Effect of CLN3-loss-of-function on cellular metabolism and signalling

Dissertation

for the award of the degree "Doctor rerum naturalium" (Dr.rer.nat.)

of the Georg-August-Universität Göttingen

within the doctoral program Molecular Medicine

of the Georg-August University School of Science (GAUSS)

submitted by

Katarzyna Więciorek-Płuciennik

from Brzeziny, Poland

Göttingen, 2021

Thesis Committee

Nuno Raimundo, PhD (1st reviewer)	Department of Cellular and Molecular Physiology The Pennsylvania State University Pennsylvania, United States of America & Multidisciplinary Institute of Ageing University of Coimbra Coimbra, Portugal
Prof. Dr Tiago F. Outeiro (2nd reviewer)	Department of Experimental Neurodegeneration University Medical Center Göttingen Göttingen, Germany
Prof. Dr Halyna R. Shcherbata	Institute of Cell Biochemistry Hannover Medical School Hannover, Germany

Further members of the Examination Board:

PD. Dr rer. nat. Laura Zelarayán-Behrend	Institute of Pharmacology and Toxicology University Medical Center Göttingen Göttingen, Germany
Prof. Dr Michael Meinecke	Department of Cellular Biochemistry University Medical Center Göttingen Göttingen, Germany
Prof. Dr Sven Thoms	Department for Child and Adolescent Health University Medical Center Göttingen Göttingen, Germany & Biochemistry and Molecular Medicine Bielefeld University Bielefeld, Germany

Date of the oral examination: 17.09.2021

You live here, now. Hic et nunc.

You have one life, one diary, one book.

What you get done such will stay.

Even if others have odd things to say.

You are not at large, not free yet still

Even if you were a pebble in a field,

Avalanches change their course to such degree,

As the rocks they roll down along you see.

And as others will say in shortest shrift,

Avalanches' course you should try to shift.

Czesław Miłosz

Translated by Marek Kazmierski

Nothing can ever happen twice.

In consequence, the sorry fact is

that we arrive here improvised

and leave without the chance to practice.

Wisława Szymborska

Translated by Stanislaw Barańczak and Clare Cavanagh

To children with Batten disease and their parents

Acknowledgements

The completion of my dissertation would not have been possible without the great effort of Nuno Raimundo, PhD. I wish to thank for the opportunity to work on such an exciting project and develop a variety of skills. I very much appreciate the valuable experience, guidance and support. Special thanks for creating working conditions, which foster my advancement.

I am deeply indebted to The NCL Foundation, which not only awarded me the fellowship but also invited me to their very supportive and competent research community. I am extremely grateful to Dr Herman van der Putten for his kind supervision and invaluable suggestions. Thanks should also go to Dr Frank Stehr for patience and help that cannot be underestimated.

I would like to express my deepest appreciation to the remaining members of my Thesis Advisory Committee for providing me with encouragement and patience throughout this project. Many thanks to Prof. Dr Tiago F. Outeiro and Prof. Dr Halyna R. Shcherbata for valuable advice and useful contributions.

I gratefully acknowledge the help of Georg-August University School of Science, especially Dr Steffen Burkhardt and Kirsten Pöhlker who extended a great deal of counselling. I would like to thank the whole Molecular Medicine doctoral programme for the support and organization of amazing events, particularly Prof. Dr Thomas Bayer.

I am also grateful to our committed collaborators. Particularly helpful to me during this time were Udhaya Bhaskar Sathya Narayanan, Nicolás Lemus-Diaz, MD PhD, and Metin Özdemir, who significantly contributed to the project. I would like to thank Ira Milosevic, PhD, for facilitating access to her laboratory.

Furthermore, I had the great pleasure of working with all former and current members of Nuno Raimundo and Ira Milosevic research groups. I would like to recognize the assistance that I received from King Faisal Yambire, PhD and Sindhuja Gowrisankaran, PhD. I very much appreciate their ingenious suggestions and unwavering mentoring. I also wish to thank Dr rer. nat. Mandy Mai, Indrani Mukherjee and other employees of the Department of Cellular Biochemistry for the friendly atmosphere and help.

Last but not least, I would like to extend my sincere thanks to my family and friends for their profound belief in my work and abilities. I very much appreciate the relentless support and love. Special thanks to my parents and husband for creating conditions that foster my further education.

Table of contents

List of figures

List of tables

List of abbreviations

4E-BP1	eukaryotic translation initiation factor 4E-binding protein 1
4E-BP2	eukaryotic translation initiation factor 4E-binding protein 2
AAV9	adeno-associated virus serotype 9
ADP	adenosine diphosphate
Akt	protein kinase B
AMOT	angiomotin
AMP	adenosine monophosphate
AMPK	AMP-activated protein kinase
AP-1	activator protein 1
APS	ammonium persulfate
ATF	activating transcription factor
ATP	adenosine triphosphate
ATP1A1	sodium/potassium-transporting ATPase subunit α1
ATP5A	ATP synthase subunit α
ATP5B	ATP synthase F1 subunit β
BAK	Bcl-2 homologous antagonist/killer
BAX	apoptosis regulator BAX
BI-1	BAX inhibitor 1
BIM	Bcl-2-like protein 11
BN-PAGE	blue native polyacrylamide gel electrophoresis
BSA	bovine serum albumin
Ca^{2+}	calcium
Cdk5	cyclin-dependent kinase 5
Cdk7	cyclin dependent kinase 7
cDNA	complementary DNA
CHOP	proapoptotic factor CCAAT/enhancer-binding protein homologous protein
CLEAR	coordinated lysosomal expression and regulation
CLN	ceroid lipofuscinosis, neuronal

$CLN3^{\Delta ex7/8}$	CLN3 with genomic deletion of 996bp corresponding to two coding exons 7 and 8
Cn	calcineurin
CO_2	carbon dioxide
COASY	coenzyme A synthase
CREB	cAMP-responsive element-binding protein
CReP	constitutive repressor of eIF2α phosphorylation
CTTN	cortactin
ddH2O	double-distilled water
DEG	differentially expressed genes
DH	dehydrogenase
DMEM	Dulbecco's Modified Eagle Medium
DMSO	dimethyl sulfoxide
DNA	deoxyribonucleic acid
dNTP	deoxynucleotide
DR5	death receptor 5
DRP1	dynamin-related protein 1
DTT	dithiothreitol
ECAR	extracellular acidification rate
EDTA	ethylenediaminetetraacetic acid
eEF2K	eukaryotic elongation factor 2 kinase
EGFR	epidermal growth factor receptor
eIF2α	eukaryotic translation initiation factor 2 subunit-α
eIF4B	eukaryotic translation initiation factor 4B
EPRS	glutamyl-prolyl tRNA synthetase
ER	endoplasmic reticulum
ERAD	ER- associated protein degradation
ERT	enzyme replacement therapy
FADH2	hydroquinone form of flavin adenine dinucleotide
FBS	Fetal Bovine Serum Heat Inactivated

FCCP	carbonyl cyanide-p-trifluoromethoxyphenylhydrazone
FDR	false discovery rate
FIS1	mitochondrial fission 1 protein
FKBP12	FK506 binding protein 12
FKBP8	peptidyl-prolyl cis-trans isomerase FKBP8
GBL	G protein β subunit-like
GCN2	general control nonderepressible 2
GP	glutathione peroxidase
GRINA	protein lifeguard 1
gRNA	guide RNA
GSH	glutathione
GSSG	glutathione disulfide
GTP	guanosine-5'-triphosphate
H^+	protons
H_2O	water
HEK	human embryonic kidney 293
HG	high glucose medium
HRI	heme-regulated inhibitor
IGF-1	insulin-like growth factor 1
IL-1β	interleukin-1β
IMM	inner mitochondrial membrane
IMS	intermembrane space
IP3R	inositol 1,4,5- trisphosphate receptor
IPA	Ingenuity Pathway Analysis
IRE1	inositol-requiring enzyme 1
ISR	integrated stress response
JNK	c-Jun N-terminal kinase
KO	knockout
LATS1	large tumour suppressor kinase 1

LATS2	large tumour suppressor kinase 2
LCN2	lipocalin 2
LD	lipid droplets
l-OPA1	long isoform of OPA1
LSD	lysosomal storage disease
MAP4K4	mitogen-activated protein kinase 4
MAPK	mitogen-activated protein kinase
MCOLN1	mucolipin TRP cation channel 1
MCS	membrane contact sites
MFF	mitochondrial fission factor
MFN	mitofusin
MFSD8	MFS domain-containing protein 8
miRNA	microRNA
MITF	melanocyte inducing transcription factor
mLST8	mammalian lethal with SEC13 protein 8
MOB	MOB kinase activator
mRNA	messenger RNA
MST1	mammalian STE-like protein 1
MST2	mammalian STE-like protein 2
MtCO1	mitochondrially encoded cytochrome c oxidase I
mtDNA	mitochondrial DNA
mTOR	mechanistic target of rapamycin
mTORC1	mTOR complex 1
mTORC2	mTOR complex 2
NADH	nicotinamide adenine dinucleotide
NaN3	sodium azide
NCL	neuronal ceroid lipofuscinosis
NDR1	nuclear Dbf2-related kinase 1
NDR2	nuclear Dbf2-related kinase 2

NDUFB8	NADH:ubiquinone oxidoreductase subunit B8
NGS	next-generation sequencing
NLK	Nemo-like kinases
NLRP3	NACHT, LRR and pyrin domain-containing 3
NOG	no glucose medium
NOXA	phorbol-12-myristate-13-acetate-induced protein 1
Nrf1	nuclear respiratory factor 1
Nrf2	nuclear respiratory factor 2
O_2	oxygen
$O_2^{\bullet-}$	superoxide radical
OCR	oxygen consumption rate
OMM	outer mitochondrial membrane
OPA1	optic atrophy 1
OxPhos	oxidative phosphorylation
P/S	penicillin/streptomycin
PBS	phosphate buffered saline
PCR	polymerase chain reaction
PERK	protein kinase-like endoplasmic reticulum kinase
Pex	peroxin, peroxisomal biogenesis factor
Pex11B	peroxisomal biogenesis factor 11β
Pex3	peroxisomal biogenesis factor 3
Pex5	peroxisomal targeting signal 1 receptor
Pgc1	peroxisome proliferator-activated receptor-gamma coactivator 1
Pi	phosphate ions
PI3K	phosphoinositide 3-kinase
PIP_3	phosphatidylinositol (3,4,5)-trisphosphate
PKA	protein kinase A
PKC	protein kinase C
PKG	protein kinase G

PKR	protein kinase R
PMP	peroxisomal membrane proteins
PMSF	phenylmethylsulphonyl fluoride
POLR2JRNA	polymerase II containing minor isoform of the subunit hRPB11
PP1	protein phosphatase 1
PRAS40	proline-rich Akt1 substrate 1
PRP4K	PRP4 pre-mRNA-processing factor 4 homolog
Prx	peroxiredoxin
PTEN	PIP3-phosphatase and dual-specificity protein phosphatase
PUMA	Bcl-2-binding component 3, isoforms 1/2
PVDF	polyvinylidene fluoride
PX459	plasmid pSpCas9(BB)-2A-Puro
PYR	no glucose medium supplemented with 1 mM pyruvate
qPCR	quantitative polymerase chain reaction
qPCR	quantitative polymerase chain reaction
Raptor	regulatory-associated protein of mTOR
Rheb	GTP-binding protein Rheb
Rictor	rapamycin-insensitive companion of mTOR
RIDD	regulated IRE1-dependent decay
Rieske	cytochrome b-c1 complex subunit Rieske
RNA	ribonucleic acid
RNS	reactive nitrogen species
ROS	reactive oxygen species
RPS6	ribosomal protein S6
S1P	site-1 protease
S2P	site-2 protease
S6K1	p70 S6 Kinase 1
SAV1	protein salvador homolog 1
SD	standard deviation

SDHA	succinate dehydrogenase complex flavoprotein subunit A
SDHB	succinate dehydrogenase complex iron sulfur subunit B
SDS	sodium dodecyl sulphate
SDS	sodium dodecyl sulphate
SDS-PAGE	sodium dodecyl sulfate-polyacrylamide gel electrophoresis
SEM	standard error of the mean
Ser	serine
Sin1	mitogen-activated protein kinase-interacting protein
SOD	superoxide dismutase
s-OPA1	short isoform of OPA1
Src	proto-oncogene tyrosine-protein kinase Src
STK11	serine/threonine-protein kinase 11
TAZ	transcriptional coactivator with PDZ-binding motif
TBC1D7	TBC1 Domain Family Member 7
TEAD	DNA-binding TEA domain transcription factor
TEMED	tetramethyl ethylenediamine
Tfam	mitochondrial transcription factor A
TFEB	transcription factor EB
Thr	threonine
TIF-1A	transcription initiation factor 1A
TPP-1	tripeptidyl peptidase I
TRAF	tumour necrosis factor receptor-associated factor
tRNA	transfer RNA
$Trx(SH)_2$	reduced thioredoxin
$TrxS_2$	oxidised thioredoxin
TSC	tuberous sclerosis complex
TUBA	α-Tubulin
TXNIP	thioredoxin-interacting protein
UBF	upstream binding factor

UCP	uncoupling protein
ULK1	Unc-51 like autophagy activating kinase 1
UPR	unfolded protein response
UQ	ubiquinol
UQCRC2	ubiquinol-cytochrome c reductase core protein 2
VDAC1	voltage-dependent anion-selective channel protein 1
WT	wild type
XBP1	transcription factor X-box-binding protein 1
YAP	Yes-associated protein

Abstract

Since a coordinated function of all organelles is essential for the proper health of a eukaryotic cell, defect in a single organelle can affect the condition of other organelles. For instance, mitochondrial dysfunction was reported in most of the lysosomal storage diseases and abnormal mitochondria-lysosome crosstalk was observed in several neurodegenerative disorders. Batten disease is a lysosomal storage disease and the most frequent cause of dementia in children, although, its precise mechanism remains unclear. Thereby, we aimed to advance the understanding of the role of organelle crosstalk in the disease progression and identify signaling pathways that might be later tested as potential therapeutic targets in Batten disease.

Analysis of our transcriptome data indicates a lack of significant effect of CLN3 KO on organelle biogenesis in HEK cells grown in high glucose medium, while mitochondrial and ER biogenesis are transcriptionally repressed in CLN3 KO HEK cells starved in no glucose medium. Moreover, we observed a substantial reduction in levels of proteins that belong to respiratory chain subunits in whole cell extracts, apart from complex V. On the contrary, the level of native OxPhos complexes in mitochondria isolated from HEK cells grown in a high glucose medium remains unaltered. Importantly, we report compromised mitochondrial respiration, increased mitochondrial superoxide levels, a decline in mitochondrial membrane potential and reduced cell viability in CLN3 KO HEK cells in both, high glucose and no glucose condition. Overall, we introduce extensive evidence of mitochondrial dysfunction in CLN3 KO HEK cells.

In addition, pathway analysis completed on transcriptome data revealed multiple signaling pathways that are significantly affected by CLN3 KO and may play an important role in Batten disease progression. Particular attention should be given to cell proliferation signaling, including Hippo, mTOR, p70 S6K1 signalling pathways, as well as stress response mechanisms, such as unfolded protein response and eIF2 signaling. Additionally, transcription factor analysis performed on the transcriptome data suggested that YAP, which is regulated by Hippo and mTOR signaling, is probably a key regulator of the cellular response to CLN3-loss-of-function. Indeed, our immunoblotting results indicate increased YAP activity in CLN3 KO HEK under both normal and starvation conditions. Likewise, we observed higher activity of S6K1 and mTORC1 in CLN3 KO HEK cells under starvation. Moreover, integrated stress response and unfolded protein response are upregulated in starved CLN3 KO HEK cells. In conclusion, our findings indicate several potential therapeutic targets and offer insight into the Batten disease mechanism.

1. Introduction

1.1. Eukaryotic cell

Each living organism is built of various individual cells, whose type, size and number ultimately determine the structure and functions of the organ and therefore the whole body. The human organism is made of approximately 37.2 trillion cells (Bianconi et al., 2013). A eukaryotic cell is organized into membrane-bound compartments, named organelles: mitochondria, peroxisomes, endoplasmic reticulum (ER), Golgi, nucleus, lipid droplets (LD), lysosomes and other vesicular compartments like endosomes, autophagosomes and multivesicular bodies (Figure 1). Such arrangement allows for spatial and temporal isolation of incompatible biochemical processes, which must be coordinated to guarantee proper cellular function (Cohen et al., 2018). The coordinated function of diverse organelles requires control over their biogenesis, position, performance and degradation. Inversely, the organelle has to stay in continuous contact with the cell to report its status and needs to ensure appropriate and timely reaction (Deus et al., 2019). Organelle interactions facilitate metabolite exchange and organelle biogenesis, growth and remodelling (Phillips and Voeltz, 2016; Rowland et al., 2014; Helle et al., 2013). Expectedly, malfunction of a single organelle due to, e.g., genetic defect, affects the condition of other organelles due to their strong interdependence (Deus et al., 2019; Sargsyan and Thoms, 2019).

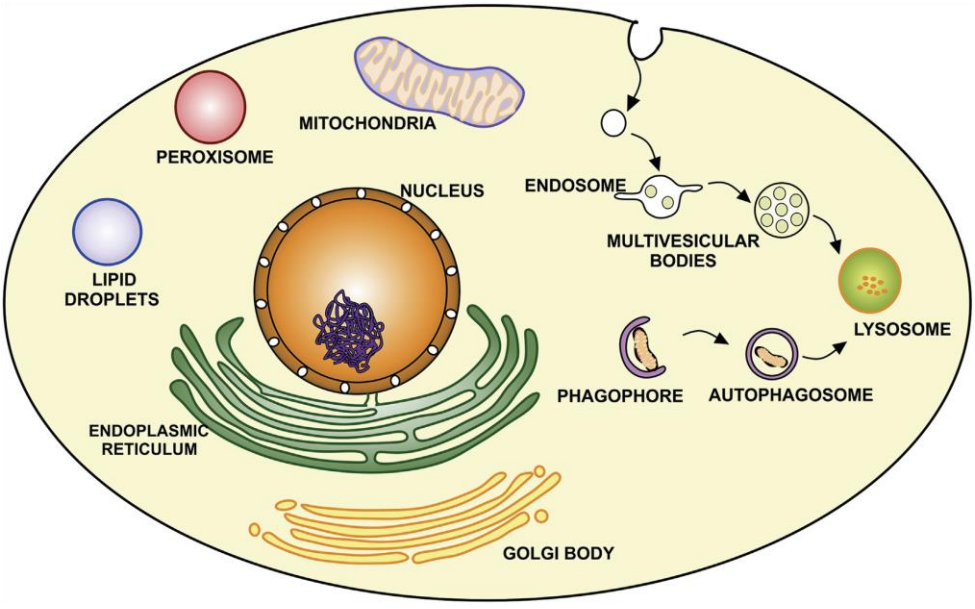

Figure 1. Illustration of the structure of a eukaryotic cell. A eukaryotic cell contains the following organelles: mitochondria, peroxisomes, endoplasmic reticulum, Golgi, nucleus, lipid droplets, lysosomes and other vesicular compartments like endosomes, autophagosomes and multivesicular bodies (Glingston et al., 2019).

1.1.1. Organelle crosstalk

Besides signaling pathways, organelles can communicate with each other via membrane contact sites (MCS), which are established by membrane proteins that function as tethers on the interacting organelles (Eisenberg-Bord et al., 2016). MCS serve for the exchange of ions, lipids and proteins. In

particular, the exchange of calcium (Ca^{2+}) takes place at different types of MCS, such as ER-plasma membrane, ER-mitochondria and ER-endosome contacts (Phillips and Voeltz, 2016). Moreover, lipid transfer was suggested to occur at most of the reported MCS, e.g., ER-mitochondria, LD-mitochondria and ER-LD contacts (Gatta and Levine, 2017; Phillips and Voeltz, 2016; Rambold et al., 2015). Importantly, lysosome-peroxisome contacts are critical for cholesterol metabolism (Chu et al., 2015). Heretofore, the exchange of proteins has only been described at ER-LD MCS.

Interestingly, organelle crosstalk can significantly contribute to organelle biogenesis and division. For instance, autophagosomes originate from various cellular compartments, including mitochondria, ER and plasma membrane (Ge et al., 2013; Hamasaki et al., 2013; Guo et al., 2012; Hailey et al., 2010; Ravikumar et al., 2010; Axe et al., 2008). Furthermore, ER-mitochondria MCS enhance autophagy specifically in answer to starvation. Notably, lysosome-mitochondria and ER-mitochondria contacts mark sites of mitochondrial fission (Wong et al., 2018; Elgass et al., 2015; Friedman et al., 2011).

1.1.2. Lysosomes

As comprehensively reviewed in Lamming and Bar-Peled et al. (2019), lysosomes were first observed in the 1950s (de Duve, 2005) and for the next several decades were mostly viewed as the degradative endpoint of the endosomal pathway (Straus, 1954). Only recently lysosomes were recognized as an important hub for metabolic signaling pathways, inter alia protein kinase mechanistic target of rapamycin (mTOR) signaling. Lysosomes play an essential part in nutrient sensing and cellular homeostasis, their malfunction results therefore in numerous disorders, collectively called lysosomal storage diseases (Cox and Cachón-González, 2012). Lysosomes also contribute to multiple common human pathologies, including neurodegeneration, obesity and cancer (Balabio, 2016).

Lysosomes are responsible for the degradation of major molecules, e.g., lipids, polysaccharides and proteins (Settembre et al., 2013). Resultant free fatty acids, monosaccharides and amino acids are translocated to the cytoplasm by specialized permeases for further use in anabolic processes (Perera and Zoncu, 2016). Hence, lysosomes are considered a recycling centre of the cell. Their degradative function requires the activity of circa 60 different catalytic enzymes, named hydrolases and an acidic environment with pH around 4.5, which is provided by the lysosomal v-ATPase (Balabio, 2016; Forgac, 2007). Extracellular material is delivered to the lysosome through endocytosis and phagocytosis, whereas intracellular material is supplied by autophagy (Balabio, 2016).

1.1.2.1 Metabolic signaling

1.1.2.1.1 Mechanistic target of rapamycin signaling

Protein phosphorylation is a common, post-translational modification, which defines metabolic and immunologic reactions to a host of stimuli (Pawson and Scott, 2005). Overall, the human body incorporates more than 500 kinases that drive phosphorylation, 150 phosphatases that can reverse phosphorylation, and 250 thousand non-redundant phosphorylation sites in over 20 thousand proteins (Alonso et al., 2004; Hornbeck et al., 2012; Khoury et al., 2011; Manning et al., 2002). Phosphorylation of a kinase normally controls its activity and can determine cellular localization

(Johnson and Lewis, 2001; Ubersax and Ferrell, 2007). Multisite phosphorylation, i.e., phosphorylation of more than one site of a protein, can regulate its activity, localization, stability, and interactions (Cohen, 2000; Holmberg et al., 2002).

The mechanistic target of rapamycin (mTOR) is a serine/threonine protein kinase in the phosphatidylinositol 3-kinase (PI3K)-related protein kinases family (Keith and Schreiber, 1995). Predictably, it was first noticed during studies on molecular mechanisms, by which rapamycin can slow or arrest cell proliferation. Rapamycin, also called sirolimus, forms a complex with the intracellular receptor FK506 binding protein 12 (FKBP12), which inhibits mTOR (Sabers et al., 1995; Brown et al., 1994; Sabatini et al., 1994). In mammals, mTOR acts as a catalytic subunit of two distinct complexes, later described as mTOR complex 1 (mTORC1) and mTOR complex 2 (mTORC2). These complexes differ concerning their sensitivity to rapamycin, substrates and functions (Liu and Sabatini, 2020).

An association of mTOR with the adaptor proteins regulatory-associated protein of mTOR (Raptor) and mammalian lethal with SEC13 protein 8 (mLST8, also called GBL) creates mTORC1, which is highly sensitive to rapamycin (Kim et al., 2003; Kim et al., 2002; Hara et al., 2002). On contrary, the association of mTOR with the adaptor proteins rapamycin-insensitive companion of mTOR (Rictor), mLST8 and mitogen-activated protein kinase (MAPK)-interacting protein (Sin1) forms rapamycin resistant mTORC2 (Kennedy and Lamming, 2016; Frias et al., 2006; Jacinto et al., 2004; Sarbassov et al., 2004).

Both mTOR complexes are essential for the regulation of metabolism, as depicted in Figure 2. Protein kinase mTOR integrates various environmental signals, including growth factors, stress, availability of nutrients and energy, to adjust material accumulation and metabolism by regulating essential cellular processes, such as autophagy, lipid and protein synthesis. Therefore, mTOR plays a key role in maintaining cellular and physiological homeostasis (Liu and Sabatini, 2020).

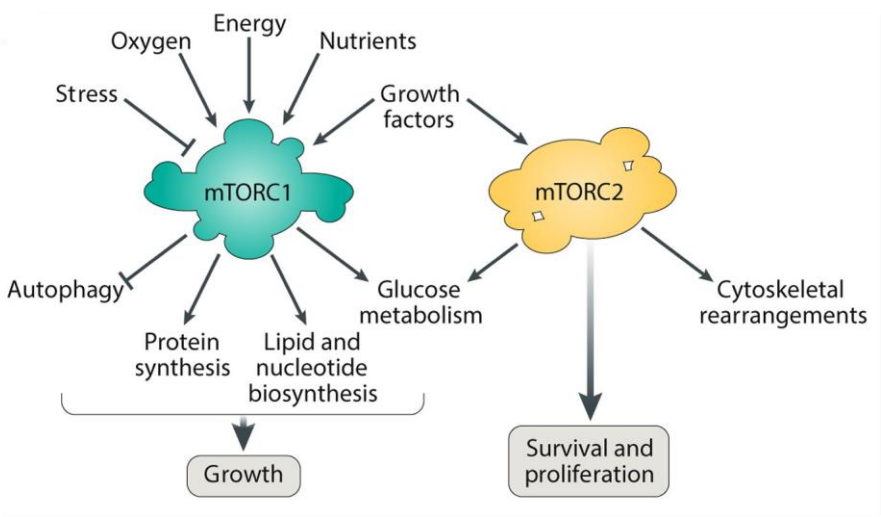

Figure 2. Diagram of mTOR signaling roles concerning mTORC1 and mTORC2. Briefly, mTORC1 combines information about the availability of nutrients and environmental conditions to regulate cellular anabolism and catabolism, while mTORC2 controls cytoskeletal arrangement and can activate various pro-survival pathways (Liu and Sabatini, 2020).

1.1.2.1.1.1 Mechanistic target of rapamycin complex 1

Expectedly, the two mTOR complexes play different cellular roles. The kinase complex mTORC1 integrates environmental and hormonal signals and senses the availability of amino acids, glucose and cholesterol (Lamming, 2014; Park and Ahima, 2014; Wang et al., 2007; Barb et al., 2007; Zhang et al., 2003). When these conditions favour cell growth and anabolism, mTORC1 locates to the lysosomal surface, where it interacts with its obligate activator guanosine-5'-triphosphate (GTP)-binding protein Rheb (Rheb) to phosphorylate multiple substrates, such as p70 S6 Kinase 1 (S6K1), eukaryotic translation initiation factor 4E-binding protein (4E-BP) 1 and Unc-51 like autophagy activating kinase 1 (ULK1), to increase the production of ATP, proteins, lipids and nucleotides, while inhibiting autophagy (Kennedy and Lamming, 2016; Kang et al., 2013; Egan et al., 2011; Kim et al., 2011; Zid et al., 2009; Cunningham et al., 2007). Otherwise, mTORC1 stays inactive in the cytoplasm; therefore, anabolic processes are inhibited, whereas autophagy is activated. Notably, mTORC1 controls multiple cellular functions, including ribosomal biogenesis and translation, lipogenesis amino acid transport and nucleotide synthesis (Kennedy and Lamming, 2016; Rosario et al., 2016; Lamming and Sabatini, 2013).

Interaction of mTORC1 with Rheb is possible only at the lysosomal surface, thus recruitment of Rheb and mTORC1 to the lysosome is required for activation of mTORC1. Lysosomal recruitment of Rheb is controlled by amino acids (Yang et al., 2017). The kinase complex mTORC1 is a part of a complex signaling network responsive to the variable lysosomal amino acid content via a nutrient-sensing mechanism. Amino acids interact with sensor proteins at the lysosomal surface that regulate the nucleotide loading of the ras-related GTP-binding proteins (Rags), which strongly interact with mTORC1 through its Raptor subunit to activate mTORC1 (Kim et al., 2008; Sancak et al., 2008). Negative regulation of mTOR involves peptidyl-prolyl cis-trans isomerase FKBP8 (FKBP8), which precludes Rheb from activating mTORC1, and proline-rich Akt1 substrate 1 (PRAS40), which competes with Raptor for binding to S6K1 and 4E-BP1 (Dancey, 2010).

Noteworthy, Rheb is also regulated by the tuberous sclerosis complex (TSC), consisted of TSC1, TSC2 and TBC1 Domain Family Member 7 (TBC1D7) (Dibble et al., 2012). Different residues of TSC1 and TSC2 are phosphorylated by various kinases, e.g., protein kinase B (Akt) and 5' adenosine monophosphate (AMP)-activated protein kinase (AMPK), to adjust mTORC1 activity by changing the GTPase activating potential of TSC towards Rheb (Tian et al., 2017; Lee et al., 2007; Inoki et al., 2006; Ma et al., 2005). Relative depletion of intracellular adenosine triphosphate (ATP) in proportion to AMP leads to phosphorylation of TSC1/2 by AMPK and its upstream regulator serine/threonine-protein kinase 11 (STK11), and consequently to inhibition of Rheb and mTORC1 signalling (Dancey, 2010). Importantly, the activity of TSC is also regulated by localization. The departure of TSC from lysosome results from phosphorylation of TSC2 by Akt in response to insulin-PI3K signalling. Therefore, TSC cannot inhibit Rheb, which allows for mTORC1 activation. Otherwise, in the absence of insulin signalling, TSC is located to the lysosome and inhibits Rheb. Briefly, Akt facilitates crosstalk between the mTORC1 and mTORC2 by phosphorylation of TSC2 and mSin1 (Humphrey et al., 2013; Inoki et al., 2002), as illustrated in Figure 3.

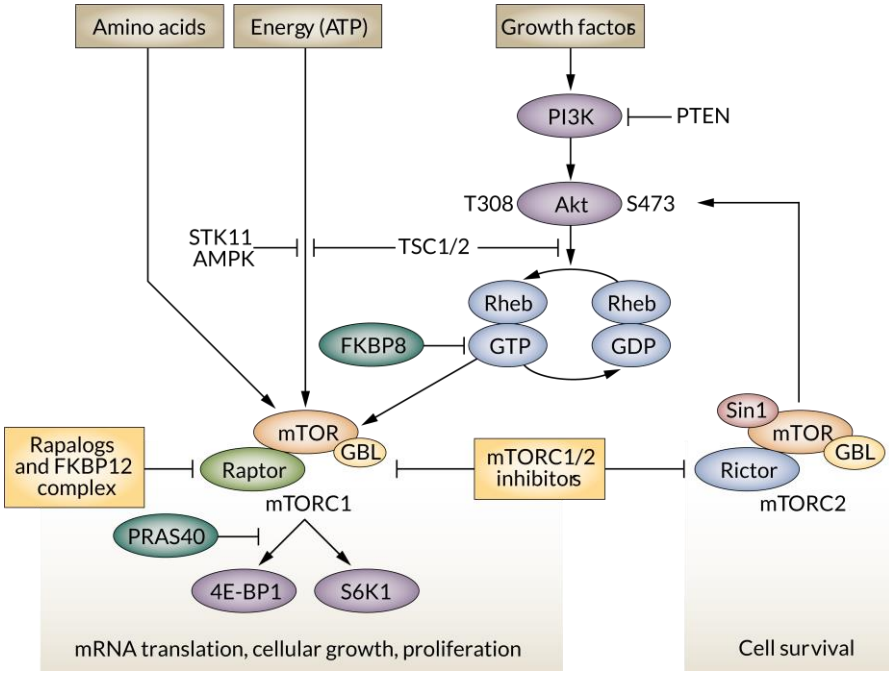

Figure 3. Schematic representation of mTOR signaling network depicting crosstalk between the mTORC1 and mTORC2. Akt mediates crosstalk between the mTORC1 and mTORC2 since it is a downstream effector of mTORC2 and an upstream activator of mTORC1. Following activation of the PI3K-Akt axis, Akt phosphorylates TSC2 and consequently inhibits repression of Rheb. Resultant mTORC1 activation leads to phosphorylation of S6K1 and 4E-BP1. On the other hand, mTORC2 phosphorylates Akt to enhance its activity and stability. Moreover, relative depletion of intracellular ATP in proportion to AMP results in phosphorylation of TSC1/2 by AMPK and its upstream regulator STK11; therefore inhibition of Rheb and mTORC1 signalling. Moreover, mTORC1 can be negatively regulated by FKBP8 and PRAS40. Rapamycin analogues (Rapalogs) form a complex with FKBP12 and preferentially disrupt mTORC1, while small molecule mTOR kinase inhibitors deactivate both mTOR complexes (Dancey, 2010).

1.1.2.1.1.2 Mechanistic target of rapamycin complex 2

On the other hand, mTORC2 is mainly an effector of the insulin-IGF1-PI3K signalling pathway, while IGF1 signifies insulin-like growth factor 1. Complexes have also different cellular localization, mTORC2 is physically associated with the ribosome (Zinzalla et al., 2001) and localizes to the mitochondria-associated ER, where it interacts with a particular mitochondrial tethering complex (Betz et al., 2013). Intriguingly, recent evidence links mTORC2 to lysosomal acidification (Monteith et al., 2018). Notably, mTORC2 regulates numerous processes, inter alia metabolism, apoptosis, amino acid and ion homeostasis (Gu et al., 2017; Kennedy and Lamming, 2016; Sciarretta et al., 2015).

The kinase complex mTORC2 can be directly activated by phosphatidylinositol (3,4,5)-trisphosphate (PIP_3) by relieving an inhibitory interaction with Sin1 (Liu et al., 2015). PIP_3-phosphatase and dual-specificity protein phosphatase PTEN (PTEN) negatively modulates the PI3K-Akt signalling pathway by dephosphorylating phosphoinositides. Moreover, mTORC2 activity responds to fatty acids (Tripathy and Jump, 2013) and probably requires interaction with ribosomal protein subunits (Zinzalla et al., 2011). After activation, mTORC2 phosphorylates multiple AGC kinases, such as Akt and protein kinase C α (PKCα), usually to enhance their activity and stability (Liu et al., 2014; Ikenoue et al., 2008;

Sarbassov et al., 2005). Akt in turn mediates the cellular insulin response and enhances proliferation as a key early effector in the PI3K pathway. Figure 3 presents a simplified scheme of just described mTOR signaling. Lysosomes are not only the recycling centre of the cell but also a signalling platform essential for the coordination of environmental and hormonal signals with mTORC1 and mTORC2 activity.

1.1.2.1.1.3 P70 S6 Kinase 1 signalling

As previously mentioned, S6K1 is activated by phosphorylation at threonine 389 mediated by mTORC1. Noteworthy, S6K1 can be phosphorylated at eight or more sites in response to various cues (Magnuson et al., 2012). Along with the aforementioned phosphorylation at threonine 389, phosphorylation at threonine 229 and serine 371 plays an essential role in canonical S6K1 activation (Ma and Blenis, 2009; Pullen et al., 1998; Moser et al., 1997). Importantly, the mTORC1-S6K1 kinase axis has a key role in the metabolic pathways network, since it integrates intracellular and extracellular cues and regulates nutrient driven metabolic pathways with an evident link to inflammation (Saxton and Sabatini, 2017; Dibble and Cantley, 2015; Fontana et al., 2010; Ma and Blenis, 2009; Hotamisligil and Erbay, 2008; Ruvinsky et al., 2005).

Interestingly, multisite phosphorylation of S6K1 determines target selection, i.e., phosphorylation of several proteins by S6K1 is feasible only if S6K1 is phosphorylated by both, mTORC1 at threonine 389 (T389) and cyclin-dependent kinase 5 (Cdk5) at serines 424 and 429 (S424 and S429, respectively). Phosphorylation of S6K1 by Cdk5 stimulates a conformational switch, which enables high-affinity binding and phosphorylation of glutamyl-prolyl tRNA synthetase (EPRS), coenzyme A synthase (COASY), cortactin (CTTN) and lipocalin 2 (LCN2) (Arif et al., 2019). In adipocytes, insulin- and obesity-induced activation of Cdk5 is essential for glucose uptake and promotion of a diabetogenic expression program (Banks et al., 2015; Li et al., 2011; Lalioti et al., 2009). Overall, S6K1 responds to signals from mTORC1 and Cdk5 to regulate lipid metabolism in adipocytes.

However, phosphorylation of S6K1 by Cdk5 is neither required nor impediment for phosphorylation of canonical S6K1 targets, such as eukaryotic translation initiation factor 4B (eIF4B), eukaryotic elongation factor 2 kinase (eEF2K) and ribosomal protein S6 (RPS6) (Arif et al., 2019), which lead global induction of translation (Ma and Blenis, 2009; Ruvinsky et al., 2005). Figure 4 is a schematic representation of S6 K1 signalling described above.

Parenthetically, S6K1 and mTOR can also stimulate translation more directly, by increasing the activity of RNA polymerase I and RNA polymerase III through phosphorylation of the regulatory factors upstream binding factor (UBF) (Hannan et al., 2003), transcription initiation factor 1A (TIF-1A) (Mayer et al., 2004) and MAF1 (Michels et al., 2010; Shor et al., 2010), thus upregulating transcription of ribosomal RNA.

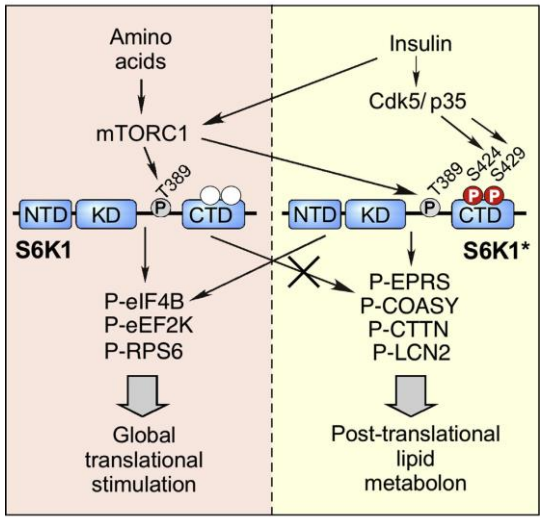

Figure 4. Simplified scheme of S6K1 signaling concerning a role of multisite phosphorylation in substrate selection. Briefly, mTORC1-mediated phosphorylation of S6K1 allows for phosphorylation of its canonical targets, including eIF4B, eEF2K and RPS6. Additional phosphorylation of S6K1 by Cdk5 is required for phosphorylation of EPRS, COASY, CTTN and LCN2. P indicates phosphorylation at threonine (T) or serine (S). NTD, KD and CTD signify the N-terminal domain, kinase domain and C-terminal domain of S6K1, respectively (Arif et al., 2019).

1.1.2.1.1.4 Lysosomal biogenesis

As neatly summarized in Balabio (2016), lysosomal biogenesis and autophagy are transcriptionally controlled by the CLEAR gene network and its master regulator, transcription factor EB (TFEB) (Sardiello et al., 2009; Settembre et al., 2011). The lysosomal gene network regulates cellular clearance and metabolism. Stressors like starvation lead to a great enhancement of degradation through autophagy, which plays a key role in restoring homeostasis throughout metabolic imbalance. Lysosome-to-nucleus signalling allows adapting lysosomal function to nutrient availability, i.e., switch between cellular anabolic and catabolic pathways (Settembre et al., 2012).

Under the normal, nutrient-rich condition, TFEB is inactivated by mTORC1 by phosphorylation on the lysosomal surface. Moreover, Akt can phosphorylate TFEB independently of mTORC1 (Palmieri et al., 2017). Subsequently, TFEB is sequestered in the cytoplasm by 14-3-3 proteins, and unable to translocate to the nucleus as a result (Martina et al., 2012; Roczniak-Ferguson et al., 2012; Settembre et al., 2012). On the contrary, due to stressors like starvation, mTORC1 is inhibited and relocates to the cytoplasm. The lysosome releases calcium through mucolipin TRP cation channel 1 (MCOLN1), which leads to local activation of calcineurin (Cn) and dephosphorylation of TFEB. Consequently, TFEB dephosphorylation prevents 14-3-3 proteins binding, therefore, TFEB can translocate to the nucleus and activate the lysosomal pathway (Medina et al., 2015). As a result, freshly formed lysosomes degrade proteins, release amino acids back to the cytoplasm and regenerate the pool of cellular amino acids, allowing for reactivation of mTORC1 (Yu et al., 2010). Just described lysosome-to-nucleus signalling mechanism is illustrated in Figure 5. Parenthetically, the lysosomal function can be also regulated by protein networks through protein-protein interactions.

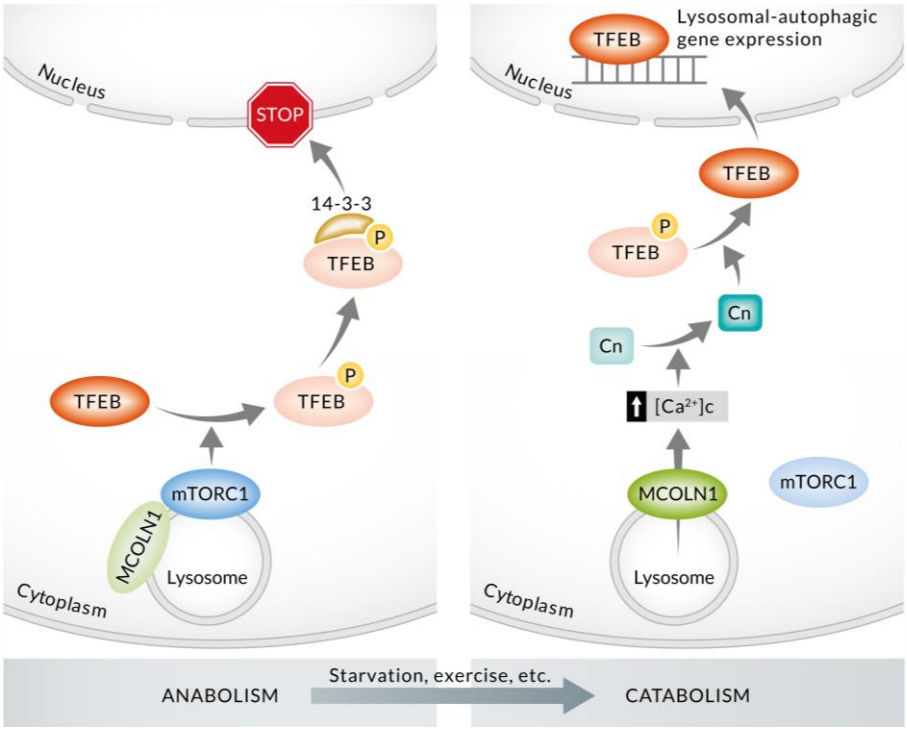

Figure 5. Schematic representation of lysosome-to-nucleus signalling. Under the nutrient-rich condition, mTORC1 locates on the lysosomal surface and inhibits TFEB by phosphorylation. Then, TFEB is sequestered in the cytoplasm by 14-3-3 proteins, and consequently incapable of translocation to the nucleus. In contrast, in response to stressors like starvation, mTORC1 is inhibited and repositions to the cytoplasm. The lysosome releases calcium (Ca^{2+}) through MCOLN1, causing local activation of calcineurin and dephosphorylation of TFEB. TFEB dephosphorylation precludes 14-3-3 proteins binding; therefore, TFEB can translocate to the nucleus and activate the lysosomal pathway (Balabio, 2016).

1.1.2.1.1.5 Role of the mechanistic target of rapamycin in health and disease

Protein kinase mTOR is an essential regulator of glucose metabolism and lipogenesis across different tissues, hence, it plays a key role in many metabolic diseases, including obesity and type 2 diabetes (Liu and Sabatini, 2020). The mTOR pathway controls brain physiology and function by coordinating multiple neuronal functions and stages of development, including shaping basic cortical architecture and remodelling of neuronal circuitry in response to experience (Lipton and Sahin, 2014; Graber et al., 2013). Interestingly, mTOR activity is perceived as a critical driver of ageing (Liu and Sabatini, 2020).

1.1.2.1.2 Hippo signalling

As neatly summarized in Ibar and Irvine (2020), Hippo-YAP signalling harmonizes organ growth and homeostasis with nutrition and metabolism through the integration of signals that regulate cellular proliferation and differentiation. The Hippo signalling network reacts to a variety of environmental cues, such as cell density and polarity, Wnts, mechanical force, as well as energy and ER stress (Zheng and Pan, 2019; Misra and Irvine, 2018).

The key components of the mammalian Hippo network are transcription factors, Yes-associated protein (YAP) and transcriptional coactivator with PDZ-binding motif (TAZ), which can be collectively

called YAP proteins. YAP proteins are regulated by Hippo signalling through phosphorylation by large tumour suppressor kinases (LATS), which promotes their cytoplasmic localization and degradation (Oh and Irvine, 2008; Dong et al., 2007; Zhao et al., 2007). Otherwise, not phosphorylated YAP proteins locate to the nucleus, where they activate gene expression through interactions with partner proteins, such as the DNA-binding TEA domain transcription factors (TEAD) (Wu et al., 2008; Zhang et al., 2008; Zhao et al., 2008). Furthermore, YAP proteins can induce transcription of secreted growth factors like Wnts (Hansen et al., 2015; Varelas, 2014). Under conditions of growth, YAP proteins are critical to promote and orchestrate nutrient uptake, energy availability and anabolic processes. Alterations in Hippo-YAP signalling contribute to the pathogenesis of several metabolic diseases, including type 2 diabetes, fatty liver and cardiovascular diseases.

Ste20 family kinases, primarily mammalian STE-like proteins (MST), or mitogen-activated protein kinase 4 (MAP4K4) activate LATS kinases through phosphorylation. MST form a stable complex with protein salvador homolog (SAV1), which is required for phosphorylation of the downstream LATS/MOB complex (Lin et al., 2020). Independent of Hippo signalling, YAP proteins activity can be inhibited through phosphorylation by nuclear Dbf2-related kinases (NDR) (Zhang et al., 2015) and PRP4 pre-mRNA-processing factor 4 homolog (PRP4K) (Cho et al., 2018). On the other hand, phosphorylation by cyclin-dependent kinase 7 (Cdk7), Nemo-like kinases (NLK) (Cho et al., 2020; Hong et al., 2017; Moon et al., 2017) or Src family kinases increases YAP activity (Li et al., 2016; Taniguchi et al., 2015). YAP can be also controlled by cytoplasmic sequestration through binding to upstream regulators, including angiomotin (AMOT) in mammals and expanded (Ex) in Drosophila (Chan et al., 2011; Oh et al., 2009; Wang et al., 2011; Zhao et al., 2011). Figure 6 presents a simplified schematic of the Hippo-YAP signalling network.

Hippo-YAP signaling is a part of feedback networks, where controls and is controlled by metabolism. For instance, YAP proteins modulate glucose metabolism by, inter alia, upregulation of glucose transporters and regulation of insulin signalling (Hwang et al., 2019; Cox et al., 2018). On the other hand, energy stress activates AMPK (Hardie et al., 2012), which directly phosphorylates YAP proteins (Mo et al., 2015; Wang et al., 2015) or promotes LATS activation (DeRan et al., 2014) to impair YAP activity. On contrary, under high glucose conditions, YAP is O-linked-N-acetylglucosaminylated (O-GlcNAcylated) at multiple sites to suppress its inhibition (Peng et al., 2017; Zhang et al., 2017).

Moreover, YAP proteins can promote the transcription of amino acid transporters to increase the uptake of amino acids (Edwards et al., 2017; Park et al., 2016). Interestingly, YAP controls protein synthesis by stimulating Myc expression, which in turn promotes the expression of genes implicated in ribosome biogenesis. Importantly, YAP proteins can enhance mTOR signalling through miRNA-mediated inhibition of PTEN (Tumaneng et al., 2012). Conversely, the previously mentioned effector of the insulin-PI3K signalling pathway, Akt can indirectly increase the activity of YAP proteins through inhibition of MST1/2 (Borreguero-Muñoz et al., 2019). YAP activity is also regulated by mTORC2, which phosphorylates MST1 (Sciarretta et al., 2015) and AMOT (Artinian et al., 2015).

Furthermore, Hippo signalling controls autophagy through crosstalk with mTOR pathway and MST1-dependent regulation of Beclin-1 (Zhang et al., 2016; Lin et al., 2016; Maejima et al., 2013). Defective autophagy results in increased cellular YAP levels and activity (Lee et al., 2018; Liang et al., 2014). Similarly, crosstalk between lipid metabolism and hippo signalling is evident from several publications. Regulation of YAP proteins is connected to the mevalonate synthesis pathway and fatty acid metabolism (Noto et al., 2017, Sorrentino et al., 2014; Wang et al., 2014). The Hippo signalling network, in turn, regulates adipose cell proliferation and differentiation (Huang et al., 2013; Dupont et al., 2011).

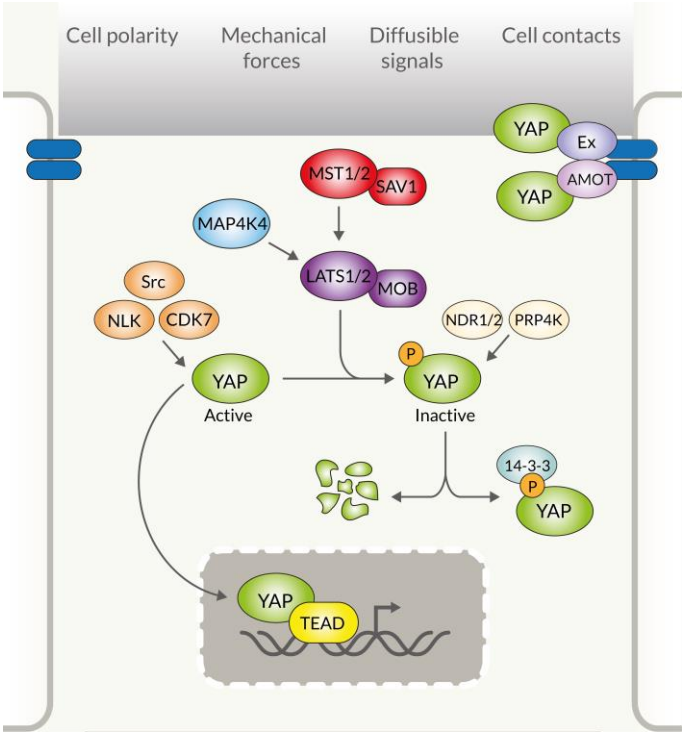

Figure 6. A schematic representation of the Hippo-YAP signalling network. The activity of kinases MAP4P4, MST1/2 and LATS1/2 is regulated by the environmental signals. YAP is phosphorylated by LATS1/2, NDR1/2 or PRP4K to promote is cytoplasmic localization through binding to 14-3-3 proteins and degradation. On contrary, Src, CDK7 and NLK phosphorylate YAP to increase its activity. YAP can be also regulated by cytoplasmic sequestration through binding to AMOT. Active YAP translocates to the nucleus, where it induces gene expression through interactions with TEAD (Ibar and Irvine, 2020).

1.1.2.2 Lysosomal storage diseases

Mutations in genes encoding proteins engaged in lysosomal function result in lysosomal storage diseases (LSD), distinguished by the gradual accumulation of undegraded material inside the lysosome. Patients with LSD show severe multisystemic phenotype, often including early-onset neurodegeneration. Pathological lysosomal storage usually results in defective autophagy and consequent accumulation of autophagy substrates (Balabio, 2016). Interestingly, the amount of accumulated material can be decreased through the initiation of the lysosomal-autophagic pathway caused by overexpression of TFEB (Palmieri et al. 2016; Settembre et al., 2013). Moreover, safe and successful

means to improve lysosomal function and enhance autophagy might play a key role in healthy ageing and treatment of various age-associated diseases (Fujikake et al., 2018; Peng et al., 2016; Peng and Puglielli, 2016).

1.1.3. Mitochondria

Mitochondria are the main source of an energy-rich compound, ATP, necessary for essential cell functions in all eukaryotes independent of photosynthesis; therefore, they are commonly known as the powerhouses of the cell. Noteworthy, mitochondria are also responsible for nicotinamide adenine dinucleotide (NADH) and guanosine-5'-triphosphate (GTP) production, synthesis of phospholipids, amino acids, heme groups and iron-sulfur clusters (Kühlbrandt, 2015). Moreover, similarly to lysosomes, they function as cellular signalling hubs involved in calcium signalling and stress response mechanisms (Chandel, 2015; Pellegrino and Haynes, 2015; Rizzuto et al., 2012). Mitochondrial morphology and function are impaired in numerous neurodegenerative disorders leading to lowered ATP generation, an overabundance of reactive oxygen species and apoptosis (Area-Gomez et al., 2019; Jodeiri Farshbaf and Ghaedi, 2017).

1.1.3.1 Mitochondrial structure

Mitochondria are semi-autonomous cellular organelles isolated from the cytoplasm of a cell by the outer and inner mitochondrial membrane. Porins in the outer mitochondrial membrane allow for passive diffusion of small, uncharged molecules and ions (Bayrhuber et al., 2008), whereas specific enzymes called translocases are involved in the transfer of larger molecules, e.g., proteins (Kühlbrandt, 2015). On the contrary, the inner mitochondrial membrane is greatly impermeant and functions as a principal barrier between the mitochondrial matrix and the cytosol. Expectedly, the gap between mitochondrial membranes is termed intermembrane space (IMS). There are three morphologically distinct structures of the inner membrane: cristae, cristae junctions and boundary membranes. Interestingly, their shape changes according to the cell's requirements (Hoppins et al., 2011; Von der Malsburg et al., 2011). The mitochondrial structure is illustrated in Figure 7 in a simplified manner. Aerobic ATP production can be reinforced through an increase in the number of mitochondria and expansion of the surface area of cristae membranes (Cogliati et al., 2016; Perkins et al., 2003).

1.1.3.2 Respiratory chain

As extensively reviewed in Kausar et al. (2018), the human brain consumes nearly 20% of the basal oxygen from the total inhaled oxygen to ensure sufficient energy supply for the usual activity of more than 85 billion neurons (Magistretti and Allaman, 2015). The vast majority of the oxygen is utilized by mitochondria in the respiratory chain to synthesize ATP through oxidative phosphorylation for various cellular activities, while reactive oxygen species (ROS) are generated as a by-product.

Oxidative phosphorylation (OxPhos) is characterized as an electron transport chain driven by substrate oxidation that is coupled to ATP synthesis through an electrochemical transmembrane gradient (Cardol et al., 2009). The mitochondrial respiratory chain consists of four electron transport

complexes: NADH dehydrogenase - complex I, succinate dehydrogenase – complex II, cytochrome c reductase – complex III, cytochrome c oxidase – complex IV, and the fifth complex is mitochondrial ATP synthase. Complexes I, III and IV generate the proton gradient necessary for ATP synthesis by pumping protons across the membrane. Successively, complex V produces ATP from adenosine diphosphate (ADP) and phosphate ions (Pi), which result from ATP hydrolysis (Kühlbrandt, 2015). Figure 8 presents a simple model of respiratory chain complexes. Electron transport complexes (I-IV) are found on the flat cristae surface, while ATP synthase (complex V) dimer is located at the cristae edge (Davies et al., 2011). Optic atrophy 1 (OPA1) is a dynamin-related GTPase, which fastens the crista junction (Varanita et al., 2015; Frezza et al., 2006), as illustrated in Figure 7.

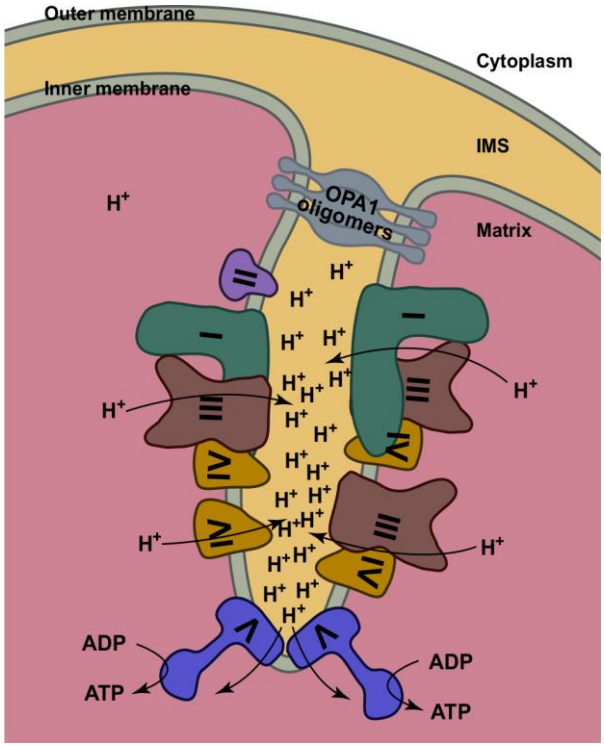

Figure 7. A simple model of cristae and respiratory chain complexes. Electron transport chain complexes I-IV are situated on the planar surface of cristae, whereas ATP synthase (complex V) dimers form ribbons at the edge of cristae. OPA1 oligomers fasten the root of cristae. Traces of protons (H^+) are indicated by arrows (Guo et al., 2017).

As discussed in Cadenas (2018), protons can leak across the inner mitochondrial membrane and return to the mitochondrial matrix independently of ATP synthase. Mitochondrial OxPhos is not therefore completely coupled (Stuart et al., 2001; Rolfe et al., 1999; Nobes et al., 1990). Mitochondrial superoxide production notably depends on mitochondrial membrane potential, thereby, proton leak affects ROS generation (Korshunov et al., 1997; Liu, 1997). Uncoupling proteins (UCP), which are located in the inner membrane, can induce proton leak to lower the overall mitochondrial membrane potential (Ricquier, 2017). Minor uncoupling of mitochondrial oxidative phosphorylation is considered a cytoprotective strategy in presence of oxidative stress since it can enhance the respiration simultaneously reducing ROS production through a change of the redox state of coenzyme Q (Brookes, 2004; Brand, 2000; Papa and Skulachev, 1997; Boveris and Chance, 1973).

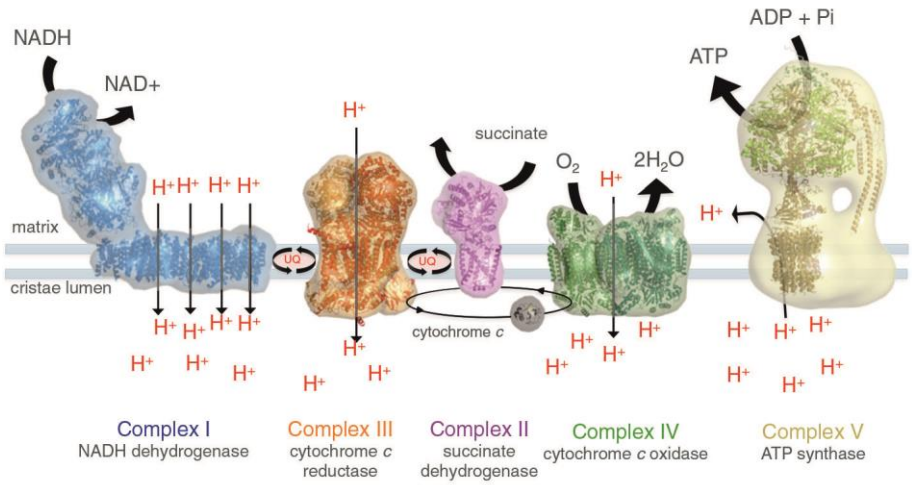

Figure 8. A simple model of membrane protein complexes of the respiratory chain. We discern four electron transport complexes: NADH dehydrogenase (blue), succinate dehydrogenase (pink), cytochrome c reductase (orange) and cytochrome c oxidase (green). The fifth OxPhos complex is the mitochondrial ATP synthase (tan). Traces of protons (H+) are indicated by arrows; UQ: ubiquinol (Kühlbrandt, 2015).

Individual OxPhos complexes can be combined into supercomplexes to enhance electron transfer efficiency and reduce ROS production (Cogliati et al., 2016; Cogliati et al., 2013; Diaz et al., 2012; Friedrich and Hellwig, 2010; Baracca et al., 2009). Interestingly, deficient supercomplexes assembly is implied in the pathogenesis of several neuromuscular disorders (Lopez-Fabuel et al., 2017; Antoun et al., 2015).

1.1.3.3 Reactive oxygen species

Importantly, mitochondria produce nearly 90% of total cellular ROS (Balaban et al., 2005) and respiratory chain complexes I, II and III are considered key contributors (Brand et al., 2010; Lenaz, 2001). As discussed in Snezhkina et al. (2019), oxidative ATP production relies on the reduction of molecular oxygen to water in the electron transport chain (Brand et al., 2010). The resultant superoxide radical is converted by manganese superoxide dismutase to hydrogen peroxide in the mitochondrial matrix or by Copper Zinc superoxide dismutase in the intermembrane space or cytosol (Okado-Matsumoto and Fridovich, 2001). Then, mitochondrial aconitase converts hydrogen peroxide to a hydroxyl radical via a Fenton reaction in the mitochondrial matrix (Vasquez-Vivar et al., 2000). Furthermore, mitochondrial ROS are produced in the cytochrome catalytic cycle, which is responsible for the metabolism of diverse organic substrates (Yasui et al., 2005). Besides superoxide dismutases, several antioxidant systems shield mitochondria from ROS, including glutathione peroxidase, peroxiredoxins, glutathione, cytochrome c oxidase (complex IV), coenzyme Q (CoQ) (Marí et al., 2009; Fernando et al., 2006; Rabilloud et al., 2001; Hanukoglu, 2001; Ham and Liebler, 1995; Beyer, 1990; Orii, 1982). Figure 9 presents a simple model of the mitochondrial respiratory chain and its contribution to total ROS, as well as antioxidant scavenger reactions.

Noteworthy, ROS are also generated in peroxisomes and ER. Moreover, ROS are also produced due to, inter alia, transition metal ions, oxidase activity, thymidine and polyamine catabolism (Kudryavtseva et al., 2019; Amendola et al., 2014; Tabata et al., 2012; Storz, 2005; Dansen and Wirtz, 2001). Multiple antioxidant defence mechanisms control metabolic and signalling pathways to regulate ROS production and preserve oxidative homoeostasis. Antioxidant systems can also induce cell death in response to a chronic increase of ROS levels (Galadari et al., 2019). High level of ROS leads to oxidative stress, which impairs various molecules, cellular structures and functions contributing to pathological changes associated with inflammation, ageing, neurodegeneration and cancer (Kudryavtseva et al., 2019; Kirkinezos and Moraes, 2001; Rimessi et al., 2016; Newsholme et al., 2007; van der Vliet et al., 2018). Furthermore, the malfunction of antioxidant defence is a significant component in neurodegeneration (Sayre et al., 2008).

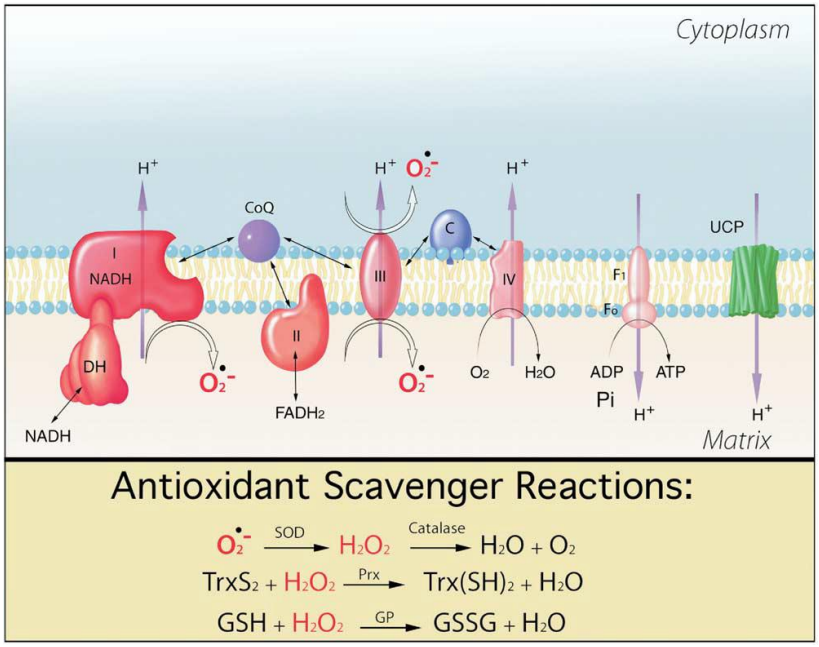

Figure 9. A simple model of mitochondrial ROS generation by respiratory chain, and antioxidant scavenger reactions. Colours of the respiratory chain complexes denote their contribution to the total ROS produced, with red being the biggest and pink the smallest. Superoxide radical ($O_2^{\bullet -}$) is converted by superoxide dismutase (SOD) to hydrogen peroxide (H_2O_2), which in turn is converted by catalase to water (H_2O) and oxygen (O_2). The enzymatic action of the peroxiredoxin (Prx) involves other cellular dithiol proteins, e.g., thioredoxin ($TrxS_2$), resulting then in reduced thioredoxin ($Trx(SH)_2$) and water. Likewise, the scavenger reaction of glutathione peroxidase (GP) requires glutathione (GSH) to produce glutathione disulfide (GSSG) and water. Traces of protons (H^+) are indicated by violet arrows. Importantly, uncoupling proteins (UCP) can lower the overall mitochondrial membrane potential; DH: dehydrogenase, $FADH_2$: hydroquinone form of flavin adenine dinucleotide (Balaban et al., 2005).

1.1.3.4 Mitochondrial DNA

Mitochondria are believed to descend from an ancient prokaryote, alpha-proteobacteria based on their close homology detected by phylogenetic analysis of mitochondrial genes. Intriguingly, mitochondria have their genetic system with a DNA code (mtDNA) dissimilar from that of their bacterial ancestors and their hosts (Gray et al., 1998). Throughout evolution mitochondria transferred the vast

majority of their genes to the nucleus, hence, most mitochondrial proteins are made in the cytoplasm and later transferred into the organelle by specialized enzymes, called protein translocases (Schmidt et al., 2010). Among circa 1000 mitochondrial proteins in a human body, only 13 are mtDNA encoded, all being essential subunits of OxPhos complexes. The remaining genes on the human mtDNA encode for mitochondrial translation machinery, including 2 ribosomal RNAs and 22 transfer RNAs. All mtDNA encoded genes are therefore crucial for proper mitochondrial function (Chan, 2019).

1.1.3.5 Mitochondrial dynamics

As reviewed by Chan (2019), mitochondrial dynamics comprises several processes: fusion, fission, transport and selective degradation, which are essential for proper mitochondrial function. Mitochondrial dynamics enables control over morphology and mitochondria inheritance, content exchange, maintenance of mtDNA and OxPhos activity.

Fusion and fission control mitochondrial morphology, which varies between cell types and conditions (Twig et al., 2008; Chen et al., 2003). Mitochondrial fusion is a unification of two mitochondria through the coordinated action of mitofusins (MFN1 and MFN2) and Optic Atrophy 1 (OPA1), which are members of the dynamin superfamily of GTPases. Mitofusins are situated on the outer mitochondrial membrane (OMM) and are crucial for its fusion, whereas OPA1 mediates fusion of the inner mitochondrial membrane (IMM). As illustrated in Figure 10A, tethering between two mitochondria in close contact by MFN complexes can be followed by fusions of inner and outer mitochondrial membrane coordinated by short isoforms of OPA1 (s-OPA1) bridging of MFN complexes and membrane-bound long isoforms of OPA1 (l-OPA1). Alternatively, IMM fusion can occur as a separate step following OMM fusion.

On contrary, mitochondrial fission is the division of a single mitochondrion into two smaller mitochondria. Fission events are mediated by GTP-hydrolysing enzyme called dynamin-related protein 1 (DRP1), which is recruited to mitochondria by mitochondrial fission factor (MFF), mitochondrial dynamics proteins MiD49 and MiD51 (Pagliuso et al., 2018; Otera et al., 2016; Osellame et al., 2016; Losón et al., 2013). Additionally, mammalian mitochondrial fission 1 protein (FIS1) plays a key role in mitophagy (Rojansky et al., 2016; Shen et al., 2014; Yamano et al., 2014), whereas in yeast FIS1 is substantial for DRP1 recruitment (Bui and Shaw, 2013). Interestingly, sites of mitochondrial fission are dependent on the dynamics of mtDNA (Lewis et al., 2016) and physical interactions between mitochondria and ER or lysosome (Wong et al., 2018; Elgass et al., 2015; Friedman et al., 2011). Mitochondrial fission is illustrated in Figure 10B.

As discussed in Popov (2020), the homeostasis of a healthy cell requires strict regulation of mitochondrial mass and function to adapt to variable energy demand. Mitochondrial biogenesis is a self-regeneration process, in which new mitochondria are created from the existing ones. More specifically, novel proteins are recruited by the existing mitochondria, which are later fragmented by fission (Zhang and Xu, 2016). This process can be enhanced to address high energy demand.

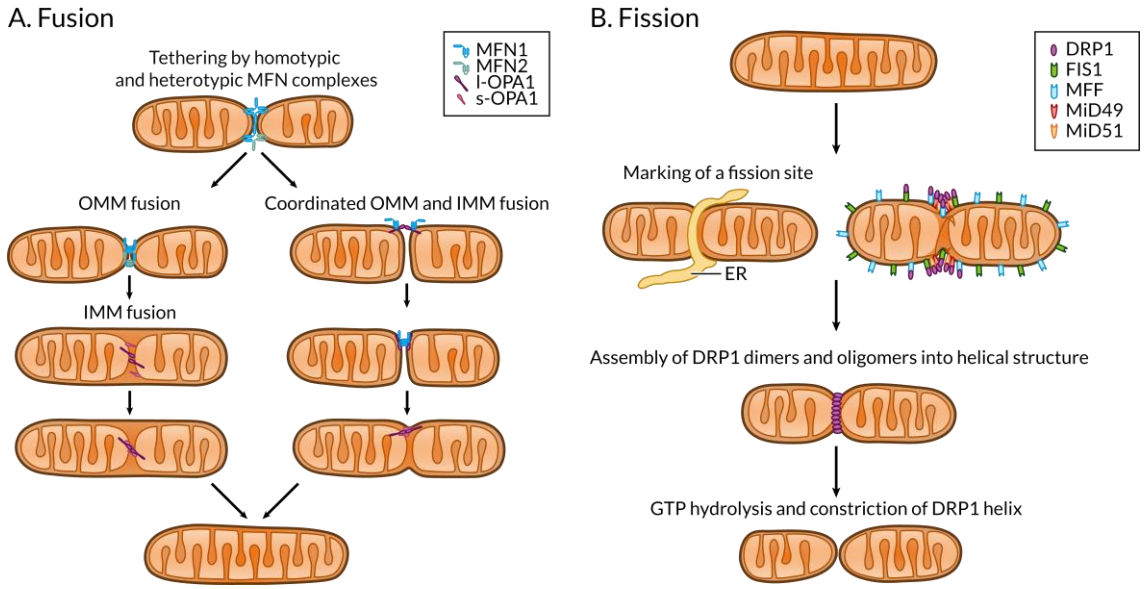

Figure 10. Schematic representation of mitochondrial fusion and fission events. A. Fusion. Initially, two mitochondria in close proximity are tethered by MFN complexes. Then, fusions of OMM and IMM are coordinated by s-OPA1 bridging of MFN complexes and membrane-bound l-OPA1. Otherwise, IMM fusion can take place as a separate step following OMM fusion. B. Fission. Wrapping around mitochondrion by ER tubule is probably the initial step of mitochondrial fission, which is followed by recruitment of DRP1 by MFF, MiD49 and MiD51 at a preconstricted fission site. Then, DRP1 form a helical structure around the marked fission site. Subsequently, DRP1 hydrolyse GTP and divides the OMM and IMM, creating two daughter mitochondria. Adapted from Pernas and Scorrano (2016).

Mitochondrial biogenesis involves coordination between mitochondrial and nuclear genome in a relatively complex procedure. Initially, a family of peroxisome proliferator-activated receptor-gamma coactivator 1 (Pgc1) proteins induce mtDNA transcription. Initiation of the pathway by activation of Pgc1α, the master regulator of mitochondrial biogenesis, is followed by stimulation of a sequence of nuclear transcription factors, namely respiratory factors 1 (Nrf1) and 2 (Nrf2), as well as oestrogen-related receptor. Consequently, expression of the final effector of mtDNA transcription and replication, mitochondrial transcription factor A (Tfam) increases (dos Santos et al., 2018; Cameron et al., 2017; Cameron et al., 2016). Subsequently, particular translation factors facilitate the translation of mtDNA-encoded genes into proteins (Yokokawa et al., 2018). Meanwhile, nuclear-encoded mitochondrial proteins are created from the preproteins, which were synthesized within the cytosol and have an amino-terminal cleavable targeting signal. The signal is targeted toward the mitochondrial matrix, where proteins assemble and are directed toward their exact location.

Selective degradation aimed at removing damaged mitochondria, named mitophagy, is a key mechanism of mitochondrial quality control. Inner mitochondrial membrane depolarization leads to inactivation of OPA1 (Twig et al., 2008; Duvezin-Caubet et al., 2006; Ishihara et al., 2006), which is essential for OxPhos activity. Inactive mitochondria cannot fuse (Mishra et al., 2014), in contrast, they are engulfed by autophagosomes and trafficked to the lysosome for degradation.

1.1.4. Peroxisomes

As comprehensively reviewed in Islinger et al. (2018), peroxisomes play an important role in the metabolism of reactive oxygen/nitrogen species (ROS/RNS), especially hydrogen peroxide, and lipid metabolism. In particular, peroxisomes are involved in the anabolism and catabolism of fatty acids, synthesis of ether lipid, bile and myelin sheath lipids. Moreover, peroxisomes perform vital non-metabolic functions, e.g., in cellular stress responses, antiviral defence and healthy ageing. Similarly to mitochondria and lysosomes, peroxisomes serve as cellular signalling platforms. Peroxisomes are considered to have a protective role, which is essential for human health and plays a part in multiple frequent pathological conditions, including obesity, cancer, neurodegeneration and age-related disorders. Predictably, peroxisomal dysfunction has been associated with grievous metabolic disorders. Moreover, a common characteristic of many peroxisomal inherited disorders is the burdensome neuropathological phenotype.

Peroxisomes are morphologically heterogeneous and functionally flexible organelles, which can specifically adapt to cell type, variable conditions and requirements. As discussed in Sargsyan and Thoms (2019), peroxisomes regularly interact with other organelles, especially ER and mitochondria, but also lipid droplets, lysosomes and autophagosomes to share signals, metabolites and proteins. Thanks to their relatively small size, peroxisomes can easily fit between larger organelles. Vesicular transfer (Farré et al., 2019), soluble lipid-transfer proteins (Wong et al., 2019) and MCS allow for close cooperation of the organelles.

Impressively, more than 90% of peroxisomes are in the vicinity of the ER (Valm et al., 2017). Peroxisomes tightly cooperate with mitochondria in lipid metabolism. For instance, lipid oxidation in peroxisomes necessitates constant replenishment of nicotinamide adenine dinucleotide (NAD^+) and results in the generation of NADH, which is supplied to the mitochondrial respiratory chain (Baumgart et al., 1996). Peroxisomes are also functionally linked to lysosomes by cholesterol transport and metabolism.

1.1.4.1 Peroxisomal dynamics

Similarly to mitochondria, peroxisomes are dynamic organelles, which multiply by fission, i.e., membrane growth and division of existing peroxisomes (Schrader et al., 2016). Furthermore, mitochondria and peroxisomes share proteins of their fission machinery, including aforementioned FIS1 (Koch et al., 2005), MFF (Gandre-Babbe and van der Bliek, 2008) and DRP1 (Li and Gould, 2003; Koch et al., 2003). Sharing division factors is viewed as a popular, evolutionary conserved strategy to reinforce cooperation between mitochondria and peroxisomes to promote a healthy lifespan (Weir et al., 2017; Koch et al., 2016; Schrader et al., 2015). On the other hand, peroxisome-ER tethering is required for peroxisome elongation (Hua et al., 2017; Costello et al., 2017).

An increase in the number of peroxisomes may also result from de novo formation from the ER (Kim, 2017; Smith and Aitchison, 2013). Intriguingly, mitochondria-derived vesicles were recently reported to contribute to peroxisomal biogenesis. Specifically, mitochondria-derived pre-peroxisomal

vesicles containing peroxisomal biogenesis factor 3 (Pex3) fuse with ER-derived vesicles to form mature peroxisomes (Sugiura et al., 2017). Additionally, peroxisomes and mitochondria are connected at the transcriptional level since peroxisome proliferator-activated receptor-gamma coactivator 1 (Pgc1)α regulates both, peroxisomal and mitochondrial biogenesis (Fransen et al., 2017).

Peroxisome biogenesis includes the generation of the peroxisomal membrane, followed by targeting and insertion of peroxisomal membrane proteins (PMP) into the lipid bilayer, and the transfer of proteins into the peroxisomal matrix. Interestingly, peroxisomes have a unique capability to import completely folded and oligomeric or cofactor-bound proteins through a dynamic protein translocon (Dias et al., 2017; Montilla-Martinez et al., 2015; Meinecke et al., 2010). Peroxins (Pex) are crucial biogenesis factors, which establish the import machinery. For instance, Pex5 is a peroxisomal targeting signal receptor, which can function as a stress senor to retain peroxisomal catalase in the cytosol, thereby, contend with oxidative stress of non-peroxisomal origin (Walton et al., 2017). Additionally, Pex11 proteins contribute to the regulation of peroxisome size and number. Similarly to mitochondria, the balance between biogenesis and degradation of peroxisomes by autophagy is critical for the regulation of peroxisome copiousness (Sargsyan and Thoms, 2019).

1.1.5. Endoplasmic reticulum

As neatly summarized in Hetz et al. (2020), ER serves as a calcium reservoir, a facility for protein folding and assembly, as well as a site for lipid and sterol biosynthesis. Importantly, the ER functions as a signalling platform and a key node in the organelle interactome, since it structures a network throughout the cell that maintains numerous MCS (Sargsyan and Thoms, 2019).

The secretory pathway is in charge of the synthesis of one-third of all eukaryotic cell proteins, their post-translational modification and assembly into complexes, followed by their transport to final destinations inside the cell or their release into the extracellular space. Unfolded proteins are translocated from the cytosol into the ER, where they undergo chaperone-assisted folding, i.e., become biologically functional proteins in their native 3D structure. Noteworthy, defective ER protein homeostasis (proteostasis) and aberrant unfolded protein response (UPR) signalling were documented in multiple human diseases, such as neurodegeneration, metabolic diseases and cancer.

1.1.5.1 Endoplasmic reticulum stress

Importantly, protein folding is a particularly error-prone process (Hebert and Molinari, 2007). Intensified protein secretion or impaired protein folding can result in the accumulation of unfolded or misfolded proteins in the ER lumen, i.e., ER stress. UPR is a signalling network responsible for the maintenance of ER functions and proteostasis through gene transcription reprograming, mRNA translation and protein modifications (Balch et al., 2008). Apart from impaired protein folding, UPR integrates a variety of stimuli, such as variable nutrient availability, energy status and redox balance. Moreover, UPR reacts to alterations in cellular growth and differentiation, as well as extracellular responses to hormones, growth factors and small ligands that bind cell surface receptors.

Activated UPR affects almost every facet of the secretory pathway, including the rate of protein synthesis and translocation into the ER, protein folding, quality control and trafficking, as well as elimination of misfolded proteins. Besides ER proteostasis, UPR plays an important role in bioenergetics (Carreras-Sureda et al., 2019; Munoz et al., 2013; Verfaillie et al., 2012), cytoskeletal dynamics (Urra et al., 2018; Ishiwata-Kimata et al., 2013) and DNA damage response (Dufey et al., 2020; Huang et al., 2017). Moreover, UPR components play a role in cell differentiation, metabolism (Kim et al., 2019; Wang et al., 2018; Kim et al., 2017; Zheng et al., 2016), and neuronal plasticity (Saito et al., 2018; Hayashi et al., 2007). Altogether, UPR is a group of signalling pathways that modify dynamically the ER folding capacity to preserve ER proteostasis and maintain cell function under ER stress. Interestingly, UPR plays an important role in the regulation of neuronal physiology and cognition, as well as brain development. Altered ER function was reported in multiple neurodegenerative diseases, e.g., Alzheimer disease, Huntington disease, Parkinson disease and amyotrophic lateral sclerosis (Hetz and Saxena, 2017; Freeman and Mallucci, 2016).

In mammals, the UPR network is composed of three main signalling pathways downstream of ER transmembrane protein sensors: inositol-requiring enzyme 1 (IRE1)α, protein kinase-like endoplasmic reticulum kinase (PERK) and activating transcription factor (ATF) 6 (Kaufman, 2002). ER luminal domains of these proteins recognize unfolded protein peptides and signal through the transcriptional or translational machinery, as well as interactions with signalling molecules. Each UPR sensor can be individually modulated through post-translational modifications or binding to particular factors. Thereby, the level of ER stress required to activate each UPR sensor depends on specific interactomes, which control UPR signalling (Shi et al., 2018; Morita et al., 2017; Pinkaew et al., 2017; Tyagi et al., 2015; Tsukumo et al., 2014; Huber et al., 2013; Rodriguez et al., 2012). Intriguingly, IRE1α and PERK localize to ER-mitochondria contact sites (Carreras-Sureda et al., 2019; Verfaillie et al., 2012). PERK regulates ROS transmission under ER stress and interacts with MFN2 (Munoz et al., 2013), impacting ER-to-mitochondrion tethering.

1.1.5.1.1 Adaptive unfolded protein response

Rapid adaptive response to ER stress is the transient attenuation of protein synthesis. Specifically, phosphorylation of eukaryotic translation initiation factor 2 subunit-α (eIF2α) by PERK precludes the influx of freshly synthesized proteins into the ER (Ron and Walter, 2007). Subsequently, phosphorylated eIF2α induces the translation of specific mRNAs, which contain at least one upstream open reading frame in their 5' untranslated regions (Lu et al., 2004; Vattem and Wek, 2004). For instance, a stress-inducible ATF4 initiates the expression of genes implicated in redox homeostasis, amino acid metabolism and protein synthesis, apoptosis, as well as autophagy. Importantly, ATF4 is a part of a feedback loop that restores protein synthesis by dephosphorylation of eIF2α (Harding et al., 2003; Jousse et al., 2003; Novoa et al., 2001).

Another adaptive response to ER stress is an enhancement of RNase activity of IRE1α by its oligomerization and autophosphorylation (Zhou et al., 2006; Credle et al., 2005). IRE1α deletes small intron to

shift the translational open reading frame in the transcription factor X-box-binding protein 1 (XBP1). Resultant active XBP1 upregulates the expression of genes implicated in ER proteostasis and cell pathophysiology (Kaufman, 2002). Moreover, regulated IRE1-dependent decay (RIDD) enables the reduction of mRNA abundance and protein folding load in the ER as a result. RIDD also adjusts metabolism and inflammation. In this process, IRE1α cleaves a small group of mRNAs or precursor microRNAs, leading to their degradation (Figure 11). Importantly, IRE1α association with adapter proteins enables crosstalk with other stress response pathways, such as macroautophagy and the MAPK pathway (Hetz and Papa, 2018).

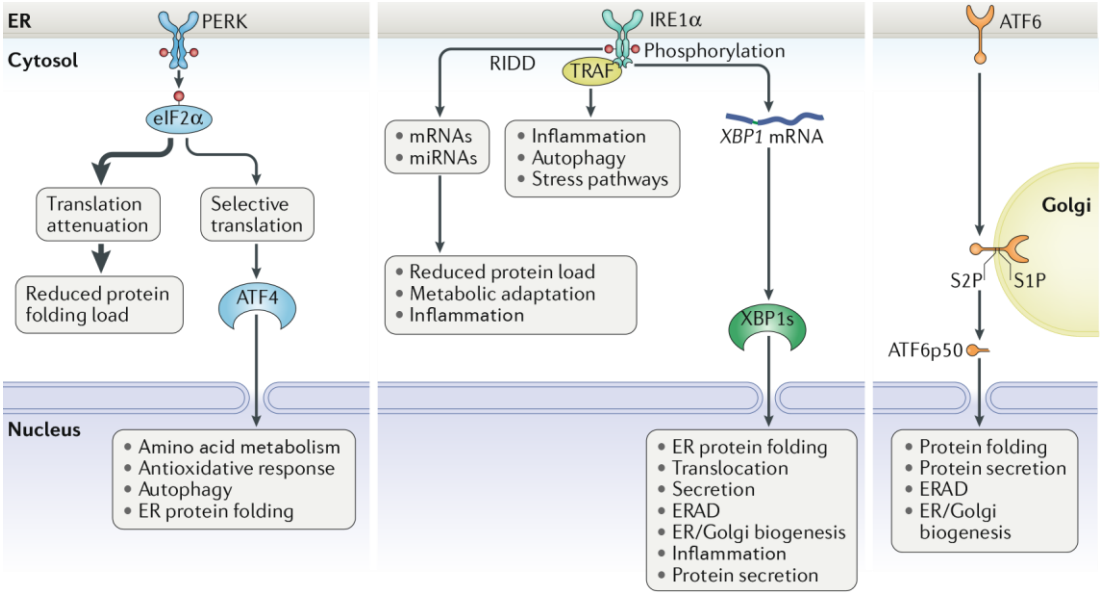

Figure 11. Schematic representation of adaptive unfolded protein response signalling initiated from the ER. It consists of three pathways downstream of ER transmembrane protein sensors: PERK, IRE1α and ATF6. PERK phosphorylates eIF2α to reduce overall protein synthesis and induce selective translation of particular mRNAs, such as ATF4. ATF4 triggers the transcription of UPR target genes, which encode factors implicated in amino acid metabolism, antioxidant defence, autophagy and apoptosis. In parallel, IRE1α splices XBP1 mRNA, which in active form upregulates the expression of genes implicated in ER proteostasis. The IRE1α can recruit adaptor proteins, such as tumour necrosis factor receptor-associated factor (TRAF) family members, to induce inflammatory responses. Moreover, RIDD reduces mRNA abundance and protein folding load in the ER in consequence. Additionally, ATF6 translocates from the ER to the Golgi apparatus, where it is cleaved by S1P and S2P. The resultant active cytosolic ATF6 fragment transits to the nucleus to stimulate transcription of the UPR target genes, which participate in ER proteostasis and cell physiology. Both, IRE1α and ATF6 signalling pathways enhance ER and Golgi biogenesis, as well as ERAD (Hetz et al., 2020).

Furthermore, due to ER stress, full-length ATF6 translocates from the ER to Golgi apparatus, where it is cleaved by site-1 protease (S1P) and site-2 protease (S2P) to release a fragment including a basic leucine zipper transcription factor. The fragment (ATF6p50) subsequently transits to the nucleus to regulate expression of genes encoding ER chaperones and enzymes implicated in ER protein translocation, folding and secretion, but also removal of misfolded proteins through ER-associated protein degradation (ERAD) (Hassler et al., 2015; Shoulders et al., 2013; Wu et al., 2007). The coordinated

action of ATF6p50 and XBP1 also stimulates ER and Golgi biogenesis to improve the secretory capacity of the cell (Bommiasamy et al., 2009; Shaffer et al., 2004). The aforementioned responses to ER stress are considered collectively as adaptive UPR and are illustrated in Figure 11.

Similarly to ATF6, hepatic-specific cAMP-responsive element-binding protein (CREBH) transits from the ER to the Golgi apparatus due to ER stress or inflammatory challenges. It is activated there through regulated intramembrane proteolysis. The resultant CREB transcription factor modulates the expression of key genes encoding metabolic regulators and enzymes (Kim et al., 2019; Kim et al., 2017; Zheng et al., 2016).

1.1.5.1.2 Proapoptotic unfolded protein response

If ER stress overpowers the UPR capacity to maintain proteostasis, the cell enters apoptotic programmes (Ron and Walter, 2007). Predictably, the consequences of ER stress can be different depending on its toxicity and duration (Pedraza and van Oudenaarden, 2005). Irreversible ER damage results in activation of the canonical apoptosis pathway, including activation of proapoptotic Bcl-2 family members at the mitochondria, namely apoptosis regulator (BAX) and Bcl-2 homologous antagonist/killer (BAK), subsequent assembly of apoptosome and activation of caspase 3 (Hetz et al., 2006; Wei et al., 2001). Downstream of PERK, ATF4 and proapoptotic factor CCAAT/enhancer-binding protein homologous protein (CHOP) activate genes encoding translational components to amplify protein synthesis, ROS generation and proteotoxicity, leading to cell death (Han et al., 2013; Marciniak et al., 2004). For instance, CHOP activates the protein phosphatase 1 (PP1) regulatory subunit (GADD34). Subsequently, GADD34 and constitutive repressor of eIF2α phosphorylation (CReP) form complexes with PP1 to dephosphorylate eIF2α and thus restore protein synthesis. Besides GADD34, CHOP modulates Bcl-2-like protein 11 (BIM), phorbol-12-myristate-13-acetate-induced protein 1 (NOXA) and Bcl-2-binding component 3 (PUMA).

Furthermore, continuous RIDD causes a reduction of miRNAs that negatively regulate caspase 2 and thioredoxin-interacting protein (TXNIP). Prolonged IRE1α activity leads therefore to sterile inflammation triggered by interleukin-1β (IL-1β) or NACHT, LRR and pyrin domain-containing 3 (NLRP3) inflammasome activation and consequent cell death (Bronner et al., 2015; Lerner et al., 2012; Upton et al., 2012). Additionally, tumour necrosis factor receptor-associated factor 2 (TRAF2) –JUN N-terminal kinase (JNK) signalling activated by IRE1α, as well as RIDD contribute to caspase 2-dependent, caspase 8-dependent or BAX/BAK-dependent apoptosis (Zhu et al., 2014; Han et al., 2009).

Under sustained ER stress, a key UPR prosurvival mechanism is lacking due to alleviation of XBP1 mRNA splicing, while PERK-CHOP signalling is still present (Lin et al., 2007). Downstream of CHOP and IRE1α, ER stress-induced apoptosis is controlled by death receptor 5 (DR5) and its effector caspase 8 (Lam et al., 2018; Munoz-Pinedo and Lopez-Rivas, 2018). Finally, yet importantly, calcium release from ER contributes to a switch to a proapoptotic response. ER releases calcium via inositol 1,4,5-trisphosphate receptor (IP_3R), which interacts with the BAX inhibitor 1 (BI-1) and protein lifeguard 1 (GRINA). Mitochondrial calcium uptake leads to a cytochrome c release and consequent

apoptosome formation (Rojas-Rivera et al., 2012; Chae et al., 2004). The abovementioned responses to ER stress are considered collectively as proapoptotic UPR and are illustrated in Figure 12.

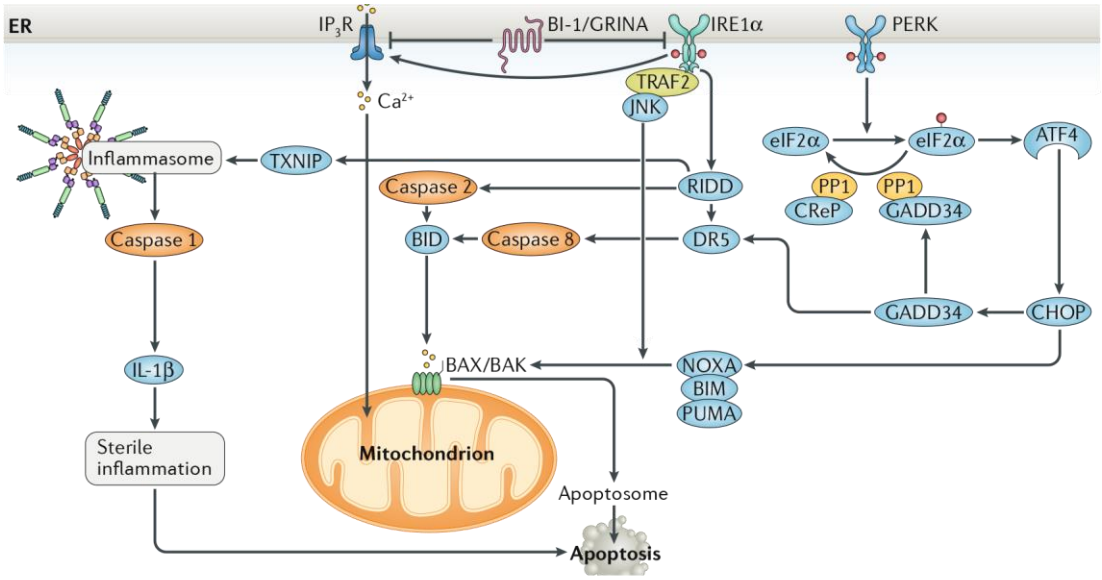

Figure 12. Schematic representation of proapoptotic unfolded protein response signalling initiated from the ER. Due to ER stress, PERK phosphorylates eIF2α to induce selective translation of particular mRNAs, such as ATF4. ATF4, in turn, activates the expression of CHOP and GADD34. GADD34 and CReP form complexes with PP1 to dephosphorylate eIF2α and consequently reinstate mRNA translation. Overall, CHOP regulates GADD34, DR5, as well as NOXA, BIM and PUMA, to promote protein synthesis and worsen protein folding deficiency. In parallel, RIDD and IRE1α-mediated activation of TRAF2–JNK signalling contribute to caspase 2-dependent, caspase 8-dependent or BAX/BAK-dependent apoptosis. Moreover, RIDD modulates TXNIP to activate sterile inflammation, resulting in apoptosis. ER releases calcium via IP3R, which interacts with the BI-1 and GRINA. Mitochondrial calcium uptake leads to reactive oxygen species release and the activation of the BAX/BAK-dependent apoptosome (Hetz et al., 2020).

1.1.5.2 Integrated stress response

As reviewed in Costa-Mattioli and Walter (2020), integrated stress response (ISR) responds to a variety of environmental and pathological changes, such as proteostasis defects, nutrient deprivation, viral infection and oxidative stress, by reprogramming translation to restore homeostasis. The diverse stresses are detected by specialised kinases: protein kinase R (PKR), heme-regulated inhibitor (HRI), general control nonderepressible 2 (GCN2) and already introduced PERK. All the four kinases converge on phosphorylation of eIF2α at serine 51, which effects were described above (1.1.5.1.1). Similarly to UPR, ISR can induce apoptosis if the stress cannot be alleviated. Noteworthy, mutations in essential components of the ISR are associated with intellectual disability (Gregory et al., 2019; Skopkova et al., 2017; Abdulkarim et al., 2015; Borck et al., 2012). Additionally, the ISR is activated in a variety of disorders of the brain (Moon et al., 2018; Smith and Mallucci, 2016; Buffington et al., 2014).

All ISR sensors have conserved kinase domains and different regulatory domains, which allow them to sense disparate signals. Stress stimuli recognized by the regulatory domains induce kinase activation by dimerization and transautophosphorylation (Lavoie et al., 2014). For instance, GCN2 detects, inter alia, amino acid deprivation, oxidative stress and viral infection (Harding et al., 2000). HRI is activated in response to low heme concentrations, cytosolic protein aggregation, oxidative and mitochondrial stress (Guo et al., 2020; Chen, 2014), while PKR activation results from of binding of double-stranded RNA of viral origin (García et al., 2007). As illustrated in Figure 13, PERK is a common sensor of UPR and ISR, which activates due to the accumulation of mis- or unfolded proteins (Wang et al., 2018), as well as alterations in lipid bilayer fluidity (Volmer et al., 2013).

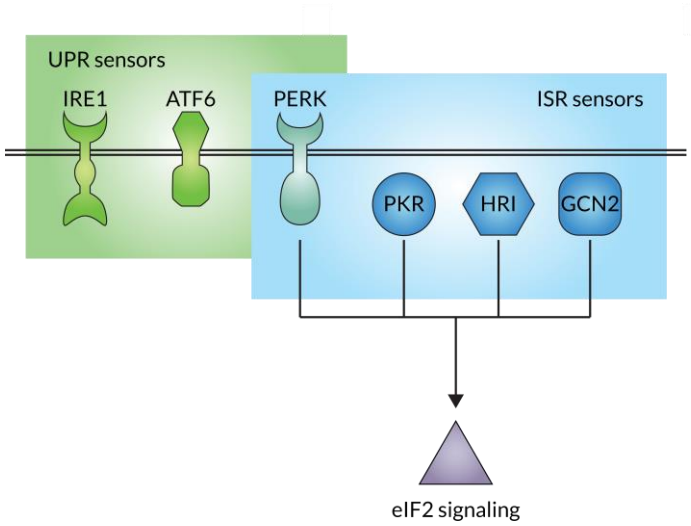

Figure 13. Integrated stress response sensor kinases, PERK, PKR, HRI and GCN2, phosphorylate eIF2α in response to a variety of cellular stresses. PERK is a common kinase of ISR and UPR. Adapted from Costa-Mattioli and Walter (2020).

1.2. Batten disease

Neuronal ceroid lipofuscinoses (NCL) is a group of lysosomal storage diseases that taken together are the most prevalent cause of dementia in children. The incidence of NCL varies from 1:12,500 to 1:100,000 depending on the country (Mole and Haltia, 2015; Augestad and Diderichsen, 2006; Cardona and Rosati, 1995; Claussen et al., 1992). Heretofore, 13 autosomal recessive and one autosomal dominant NCL have been reported (Johnson et al., 2019; Mole et al., 2019; Donsante and Boulis, 2018), while the genetic cause of CLN9 disease remains unknown. Almost 500 mutations in 13 distinct genes were recorded thus far in the *NCL mutation database* (Mole and Cotman, 2015).

NCL have been grouped because of common clinical and pathological characteristics, such as accumulation of autofluorescent storage material, progressive neuron loss and activation of the innate immune system (Cooper et al., 2015). However, the NCL vary considerably in aetiology, age of onset and symptoms. Overall, children with NCL initially present normal development and later regress in motor and language skills. Moreover, many patients exhibit cognitive decline, balance impairments, visual deterioration and epileptic seizures (Mink et al., 2013; Jalanko and Braulke, 2009). The consequences of disease-causing mutations are devastating mainly upon the brain, but can also extend to

peripheral and autonomic nervous systems, as well as somatic tissues (Rietdorf et al., 2020; Katz et al., 2017; Ostergaard et al., 2011; Galvin et al., 2008).

The juvenile NCL, later called Batten disease or CLN3 disease, was first described more than 100 years ago (Stengel, 1826), while the underlying genetic defect was determined over 2 decades ago (International Batten Disease Consortium, 1995). Heretofore, around 80 different mutations in the CLN3 gene were detected in over 420 patients and described in the *NCL mutation database*. The most frequent genetic defect is a genomic deletion of 996bp corresponding to two coding exons 7 and 8, commonly referred to as 1kb deletion or $CLN3^{\Delta ex7/8}$ in the case of animal models (International Batten Disease Consortium, 1995). First disease symptoms are usually observed in children aged 4 to 10 years, including visual impairment due to retinal degeneration, as well as cognitive and motor decline (Kuper et al., 2019; Kuper et al., 2018; Marshall et al., 2005). Seizures and behavioural problems arise along with the disease progression, eventually, patients become wheelchair-bound, bedridden and die prematurely, in their 20s (Ostergaard, 2016; Mole et al., 2011). Besides brain abnormalities, nearly half of patients have alterations in other organs and tissues, including cardio defects (Rietdorf et al., 2020) and skeletal muscle atrophy (Radke et al., 2018). Detailed medical history, high-resolution retinal imaging, microscopy and genetic testing allow for early diagnosis of Batten disease (Wright et al., 2020; Preising et al., 2017). Quantification of lymphocyte vacuolization provides information about CLN3 disease severity (Kuper et al., 2020).

1.2.1. CLN3 gene

Ceroid lipofuscinosis, the neuronal 3 (CLN3) gene, less often referred to as Battenin, is located on the short arm of chromosome 16 at position 12.1 (Järvelä et al., 1995; Mitchison et al., 1995, 1993). The experimental history of a CLN3 gene and protein is reviewed in detail in Mirza et al. (2019). Briefly, the CLN3 gene is highly evolutionary conserved (Mitchell et al., 2001; Katz et al., 1999; Mitchell et al., 1997), ubiquitously expressed (Ding et al., 2011; Eliason et al., 2007) and has 6 transcript variants documented in the NCBI Reference Sequence database (Pruitt et al., 2014; Kent et al., 2002). Regrettably, evidence demonstrating which transcripts are expressed under different conditions is lacking (Zerbino et al., 2018). Interestingly, the human CLN3 gene has 2 different transcription start points with perhaps disparate regulation. The identical full-length human CLN3 protein can be synthesized from two distinct mRNAs transcribed from the same gene using differently regulated promoters. Furthermore, one of the transcripts is probably generated by a particular form of RNA polymerase II containing a minor isoform of the subunit hRPB11 (POLR2J) encoded by the POLR2J2 gene, which was defined as a biomarker for Batten disease (Shematorova and Shpakovski, 2020; Lebrun et al., 2011).

Although the CLN3 gene contains multiple potential transcription regulatory elements (Mitchison et al., 1997), an endogenous promoter of CLN3 has not been exactly defined yet. Several transcription factors were suggested to regulate CLN3 expression pattern by physical binding to the putative promoter region or by indirect interaction through protein partners (Ramirez et al., 2012; Pandey et al., 2011; Bolotin et al., 2010; Abdelmohsen et al., 2009; Boyd et al., 2009; Hollenhorst et al., 2009; Bieda

et al., 2006; Jin et al., 2006). Besides transcription factors, diverse molecules were reported to indirectly regulate the expression of CLN3 (Kim et al., 2013; Bertolotto et al., 2011; Pandey et al., 2011; Nishiyama et al., 2009; Chen et al., 2008). TFEB was demonstrated to bind to the CLEAR motif on the proximal promoter of CLN3, which increases CLN3 transcription (Palmieri et al., 2011; Sardiello et al., 2009).

1.2.2. CLN3 protein

The CLN3 gene encodes a very hydrophobic protein of 438 amino acids. A 3D structure of CLN3 can be only revealed using high-resolution methods, which require a significant amount of properly folded pure CLN3 protein. Since proper biochemical tools are lacking, production or isolation of a sufficient amount of CLN3 is not feasible. The widely accepted secondary structure model is based on experimental data and in silico predictions. It depicts CLN3 as a multi-membrane spanning protein with six transmembrane domains and N- and C-termini facing the cytosol (Ratajczak et al., 2014).

Mapping the mutations causative of Batten disease on the CLN3 topological model demonstrated that most of these mutations, including the most common 1kb deletion, face the luminal side of the intracellular compartments; therefore, luminal regions of CLN3 might be critical for its interaction and function (Cotman and Staropoli, 2012; Gachet et al., 2005; Muzaffar and Pearce, 2008; Kousi et al., 2012; Nugent et al., 2008). The CLN3 protein sequence does not resemble any protein of known function (Muzaffar and Pearce, 2008). Noteworthy, the domain structure of CLN3 is consistent with members of the major facilitator superfamily (MFS), which is a large group of membrane transporters. Interestingly, mutations in MFS domain-containing protein 8 (MFSD8) result in CLN7 disease.

Furthermore, CLN3 has multiple potential post-translational modification motifs, including four N-glycosylation sites, two O-glycosylation sites, as well as consensus sequences for phosphorylation, myristoylation, and farnesylation (Sigrist et al., 2013; Nugent et al., 2008; Storch et al., 2007; Mao et al., 2003; Haskell et al., 2000; Golabek et al., 1999; Kaczmarski et al., 1999; Kida et al., 1999; Järvelä et al., 1998; Michalewski et al., 1999, 1998; Pullarkat and Morris, 1997; Taschner 1997). Indeed, the presence of N-glycosylated forms of CLN3 was confirmed in human cell lines (Järvelä et al., 1998). Noteworthy, CLN3 exhibits tissue-dependent glycosylation patterns (Ezaki et al., 2003). Consequently, the apparent molecular weight of glycosylated CLN3 protein may vary depending on cell type and species (Golabek et al., 1999). Moreover, CLN3 is phosphorylated by cAMP-dependent protein kinases PKA, PKG and casein kinase II, and dephosphorylated by protein phosphatase 1 or protein phosphatase 2A (Michalewski et al., 1999, 1998). Additionally, CLN3 contains a farnesylation site, which is not necessary for its lysosomal localization (Haskell et al., 2000; Pullarkat and Morris, 1997). Nevertheless, the roles of CLN3 phosphorylation and farnesylation require clarification.

1.2.2.1 Localization of CLN3 protein

Data concerning biosynthesis, intracellular localization and trafficking remain discrepant for either wild type, mutant or variant forms of CLN3 protein because of low expression and hydrophobic nature of CLN3, as well as lack of reliable antibody. Analysis of CLN3 protein sequence implies several

putative trafficking and sorting signals; therefore, CLN3 might localize to various organelles, including mitochondria (Janes et al., 1996). CLN3 contains several lysosomal targeting signals and all are necessary for optimal transport efficiency (Kyttälä et al., 2005, 2004; Storch et al., 2004; Kida et al., 1999; Järvelä et al., 1998). Overexpression studies suggest that wild type CLN3 colocalizes mostly with lysosomes, yet signal occasionally overlaps with ER and endosomes (Kyttälä et al., 2004; Luiro et al., 2004; Järvelä et al., 1999, 1998; Girotti and Banting, 1996; Reaves and Banting, 1994). Lysosomal localization of endogenous CLN3 was reported in placental lysosomes, mouse and rat livers (Schröder et al., 2007; Ezaki et al., 2003).

On the other hand, truncated CLN3 protein resulting from 1kb deletion lacks three or four transmembrane domains, the cytosolic loop and C-terminal domain containing the lysosomal sorting motif and farnesylation site (Storch et al., 2007; Kyttälä et al., 2004). It remains unclear if patients with Batten disease can produce a biologically active mutant protein due to contradictory evidence. When some studies imply that partial or complete loss of CLN3 leads to nonsense-mediated decay (Miller et al., 2013; Chan et al., 2008), results of other investigations suggest that at least certain mutations in CLN3 cause retention of the protein in ER, while other mutations do not prevent lysosomal localization (Kyttälä et al., 2004; Haskell et al., 2000; Järvelä et al., 1999, Kida et al., 1999). Another study shows that wildtype CLN3 protein transfers from Golgi to lipid rafts at the plasma membrane via Rab4- and Rab11-positive endosomes, while mutant is mostly retained within the Golgi (Persaud-Sawin et al., 2004).

Although the effects of disease-causing mutations are devastating primarily upon the brain, CLN3 protein is widely expressed in various human tissues. CLN3 gene and protein expression was reported in the nervous and secretory systems, skeletal muscle, gastrointestinal tract, as well as cancer tissues (Persaud-Sawin et al., 2004; Rylova et al., 2002; Chattopadhyay and Pearce, 2000; Margraf et al., 1999). Interestingly, the highest CLN3 expression is attributed to the placenta and leukocyte-associated tissues (Mirza et al., 2019). Focusing on the brain, CLN3 was found in astrocytes and neurons, especially in the grey matter. Generally, the intensity and distribution of the signal are similar in all of the areas of the brain analysed. Noteworthy, peripheral nerves and capillary endothelium also express CLN3 (Persaud-Sawin et al., 2004; Chattopadhyay and Pearce, 2000; Margraf et al., 1999).

1.2.2.2 The function of CLN3 protein and its potential effects on disease mechanism

As thoroughly discussed in Shematorova and Shpakovski (2020), the molecular mechanism of Batten disease is not yet fully understood and many aspects of CLN3 function necessitate elucidation. Various physiological changes are considered to contribute to Batten disease progression, while deficient endosomal-lysosomal system and defective autophagy appear to play a key role.

1.2.2.2.1 Endosomal and lysosomal function

Lysosomes and endosomes are important sites of CLN3 activity. CLN5, which was proven to interact with CLN3 (Lyly et al., 2009; Vesa et al., 2002), controls retromer function by modulating interactions

between CLN3, Ras-related protein Rab-7a (Rab7a), retromer and sortilin. CLN3 serves as a platform for the Rab7a–retromer and retromer–sortilin interactions. CLN3 and CLN5 function as an endosomal complex essential for the efficient endosome-to-TGN trafficking of sortilin. Impaired recycling leads to defective lysosomal function; therefore, these recent findings bring us closer to understanding potential disease mechanism (Yasa et al., 2021; Yasa et al., 2020).

Available literature indicates that endocytosis (Fossale et al., 2004), amino acid transport (Kim et al., 2003), autophagosomal maturation and fusion of endosomes with lysosomes are impaired in CLN3 disease patients cells (Cao et al., 2006). Study of lysosomal proteomes of murine $Cln3^{\Delta ex7/8}$ cerebellar cells demonstrates that common 1kb deletion in CLN3 gene negatively affects abundance and activity of numerous lysosomal proteins, degradation of lipid droplets and composition of membrane lipids, as well as transport efficiency of endocytic cargo receptors (Schmidtke et al., 2019; Sleat et al., 2019).

Moreover, CLN3 was implicated in the regulation of cytoskeletal dynamics due to its interactions with microtubule-binding protein Hook1 and myosin IIB (Getty et al., 2011; Luiro et al., 2004). CLN3 interacts also with the cytoskeletal protein β-fodrin and its interaction partner sodium/potassium-transporting ATPase subunit α1 (ATP1A1). Expectedly, CLN3 defects result in alterations in the fodrin cytoskeleton and subcellular distribution of ATP1A1 (Scifo et al., 2013; Uusi-Rauva et al., 2008). ATP1A1 in turn interacts with Src and regulates its activity in a conformation-dependent manner (Tian et al., 2006). CLN3 mutations lead to impaired endocytosis, which can alter neurotransmitter release, as well as the surface expression of receptors (Luiro et al., 2001) and ion channels in neurons (Chang et al., 2007), resulting in compromised neurotransmission and neuronal cell death.

1.2.2.2.2 The role of microglia and astrocytes

Another key aspect of the Batten disease mechanism is the hyperactivation of glial cells and astrocytes. Microglia are the immune cells within the parenchyma of the central nervous system. They are responsible for the phagocytosis of dead cells and the release of pro-inflammatory mediators. Anomalous neuron-microglia interactions play a part in the pathogenesis of several neurodegenerative diseases, such as Parkinson's and Alzheimer's diseases (Tejera and Heneka, 2019). Activated microglia were also observed in the brains of Batten disease patients, as well as CLN3 KO and $CLN3^{\Delta ex7/8}$ mice (Pontikis et al., 2004, 2005). $CLN3^{\Delta ex7/8}$ microglia are in a pro-inflammatory state and upon stimulation release significantly more mediators, including tumour necrosis factor α, interleukins 1, 1α, 9, and 15. On the other hand, $CLN3^{\Delta ex7/8}$ astrocytes display reduced secretion of various neuroprotective factors, mitogens, chemokines and cytokines, as well as impaired calcium signalling and glutamate clearance. Co-culture with $CLN3^{\Delta ex7/8}$ astrocytes and microglia negatively affected survival and morphology of both wild type and $CLN3^{\Delta ex7/8}$ neurons. Overall, astrocytes and microglia are functionally compromised and may play an active role in neuron loss in Batten disease (Xiong and Kielian, 2013; Lange et al., 2018).

1.2.2.2.3 The endoplasmic reticulum stress response

Based on the similarity of clinical characteristics, NCL proteins are hypothesised to be a part of the same signalling pathway or network, which implies a certain degree of interaction. Besides CLN5, CLN3 interacts with tripeptidyl peptidase I (TPP-1 or CLN2) (Scifo et al., 2013; Persaud-Sawin et al., 2007). Available literature suggests that CLN3 interacts also with transmembrane proteins CLN6 and CLN8, whereas it remains unknown whether the interaction is direct (Scifo et al., 2013; Persaud-Sawin et al., 2007). Interestingly, most CLN5 interactors also interact with CLN3 (Scifo et al., 2013).

Eight NCL proteins can be linked in a single protein network centred on epidermal growth factor receptor (EGFR), which is activated by Src (Shematorova et al., 2018). Their interactions are possible only in ER; therefore these proteins can have also certain ER-associated functions. As previously mentioned, the accumulation of misfolded proteins causes ER stress and perturbs neuronal homeostasis, which is a shared characteristic of many neurodegenerative diseases (Hetz et al., 2020; Marotta et al., 2017). A study of ER stress in SH-SY5Y cells treated with tunicamycin revealed that loss of CLN3 function leads to alterations in the ER stress response and consequent apoptosis. On the contrary, increased CLN3 gene expression resulted in a higher level of ER chaperone BiP and a reduced level of CHOP (Wu et al., 2014). CLN3 was therefore suggested to function as an ER chaperone involved in the folding of glycoproteins and ER stress might significantly contribute to the development of Batten disease.

1.2.2.2.4 Calcium homeostasis

Furthermore, CLN3 can suppress apoptosis through modulating endogenous ceramide synthesis (Puranam et al., 1999), while C2-ceramide promotes the expression of CLN3 (Decraene et al., 2002). Interestingly, a calcium-binding protein, calsenilin interacts with CLN3 ortholog in yeast in a calcium-dependent manner. Although the CLN3-calsenilin interaction was not confirmed in human cells (Seifert et al., 2020; Scifo et al., 2013), CLN3-deficient cells are more sensitive to thapsigargin treatment, which increases cytosolic calcium and induces calcium-mediated apoptosis (Chang et al., 2007). Recent data indicate that CLN3 is involved in Kv4.2/calsenilin somatodendritic A-type channel formation, trafficking, and function in human cells (Seifert et al., 2020). Additionally, autophagosome accumulation in CLN3$^{\Delta ex7/8}$ cells could be reversed by cytosolic calcium chelation. ER, mitochondrial, and lysosomal calcium pools, as well as instore-operated calcium uptake, are altered in CLN3 mutant cells (Chandrachud et al., 2015). Importantly, murine CLN3$^{\Delta ex7/8}$ astrocytes have lower spontaneous calcium oscillations under resting conditions and following exposure to glutamate, pro-inflammatory cytokines or ATP (Bosch and Kielian, 2019; Parviainen et al., 2017). Overall, CLN3-loss-of-function negatively affects calcium homeostasis.

1.2.2.2.5 Mitochondrial function

Consistently with deregulated calcium homeostasis and findings in other LSD, mitochondrial dysfunction and excess ROS are considered to play an important role in Batten disease progression. Several NCL, including CLN3 disease, are characterized by selective loss of inhibitory GABAergic interneurons rich in mitochondria, which are particularly vulnerable to compromised energy

production (Luiro et al., 2006). Moreover, neuron loss is predominantly observed in these brain areas, which are the most metabolically active and rich in mitochondria (cortical layers IV-V) (Braak and Goebel, 1978). Morphological abnormalities of mitochondria, such as elongation and enlargement, were the first mitochondrial defects described in patients cells (Zeman and Donahue, 1963). A lower rate of mitochondrial fatty acid synthesis results in mitochondrial membrane defect reported in intact skin fibroblasts from CLN2 and CLN3 patients (Dawson et al., 1996). Importantly, basal activity of ATP synthase, as well as concentrations of AMP, ADP and ATP are reduced in skin fibroblasts from patients with Batten disease (Das et al., 1999, 2001). Activities of the mitochondrial respiratory chain complexes and mitochondrial oxygen consumption were slightly decreased in mitochondria isolated from murine CLN3 KO brains. Increased expression of glycolytic genes observed in embryonic primary culture of the murine CLN3 KO neurons suggests that glycolysis upregulation serves as a compensatory mechanism for inefficient energy production (Luiro et al., 2006).

As previously mentioned, excess cellular ROS causes damage to proteins, nucleic acids, lipids and organelles, leading to activation of apoptosis if oxidative stress cannot be alleviated. Significantly elevated ROS levels were observed in Batten disease patients fibroblasts (Vidal-Donet et al., 2013). Interestingly, CLN3 in Drosophila melanogaster interacts genetically with critical components of stress signalling pathways, such as JNK, and constituents of stress granules. CLN3 loss of function led to hypersensitivity to oxidative stress, yet not to other physiological stresses. CLN3 mutant flies can recognize oxidative stress correctly, but their ability to react and detoxify ROS is compromised (Tuxworth et al., 2011). Notably, increased generation of intracellular ROS and deregulated redox homeostasis affect several signalling pathways, including PI3K-Akt and MAPK signalling, as well as ubiquitination/proteasome systems (Zhang et al., 2016). Interestingly, screen for genetic interactions with CLN3 ortholog in yeast indicated signalling hub including two major MAPK cascades, which centres on the Tor kinase complexes (Bond et al., 2015). Under starvation, social amoeba Dictyostelium discoideum CLN3 KO cells presented delayed migration and aggregation, as well as upregulation of genes encoding MAPK signalling cascade proteins (Huber and Mathavarajah, 2019; Huber, 2017).

1.2.2.2.6 Osmoregulation and pH homeostasis

Moreover, CLN3 was implicated to play a role in pH homeostasis and osmoregulation. Yeast strains lacking CLN3 ortholog display an increased activity of the plasma membrane hydrogen ATPase because of an aberrantly high vacuolar acidity during the early phase of growth (Padilla-López and Pearce, 2006). In Dictyostelium discoideum, the CLN3 protein is found mainly in the contractile vacuole system, which is a network of tubules that deliver water to the bladders. CLN3 KO cells are susceptible to both hypotonic and hypertensive stress, which eventually negatively impacts their viability and multicellular development (Mathavarajah et al., 2018). Additionally, hypertensive stress resulted in CLN3 gene upregulation in the kidney cells of young hamsters and affected the localization of the protein (Getty et al., 2013). A study in mice indicated a role for CLN3 in renal regulation of

water and/or ionic homeostasis (Stein et al., 2010). Importantly, regulatory volume depletion is impaired in brain endothelial cells derived from CLN3-deficient mice (Tecedor et al., 2013). Hence, defective osmoregulation fails to displace excess water and cell destruction in consequence.

1.2.2.2.7 Storage material in neuronal ceroid lipofuscinoses

As discussed in Palmer (2015), a defining characteristic of NCL is the accumulation of fluorescent, electron-dense, lysosome derived storage material in cells throughout the body. Direct sequencing of storage body proteins determined specific storage of complete and normal subunit c of mitochondrial ATP synthase in CLN2, CLN3, CLN5, CLN6, CLN7 and CLN8 disease models (Haltia, 2006; Tammen et al., 2006; Ezaki et al., 2000; Faust et al., 1994; Fearnley et al., 1990; Palmer et al., 1989, 1992), while sphingolipid activator proteins A and D are main components of storage material in CLN1 and CLN10 disease models (Nosková et al., 2011; Nijssen et al., 2003; Palmer et al., 1997; Tyynelä et al., 1993). Noteworthy, the fluorescence of storage bodies is an aggregate property of non-fluorescent compounds (Palmer et al., 1986, 1993, 2002).

Importantly, the presence of storage material does not correlate with disease-related changes. Storage bodies containing subunit c of mitochondrial ATP synthase accumulate in the majority of cells in most tissues and do not cause organ malfunction or impairment of cellular functions (Palmer et al., 2013; Kay et al., 2011; Oswald et al., 2005). Detected trimethylation of lysine-43 and cleavage of the lead sequence of stored protein implies that the protein has been processed through mitochondria before accumulation in lysosomes, yet has not been subjected to degradation. These observations raised a hypothesis that some CLN proteins may be critical for de-methylation of lysine-43, and therefore turnover of subunit c of mitochondrial ATP synthase. However, evidence for direct interaction between CLN3 and subunit c is lacking (Mirza et al., 2019; Leung et al., 2001). On the other hand, TPP-1 was demonstrated to degrade the stable subunit c in the mitochondrial-lysosomal fractions from cells of a patient with late infantile NCL (Ezaki et al., 2000).

1.2.3. Therapeutic targets for Batten disease studied thus far

As comprehensively reviewed in Specchio et al. (2021), despite decades of committed research and significant developments toward potential treatments for NCL, the only treatment available in the market is enzyme replacement therapy (ERT) for CLN2 disease (Trivisano and Specchio, 2020; Schulz et al., 2018; Markham, 2017). Overall, potential treatments include ERT, gene and stem-cell therapies, as well as pharmacological drugs (Johnson et al., 2019; Sima et al., 2018; Sondhi et al., 2016; Kruer et al., 2013; Selden et al., 2013; Tamaki et al., 2009). These interventions have mostly disease-modifying potential, i.e., they might slow or arrest disease progression. While few of them might partially reverse the disease, complete reversal is doubtful. Even damage-limiting therapies would improve patient's quality of life and reduce the burden on families.

Due to variability in aetiology, age of onset and symptoms, each NCL requires individual clinical management, i.e., many treatments are effective for specific gene defects or enzyme deficit. In general, any therapy would have to be introduced as rapidly as possible, preferably in a presymptomatic

phase, to result in long-term clinical benefits (Trivisano and Specchio, 2020; Fietz et al., 2016). Successful treatment requires therefore an early diagnosis, which could be provided by neonatal screening programs. Recent advancements include optimalisation of mutation-detection methods and enzyme diagnostics, development of animal models and initiation of several novel clinical trials (Rosenberg et al., 2019; Shacka, 2012). Insufficient understanding of natural history and associated biomarkers poses a challenge for the development of adequate medical care besides current palliative treatment (Sleat et al., 2017).

In respect of Batten disease, gene therapy and pharmacological treatments are investigated. Pre-clinical studies of gene therapy have shown at least partial efficacy in cellular and animal models (Burnight et al., 2018; Bosch et al., 2016; Wiley et al., 2016; Sondhi et al., 2014). Moreover, there is an ongoing phase 1/2 clinical trial with patients diagnosed with Batten disease, aged 3 to 10 years. An adeno-associated virus serotype 9 (AAV9) vector carrying a CLN3 gene is delivered intrathecally into the lumbar spinal cord region of children (ClinicalTrials.gov identifier: NCT03770572). The presence of naturally occurring antibodies against AAV and unstable transgene expression still pose a challenge for the gene therapy method.

On the other hand, examined pharmacological treatments use antiapoptotic drugs, TFEB modulators and immunosuppressive agents, as well as medications known for their neuroprotective and anti-inflammatory effects (Hong et al., 2016). For instance, three phosphodiesterase-4 inhibitors significantly ameliorated phenotype in CLN3-KO mice, including improved motor and lysosomal function, reduced neuronal apoptosis and neuroinflammation (Aldrich et al., 2016). The anticonvulsant retigabine saved patient-derived lymphoblasts from accelerated apoptosis and had a neuroprotective impact in CLN3-defective cultured cells (Makoukji et al., 2018). Moreover, oral administration of the Akt inhibitor, trehalose successfully extended lifespan, improved lysosomal storage clearance along with reduction of neuroinflammation and neurodegeneration in a CLN3 mouse model (Palmieri et al., 2017). Treatment involving the immunosuppressant mycophenolate mofetil reduced disease severity and improved motor skills in CLN3-deficient mice (Seehafer et al., 2011); therefore, it was tested in patients with Batten disease to prove good tolerability (Adams et al., 2019; Augustine et al., 2019). Additionally, administration of mycophenolate mofetil in combination with other immunosuppressive medications over 2 years prevented ambulatory vision loss in one of the patients (Drack et al., 2015).

1.3. Aims

Batten disease is the most common neurodegenerative, metabolic disorder of childhood characterized by accumulation of autofluorescent storage material in lysosomes. The malady results from mutations in the CLN3 gene, while its exact mechanism remains unknown (Shematorova and Shpakovski, 2020). The health and proper function of a eukaryotic cell require coordinated function and biogenesis of its organelles. Predictably, the deficiency of a single organelle has an impact on the condition of other compartments because of their strong interdependence (Deus et al., 2019; Sargsyan

and Thoms, 2019). Mitochondrial dysfunction was observed in most of the lysosomal storage diseases and defective mitochondria-lysosome crosstalk was reported in several neurodegenerative disorders (Deus et al., 2019; Raimundo and Krisko, 2019). Hence, we concentrated our efforts on the evaluation of organelle biogenesis and function in a cellular model lacking CLN3 to improve our understanding of the role of organelle crosstalk in Batten disease pathogenesis.

Moreover, we applied an unbiased, multi-dimensional genomics approach to discern signaling pathways and transcriptional regulators that are particularly affected by CLN3-loss-of-function and may play an important role in Batten disease progression. These results were complemented by western blot experiments to determine if CLN3-loss-of-function had an impact on identified signalling pathways also at the protein level. A deeper comprehension of the signaling pathways and transcription factors strongly influenced by CLN3-loss-of-function can aid in finding therapeutic targets that are closer to the origin of the problem.

To achieve above-mentioned the objectives, we generated a cellular model modifying the human embryonic kidney 293 (HEK) cell line with CRISPR/Cas9 technology. Choice of the cell line was inspired by its popularity in the fields of cellular signalling related to lysosomal function and NCL, which enables comparison and perhaps a combination of our data with published and confidentially shared results.

1.3.1. Genome editing with Clustered Regularly Interspaced Short Palindromic Repeats-Cas CRISPR-associated protein 9

Clustered Regularly Interspaced Short Palindromic Repeats-Cas CRISPR-associated protein 9 (CRISPR–Cas9) is a technology that in this project serves as a framework to knockout (KO) CLN3 in HEK cells. Overall, it has a great potential in genome editing and gene therapy for various diseases, not only genetic disorders but also some conditions associated with cancer and infections (Doudna and Charpentier, 2014; Hsu et al., 2014). The inspiration was drawn from adaptive immunity in archaeal and bacterial genomes, which results from the existence of CRISPR–Cas structure that targets foreign mobile genetic elements to eliminate them eventually (Barrangou et al., 2007; Van Der Oost et al., 2014). The Cas9 endonuclease comes from the bacterium Streptococcus pyogenes and is widely used for genome modifications where the guide RNA directs the Cas9 toward the target sites for cleaving based on DNA-RNA hybridization (Sander and Joung, 2014; Barman et al., 2020).

2. Materials and methods

2.1. Materials

2.1.1. Reagents

A variety of chemicals was used throughout this project. They are listed below with their correspondent suppliers and codes (Table 1).

Table 1. List of reagents, their suppliers and catalogue numbers.

Product	Supplier	Code
1 kb DNA Ladder	New England BioLabs	N3232S
100 bp DNA Ladder	New England BioLabs	N3231S
2-deoxy-D-Glucose	Sigma-Aldrich	D8375
2-Mercapthoethanol	Carl Roth	4227.3
4-(2-hydroxyethyl)-1-piperazineethanesulfonic acid (HEPES)	Carl Roth	HN77.2
Acetic acid	Carl Roth	7332.3
Acrylamide solution 40%	AppliChem	A0385
Ammonium Persulfate (APS)	AMRESCO	0486
Antimycin A	Sigma Aldrich	A8674
Biozym LE Agarose	Biozym	840004
Bovine serum albumin (BSA)	Sigma Aldrich	A7906
Bromophenol blue	Carl Roth	T116.1
Carbonyl cyanide-p-trifluoromethoxyphenylhydrazone (FCCP)	Sigma Aldrich	C2920
Coomassie Brilliant Blue G	Carl Roth	9598.2
D-Glucose	Carl Roth	275227941
Dialyzed Fetal Bovine Serum	Gibco	A3382001
Digitonin	Merck	11024-24-1
Dimethyl sulfoxide (DMSO)	Sigma Aldrich	D8418
Dithiothreitol (DTT)	AppliChem	A2948
DMEM - no glucose	Gibco	11966-025

Product	Supplier	Code
DMEM Base 8.3g/L	Sigma Aldrich	D5030-1L
Dulbecco's Modified Eagle Medium (DMEM) - high glucose	Gibco	41965-039
Ethanol 70%	VWR	84858.440
Ethanol Absolut	BD Bioscience	354052
Ethidium bromide	VWR	E406
Ethylenediaminetetraacetic acid (EDTA)	Carl Roth	8043.2
Fetal Bovine Serum Heat Inactivated (FBS)	Gibco	10500-064
Glutamax (100x)	Gibco	35050-061
Glycerol	Carl Roth	7530.1
Glycine	VWR	0167
H_2O Nuclease-free	VWR	E476
Halt™ Protease & Phosphatase single use Inhibitor Cocktail	Thermo Scientific	78442
Methanol	VWR	20903.368
N-dodecylmaltoside	Carl Roth	CN26.2
Oligomycin	Sigma Aldrich	O4876
Opti-MEM I Reduced Serum Medium	Gibco	11058021
PageRuler Plus Prestained Protein Ladder	Thermo Scientific	26619
Penicillin/Streptomycin (P/S)	Gibco	15140-062
phenylmethylsulphonyl fluoride (PMSF)	Sigma	P7626
Phosphate buffered saline (PBS) tablets	Sigma	P44177-100TAB
Potassium chloride (KCl)	Volu-Sol	83608.26
Precision Plus Protein™ standard All Blue	Bio-Rad	1610393
Proteinase K	Amresco	0706
Puromycin 100mg	Fisher Scientific	BP2956-100
Skim Milk Powder	Fluka	70166

Product	Supplier	Code
Sodium azide (NaN_3)	Sigma Aldrich	52002-1006
Sodium chloride (NaCl)	AppliChem	A1430,0010
Sodium dodecyl sulphate (SDS)	Sigma Aldrich	L4509-500G
Sodium Pyruvate	Sigma	S8636
TE Buffer	Macherey-Nagel	740797.1
Tetramethyl ethylenediamine (TEMED)	Sigma Aldrich	T7024
Trehalose	Carl Roth	5151.3
Tris Base	Sigma Aldrich	T1503
Tris-HCl	Carl Roth	9090.2
Triton X 100	Carl Roth	3051.3
TrypLE Express (1X)	Gibco	12605-010
Tween 20	AMRESCO	0777-1L
ε-Amino n-caproic acid	Merck	CAS6032-2

2.1.2. Kits and consumables

The table below presents a list of kits and consumables used to perform experiments described in this thesis, with their correspondent suppliers and codes (Table 2).

Table 2. Kits and consumables.

Product	Supplier	Code
Amersham Hybond PO45 PVDF	GE Healthcare	10600023
BbsI-HF®	New England Biolabs	R3539S
CellTiter-Glo® Luminescent Cell Viability Assay	Promega	G7572
Centrifuge tubes 15ml Corning CentriStar	Corning	430791
Centrifuge tubes 50ml Corning CentriStar	Corning	430829
CRYSTAL RNA Mini Kit	New England Biolabs	31-010-404
Cuvettes PMMA	VWR-International	634-0678
Deoxynucleotide (dNTP) Solution Mix	New England Biolabs	N0447S
DQ™ Red BSA	Life Technologies	D12051

Product	Supplier	Code
FACS Tubes Polystyrene Round-Bottom 5ml	Corning	352052
GoTaq® G2 Flexi DNA Polymerase	Promega	M7801
High-Performance chemiluminescence film	GE Healthcare	28906837
Hoechst 33342 Fluorescent Stain	Thermo Fisher Scientific	62249
iScript cDNA Synthesis Kit	Bio-Rad	170-8891
Lipofectamin 3000 Reagent	Invitrogen	11668-019
Luminata™ Classico Western HRP Substrate	Millipore	WBLUC0500
Luna® Universal qPCR Master Mix	New England Biolabs	M3003
Medical X-Ray Film	Foma	-----
Microseal B seal	Bio-Rad	MSB1001
MitoSOX™ Red Mitochondrial Superoxide Indicator	Thermo Fisher Scientific	M36008
Molecular Probes™ MitoProbe™ JC-1 Assay Kit	Thermo Fisher Scientific	M34152
NucleoSpin Gel and PCR Clean-up	Macherey-Nagel	740609.50
PCR plate 384-well skirted ABI-Type (Universal)	StartLab	E1042-3840
Protein Assay Dye Reagent Concentrate	Bio-Rad	500-0006
Serological Pipette 10ml	StartLab	E4860-1011
Serological Pipette 25ml	StartLab	E4860-2511
Serological Pipette 5ml	StartLab	E4860-0511
T4 DNA Ligase (5U/µl)	Thermo Fisher Scientific	EL0011
Test Tube Soda Glass	VWR International	212-003
Tips 10µl TipOne	StartLab	S1111-3210
Tips 1000µl TipOne	StartLab	S1111-6810
Tips 200µl TipOne	StartLab	S1111-1810
Filter Tips 10µl TipOne	StartLab	S1120-3810
Filter Tips 1000µl TipOne	StartLab	S1126-7710
Filter Tips 200µl TipOne	StartLab	S1120-8710
0.5ml Microcentrifuge Tube	StartLab	E1405-0010

Product	Supplier	Code
1.5ml Crystal Clear Microcentrifuge Tube	StartLab	E1415-1500
2.0ml TubeOne® Microcentrifuge Tubes, Natural	StartLab	S1620-2700
Tubes 15ml opaque sterile Greiner Bio-One	Kisker Biotech	188280
Tubes 8 Twin Strip Start PCR	StartLab	11402-3700
Western Blot Paper	Th. Geyer	4-01-60-0041
XL10-Gold® Ultracompetent Cells	Agilent	200314
XFe 96 extracellular flux assay kit Seahorse	Agilent	102416-100

2.1.3. Cell culture consumables

Besides media, diverse products dedicated to cell culture were needed throughout this project. The list of products with their supplier and code can be found below, in Table 3.

Table 3. Cell culture consumables.

Product	Supplier	Code
100 x 20mm TC dish	CytoOne	CC7682-3394
12-well TC plate	CytoOne	CC7682-7512
150 x 20mm TC dish	CytoOne	CC7682-3617
60 x 20mm TC dish	CytoOne	CC7682-3354
6-well TC plate	CytoOne	CC7682-7506
96-well TC plate	CytoOne	CC7682-7596
96-well TC plate black	Thermo Scientific	137104
Cell scrapper	StartLab	CC7600-0202
Countess cell counting chamber slides	Invitrogen	C10283
Coverslips	Marienfeld	017580
Cryogenic vial 2ml	Fisher Brand	1050026
Trypan Blue 0.4%	Life Technologies	T10282

2.1.4. Buffers and solutions

The table below presents a composition of buffers and solutions used to perform experiments described in this thesis (Table 4).

Table 4. Buffers and solutions.

Buffer / solution	Composition
Anode buffer 10x	500mM Tris-HCl pH 7.0.
Blocking buffer	5% (w/v) Skimmed milk or BSA in TBS-T.
BN-gel buffer 3x	200mM E-Amino n-caproic acid, 150mM Tris-HCl pH 7.0.
BN-loading dye 10x	5% Coomassie blue G, 500mM E-Amino n-caproic acid in 100mM Tris pH 7.0.
Cathode buffer 10x	500mM Tricine pH 7.0, 150mM Tris, 0.2% Coomassie G.
DNA extraction buffer	50mM Tris-HCl pH 8.5, 0.25% SDS, 1mM EDTA and 5mM DTT.
NaN_3	10% NaN_3.
PBS	5 PBS tablets dissolved in 1l of double-distilled water ($_{dd}H_2O$) and autoclaved.
Resolving gel 12%	375mM Tris, pH 8.8, 0.1% SDS, 12% Polyacrylamide, 0.1% APS, 0.04% TEMED.
Running buffer 5x	125mM Tris Base, 0.96M Glycine, 0.5% SDS.
SDS loading buffer	62.5mM Tris, pH 6.8, 50% (v/v) Glycerol, 12% (w/v) SDS, 0.06% (w/v) Bromophenol blue. 5% 2-Mercaptoetanol added freshly prior to use.
Solubilization buffer	1% Digitonin, 20mM Tris-HCl pH 7.4, 0.1mM EDTA pH 8.0, 50mM NaCl, 10% glycerol, 1mM PMSF freshly added.
Stacking gel 5%	62.5mM Tris pH 6.8, 0.1% SDS, 5% Polyacrylamide, 0.1% APS, 0.1% TEMED.
TAE buffer 50x	2mM Tris, 50mM EDTA, 1M Glacial acetic acid pH 8.0.
TBS-T 10x	200mM Tris, 1.5M NaCl, 1% Tween 20, pH 7.4.
TH-buffer	300mM Trehalose, 10mM KCl, 10mM HEPES pH 7.4; 0.2% BSA and 1x protease/phosphatase inhibitor cocktail freshly added before use.
Transfer buffer 10x	250mM Tris, 1.92M Glycine. 1x dilution contains 20% (v/v) Methanol.

Buffer / solution	Composition
Whole cell extraction buffer	1.5% N-dodecylmaltoside in PBS supplemented with fresh 1x protease/phosphatase inhibitor.
XF Seahorse assay media for Cell Mito Stress Test	8.3g DMEM base, 2mM L-Glutamine (Glutamax), 1mM Sodium pyruvate, 1.85g NaCl made up to 1l with ddH_2O; filtered sterile; 20mM D-Glucose freshly added and pH adjusted to 7.4 before use.
XF Seahorse assay media for Glycolysis Stress Test	8.3g DMEM base, 2mM L-Glutamine (Glutamax), 1.85g NaCl made up to 1l with ddH_2O; filtered sterile; pH adjusted to 7.4 before use.

2.1.5. Primers

Sequences of the primers applied in a quantitative polymerase chain reaction (qPCR) in the context of this thesis were obtained with the use of Primer Bank (Harvard Medical School) and ordered from Integrated DNA Technologies. They were diluted to attain a concentration of 100µM according to the supplier's instruction and stored at -20°C. The primers are listed below, in Table 5.

Table 5. List of primers.

Gene	Forward sequence (5'→3')	Reverse sequence (5'→3')
mtDNA	CGAAAGGACAAGAGAAATAAGG	CTGTAAAGTTTTAAGTTTTATGCG
β-globin	CAACTTCATCCACGTTCACC	GAAGAGCCAAGGACAGGTAC
TFEB	ACCTGTCCGAGACCTATGGG	CGTCCAGACGCATAATGTTGTC
LAMP1	CAGATGTGTTAGTGGCACCCA	TTGGAAAGGTACGCCTGGATG
NRF1	AGGAACACGGAGTGACCCAA	TATGCTCGGTGTAAGTAGCCA
NDUFS3	TGTGGCTGAAATCTTGCCCAA	AGTTGAAGCGCAGAGACAACA
COX5a	ATCCAGTCAGTTCGCTGCTAT	CCAGGCATCTATATCTGGCTTG
TFAM	ATGGCGTTTCTCCGAAGCAT	TCCGCCCTATAAGCATCTTGA
CTSC	CGATGTCAACTGCTCGGTTAT	AAGGCAAACCACTTGTAGTCATT
CTSD	ATTCAGGGCGAGTACATGATCC	CGACACCTTGAGCGTGTAG
ATP6V0E1	GTCCTAACCGGGGAGTTATCA	AAAGAGAGGGTTGAGTTGGGC
ATP6V1H	GCTGCTGTCCCCACCAATAT	GCTTCTCTTCAGGGCTTCGT
ATP6V1A	GGGTGCAGCCATGTATGAG	TGCGAAGTACAGGATCTCCAA

Gene	Forward sequence (5'→3')	Reverse sequence (5'→3')
CTSA	TCCCAGCATGAACCTTCAGG	AGTAGGCAAAGTAGACCAGGG
CTSF	AGAGAGGCCCAATCTCCGT	GCATGGTCAATGAGCCAAGG
UQCRC1	GGGGCACAAGTGCTATTGC	GTTGTCCAGCAGGCTAACC
PEX5	AGCAGATTGAGCAGTCAAACTT	TTGGGACCAGTCAGTCTCATT
SDHA	CAGCATGTGTTACCAAGCTGT	GGTGTCGTAGAAATGCCACCT
MITF	GCCTCCAAGCCTCCGATAAG	GCACTCTCTGTTGCATGAACT
12S	GGCGGTGCTTCATATCCCTCT	ACGTGGGTACTTGCGCTTACT
ND1	CAAAGGCCCCAACGTTGTAGG	AGGGTGATGGTAGATGTGGCG
PGC1A	TCTGAGTCTGTATGGAGTGACAT	CCAAGTCGTTCACATCTAGTTCA
CTSB	ACAACGTGGACATGAGCTACT	TCGGTAAACATAACTCTCTGGGG
ATF4	CCCTTCACCTTCTTACAACCTC	TGCCCAGCTCTAAACTAAAGGA
CHOP	GGAAACAGAGTGGTCATTCCC	CTGCTTGAGCCGTTCATTCTC
CAT	TGGAGCTGGTAACCCAGTAGG	CCTTTGCCTTGGAGTATTTGGTA
SOD2	GCTCCGGTTTTGGGGTATCTG	GCGTTGATGTGAGGTTCCAG
NRF2	TTAAACCTGCGGACACTGTTG	GTATCCCAAGGCGTTCTTGTT
HMOX1	AAGACTGCGTTCCTGCTCAAC	AAAGCCCTACAGCAACTGTCG
EDEM1	CGGACGAGTACGAGAAGCG	CGTAGCCAAAGACGAACATGC
XBP1	TGCTGAGTCCGCAGCAGGTG	GCTGGCAGGCTCTGGGGAAG
KLF2	TTCGGTCTCTTCGACGACG	TGCGAACTCTTGGTGTAGGTC
ETV1	TGGCAGTTTTTGGTAGCTCTTC	CGGAGTGAACGGCTAAGTTTATC
CLN1	TGTTTTTGGACTCCCTCGATG	CATGCCAGTATTCGGCTTGC
CLN2	CCTCCACACGGTGCAAAAATG	CTCTGCTTGTCGGATGCTCAG
CLN3	CGCCCACGACATCCTTAGC	AGCAGCCGTAGAGACAGAGTT
CLN4	CTCACGGACGCCACAAAAAG	GTTCACGTTCTCTTCCCCAAA
CLN5	CTGATGGCGCAGGAGGTAG	TTTTGGACGGAAGTCAAAGCG
CLN6	TGCCATGCTGGTATTCCCTC	TGATGACGTTGTAGGCCATGT
CLN7	GCTGGTTGCTCGTGGATTG	ACCTAATGCTTGACACATGCTTA

Gene	Forward sequence (5'→3')	Reverse sequence (5'→3')
CLN8	AATGCCACTTACCGTTCTTTGG	CTGTCGTGATGTGAAACCAGC
CLN11	ATCTTTACCGTCTCAGGGACTT	CCATCGACCATAACACAGCAC
CLN12	AGGGACATCAATAGATCCCCTC	CACGACGTGATAGCCGATGA
CLN14	GAGGGCCGGTACTTCATCG	CATGAGTCCCAGAAACGCTTG
CYCC	AGCAAGTTTCATCGTGTCATCA	TGGAAATGTCTCACCATAGATGC
PEX1	CATGCCGTAGTCAGGATAACTC	TGGTGGTAGTAGACTGCTGTAG
PEX11A	AGCCTTGTCAGGGATCTGTAT	CCACGCTGAACCAAAGAGGA
PEX14	GCCACGGCAGTGAAGTTTCTA	GCTGGAAGGCCATATCAATCTC
PEX12	TTCCTGGCAGCCTACCCAT	TGCTCCAGAGCTTGTATATCCT
PEX10	TCTGCTGGGAGTGCATCAC	CGAAGGTAGATGAGCTTCTGGG
GSTA1	CTGCCCGTATGTCCACCTG	AGCTCCTCGACGTAGTAGAGA
GNPAT	GAGGAGGCATGTCGATGACTT	ACAAAACCGAATGGCTCCAAG
AGPS	TGAGTACCAATGAGTGCAAAGC	GGTAAACCCATGCCACTAAGAG

2.1.6. Antibodies

Several primary and secondary antibodies were used for immunoblotting throughout this project, they are presented in Table 6. Antibodies used after blue native polyacrylamide gel electrophoresis (BN-PAGE) were a kind gift from Prof. Dr Peter Rehling.

Table 6. Primary and secondary antibodies for western blot.

Antibody	Supplier	Catalogue number	Dilution
Goat anti-mouse IgG	Dianova	115-035-146	1:4000
Goat anti-rabbit IgG	Dianova	115-035-144	1:4000
Akt (pan)	CS	4691	1:1000
Akt (Ser473)-P	CS	4060	1:1000
Akt (Thr308)-P	CS	2965	1:1000
CREB	CS	9197	1:1000
CREB (Ser133)-P	CS	9198	1:1000
Drp1	BD Biosciences	611113	1:1000

Drp1 (Ser616)-P	CS	3455	1:1000
Drp1 (Ser637)-P	CS	4867	1:1000
eIF2α	SC	sc-11386	1:1000
eIF2α (Ser51)-P	CS	119A11	1:1000
MFF (Ser146)-P	CS	49281S	1:1000
MFF	Proteintech	17090-1-AP	1:1000
MFN2	Abcam	ab56889	1:1000
NRF1	Abcam	ab175932	1:1000
OXPHOS Cocktail	Abcam	ab110413	1:1000
p70 S6 Kinase	CS	2708	1:1000
p70 S6 Kinase (Thr389)-P	CS	9234	1:1000
PERK	CS	3192	1:1000
PERK (Thr981)-P	SC	SC-32577	1:1000
PEX11B	ab -onli. (assaybi.)	ABIN 485770	1:1000
PEX5	Sigma-Ald.	HPA039259	1:1000
PGC1α	Proteintech	66369	1:1000
S6 Ribosomal Protein (Ser235)-P	CS	4858S	1:2000
S6 Ribosomal Protein	CS	2217	1:2000
TFAM	biomol (ABGENT)	AP10271b	1:1000
Tuberin/TSC2	CS	4308	1:1000
Tuberin/TSC2 (Ser939)-P	CS	3615	1:1000
Tubulin-α	CS	2125	1:5000
YAP	CS	4912	1:500
YAP (Ser127)-P	CS	4911	1:500

2.1.7. Equipment

A variety of devices was needed to perform experiments described in this thesis, their names and manufacturers are listed in Table 7.

Table 7. Equipment.

Device	Manufacturer
Ace Block Digital Dry Bath	Labnet
Amersham ImageQuant 800	Cytiva
Avanti J-20 XPI Centrifuge	Beckman Coulter
CAWOMAT 2000	CAWO
Centrifuge 5415R	Eppendorf
Centrifuge 5424R	Eppendorf
Centrifuge 5810R	Eppendorf
Centrifuge Allegra X-15R	Beckman Coulter
Countess C10281	Invitrogen
Epson Perfection V850 Pro Scanner	Epson
FACS Canto™ II	BD Biosciences
Gene Quant 1300	GE Healthcare
Hood Herasafe	Thermo Scientific
Incubator Heracell 150i	Thermo Scientific
Incubator INE600	Memmert
Innova™ 42 Incubator Shaker	New Brunswick Scientific
Mastercycler Epgradient Thermal Cycler	Eppendorf
Microscope Zeiss Axio Vert A1	Zeiss
MINIPULS 3 Peristaltic Pump	Gilson
Multichannel pipette	Eppendorf Research
NanoDrop™ One^{C} Microvolume UV-Vis Spectrophotometer	Thermo Scientific
Semi-Dry-Elektroblotter Owl™ HEP-1	PEQLAB Biotechnologie
pH meter pH7110	WTW Inolab
Pipette gun accu-jet pro	BRAND

Device	Manufacturer
Pipettes	Eppendorf Research
Potter S (Dounce homogenizer)	Sartorius
Power Pack HC Mini-Protean Tetra System	Bio-Rad
PowerPac Basic Power Supply	Bio-Rad
Precision balance Explorer	OHAUS
Quant Studio 6 Flex	Life Technologies
Revolver wheel	Labnet
SE600 Ruby system	GE Healthcare
Seahorse XFe96 Analyzer	Agilent
Sorvall™ RC 6 Centrifuge	Thermo Scientific
SYNERGYM1 microplate reader	BioTek
Thermocycler UNO II	Biometra
Thermomixer comfort	Eppendorf
Vortex RS-VA10	Phoenix Instrument

2.1.8. Software

The table below presents software that was used for the collection and analysis of the data obtained throughout this project (Table 8).

Table 8. Software.

Software	Company	City/State	Country
Adobe Illustrator	Adobe Systems Inc.	San Jose, CA	USA
CLC Workbench 7	Qiagen	Redwood City, CA	USA
FACS DIVA™ software	BD Biosciences	Heidelberg	Ger-many
FlowJo	FlowJo LLC	Ashland, OR	USA
GraphPad Prism	GraphPad Software Inc.	La Jolla. CA	USA
ImageJ	National Institutes of	Bethesda, MD	USA

Software	Company	City/State	Country
	Health		
IPA Ingenuity	Qiagen	Redwood City, CA	USA
Microsoft Office	Microsoft Corporation	Redmond, WA	USA
QuantStudio™ Real-Time PCR Software	Thermo Fisher Scientific Inc.	Waltham, MA	USA
Seahorse Wave Desktop Software	Agilent	Santa Clara, CA	USA

2.2. Methods

2.2.1. Cell culture

2.2.1.1 Cell lines and culture growth conditions

In the present work, HeLa and human embryonic kidney 293 (HEK) cells were used as experimental models. The HeLa cell line lacking CLN3 and respective WT control was a kind gift from Dr PD Guido Hermey from The Center for Molecular Neurobiology Hamburg (ZMNH) at the University Medical Center Hamburg-Eppendorf (UKE). The HEK cell line was purchased from ATCC (LGC Standards, Middlesex, UK) and modified using CRISPR/Cas9 technology as described later (see 2.2.1.2). The HEK cell line lacking CLN3 and respective WT control were used as a principal experimental model.

All the cell lines were deposited frozen in the liquid nitrogen vapour phase and grown in sterile DMEM high glucose medium complemented with 10% FBS and 1% P/S at 37°C and 5% CO_2. For seeding, cells were washed with sterile 1x PBS (see Table 4) and then incubated with 1 volume of TrypLE Express 1x for 5 minutes at 37°C. Thereafter, 2 volumes of complete growth medium were added to neutralize enzyme activity. A suitable aliquot of the cell suspension was added to new culture flasks or plates. This protocol was followed each time cultures reached 80-90% confluence.

For the purpose of experiments, DMEM high- and no glucose media (see Table 1) were supplemented exactly like a growth medium. Importantly, DMEM high glucose medium contains 4.500g/ml of D-Glucose and 0.580g/ml of L-Glutamine, whereas DMEM no glucose medium comprises 0.584g/ml of L-Glutamine and neither of them is supplemented with sodium pyruvate. Media were changed to high- and no glucose medium the next day after seeding and cells were harvested after another 24 hours at a maximal 80-90% confluence or used for functional assays respectively.

2.2.1.1.1 Cryogenic storage and thawing

With the intention of freezing cells, they were collected by trypsinization as described in the previous section and centrifuged at 1,300xg for 5 minutes. The cell pellet was resuspended in a freezing medium, which was a growth medium complemented with 10% DMSO. Labelled cryotubes containing 1ml aliquots of the cell suspension were placed in Mr Frosty freezing containers previously filled with isopropanol, which were then transferred to a -80°C freezer. On the next day, cryotubes were relocated to a liquid nitrogen tank. The cells were later defrosted in a water bath at 37°C and cultured as described before. Additionally, a quick wash with warm PBS and a change of medium were performed on the following day.

2.2.1.2 CLN3 KO using CRISPR-Cas9

To knock out CLN3 in HEK cells, we used Clustered Regularly Interspaced Short Palindromic Repeats-Cas CRISPR-associated protein 9 (CRISPR–Cas9) technology, which is a popular genome editing tool. Our proceeding is described in detail in the following paragraphs.

2.2.1.2.1 Agarose gel electrophoresis

Suitable mass of agarose was dissolved in 100ml of TAE buffer 1x by boiling in a microwave, then cooled to about 60°C and mixed with 3µl of 10mg/ml ethidium bromide. The solution was immediately poured into a horizontal chamber and allowed to cool to room temperature, to form an agarose gel. Samples were electrophoresed along with a standard DNA marker in the previously made agarose gel submerged in TAE buffer 1x at a steady voltage of 100V. Subsequently, the gel was imaged with a UV documentation system allowing for the determination of the size of visible DNA fragments.

2.2.1.2.2 Restriction digestion of plasmid pSpCas9(BB)-2A-Puro

Plasmid pSpCas9(BB)-2A-Puro (PX459) was a kind gift from Prof. Dr Tiago F. Outeiro. The restriction digestion mixture was composed of 2µl of 10x Cut Smart buffer, 1µl of Enzyme BbsI, 2µg of DNA and $_{dd}H_2O$ added to reach a final volume of 20µl. It was incubated at 37°C for 3 hours, mixed with Gel Loading Dye and loaded onto 0.8% agarose gel as described in the previous section (2.2.1.2.1). The band at 9kb, corresponding to the total size of the plasmid (9175 bp), was cut out from the gel and purified utilising NucleoSpin Gel and PCR Clean-up kit. Briefly, the gel slice was dissolved in Buffer NTI (200µl/100mg of agarose gel) by incubation in Thermomixer at 50°C for a few minutes and vortexing. The sample was then loaded onto PCR Clean-up Column in a 2ml Collection Tube and spun at 11,000xg for 30 seconds to enable DNA binding. The membrane was washed twice with 700µl of Buffer NT3 by centrifugation at 11,000xg for 30 seconds and dried by another centrifugation at 11,000xg for 1 minute. To elute DNA, the Column was placed into a new 1.5ml tube and 20µl of Buffer NE were added. It was then incubated at room temperature for 1 minute and spun at 11,000xg for another minute. DNA concentration was quantified using NanoDrop as described in section 2.2.6.3.

A guide RNA (gRNA) corresponding to the first exon of CLN3 protein was designed in CLC Workbench 7 based on its genomic DNA sequence available on the Ensembl (Yates et al., 2020). Suitable primers, listed in Table 9, were ordered from Integrated DNA Technologies. Annealing mixture was made of 5µl of 10x 3.1 NEB buffer, 2µl of each 10pM Primer and $_{dd}H_2O$ added to reach a final volume of 50µl. It was then incubated in a thermal cycler using the following protocol: initial denaturation at 95°C for 5 minutes and annealing at 95°C gradually decreasing to 25°C at 1°C/min.

Table 9. CLN3 guide RNA primers.

Primer	Sequence 5'→3'
Forward	CACCTGCGATGGGAGGCTGTGCAGGCTCG
Reverse	AAACCGAGCCTGCACAGCCTCCCATCGCA

2.2.1.2.3 Ligation of PX459 with gRNA and bacterial transformation

The ligation mixture was composed of 2µl of 10X T4 DNA Ligase buffer, 1µl of T4 DNA Ligase, 50µg of backbone DNA, 1µl of annealed gRNA reaction mixture and $_{dd}H_2O$ added to reach a final volume of 20µl. It was incubated at room temperature for 2 hours and added to 50µl of E.coli strain, XL10-

Gold ultracompetent cells. Then, it was further incubated on ice for 30 minutes. Next, the mixture was heat-shocked at 42°C for 1 minute and incubated on ice for another 2 minutes. Subsequently, 200µl of S.O.C. medium was added and the mixture was incubated in Thermomixer at 37°C with continuous shaking at 400rpm for 1 hour. The culture was centrifuged at 21,000xg and supernatant was discarded. Then, the pellet was resuspended in the remaining media and 200µl of the culture cells was plated onto LB plates containing ampicillin. The plates were incubated overnight at 37°C.

2.2.1.2.4 Plasmid purification

On the next day, single colonies were picked with a small pipet tip and transferred into a culture tube containing 4ml of prewarmed to room temperature LB Medium with ampicillin. Then, they were incubated overnight in an Incubator Shaker at 250rpm and 37°C. Day after, 250ml of LB medium and 1ml of mini culture were added to each 500ml flask and incubated overnight in an Incubator Shaker at 250rpm and 37°C. Subsequently, plasmids were purified with NucleoBond Xtra Midi EF Kit according to the supplier's instructions. More specifically, the midi culture was spun in a big centrifuge tube at 5,500xg, 4°C for 15 minutes. The pellet was then resuspended in 8ml of RES-EF and transferred into a fresh centrifuge tube, where 8ml of Lys-EF were added to initiate cell lysis. The sample was mixed and incubated at room temperature for 5 minutes. Thereafter, 8ml of NEU-EF was added to each sample, which was mixed until it turned colourless and incubated on ice for 5 minutes. The tubes were centrifuged at 14,500xg, 4°C for 20 minutes. Following equilibration of the column and filter with 15ml of EQU-EF, the supernatant was passed through them and they were washed with 5ml of FIL-EF. The filters were later discarded and each column was washed with 35ml of Endo-EF and 15ml of WASH-EF, consecutively. The plasmid DNA was eluted in 5ml of prewarmed to 50°C ELU-EF and collected in a 50ml centrifuge tube. Then, 3.5ml of isopropanol was added to each elution tube, which was vortexed and spun at 3,500xg, 4°C for 30 minutes. Afterwards, the supernatant was discarded with caution and the pellet was washed with 2ml of 70% endotoxin-free ethanol by centrifugation at 3,500xg, 4°C for 20 minutes. Following removal of the supernatant (ethanol), the pellet was dried in the incubator at 37.5°C for 1 hour. Finally, the DNA was reconstituted in 300µl of pre-warmed H2O-EF by shaking and 15 minutes long incubation, then transferred to an Eppendorf tube. DNA concentration was quantified using NanoDrop as described later (see 2.2.6.3). Plasmids were stored in a freezer at -20°C.

2.2.1.2.5 Transfection and selection of clonal populations

For the purpose of CLN3 KO in HEK cells, alongside a 10cm cell culture plate needed for transfection, natural puromycin resistance control and wild type (WT) control plates were grown. Transfection was performed using Lipofectamine 3000 according to the supplier's instructions. Briefly, mastermix A made of 500µl of Opti-MEM and 30µl of Lipofectamine 3000 Reagent was combined with mastermix B composed of 500µl of Opti-MEM, 15µg of DNA (plasmid) and 22.5µl of P3000 Reagent and incubated at room temperature for 15 minutes. Then the mixture was added to the plate and well mixed with the medium by shaking. After 48 hours the media in transfected and natural puromycin resistance control plates were changed to a growth medium with 2µg/ml of puromycin added to start

antibiotic selection. Selection media were changed every 2-3 days until all WT cells in the control plate were dead as determined by observation under the microscope. Single-cell colonies were obtained by flow cytometry at the Core Facility Cell-Sorting of the University Medical Center Göttingen. More specifically, single alive cells present in cell suspension were arranged in a 96-well plate with fresh DMEM high glucose enriched in additional FBS (20%). The resulting colonies were subsequently cultured in plates with a bigger surface area until collection of sufficient material for storage in the liquid nitrogen vapour phase and DNA isolation was possible.

2.2.1.2.6 DNA Sequencing

With the aim of DNA isolation, the cell pellet of each clone was resuspended in 100µl of TE buffer with 0.1% of Triton x100 and boiled at 100°C for 5 minutes. Then, it was centrifuged at 13,000xg for 10 minutes. The containing DNA supernatant was placed in a new tube, either used immediately or stored at -20°C. DNA concentration was quantified using NanoDrop as described in section 2.2.6.3.

Following DNA isolation, DNA was amplified using the GoTaq Flexi DNA polymerase kit according to the manufacturer's protocol. Briefly, each 25µl reaction was made of 5µl of 5X reaction buffer, 2µl of 25mM $MgCl_2$, 0.5µl of 10mM dNTPs, 1µl of each 10µM primer (Table 10), 0.25µl of 5U/µl Taq polymerase, 12µl of nuclease-free water and 2-3µl of DNA template (ca. 500ng). Nested reverse primers were utilized to obtain higher specificity through subsequent rounds of PCR. The following thermal cycling protocol was used for DNA amplification: initial denaturation at 95°C for 5 minutes, 35 cycles of denaturation at 95°C for 30 seconds, annealing at 69°C for 40 seconds and extension at 72°C for 1 minute, followed by 10 minutes of final extension at 72°C. The reaction was then held at 4°C indefinitely.

Table 10. Sequencing primers.

Reaction	Primer	Sequence 5'→3'
1st	Forward	GCT GTC ACG TGA TCC GAC AAA CGG C
1st	Reverse 1	CCA GGC TGC AGG GAG CTG TGA TTG C
2nd	Reverse 2	TCG CTG AAG TCT CAG GCC ACT CAC C
3rd	Reverse 3	CTA CTC TCA GGT GCA CGA CCG CTC C

25µl of final amplicon were electrophoresed in the 1.2% agarose gel as described in section 2.2.1.2.1. The corresponding bands (around 500bp) were cut out and DNA was extracted with NucleoSpin Gel and PCR Clean-up kit like before (see 2.2.1.2.2). DNA concentration was quantified using Nanodrop as described in section 2.2.6.3. Finally, 12µl of diluted DNA (ca. 80ng/µl) were mixed with 3µl of forward Primer and sent to Microsynth SEQLAB for single-tube sequencing. Obtained results were interpreted in CLC Workbench 7 to confirm deletion in CLN3 DNA sequence consistent with design

(Figure 14) and presence of STOP codons in all 3 potential forward translations (Figure 15). Clone C1.6 was selected for further experiments along with other clones with confirmed deletion.

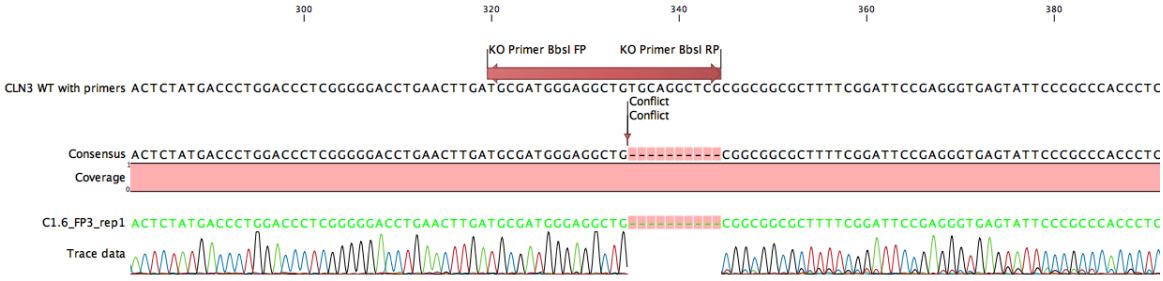

Figure 14. Deletion in CLN3 DNA sequence in of the clone C1.6.

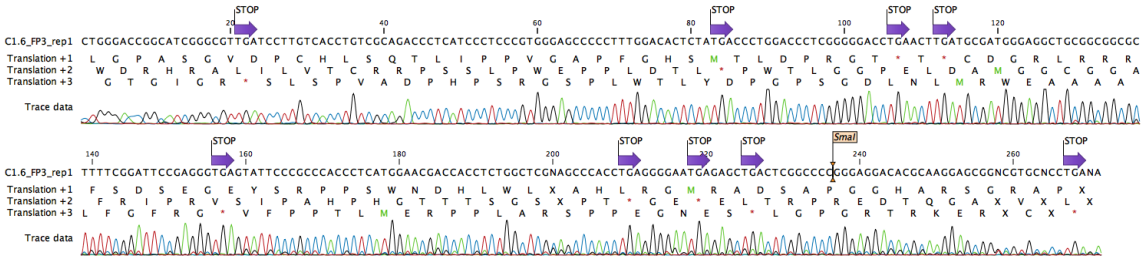

Figure 15. Multiple STOP codons are present in all possible forward translations.

2.2.2. Material harvesting

2.2.2.1 Cells harvesting

To extract RNA, DNA or protein, adherent cells were harvested on ice by aspirating the medium and rinsed with ice-cold PBS 1x. Then, cells were scraped on ice with ice-cold PBS 1x, and the cell suspension was collected and pelleted at 1,300xg, 4°C for 5 minutes. The cell pellet was usually immediately used for the required technique or frozen in liquid nitrogen and stored at -80°C for later use. Material for flow cytometry was collected differently to minimize debris content. Cells were trypsinised as described before (2.2.1.1) and enzyme activity was inhibited by adding twice the volume of prewarmed to 37°C PBS 1x. Then, the cell suspension was collected and centrifuged at 1,300xg for 5 minutes. The supernatant was discarded, and the cell pellet was resuspended in ice-cold PBS 1x.

2.2.3. Biochemical procedures

2.2.3.1 Preparation of whole cell lysates

With the aim of cell lysis, the aforementioned cell pellets were resuspended on ice in about 200-500µl of the whole cell extraction buffer (prepared as described in Table 4), depending on pellet size. Subsequently, the cell suspension was lysed by rotation at 4°C for 30 minutes and centrifuged for 20 minutes at 16,000xg. The supernatant, which is whole cell lysate, was collected and placed in a new tube. The protein concentration was quantified using Bradford Assay as described later (see 2.2.3.3). The lysates were either used for experiments or stored frozen at -20°C.

2.2.3.2 Mitochondria isolation

With the objective to isolate mitochondria, cells were collected as described before (2.2.2.1). Each cell pellet was resuspended in 4ml of TH-buffer with 0.1% BSA and 1x protease/phosphatase inhibitor freshly added and transferred into a pre-chilled 5ml Dounce homogenizer on ice. The sample was then potted on ice for 30 strokes and transferred into 2ml Eppendorf tubes to spin it down at 400xg, 4°C for 10 minutes. The supernatant was placed in fresh 1.5ml Eppendorf tubes and the pellet was handled exactly like a cell pellet before. Afterwards, the freshly obtained supernatant was also transferred into 1.5ml Eppendorf tubes and the pellet was discarded. The tubes were spun down at 800xg, 4°C for 5 minutes to remove the debris. The supernatant was placed into a fresh 1.5ml Eppendorf tube and spun at 10,000xg, 4°C for 10 minutes. Subsequently, the supernatant was discarded, and the pellets (isolated mitochondria) were combined in 300µl of TH-buffer without BSA. The tubes were washed with an additional 300µl of TH-buffer to remove BSA from the sample and spun down at 10,000xg, 4°C for 5 minutes. One more time, the supernatant was discarded, and the pellet was resuspended in 200-500µl of TH-buffer without BSA, depending on pellet size. The mitochondrial protein concentration was determined using the Bradford assay as described below. Purified mitochondria were used immediately for sample preparation and aliquoted, snap-frozen in liquid nitrogen and stored at -80°C.

2.2.3.3 Protein concentration determination using Bradford assay

Protein Assay Dye Reagent Concentrate was applied accordingly manufacturer's protocol to verify protein concentration. Specifically, 800µl of $_{dd}H_2O$, 1µl of sample or standard and 200µl of mentioned dye were mixed in a glass tube and vortexed briefly. Then, the tubes were incubated in the dark, at room temperature for 5 minutes and transferred into plastic cuvettes. The binding of the dye to protein triggers a shift in its absorption maximum from 465 to 595nm (Bradford, 1976), the latter was measured by GeneQuant 1300 spectrophotometer. The protein concentration of the cell lysates was estimated based on the standard calibration curve.

2.2.3.4 Sodium dodecyl sulfate-polyacrylamide gel electrophoresis

Sodium dodecyl sulfate-polyacrylamide gel electrophoresis (SDS-PAGE) was completed to separate complex mixtures of proteins, which is the first step in immunoblotting (Gallagher, 2012). Proteins migrate within a gel in response to an electrical field with a rate dependent on gel pore size and protein charge, size, and shape. Polyacrylamide gels were formed by copolymerization between acrylamide and bis-acrylamide initiated by the addition of APS and catalysed by TEMED. One can find a more detailed description in Table 4. Gels were stored in Running Buffer 1x at 4°C for later use, not longer than few days. Following protein quantification, the same amount of protein from cell lysates was diluted in the proper volume of $_{dd}H_2O$ and mixed with a 6x SDS loading buffer to reach equal final volume and protein concentration. Samples were usually boiled at 95°C for 5 minutes and loaded on a discontinuous vertical polyacrylamide gel electrophoresis system (Bio-Rad).

The Mini Protean Tetra System (Bio-Rad) was filled with 1x running buffer and connected to a PowerPac Basic Power Supply (Bio-Rad) outputting an initial constant voltage of 90V and increased to 160V when samples were in the resolving gel. Electrophoresis was complete when the front of the run reached the bottom end of the gel. A molecular weight standard, PageRuler plus Prestained ladder, was loaded in every gel to enable molecular weight estimation.

2.2.3.4.1 SDS-PAGE: Immunoblotting

Subsequently, proteins were transferred onto a membrane by electroblotting following the widely accepted protocol described in detail by Gallagher et al., (2008). Briefly, polyvinylidene fluoride (PVDF) membranes were pre-activated by submersion in methanol for 1 minute, wash with $_{dd}H_2O$ for another minute and equilibration in transfer buffer 1x for at least 5 minutes. Then, the gel was shortly washed in previously cooled transfer buffer and laid on a membrane in the so-called 'immunoblot sandwich'. In other words, a membrane with gel was covered by filter paper and wet sponges on both sides and pressed together by a gel holder cassette. Each cassette was then inserted into the transfer apparatus in a tank filled with still cold transfer buffer, in the correct orientation towards electrodes. Moreover, a cooling unit was placed in the tank to further reduce the heating of the transfer buffer. Protein transfer was completed at a constant voltage of 100V for 90 minutes.

Afterwards, to prevent non-specific binding, the membranes were submerged in blocking buffer and gently shaken at room temperature for 1 hour. The membranes were washed three times with TBS-T 1x for 10 minutes, cut and incubated in primary antibodies, diluted in blocking buffer, at 4°C overnight. On the following day, membranes were washed with TBS-T 1x three times for 10 minutes and incubated with corresponding HRP-conjugated secondary antibody, also diluted in blocking buffer, at room temperature for 1 hour and washed again exactly like before. The membranes were then drained to remove excess TBS-T and incubated in Luminata Western HRP substrate for 3 minutes. Chemiluminescent signals were captured on medical X-ray films, which were in turn developed in the AGFA Curix 60 processor. The films were later digitalized with the Epson Perfection V850 Pro Scanner for image processing. Band density was quantified using ImageJ after subtraction of background and normalized against loading controls (α-Tubulin).

2.2.3.5 Blue native polyacrylamide gel electrophoresis

With the intention to examine mitochondrial complex assembly in cells lacking CLN3, blue native polyacrylamide gel electrophoresis (BN-PAGE) was performed. Contrary to SDS-PAGE, it resolves non-denatured mitochondrial proteins, hence, their physiological interactions with other proteins are preserved (Schägger, 2001).

2.2.3.5.1 BN-PAGE: sample preparation

To prepare samples for BN-PAGE, 300µg of previously isolated mitochondria were centrifuged at 10,000xg, 4°C for 5 minutes. The supernatant was then discarded and each pellet was resuspended in 500µl of Solubilization buffer, prepared as described in Table 4. The samples were pipetted up and

down several times to ensure thorough solubilization, incubated on ice for 20 minutes while vortexing every 5 minutes. Subsequently, they were spun at 20,000xg for 10 minutes and 50µl of BN-loading dye was added to each. Finally, they were incubated on ice for 5 minutes and spun at 20,000xg, 4°C for 5 minutes.

2.2.3.5.2 BN-PAGE: casting gels and electrophoresis

Mitochondrial protein complexes were separated by BN-PAGE following the protocol described in Dekker et al., (1997). More specifically, the gels were cast the day before and stored at 4°C overnight. Resolving gels were made from equal volumes of 4% and 14% acrylamide in 1x BN-gel buffer (see Table 4) supplemented with 0.44% APS and TEMED, employing a gradient gel maker with pump. The stacking gel was composed of 4% acrylamide solution in 1x BN-gel buffer, 0.08% APS and 0.133% TEMED.

Previously prepared samples were loaded in the gels and overlaid with the cathode buffer with caution along with a molecular weight standard, Precision Plus Protein™ standard All Blue, to enable molecular weight estimation. Then, the gel was run in a cooled gel chamber at 600V, 15mA for 1 hour and later at 90V, 15mA overnight at 4°C using the SE600 Ruby system. The cathode buffer was replaced with the anode buffer after an initial 1-hour run. Electrophoresis was completed when the front of the run reached the bottom end of the gel.

2.2.3.5.3 BN-PAGE: immunoblotting

Thereafter, proteins were transferred onto a PVDF membrane by semi-dry electroblotting as described by Gravel (2009). Initially, the gel was incubated in a Running buffer (see Table 4) for 30 minutes. In contrast to wet blotting, the gel and membrane were placed between buffer-wetted filter papers, which were in direct contact with two closely spaced horizontal solid-plate electrodes of Semi-Dry-Elektroblotter Owl™ HEP-1. The gel was blotted at 25V, 400mA for 3 hours. Later proceeding was identical with SDS-PAGE described previously (2.2.3.4.1). Chemiluminescent signals were detected and documented by Amersham ImageQuant 800 system.

2.2.4. Microplate reader assays

2.2.4.1 Proteolytic activity

Lysosomal proteolytic capacity was determined by the Molecular Probes' DQ Red BSA assay according to the manufacturer's recommendation. More specifically, 1mg of dye was resuspended in 1ml of sterile PBS 1x, aliquoted and stored frozen at -20°C, protected from light for later use. The intermediate stock was diluted in a warm experimental medium to a working concentration of 10µg/ml. Medium in an opaque-walled, clear bottom 96 well-plate with cultured cells was changed to 100µl of the dye-containing medium per well and incubated at 37°C for 1 hour. Then, they were washed twice with warm sterile PBS 1x and supplied with 100µl of warm EBSS medium per well. DQ Red BSA is a derivative of bovine serum albumin (BSA) labelled with BODIPY TR-X dye to an extent, that the dye is strongly selfquenched. Proteolysis of the BSA results in dequenching and brightly fluorescent protein fragments. The kinetics of DQ Red BSA digestion was measured at excitation and emission

maxima of 590nm and 620nm respectively in a microplate reader every 5 minutes for 4 hours. Control wells containing medium without cells were used to obtain a value for background fluorescence. The results were exported as a Microsoft Excel file for the analysis.

2.2.4.2 Real-Time Cell Metabolic Analysis

In order to evaluate the impact of CLN3 KO on cell metabolism, the XFe 96 extracellular flux assay kit was used following the manufacturer's protocols. Briefly, cells were seeded in the XF96 cell culture plate in 100µl of growth medium. Wells in the corner of the plate were left empty to later obtain a value for the background signal. On the same day, the XFe 96 sensor cartridge plate was filled with 200µl of XF calibrant per well and hydrated in a non-CO_2 incubator at 37°C overnight. On the following day, the cultured cells were washed with PBS 1x and 160µl of warm XF Seahorse assay media, prepared as described in Table 4, were added to each well. The plate was incubated at 37°C for 1 hour without CO_2. Meanwhile, the sensor cartridge was loaded in the indicated ports with the compounds diluted in warm XF Seahorse assay media. Following modulators were applied in XF Cell Mito Stress Test: 10µM Oligomycin (20µl per well injected from Port A), 20µM FCCP (22µl per well injected from Port B) and 10µM each of Rotenone and Antimycin (25µl per well injected from Port C). Correspondingly, 90mM D-Glucose, 10µM Oligomycin and 550mM 2-deoxy-D-Glucose were used in XF Glycolysis Stress Test. Afterwards, the sensor cartridge plate was calibrated in the Seahorse XFe96 Analyzer. Once the calibration was completed, the XF96 cell culture plate was placed into the instrument at 37°C and the corresponding test was run using XFe96 Analyzer software. Concentrations of dissolved oxygen and free protons were measured every few seconds for few minutes to calculate the oxygen consumption rate (OCR) and extracellular acidification rate (ECAR), respectively. This step was repeated 4 times for each modulator. The results were exported as an XFD file for the analysis in Seahorse Wave Desktop Software.

2.2.4.3 Cell viability

With the objective to assess cell viability, CellTiter-Glo® Luminescent Cell Viability Assay was applied following the manufacturer's protocol. The assay system uses mono-oxygenation of luciferin catalysed by luciferase to generate a luminescent signal proportional to the amount of ATP present, which is, in turn, proportional to the number of metabolically active cells (Crouch et al., 1993). The CellTiter-Glo® Buffer and Substrate were both equilibrated to room temperature. Then, the CellTiter-Glo® Substrate was reconstituted in the CellTiter-Glo® Buffer in its amber bottle and mixed by vortexing to obtain a homogeneous solution. The CellTiter-Glo® Reagent was aliquoted, stored frozen at -20°C and protected from light for later use. An opaque-walled, clear bottom 96 well-plate containing cells cultured for the experiment was equilibrated at room temperature for approximately 30 minutes. Subsequently, 50µl of CellTiter-Glo® Reagent were added to 50µl of medium present in each well. The plate was immediately placed in a microplate reader and shaken orbitally for 2 minutes to induce cell lysis, followed by incubation at room temperature for 10 minutes and recording. Control wells containing medium without cells were utilized to register a value for background luminescence. The results were exported as a Microsoft Excel file for the analysis.

2.2.4.4 DNA staining

For normalization, DNA concentration per well was quantified using Hoechst 33342 following the manufacturer's suggestion in each microplate reader experiment. Hoechst dyes are bisbenzimide dyes excited by UV light and emitting blue fluorescence, which increases greatly upon DNA binding (Bucevičius et al., 2018). Briefly, the initial stock was diluted in sterile PBS 1x to a concentration of 1mg/ml and stored at -20°C for later use. The intermediate stock solution was diluted in assay media to a working concentration of 1µg/ml. Cells cultured for the experiment were loaded with a suitable volume of the dye-containing medium and incubated at 37°C for 10 minutes. Then, the blue fluorescence of Hoechst 33342 was recorded at respective excitation and emission maxima of 361nm and 486nm in a microplate reader, followed by the desired experiment. The results were exported as a Microsoft Excel file. Importantly, in each microplate reader experiment control wells containing medium without cells were used to obtain a value for background signal.

2.2.5. Flow cytometry

2.2.5.1 Measurement of mitochondrial superoxide levels

To further characterize mitochondrial function, mitochondrial superoxide levels were determined by flow cytometry using the MitoSOX™ Red Mitochondrial Superoxide Indicator according to the manufacturer's recommendation. In principle, oxidation of MitoSOX™ by superoxide in mitochondria results in red fluorescence (Puleston, 2015). Each required 50µg MitoSOX vial was resuspended in 13µl of DMSO to obtain fresh 5mM stock concentration. Then, the dye was diluted to the working concentration of 5µM in prewarmed to 37°C experimental medium. The cells, cultured as described before (2.2.1.1), were washed with PBS 1x and incubated in the corresponding MitoSOX working solution at 37°C for 15 minutes.

Following staining, cells were washed with warm PBS 1x and harvested by trypsinization as described earlier (2.2.2.1), including unstained native fluorescence control. The cell pellet was resuspended in 500-1000µl of PBS 1x supplemented with 0.5µM of glucose, depending on pellet size. Subsequently, the cell suspension was transferred to FACS tubes and mitochondrial superoxide levels were assessed by flow cytometry. Cells incubated with 100µM Antimycin A at 37°C for 20 minutes were used as a positive control. The results were analysed using Microsoft Excel and FlowJo software.

2.2.5.2 Mitochondrial membrane potential

Similarly, mitochondrial membrane potential was evaluated by flow cytometry using Mito-Probe™ JC-1 Assay Kit according to the manufacturer's instructions. The assay uses a potential-dependent accumulation of JC-1 dye in mitochondria to monitor membrane potential. The monomeric form of the probe emits green fluorescence, which shifts to red due to the concentration-dependent formation of red fluorescent aggregates (Chazotte, 2011). Specifically, 5mM JC-1 stock was prepared in DMSO and diluted to a working concentration of 20µM in prewarmed to 37°C experimental medium. The cultured cells were washed with warm PBS 1x and incubated in JC-1 working solution at 37°C for 20 minutes. Unstained cells and cells treated with 75µM of FCCP for 3 hours a prior were used as

controls. Then, the cells were washed twice with warm PBS 1x to eliminate excess dye and collected by trypsinization as previously described. The pellets were resuspended in 500-1000µl of cold PBS 1x and transferred to FACS tubes. Mitochondrial membrane potential was measured by flow cytometry and the results were analysed using Microsoft Excel and FlowJo software.

2.2.6. Molecular biology

2.2.6.1 RNA extraction

Ribonucleic acid (RNA) was extracted from cells harvested as described before (see 2.2.2.1) using the CRYSTAL RNA Mini Kit according to the manufacturer's protocol. Briefly, cells were lysed by the addition of 400µl of Lysis Solution RL complemented with 1% 2-Mercaptoethanol, incubation at room temperature for 2 minutes, resuspension and incubation at room temperature for another 3 minutes. Then, samples were transferred to Spin Filter D columns arranged in Receiver Tubes 2ml and centrifuged at 10,000xg for 2 minutes. Afterwards, the columns were removed and 400µl of 70% ethanol was added to each Receiver Tube. The content was mixed and pipetted to Spin Filter R column placed in fresh Receiver Tube and centrifuged at 10,000xg for 2 minutes. Subsequently, flow-through was discarded and 500µl of Washing Solution HS was added to each column. Samples were centrifuged at 10,000xg for 1 minute. For another wash, 700µl of Washing Solution LS was added and samples were centrifuged again at 10,000xg for 1 minute. The columns were dried in Receiver Tubes by centrifugation at 10,000xg for 2 minutes. Then, 20–50µl of nuclease-free water were added to elute the RNA into RNAse-free 1.5ml Collection Tubes. Samples were incubated at room temperature for 1 minute and centrifuged at 6,000xg for another minute. The RNA was quantified as described in section 2.2.6.3, used immediately for complementary DNA (cDNA) synthesis and later stored at -80°C.

2.2.6.2 Total DNA isolation

With a view to measure mtDNA copy number, total DNA was isolated from cells as shown in Cotney et al., (2007). More specifically, cell pellets were resuspended in 500µl of DNA extraction buffer and boiled at 95°C for 10 minutes. Lysates were cooled to room temperature and 100µg of RNAse A was added to each of them, followed by incubation at 37°C for 3 hours. Afterwards, 100µg of Proteinase K was added to each sample and they were incubated at 55°C overnight. On the next day, samples were boiled at 95°C for 5 minutes and cooled to room temperature. Similarly to RNA, the DNA was quantified, diluted to 2.0ng/µl in $_{dd}H_2O$ for qPCR and later stored at -20°C.

2.2.6.3 Quantification of nucleic acid

For quantification of isolated RNA and DNA, the NanoDrop One^C was utilized according to the manufacturer's instructions. Besides concentration, absorbances at 260nm and 280nm were measured to verify the quality. Shortly, 1.5µl of suitable blank or sample was pipetted onto the freshly cleaned pedestal and concentration and absorbances were measured in duplicates after the arm was lowered. The results were then saved as Microsoft Excel files.

2.2.6.4 Complementary DNA synthesis

With the objective to assess gene expression, the iScript cDNA Synthesis Kit was used for reverse transcription of isolated RNA into cDNA according to the manufacturer's instructions. More specifically, each reaction in PCR strip was composed of 1µg of total RNA diluted in 15µl of nuclease-free water, 4µl of 5x iScript Reaction Mix and 1µl of iScript Reverse Transcriptase. After quick spin down, the samples were incubated in a thermal cycler using the following protocol: priming at 25°C for 5 minutes, reverse transcription at 46°C for 20 minutes, reverse transcriptase inactivation at 95°C for 1 minute and held at 4°C indefinitely. The synthesized cDNA was diluted 50-fold in $_{dd}H_2O$, used for qPCR and stored at -20°C for subsequent experiments.

2.2.6.5 Quantitative real-time polymerase chain reaction

Quantitative real-time polymerase chain reaction (qPCR) was applied to obtain preliminary data on gene expression, reproduce Next Generation Sequencing results (see 2.2.7.1) and conduct further experiments. Measurements were performed with at least biological triplicates and technical duplicates using the Luna Universal qPCR Master Mix in 384-well plates. Every well was loaded with a reaction composed of 3.6µl of Luna Universal qPCR Master Mix, 0.2µl of each forward and reverse primer for every gene, and 4µl of cDNA template mentioned before.

Afterwards, the plate was secured with an adhesive seal, centrifuged at 1,000xg for 1 minute to eliminate potential air bubbles and incubated in the QuantStudio 6 Flex using the following fast thermal cycling protocol: polymerase activation at 95°C for 30 seconds, amplification for 40 cycles with steps of denaturation at 95°C for 3 seconds, annealing at 56°C for 30 seconds and extension at 60°C for 30 seconds. Melt-curve analyses were conducted at steps of 85°C for 15 seconds, 52°C for 30 seconds and 95°C for 15 seconds. Afterwards, data were collected and processed in the QuantStudio™ Real-Time PCR Software to export them later as a Microsoft Excel file for analysis employing the ΔΔCT method.

2.2.6.6 Relative mtDNA copy number assessment

Relative mtDNA copy numbers were determined using the protocol described in Cotney et al., (2007). The qPCR for mtDNA was performed similarly to the qPCR described earlier, however, some modifications were necessary. More specifically, every well contained 4.5µl of Luna Universal qPCR Master Mix, 0.25µl each of forward and reverse primer for every gene and 5.0µl of diluted total DNA template. Moreover, a different fast thermal cycling protocol was applied: hold stage and polymerase activation at 95°C for 10 minutes, amplification for 40 cycles with steps of denaturation at 95°C for 15 seconds, annealing/extension at 60°C for 1 minute. Melt-curve analyses were conducted with a temperature gradient rising at 0.5°C per step from 55 to 80°C. Measurements were taken at each step after 10 seconds of incubation.

2.2.7. Statistical analyses

The results were analysed using Microsoft Excel. Graphs present data from a representative experiment, mean values normalized to experimental controls and their corresponding error bars equal to

standard deviation (SD) or standard error of the mean (SEM) for at least three biological replicates. Use of SEM or SD arises from a type of experiment and statistical analysis performed, since standard deviation describes the variability of observations, whereas the standard error of the mean estimates the variability of the mean estimates of values of means of samples (Barde and Barde, 2012). Means were interpreted as significantly different based on p-value calculated using Student's t-test for two-parameter comparisons and indicated as follows $p < 0.05$ (*), $p < 0.01$ (**) or $p < 0.001$ (***), as routinely used in biological sciences.

2.2.7.1 Next-generation sequencing data analysis

With a view to applying an unbiased, multi-dimensional genomics approach, RNA from HEK cells grown in high glucose and starved in no glucose medium was isolated as described in section 2.2.6.1, in triplicates for each condition. Following quality assessment, RNA-sequencing was performed at the NGS Core Facility for Integrative Genomics of the University Medical Center Göttingen. The obtained data were analysed by Nicolás Lemus-Diaz, MD PhD as described in Cruz-Barrera et al. (2020).

Briefly, raw reads underwent quality control with FastQC and then were mapped against the Human Reference Genome GRCh38 (Ensembl 92 version) using STAR (v2.6.0) (Dobin et al., 2012; Dobin and Gingeras, 2015). Following alignment files manipulation with Samtools (Li et al., 2009), gene expression was quantified using RSEM (Li and Dewey, 2011) and differential expression was determined with EBSeq (Leng et al., 2013). More specifically, EBseq recognised several possible expression patterns and computed a posteriori probability (MAP) to discern the expression pattern that fits best for each gene, and a posteriori probability of equal expression in all conditions. Differentially expressed genes (DEG) were identified depending on a false discovery rate (FDR) with a significance threshold of $p < 0.05$. Functional annotation of DEG, GO enrichment and clustering analyses were completed in R (R Core Team, 2018) with org.Hs.eg.db (Carlson, 2019), clusterProfiler (Yu et al., 2012), and factoextra (Kassambara and Mundt, 2019) packages, respectively.

2.2.7.1.1 Identification of signaling pathways and transcriptional regulators

Subsequently, the DEG were examined by Nuno Raimundo, PhD, using Ingenuity Pathway Analysis (IPA) to identify signaling pathways affected by CLN3 KO and relevant for Batten disease pathogenesis. IPA indicates statistically enriched transcriptional regulators and signalling pathways applying the Fisher's exact test with the threshold at $p < 0.05$.

2.2.7.1.2 Organelle biogenesis

It was demonstrated before that average expression of organelle-specific genes is a good indicator of the biogenesis of that organelle (Yambire et al., 2019; Fernández-Mosquera et al., 2017). Lysosomal, mitochondrial (including respiratory chain subunits), peroxisomal, endoplasmic reticulum and Golgi proteomes were obtained from verified publications listed in Table 11 and the protein IDs were converted to Ensembl Stable IDs. The average expression was determined as the mean fold change of all

detected organelle-specific genes and interpreted as significantly different from corresponding control based on p-value calculated with Student's t-test with Bonferroni post hoc correction with thresholds set as described later, in section 2.2.7.

Table 11. Source of organelle-specific proteome subset.

Subset	Number of genes	Source
Mitochondria	1158	Calvo et al., 2016
Respiratory chain subunits	71	Calvo et al., 2016
Lysosomes	435	Schröder et al., 2010
Peroxisomes	87	Yifrach et al., 2018
Endoplasmic reticulum	268	Gilchrist et al., 2006
Golgi (COP I) vesicles	77	Gilchrist et al., 2006

3. Results

Batten disease is the most common neurodegenerative disorder of childhood characterized by the accumulation of autofluorescent storage material in lysosomes. The malady is caused by mutations in the CLN3 gene, while the exact disease mechanism remains obscure (Shematorova and Shpakovski, 2020). Mitochondrial dysfunction was reported in most of the lysosomal storage diseases and anomalous mitochondria-lysosome crosstalk was observed in several neurodegenerative disorders (Deus et al., 2019; Raimundo and Krisko, 2019). Therefore, we decided to study the role of organelle crosstalk in the Batten disease course and determine signalling pathways pertinent to the pathology using HEK cell line lacking CLN3, which we generated using CRISPR-Cas9. The cellular model was modulated to respond to distinct metabolic conditions, such as starvation, to evaluate the effect of CLN3-loss-of-function on metabolism. Media used in the experiments were described before (see 2.2.1.1) and are later referred to as high- and no glucose medium.

3.1. The lysosomal function is defective in CLN3 KO cells

Lysosomes are responsible for the degradation of major molecules, which requires the activity of specialized hydrolases and acidic environment (Lamming and Bar-Peled et al., 2019). Breakdown of proteins into smaller polypeptides or amino acids is referred to as proteolysis. Following confirmation of the deletion in the CLN3 gene by DNA sequencing (see 2.2.1.2.6), we verified if the genetic defect had an impact on lysosomal function using microplate reader DQ Red BSA assay. We observed significantly impaired proteolytic activity in both, CLN3 KO HeLa and HEK cells, whereas preceding starvation further worsened the proteolytic capacity of CLN3 KO HEK cells (Figure 16).

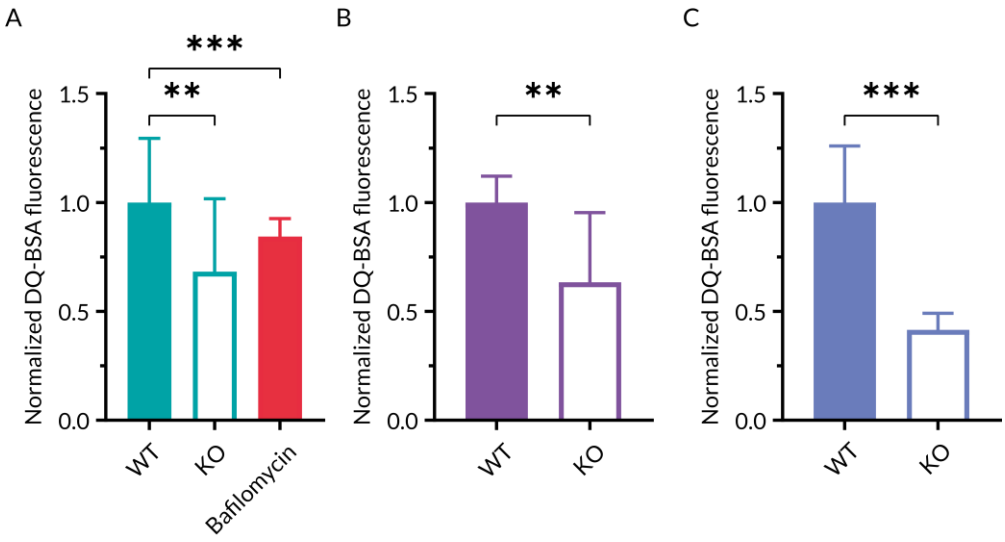

Figure 16. Lysosomal proteolytic capacity is impaired in CLN3 KO cells. A. Normalized DQ Red BSA fluorescence measured in CLN3 HeLa cells grown in high glucose medium (N=3). B. Normalized DQ Red BSA fluorescence measured in CLN3 HEK cells grown in high glucose medium (N=10). C. Normalized DQ Red BSA fluorescence measured in CLN3 HEK cells starved in no glucose medium (N=12). Proteolytic activity was measured with a DQ Red BSA assay by plate reader. Graphs represent mean ± SD of indicated number (N) of experimental replicates and differences were significant based on the Student's t-test, $p < 0.05$ (*), $p < 0.01$ (**), $p < 0.001$ (***); SD: standard deviation.

3.2. Organelle crosstalk may play an important role in Batten disease progression

3.2.1. Mitochondrial and ER biogenesis is transcriptionally repressed in starved CLN3 KO HEK cells

The organization of a eukaryotic cell into organelles allows for spatial and temporal separation of incompatible biochemical processes, which must be synchronized to guarantee appropriate cellular function (Cohen et al., 2018). Mitochondria and lysosomes play an essential role in cellular metabolism and signalling, including autophagy, proliferation and cell death. Interdependence of mitochondria and lysosomes was observed in multiple disorders, including most lysosomal storage diseases and mitochondrial diseases (Deus et al., 2019).

Although several publications report aberrant mitochondrial and ER function in NCL models (Marotta et al., 2017; Luiro et al., 2006; Fosalle et al., 2004; Jolly et al., 2002), lack of comprehensive characterization of organelle biogenesis, morphology and function impedes determination of the role of organelle crosstalk in Batten disease progression. We present below a general overview of organelle biogenesis with the use of our transcriptome data analysed as described in Methods section 2.2.7.1.2. CLN3 KO in HEK cells did not globally affect biogenesis of any of the organelles in cells grown in high glucose medium (Figure 17A), however, more than 10% of genes specific to given organelle are differentially expressed (Figure 17B). On contrary, mitochondrial and ER biogenesis is transcriptionally repressed in CLN3 KO HEK cells starved in no glucose medium compared to corresponding WT (Figure 18A). Moreover, around half of mitochondrial and ER genes are differentially expressed (Figure 18B). Overall, we observe a substantial impact of CLN3 KO on organelle biogenesis in starved cells considering the number of differentially expressed genes.

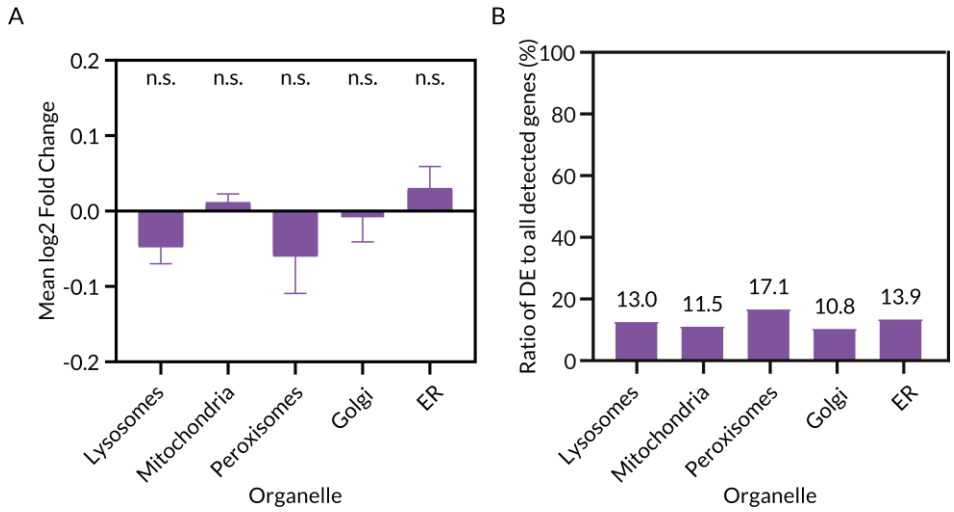

Figure 17. CLN3 KO has no statistically significant impact on organelle biogenesis in HEK cells grown in a high glucose medium. A. Mean ± SEM of the logarithm of base 2 of fold change in expression of all detected genes specific to a given organelle in CLN3 KO/WT high glucose NGS dataset; SEM: standard error of the mean. B. Ratio of differentially expressed genes to all detected genes specific to a given organelle in CLN3 KO/WT high glucose NGS dataset, in percentage. Differences between groups were considered statistically significant based on Student's t-test with post hoc Dunn–Bonferroni correction at $p < 0.05$ (*), $p < 0.01$ (**) or $p < 0.001$ (***).

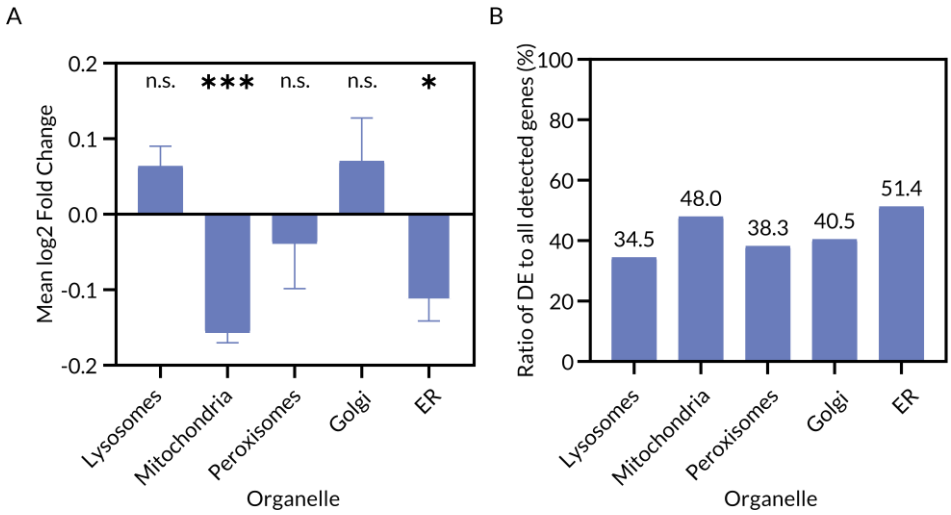

Figure 18. CLN3 KO has a substantial impact on mitochondrial and ER biogenesis in HEK cells starved in no glucose medium. A. Mean ± SEM of logarithms of base 2 of fold change in expression of all detected genes specific to a given organelle in CLN3 KO/WT no glucose NGS dataset. B. Ratio of differentially expressed genes to all detected genes specific to a given organelle in CLN3 KO/WT no glucose NGS dataset, in percentage. Differences between groups were considered statistically significant based on Student's t-test with post hoc Dunn–Bonferroni correction at $p < 0.05$ (*), $p < 0.01$ (**) or $p < 0.001$ (***); SEM: standard error of the mean.

We successfully replicated the above-mentioned transcriptome data by qPCR with another set of freshly extracted RNA samples. The goodness of fit of fold changes in expression of 50 genes, detected in CLN3 KO HEK cells grown in high glucose medium and normalized to corresponding WT control, is described by R squared equal to 0.58 (Figure 19). One should consider that observed disparity between transcriptome and qPCR data may result from significant differences between applied methods and imperfection of loading control.

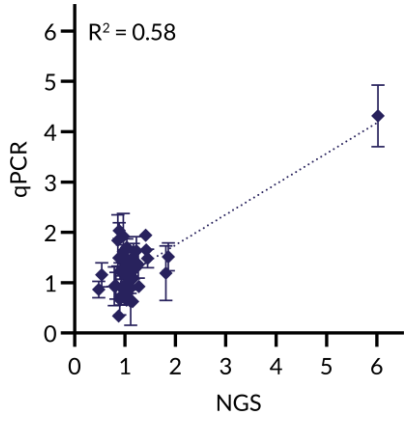

Figure 19. Transcriptome data were successfully reproduced by qPCR with another set of freshly extracted RNA samples. Fold change in expression of 50 genes detected by qPCR in CLN3 KO HEK cells grown in high glucose medium is plotted against corresponding fold change in NGS dataset. Data points represent mean ± SEM of experimental triplicates with each experimental replicate being the average of technical duplicates; SEM: standard error of the mean.

Since our transcriptome data analysis indicated repression of mitochondrial biogenesis in starved CLN3 KO HEK cells, we next assessed protein levels of mitochondrial biogenesis regulators. Intriguingly, we did not detect any statistically significant difference in protein levels of Pgc1α, Nrf1 and Tfam in CLN3 KO HEK cells grown in high glucose medium (Figure 20), nor starved in no glucose medium (Figure 21).

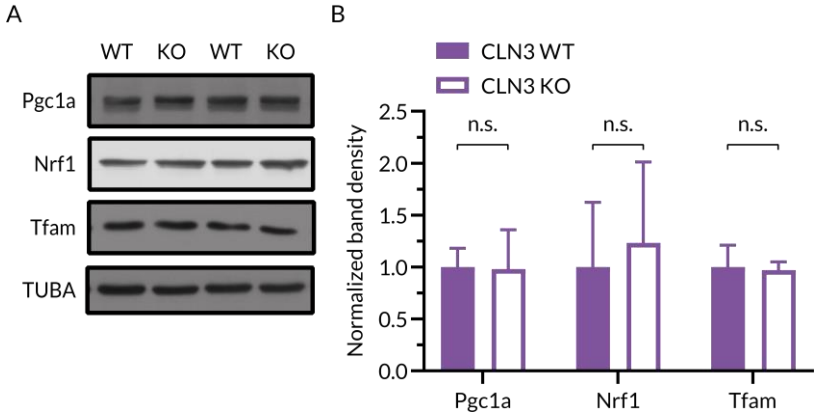

Figure 20. The protein level of mitochondrial biogenesis regulators is not affected in CLN3 KO HEK cells grown in a high glucose medium. A. Immunoblot of Pgc1α, Nrf1 and Tfam with α-Tubulin as a loading control in whole cell lysates of CLN3 HEK cells grown in high glucose medium. B. Band density quantifications from the western blot represented in A. Graph represents mean ± SD of experimental triplicates and differences were significant based on the Student's t-test, $p < 0.05$ (*), $p < 0.01$ (**), $p < 0.001$ (***); SD: standard deviation.

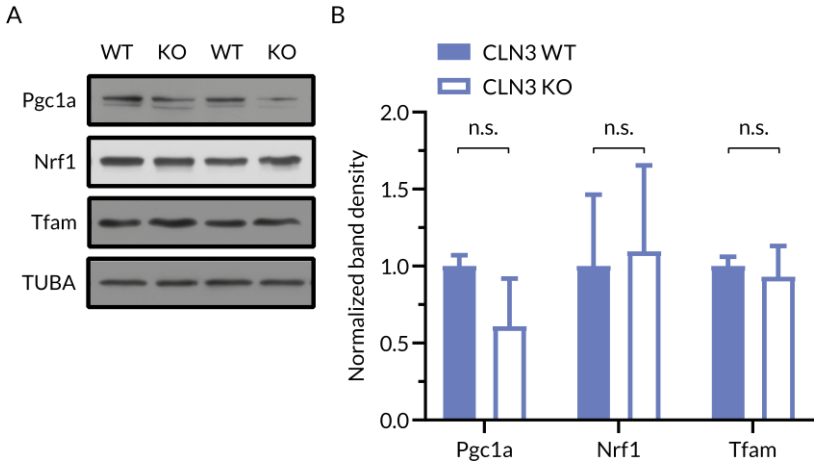

Figure 21. The protein level of mitochondrial biogenesis regulators is not statistically significantly changed in CLN3 KO HEK cells starved in no glucose medium. A. Immunoblot of Pgc1α, Nrf1 and Tfam with α-Tubulin as a loading control in whole cell lysates of CLN3 HEK cells starved in no glucose medium. B. Band density quantifications from the western blot represented in A. Graph represents mean ± SD of experimental triplicates and differences were significant based on the Student's t-test, $p < 0.05$ (*), $p < 0.01$ (**), $p < 0.001$ (***); SD: standard deviation.

3.2.2. Levels of OxPhos proteins and mtDNA copy number are reduced in HEK cells lacking CLN3

Considering the importance of OxPhos complexes, we decided to examine gene expression of their proteins separately to assess the impact of CLN3-loss-of-function on mitochondrial OxPhos biogenesis and verify if the trend is consistent with our previous observations. Interestingly, CLN3 KO

significantly affects the expression of genes encoding OxPhos proteins, upregulating them under high glucose conditions ($p < 0.05$) and downregulating in starved cells ($p < 0.001$), according to the aforementioned statistical analysis. Notably, 60% of these genes are differentially expressed in CLN3 KO HEK cells starved in no glucose medium consistently with overall mitochondrial biogenesis repression at the transcriptional level (Figure 22).

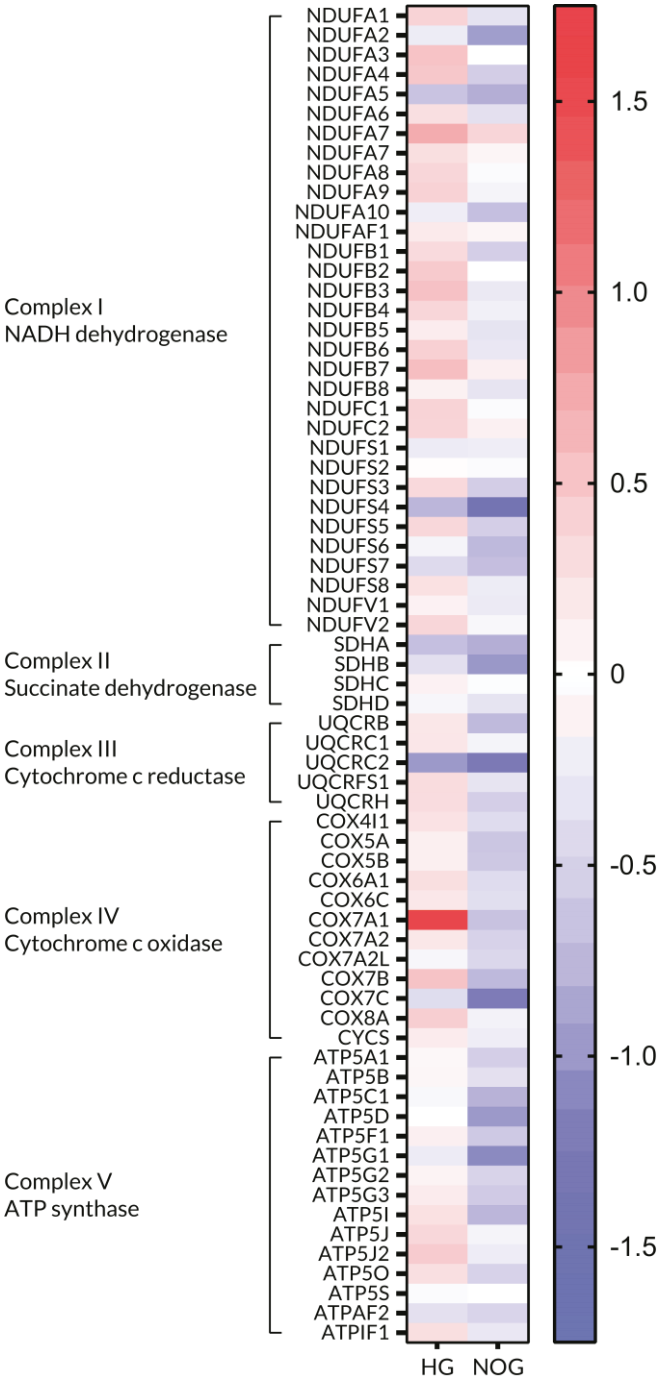

Figure 22. CLN3 KO has a substantial impact on the expression of genes encoding respiratory chain proteins in both, high glucose and no glucose condition. Heatmap represents the logarithm of base 2 of fold change in expression of a given gene in the CLN3 KO/WT NGS dataset. Differences between groups were considered statistically significant based on Student's t-test with post hoc Dunn–Bonferroni correction, $p < 0.05$.

Subsequently, we tested if the aforementioned changes in expression of mitochondrial genes correspond to any alterations in protein levels detected by immunoblotting and mtDNA copy number measured by qPCR. For mtDNA copy number assessment, the cells were grown in high glucose medium or starved in no glucose medium with or without pyruvate (1mM). In Figure 23 one can appreciate that mtDNA copy number is significantly reduced in CLN3 KO HEK cells in comparison to WT in every tested condition.

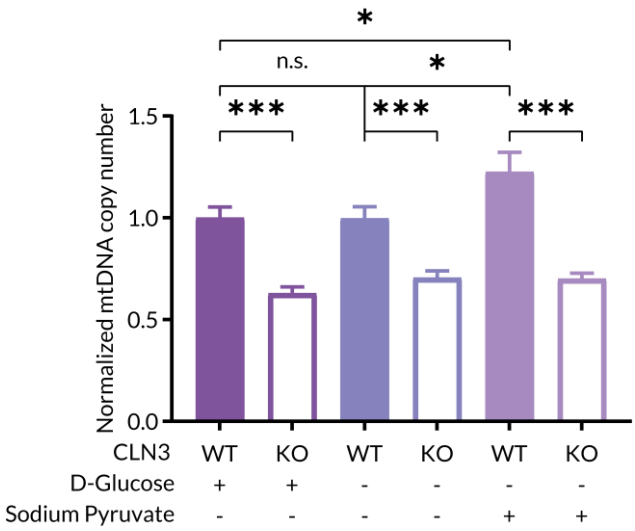

Figure 23. Mitochondrial DNA copy number level is reduced in CLN3 KO HEK cells. mtDNA copy number measured by qPCR using DNA extracted from CLN3 HEK cells grown high glucose, no glucose with or without pyruvate (1mM) media and β-Globin as a loading control. The graph represents mean ± SEM of 4 experimental replicates with each experimental replicate being the average of technical triplicates and differences were significant based on the Student's t-test, p < 0.05 (*), p < 0.01 (**), p < 0.001 (***); SEM: standard error of the mean.

Moreover, we also observed a substantial decrease in levels of proteins that belong to respiratory chain subunits in CLN3 KO HEK cells grown in normal medium, specifically NADH:ubiquinone oxidoreductase subunit B8 (NDUFB8) – complex I, succinate dehydrogenase complex iron-sulfur subunit B (SDHB) – complex II, ubiquinol-cytochrome c reductase core protein 2 (UQCRC2) – complex III and mitochondrially encoded cytochrome c oxidase I (MtCO1) – complex IV. On the other hand, ATP synthase subunit α (ATP5A), which is a part of complex V, remains unchanged (Figure 24). Similarly, levels of said proteins are substantially lower in CLN3 KO HEK cells starved in no glucose medium in comparison to the corresponding wild type, whereas ATP5A persists the same (Figure 25).

To investigate if CLN3-loss-of-function also affects the assembly of mitochondrial OxPhos complexes, we assessed the level of native complexes in mitochondria isolated from CLN3 HEK cells grown in high glucose medium and did not detect any substantial difference (Figure 26). Following proteins were used as OxPhos complexes markers: NDUFB8 – complex I, succinate dehydrogenase complex flavoprotein subunit A (SDHA) – complex II, cytochrome b-c1 complex subunit Rieske (Rieske) – complex III, MtCO1 – complex IV and ATP synthase F1 subunit β (ATP5B) – complex V.

Voltage-dependent anion-selective channel protein 1 (VDAC1) was immunoblotted as a loading control.

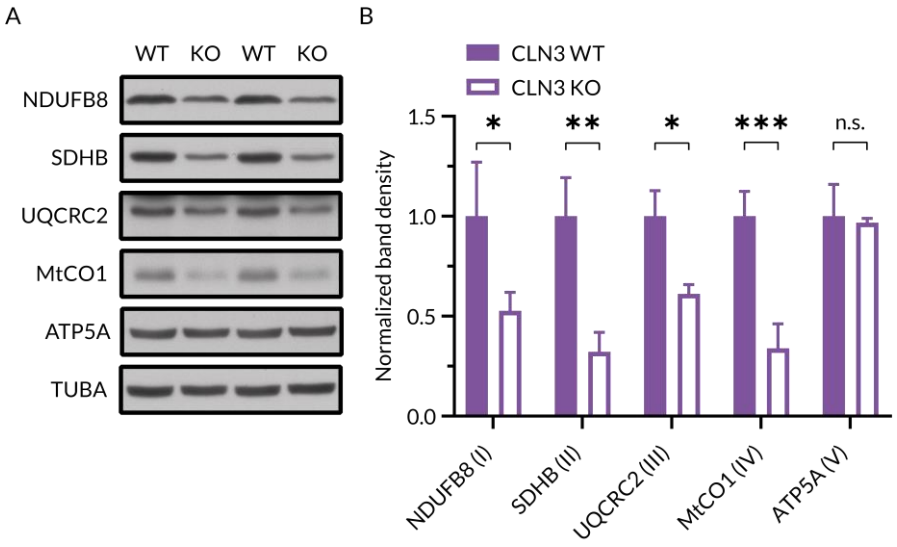

Figure 24. Level of OxPhos proteins NDUFB8, SDHB, UQCRC2 and MtCO1 is significantly reduced in CLN3 KO HEK cells grown in a high glucose medium. Immunoblot of NDUFB8, SDHB, UQCRC2, MtCO1 and ATP5A with α-Tubulin as a loading control in whole cell lysates of CLN3 HEK cells grown in high glucose medium. B. Band density quantifications from the western blot represented in A. Graph represents mean ± SD of experimental triplicates and differences were significant based on the Student's t-test, $p < 0.05$ (*), $p < 0.01$ (**), $p < 0.001$ (***); SD: standard deviation.

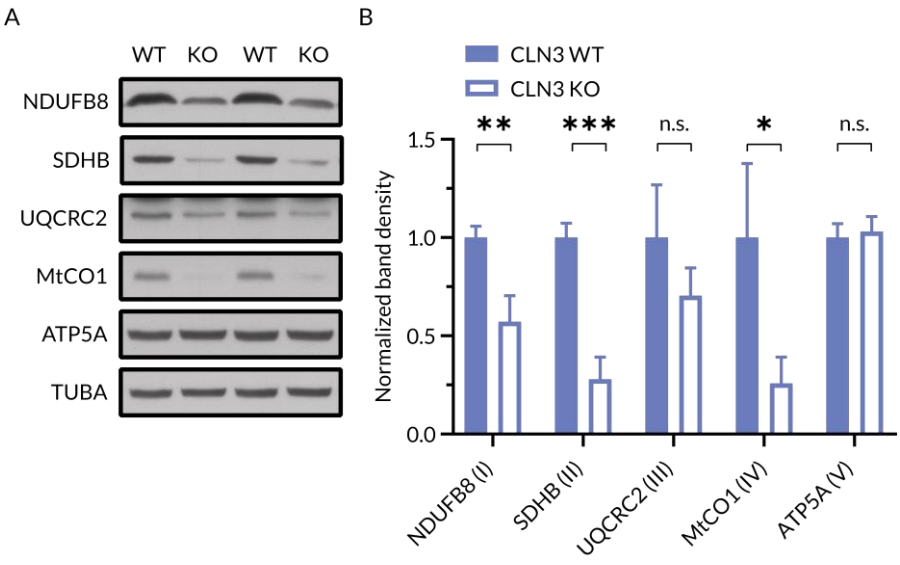

Figure 25. Level of OxPhos proteins NDUFB8, SDHB, UQCRC2 and MtCO1 is considerably decreased in CLN3 KO HEK cells starved in no glucose medium. A. Immunoblot of NDUFB8, SDHB, UQCRC2, MtCO1 and ATP5A with α-Tubulin as a loading control in whole cell lysates of CLN3 HEK cells starved in no glucose medium. B. Band density quantifications from the western blot represented in A. Graph represents mean ± SD of experimental triplicates and differences were significant based on the Student's t-test, $p < 0.05$ (*), $p < 0.01$ (**), $p < 0.001$ (***); SD: standard deviation.

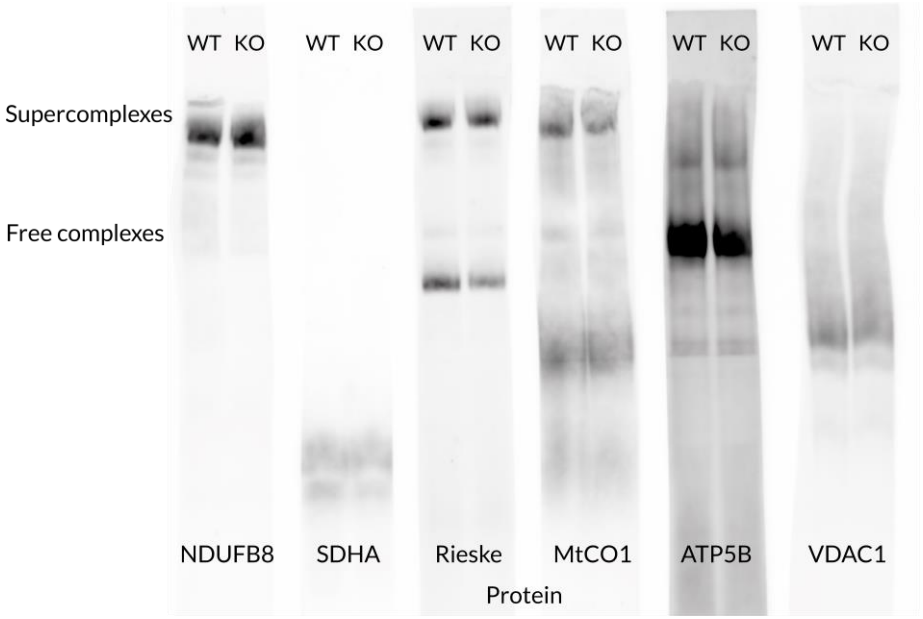

Figure 26. The level of native OxPhos complexes in isolated mitochondria is not changed in CLN3 KO HEK cells grown in a high glucose medium. Immunoblot of NDUFB8, SDHA, Rieske, MtCO1 and ATP5B with VDAC1 as a loading control in mitochondria isolated from CLN3 HEK cells grown in high glucose medium resolved by BN-PAGE.

3.2.3. Mitochondria are dysfunctional in CLN3 KO cells

The vast majority of oxygen inhaled by a human is consumed by mitochondria in the respiratory chain to synthesize ATP through oxidative phosphorylation for different cellular activities, while ROS are generated as a by-product (Kausar et al., 2018). Glycolysis and oxidative phosphorylation are the key energy-producing processes in the cell. We subsequently verified whether the previously described decrease in the level of OxPhos proteins in whole cell extracts and reduction in mtDNA copy number coincide with altered mitochondrial function. Indeed, we observed a decline in oxygen consumption rate (OCR) in CLN3 KO HEK cells, while starvation resulted in a further decrease of OCR (Figure 27A). Impaired basal mitochondrial respiration is not compensated by an increase in glycolysis, which would be reflected in the extracellular acidification rate (ECAR). Saturation of glucose concentration and inhibition of ATP synthase by oligomycin did not reveal a significant difference in glycolytic flux and maximum glycolytic capacity, respectively, between CLN3 WT and KO HEK cells (Figure 27B). These results suggest compromised energy production in CLN3 KO HEK cells, which should be later confirmed by assessment of ATP levels.

Despite lower oxygen consumption, we observed increased intensity of MitoSox Red fluorescence detected by flow cytometry in CLN3 KO HEK cells (Figure 28), which implies elevated mitochondrial superoxide level and therefore higher mitochondrial ROS abundance. Moreover, the JC-1 dye red to green fluorescence intensity ratio measured by flow cytometry is decreased in CLN3 KO HEK cells, implicating reduced mitochondrial membrane potential (Figure 29). We also observed lower cell viability of CLN3 KO HEK cells indicated by a decline in the intensity of the luminescent signal (Figure 30), which is proportional to the number of metabolically active cells. All studied aspects were consistent for high- and no glucose conditions and are characteristic for mitochondrial dysfunction.

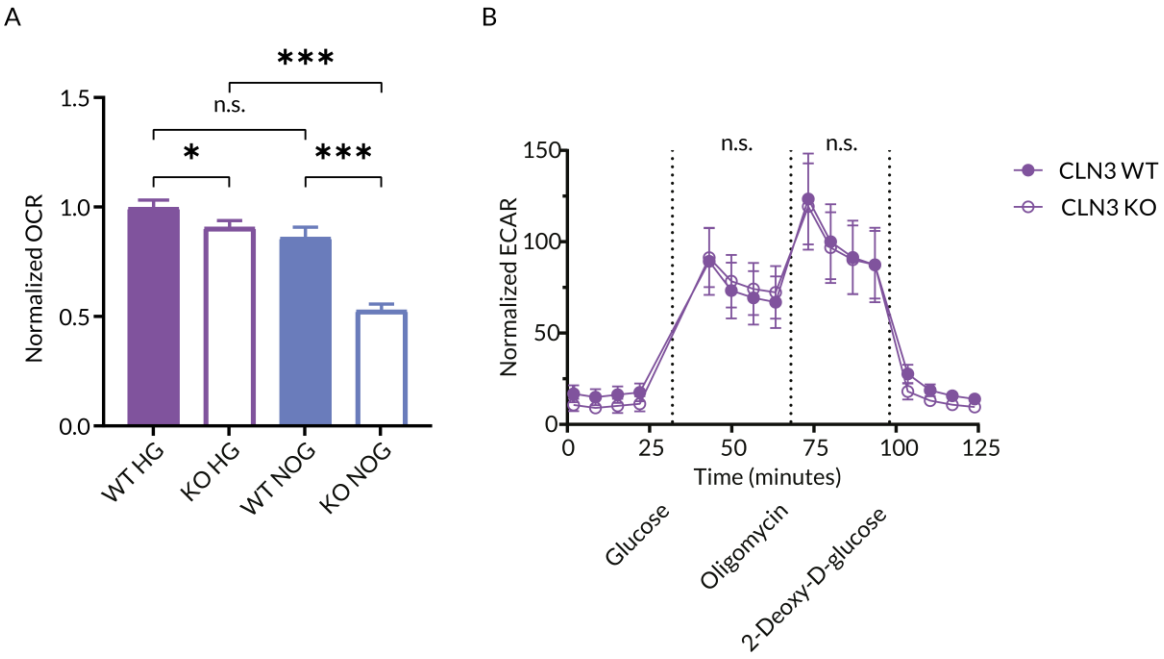

Figure 27. Basal mitochondrial respiration is impaired in CLN3 KO HEK cells in both, high glucose (HG) and no glucose (NOG) conditions. A. Quantification of basal oxygen consumption rate measured in CLN3 HEK cells by Seahorse XF Analyzer. The graph represents mean ± SEM of 11 experimental replicates; SEM: standard error of the mean. B. Extracellular acidification rate over time measured in CLN3 HEK cells by Seahorse XF Analyzer. The graph represents the mean ± SD of 24 experimental replicates. In both, differences were considered significant based on the Student's t-test, p < 0.05 (*), p < 0.01 (**), p < 0.001 (***); SD: standard deviation.

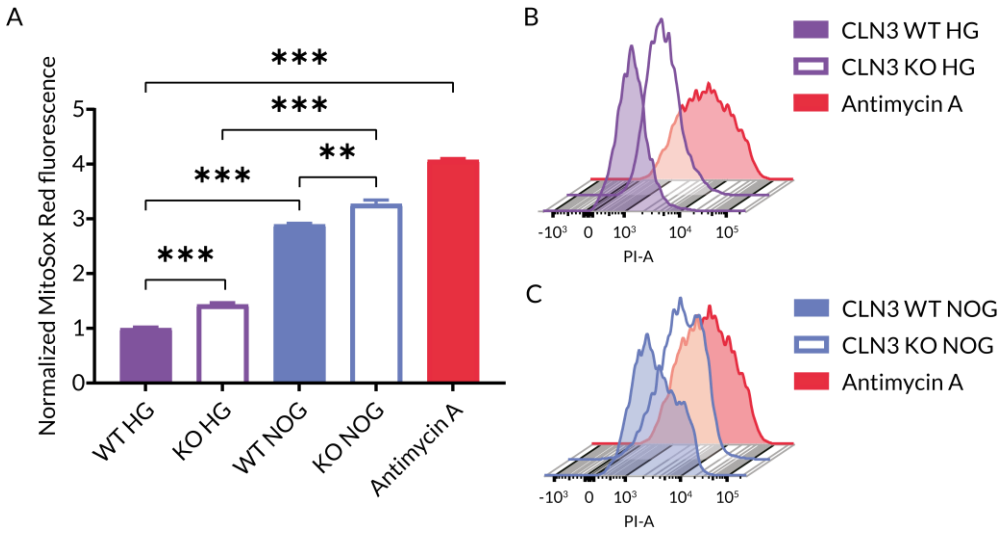

Figure 28. Mitochondrial superoxide level is increased in CLN3 KO HEK cells in both, high glucose (HG) and no glucose (NOG) conditions. A. Quantification of MitoSox Red fluorescence measured in CLN3 HEK cells by flow cytometry. The graph represents mean ± SEM of experimental triplicates and differences were significant based on the Student's t-test, p < 0.05 (*), p < 0.01 (**), p < 0.001 (***); SEM: standard error of the mean. B. Representative histogram of MitoSox Red fluorescence detected in CLN3 HEK cells grown in high glucose medium. C. Representative histogram of MitoSox Red fluorescence detected in CLN3 HEK cells starved in no glucose medium. CLN3 WT HEK cells grown in high glucose medium and incubated with antimycin A were used as a positive control.

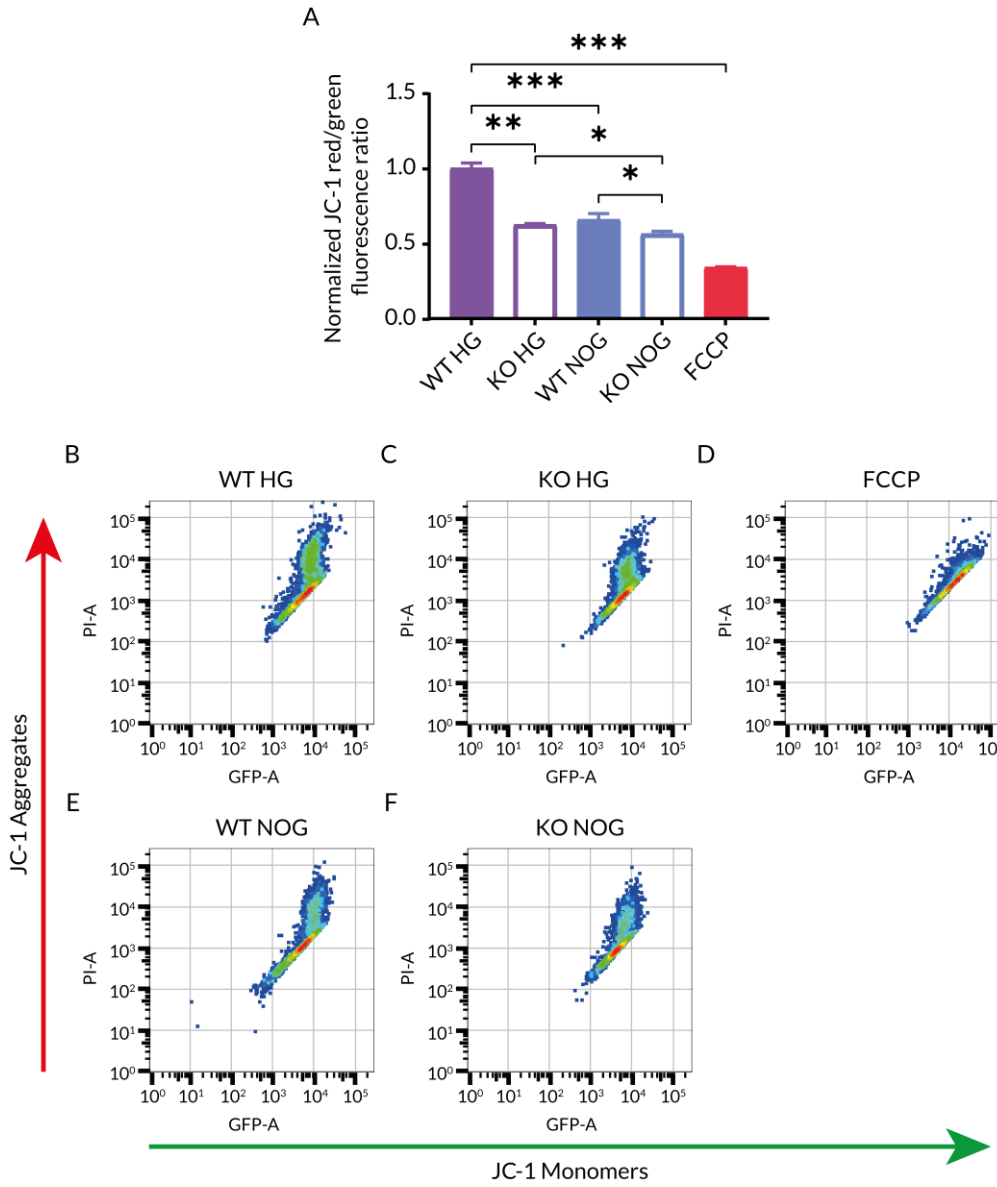

Figure 29. Mitochondrial membrane potential is reduced in CLN3 KO HEK cells in both, high glucose (HG) and no glucose (NOG) conditions. A. Quantification of JC-1 dye red/green fluorescence ratio measured in CLN3 HEK cells by flow cytometry. The graph represents mean ± SEM of experimental triplicates and differences were significant based on the Student's t-test, $p < 0.05$ (*), $p < 0.01$ (**), $p < 0.001$ (***); SEM: standard error of the mean. B. JC-1 aggregates vs. monomers dot plot for CLN3 WT HEK cells grown in high glucose medium. C. JC-1 aggregates vs. monomers dot plot for CLN3 KO HEK cells grown in high glucose medium. D. JC-1 aggregates vs. monomers dot plot for CLN3 WT HEK cells grown in high glucose medium and incubated with FCCP, as a positive control. E. JC-1 aggregates vs. monomers dot plot for CLN3 WT HEK cells starved in no glucose medium. F. JC-1 aggregates vs. monomers dot plot for CLN3 KO HEK cells starved in no glucose medium.

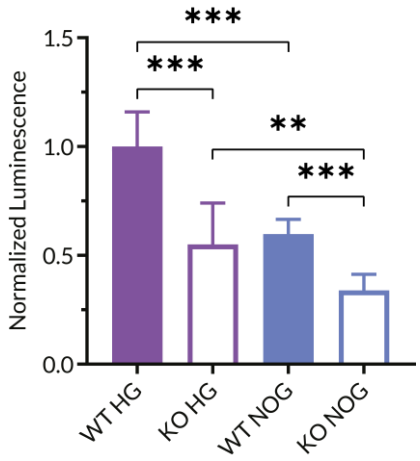

Figure 30. Cell viability is declined in CLN3 KO HEK cells in both, high glucose (HG) and no glucose (NOG) conditions. Cell viability was measured in CLN3 HEK cells with CellTiter-Glo assay by plate reader. The graph represents the mean ± SD of 12 experimental replicates and differences were significant based on the Student's t-test, p < 0.05 (*), p < 0.01 (**), p < 0.001 (***); SD: standard deviation.

We observed a similar phenotype in CLN3 KO HeLa cells grown in a high glucose medium. Specifically, we detected a decrease in basal respiration in CLN3 KO HeLa cells implicated by lower OCR measured before inhibition of ATP synthase by oligomycin, as well as reduced maximal respiration indicated by lower OCR measured following disruption of the mitochondrial membrane potential by FCCP (Figure 31). Similarly, the intensity of MitoSox Red fluorescence measured by flow cytometry is increased in CLN3 KO HeLa cells, indicating higher mitochondrial superoxide levels (Figure 32).

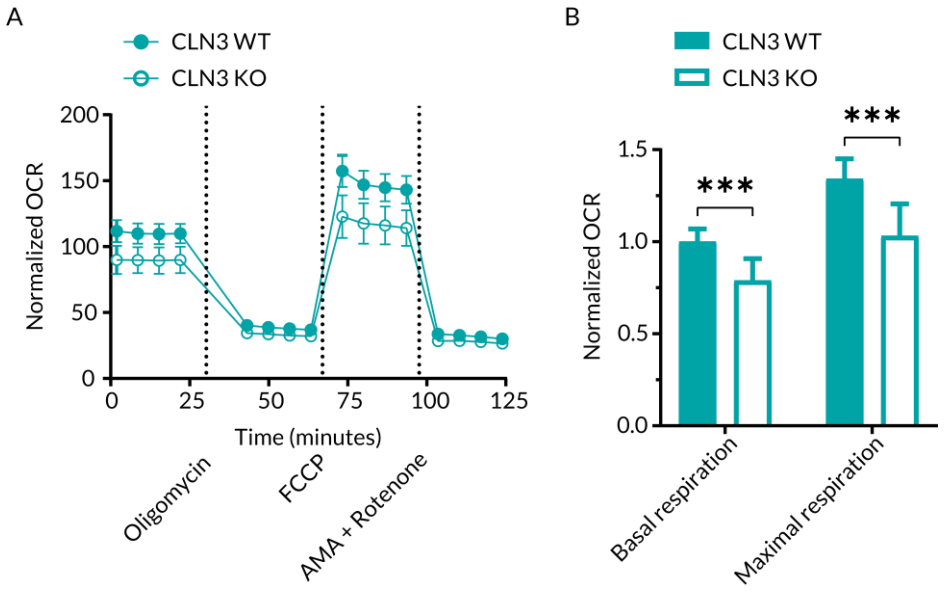

Figure 31. Mitochondrial respiration is defective in CLN3 KO HeLa cells. A. Oxygen consumption rate measured over time in CLN3 HeLa cells grown in high glucose medium by Seahorse XF Analyzer. The graph represents the mean ± SD of 12 experimental replicates; SD: standard deviation. B. Quantification of basal and maximal respiration represented in A. Graph represents mean ± SEM of 12 experimental replicates and differences were considered significant based on the Student's t-test, p < 0.05 (*), p < 0.01 (**), p < 0.001 (***); SEM: standard error of the mean.

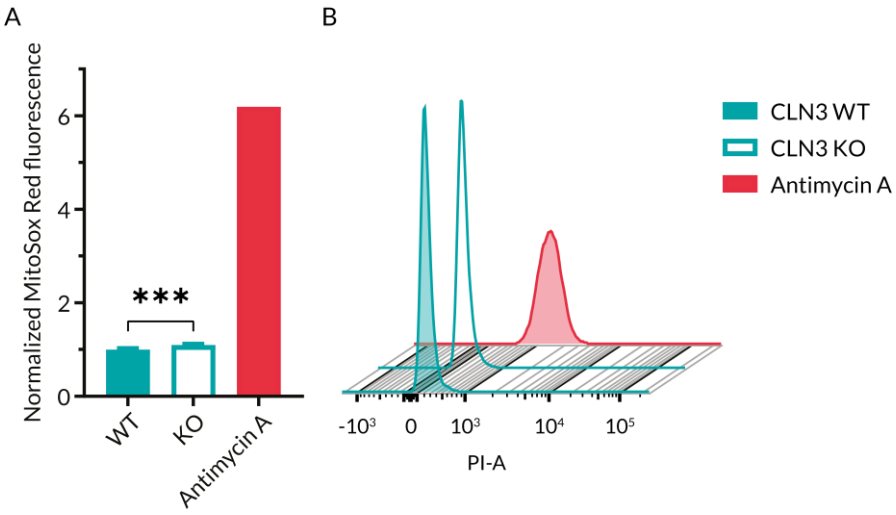

Figure 32. Mitochondrial superoxide level is elevated in CLN3 KO HeLa cells. A. Quantification of MitoSox Red fluorescence measured in CLN3 HeLa cells grown in high glucose medium by flow cytometry. The graph represents mean ± SEM of 5 experimental replicates and differences were significant based on the Student's t-test, $p < 0.05$ (*), $p < 0.01$ (**), $p < 0.001$ (***); SEM: standard error of the mean. B. Representative histogram of MitoSox Red fluorescence detected in CLN3 HeLa cells grown in high glucose medium by flow cytometry. CLN3 WT HeLa cells grown in high glucose medium and incubated with antimycin A were used as a positive control.

3.2.4. Protein levels of mitochondrial and peroxisomal morphology regulators are not significantly altered in HEK cells lacking CLN3

Mitochondrial dynamics allows for control over morphology and mitochondria inheritance, content exchange, maintenance of mtDNA and OxPhos activity (Chan, 2019). Balancing fission and fusion is critical for normal mitochondrial and peroxisomal function. Thus, we tested if observed mitochondrial dysfunction corresponds to changes in mitochondrial morphology. The effect of CLN3 KO on organelle morphology can be revealed by fluorescence imaging experiments and implied by protein levels of regulators, which in the case of mitochondria and peroxisomes are fission and fusion factors.

Drp1 belongs to the dynamin superfamily of GTPases and is essential for mitochondrial and peroxisomal division. The mitochondrial fission is partially controlled by the phosphorylation of Drp1 at serine 616 (Ser616) by Cdk1 and at serine 637 (Ser637) by protein kinase A. Drp1 stimulates mitochondrial division when phosphorylated at Ser616. On the contrary, phosphorylation of Drp1 at Ser637 inhibits fission. MFF is also involved in both, mitochondrial and peroxisomal division, and serves as one of many receptors for Drp1. AMPK phosphorylates MFF at serine 146 (Ser146) to favour the enhanced recruitment of Drp1 to the mitochondria. MFN2 participates in mitochondrial fusion (Pernas and Scorrano, 2016; Oettinghaus et al., 2011). We did not detect statistically significant differences in levels of the aforementioned proteins in cells grown in high glucose medium (Figure 33). Interestingly, the ratio of phosphorylated to total MFF is higher in CLN3 KO HEK cells starved in no glucose medium in comparison to corresponding WT, when phosphorylation of Drp1 remains unaffected (Figure 34). Importantly, mitochondrial and peroxisomal morphology should be evaluated in depth by imaging experiments.

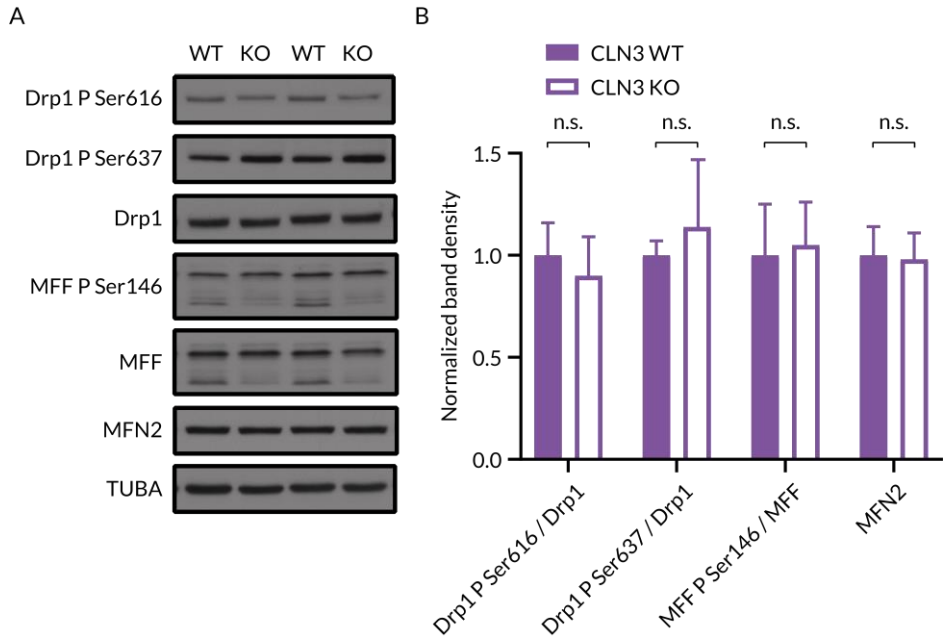

Figure 33. The level of mitochondrial and peroxisomal morphology regulators is not affected in CLN3 KO HEK cells grown in a high glucose medium. A. Immunoblot of Drp1, MFF and MFN2 with α-Tubulin as a loading control in whole cell lysates of CLN3 HEK cells grown in high glucose medium. B. Band density quantifications from the western blot represented in A. Graph represents mean ± SD of experimental triplicates and differences were significant based on the Student's t-test, p < 0.05 (*), p < 0.01 (**), p < 0.001 (***); SD: standard deviation.

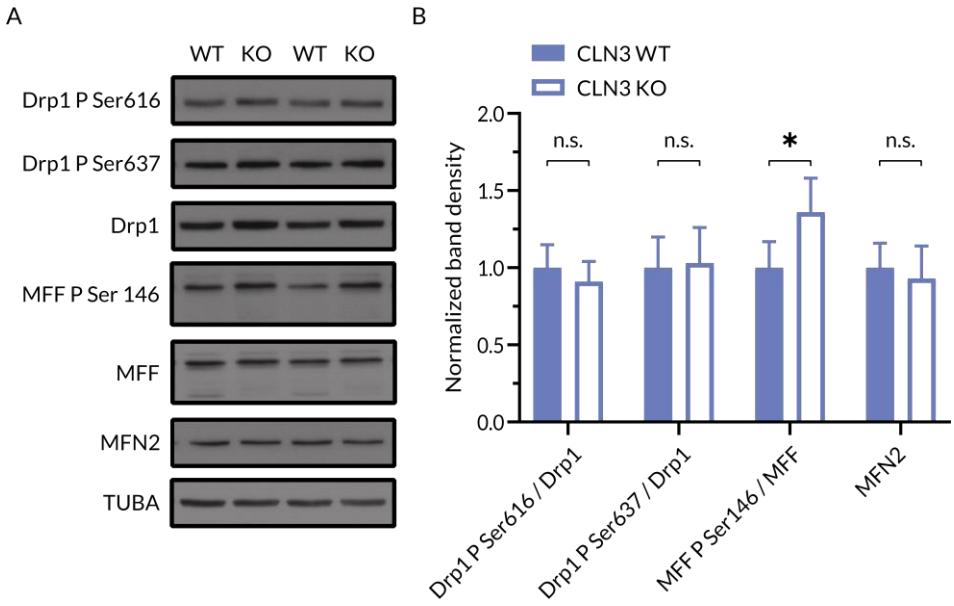

Figure 34. The ratio of phosphorylated to total peroxisomal and mitochondrial fission factor MFF is increased in CLN3 KO HEK cells starved in no glucose medium. A. Immunoblot of Drp1, MFF and MFN2 with α-Tubulin as a loading control in whole cell lysates of CLN3 HEK cells starved in no glucose medium. B. Band density quantifications from the western blot represented in A. Graph represents mean ± SD of experimental triplicates and differences were significant based on the Student's t-test, p < 0.05 (*), p <0.01 (**), p <0.001 (***); SD: standard deviation.

3.2.5. Peroxisomal mass is not affected by CLN3 KO in HEK cells

Notably, peroxisomes are essential for lipid and ROS/RNS metabolism, and often interact with other organelles, especially with ER and mitochondria. Therefore, we decided to verify if observed changes in mitochondrial mass and function coincide with alterations in peroxisomal mass. We did not detect any difference in protein levels of peroxins 5 and 11B in CLN3 HEK cells in both, high glucose (Figure 35) and no glucose conditions (Figure 36). Noteworthy, unaltered peroxisomal mass does not ensure proper peroxisomal function or morphology, which should be assessed in future.

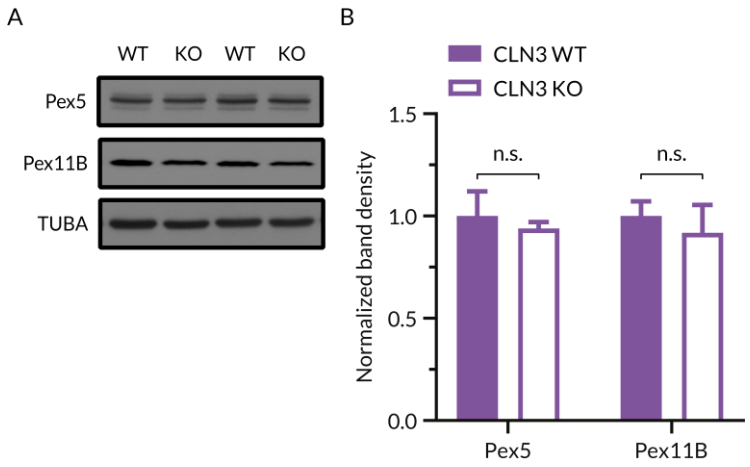

Figure 35. The level of peroxisomal proteins is not altered in CLN3 KO HEK cells grown in a high glucose medium. A. Immunoblot of Pex5 and Pex11B with α-Tubulin as a loading control in whole cell lysates of CLN3 HEK cells grown in high glucose medium. B. Band density quantifications from the western blot represented in A. Graph represents mean ± SD of experimental triplicates and differences were significant based on the Student's t-test, $p < 0.05$ (*), $p < 0.01$ (**), $p < 0.001$ (***); SD: standard deviation.

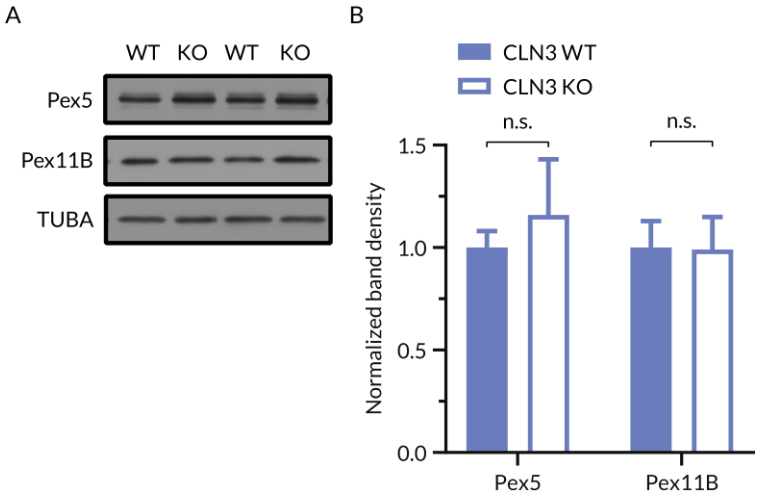

Figure 36. The level of peroxisomal proteins is not changed in CLN3 KO HEK cells starved in no glucose medium. A. Immunoblot of Pex5 and Pex11B with α-Tubulin as a loading control in whole cell lysates of CLN3 HEK cells starved in no glucose medium. B. Band density quantifications from the western blot represented in A. Graph represents mean ± SD of experimental triplicates and differences were significant based on the Student's t-test, $p < 0.05$ (*), $p < 0.01$ (**), $p < 0.001$ (***); SD: standard deviation.

3.3. Proliferation signalling and stress response mechanisms are significantly enriched in CLN3 KO HEK cells

Transcriptome data allow us not only to assess organelle biogenesis but also to find signaling pathways significantly affected by CLN3 KO, whose identification may help in finding therapeutic targets that are closer to the root of the pathogenesis (Deus et al., 2019; Raimundo, 2014). Results presented below were obtained with Ingenuity Pathway Analysis, as described in section 2.2.7.1.1. Figure 37 and Figure 38 display 20 signalling pathways, sorted by -log(p-value), which are the most enriched by CLN3 KO in HEK cells grown in high- and no glucose medium, respectively. Otherwise stated, these pathways are indicative of the processes that are impacted by the absence of CLN3. We focused on proliferative pathways like mTOR, S6K1 signaling and stress response mechanisms because these pathways scored high in the pathway analysis and can be potentially involved in Batten disease pathology.

Importantly, the enrichment analysis was accompanied by an unbiased assessment of the transcription factor activities, which determines which are the key regulators of the transcriptional changes observed. The transcription factor analysis revealed that YAP seems to be a major regulator of the cellular response to the absence of CLN3. The results obtained from the transcriptome data analysis were later complemented by western blot experiments.

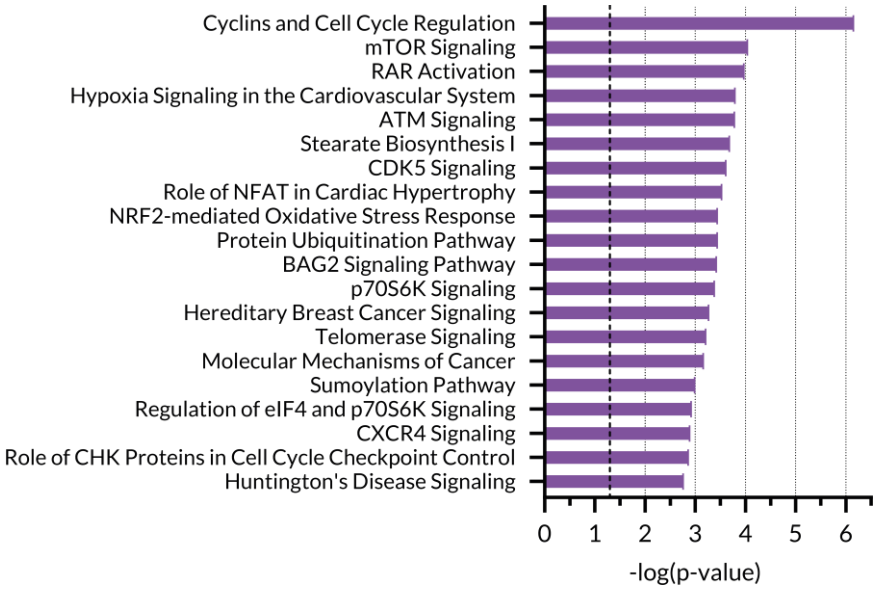

Figure 37. CLN3 KO has a significant impact on stress response mechanisms and proliferative pathways at the transcriptional level in HEK cells grown in a high glucose medium. The twenty most enriched pathways in the differentially expressed gene list of the CLN3 KO/WT high glucose NGS dataset. The graph represents -log(p-value) obtained with the use of Ingenuity Pathway Analysis. A thick dashed line indicates a p-value equal to 0.05.

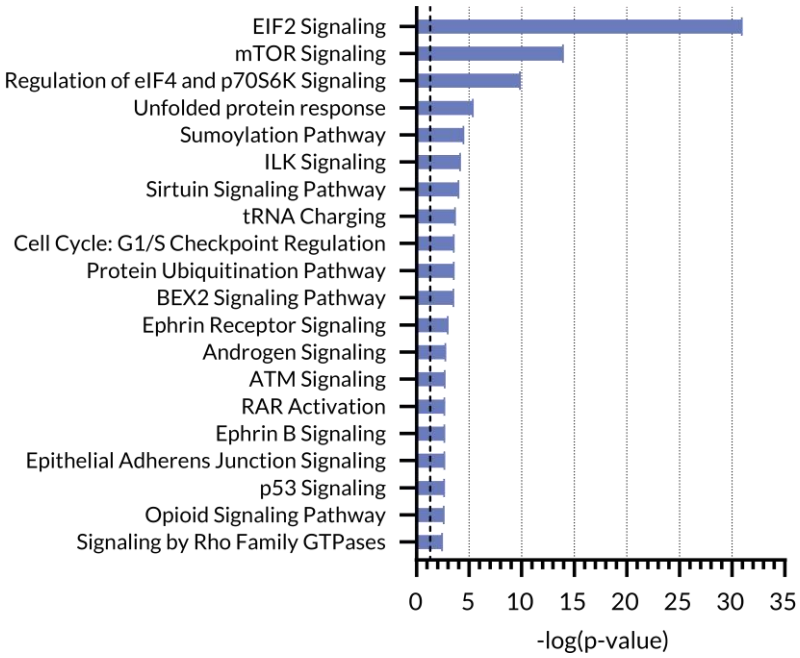

Figure 38. CLN3 KO strongly affects stress response mechanisms and proliferative pathways at the transcriptional level in HEK cells starved in no glucose medium. The twenty the most enriched pathways in the differentially expressed gene list of the CLN3 KO/WT no glucose dataset. The graph represents -log(p-value) obtained with the use of Ingenuity Pathway Analysis. A thick dashed line indicates a p-value equal to 0.05.

3.3.1. Hippo-YAP signalling is significantly altered in HEK cells lacking CLN3

The Hippo-YAP signalling pathway is an integrator of signals that regulate cellular proliferation and differentiation. It is responsive to a variety of environmental cues, e.g., cell density and polarity, energy and ER stress, as well as growth factors like Wnts (Ibar and Irvine, 2020). The Wnt signalling pathway plays a role in the control of different biological processes, such as cell proliferation, differentiation and ageing. There is evidence that Hippo signalling inhibits Wnt-β-catenin signalling. Furthermore, the Hippo signaling transcription factors YAP and TAZ are likely integral components of the β-catenin destruction complex, orchestrating the Wnt responses (Kim and Jho, 2014).

As mentioned before, YAP seems to be activated and play a crucial role as a transcription regulator in HEK cells lacking CLN3. Furthermore, the Hippo signaling pathway is significantly affected at the transcriptional level in CLN3 KO HEK cells in both, high glucose and no glucose condition as indicated by aforesaid pathway analysis. Wnt-β-catenin signaling is also significantly altered at the transcriptional level in CLN3 KO HEK cells starved in no glucose medium. Heatmaps below show the impact of CLN3 KO cells on the expression of genes involved in Hippo and Wnt-β-catenin signalling (Figure 39A and B, respectively). Shades of blue denote reduced gene expression in CLN3 KO HEK cells, indicated by negative values of the logarithm of base 2 of fold change, while shades of red, contrarily, increased gene expression in CLN3 KO HEK cells corresponding to positive values of the logarithm of base 2 of fold change.

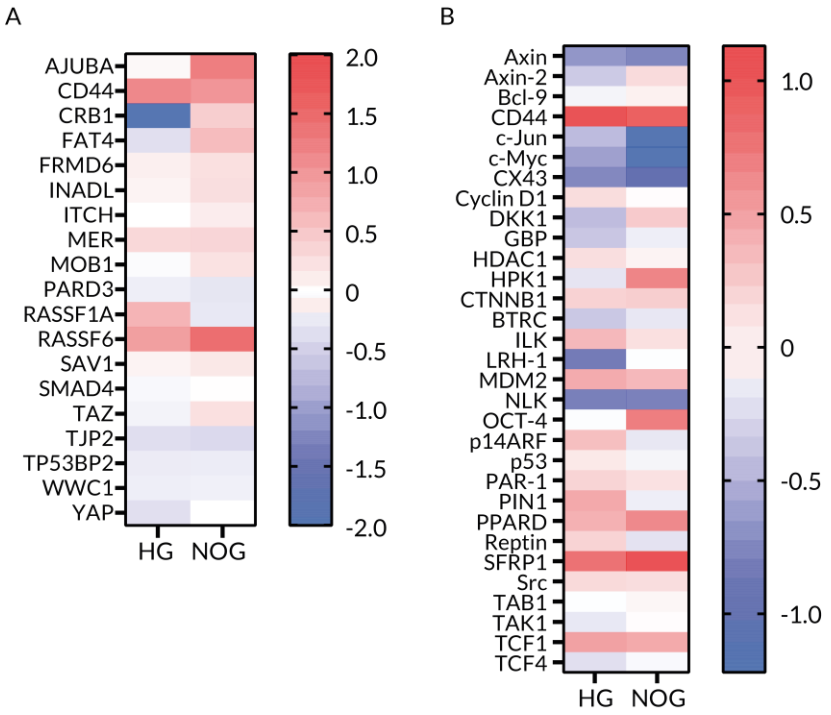

Figure 39. CLN3 KO has a significant impact on Hippo signaling at the transcriptional level in HEK cells starved in no glucose medium as revealed by Ingenuity Pathway Analysis. A. Heatmap represents the logarithm of base 2 of fold change in expression of a given gene involved in Hippo signalling in the CLN3 KO/WT NGS dataset. Genes are listed alphabetically. B. Heatmap represents the logarithm of base 2 of fold change in expression of a given gene involved in Wnt-β-catenin signalling in the CLN3 KO/WT NGS dataset. Genes are listed alphabetically.

Phosphorylation of YAP proteins at serine 127 (Ser127) by LATS1/2 or NDR1/2 promotes their cytoplasmic localization and degradation (Ibar and Irvine, 2020). Therefore, a lower ratio of phosphorylated to total YAP suggests that YAP is more active in CLN3 KO HEK cells under both, normal conditions (Figure 40) and starvation (Figure 41).

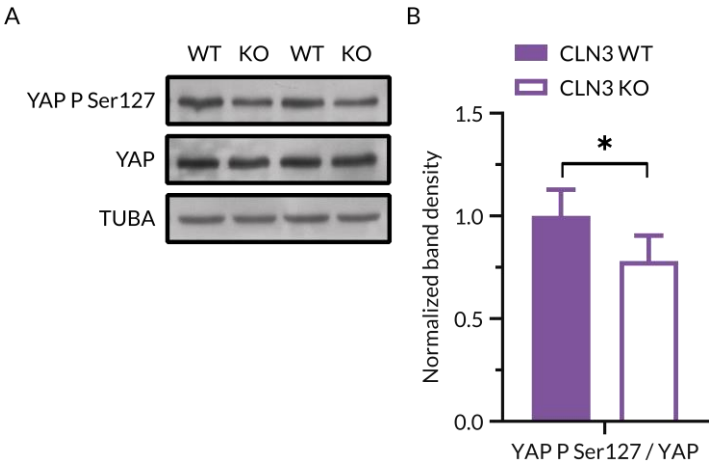

Figure 40. The activity of YAP is elevated in CLN3 KO HEK cells grown in a high glucose medium. A. Immunoblot of YAP with α-Tubulin as a loading control in whole cell lysates of CLN3 HEK cells grown in high glucose medium. B. Band density quantifications from the western blot represented in A. Graph represents mean ± SD of experimental triplicates and differences were significant based on the Student's t-test, $p < 0.05$ (*), $p < 0.01$ (**), $p < 0.001$ (***); SD: standard deviation.

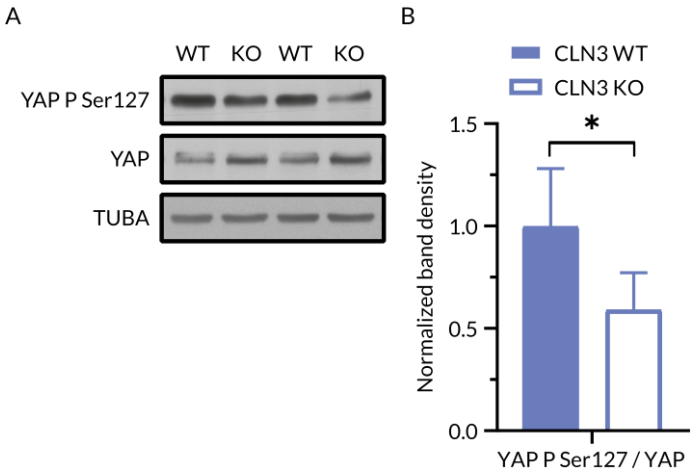

Figure 41. The activity of YAP is increased in CLN3 KO HEK cells starved in no glucose medium. A. Immunoblot of YAP with α-Tubulin as a loading control in whole cell lysates of CLN3 HEK cells starved in no glucose medium. B. Band density quantifications from the western blot represented in A. Graph represents mean ± SD of experimental triplicates and differences were significant based on the Student's t-test, $p < 0.05$ (*), $p < 0.01$ (**), $p < 0.001$ (***); SD: standard deviation.

3.3.2. mTOR-S6K1 signaling is substantially affected by CLN3 KO in HEK cells

Protein kinase mTOR integrates diverse environmental signals, including growth factors, availability of nutrients and energy, to tailor material accumulation and metabolism by controlling critical cellular processes, such as autophagy, lipid and protein synthesis. Interestingly, the aforementioned Hippo-YAP pathway is controlled by the mTOR signalling, which provides input concerning the insulin pathway and nutrients availability (Ibar and Irvine, 2020). mTOR plays an essential role in maintaining cellular and physiological homeostasis (Liu and Sabatini, 2020).

Pathway analysis performed on our transcriptome data demonstrated that CLN3 KO has a significant impact on mTOR and S6K1 signaling in both, high- and no glucose conditions. The following heatmap presents the effect of CLN3 KO on the expression of genes implicated in mTOR signalling (Figure 42). As stated before, shades of blue indicate decreased gene expression, while shades of red, in contrast, higher gene expression in CLN3 KO HEK cells inferred from the logarithm of base 2 of fold change value.

Noteworthy, the mTOR-S6K1 axis is an essential part of the metabolic pathways network, since it combines intracellular and extracellular signals to control nutrient driven metabolic pathways. Under favourable conditions for growth, S6K1 is activated by phosphorylation at threonine 389 (Thr389) mediated by mTORC1. Subsequently, phosphorylation of canonical S6K1 targets, such as RPS6 at serine 235 (Ser235), leads to global initiation of translation (Arif et al., 2019).

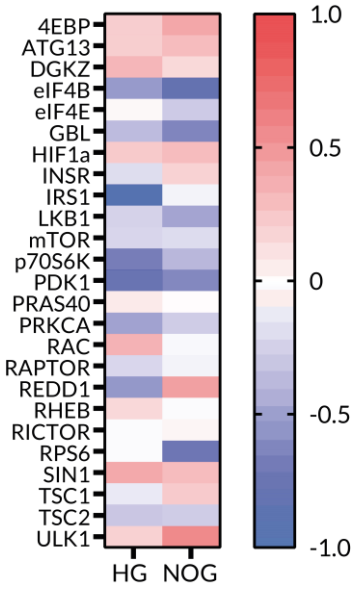

Figure 42. mTOR and p70 S6 Kinase signaling is significantly affected by CLN3 KO at the transcriptional level in both, high- and no glucose conditions as revealed by Ingenuity Pathway Analysis. Heatmap represents the logarithm of base 2 of fold change in expression of a given gene in the CLN3 KO/WT NGS dataset. Genes are listed alphabetically.

Intriguingly, only the ratio of phosphorylated RPS6 to total protein is substantially higher in CLN3 KO HEK cells grown in high glucose medium, while phosphorylation of S6K1 is not significantly changed (Figure 43). We observed an increased ratio of phosphorylated S6K1 and RPS6 to total protein in CLN3 KO HEK cells under starvation (Figure 44), which suggests the higher activity of S6K1 and mTORC1. One should also consider that tested residue of RPS6 can be phosphorylated by multiple protein kinases besides S6K1, including protein kinases A and C (Biever et al., 2015).

After activation, mTORC2 phosphorylates numerous AGC kinases, such as Akt, typically to reinforce their activity and stability. Diverse residues of TSC1 and TSC2 are phosphorylated by different kinases, such as Akt, to adjust mTORC1 activity (Lamming and Bar-Peled, 2019). The activity of mTORC2 is not changed in CLN3 KO HEK cells grown in a normal medium based on the unaltered ratio of Akt phosphorylated at serine 473 (Ser473) to total protein. The activity of Akt, which phosphorylates TSC2 at threonine 1462 (Thr1462), also remains unaffected (Figure 45). The pathway should be further studied to determine the role of their downstream effectors in Batten disease pathogenesis.

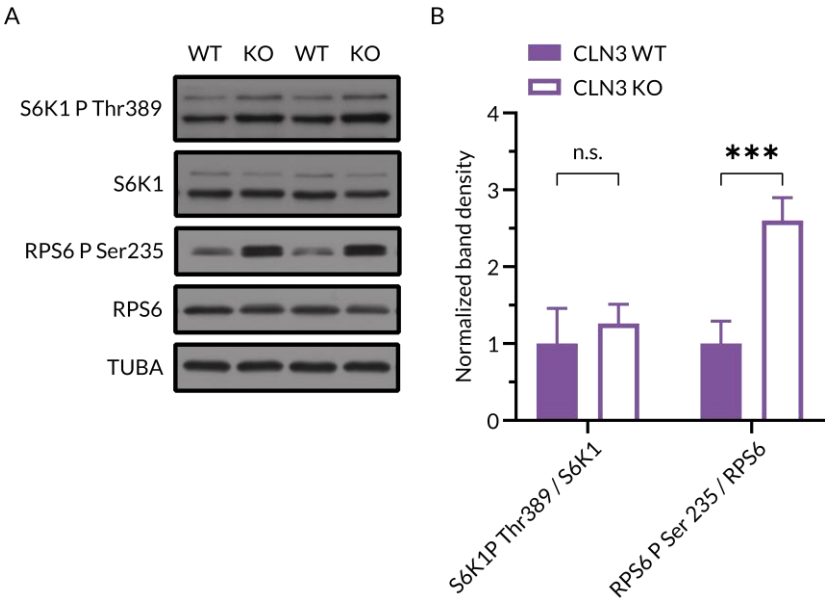

Figure 43. The ratio of phosphorylated RPS6 to total protein is significantly increased in CLN3 KO HEK cells grown in a high glucose medium. A. Immunoblot of S6K1 and RPS6 with α-Tubulin as a loading control in whole cell lysates of CLN3 HEK cells grown in high glucose medium. B. Band density quantifications from the western blot represented in A. Graph represents mean ± SD of experimental triplicates and differences were significant based on the Student's t-test, p < 0.05 (*), p < 0.01 (**), p < 0.001 (***); SD: standard deviation.

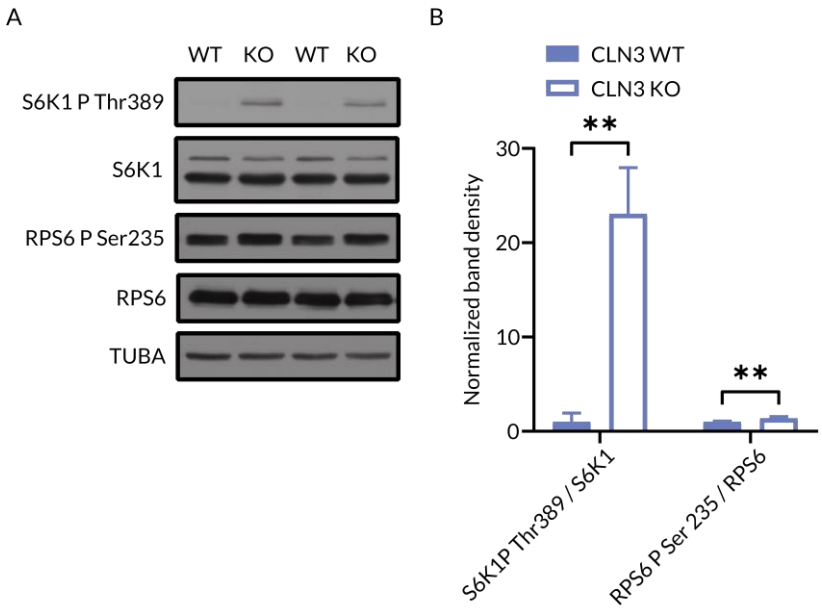

Figure 44. The ratio of phosphorylated S6K1 and S6 to total protein is substantially higher in CLN3 KO HEK cells starved in no glucose medium. A. Immunoblot of S6K1 and RPS6 with α-Tubulin as a loading control in whole cell lysates of CLN3 HEK cells starved in no glucose medium. B. Band density quantifications from the western blot represented in A. Graph represents mean ± SD of experimental triplicates and differences were significant based on the Student's t-test, p < 0.05 (*), p < 0.01 (**), p < 0.001 (***); SD: standard deviation.

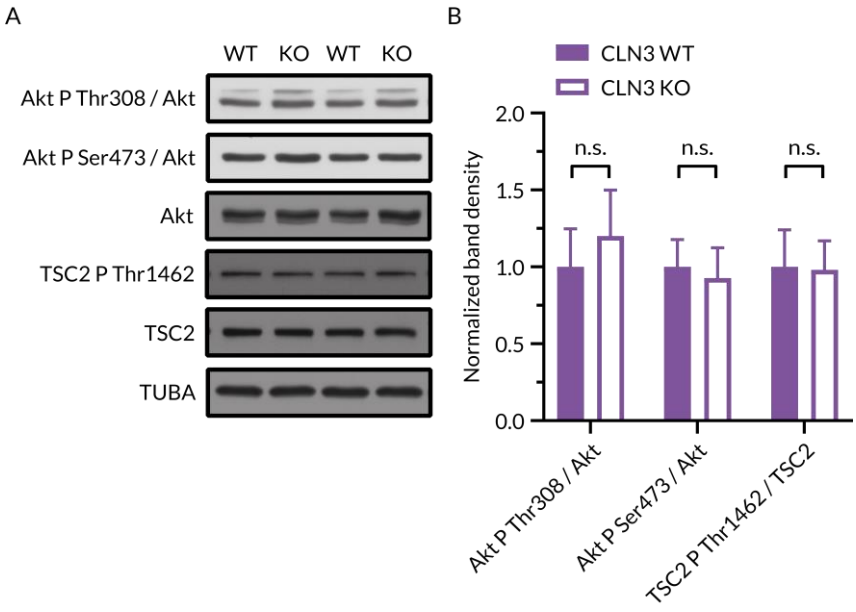

Figure 45. The activity of Akt is not significantly altered in CLN3 KO HEK cells grown in a high glucose medium. A. Immunoblot of Akt and TSC2 with α-Tubulin as a loading control in whole cell lysates of CLN3 HEK cells grown in high glucose medium. B. Band density quantifications from the western blot represented in A. Graph represents mean ± SD of experimental triplicates and differences were significant based on the Student's t-test, p < 0.05 (*), p <0.01 (**), p <0.001 (***); SD: standard deviation.

3.3.3. Integrated stress response and unfolded protein response are upregulated in CLN3 KO HEK cells starved in no glucose medium

The integrated stress response (ISR) is a signalling network that reprograms gene expression due to diverse environmental and pathological conditions such as proteostasis defects, nutrient deprivation and oxidative stress. These stresses are recognised by specialized kinases: PKR, HRI, GCN2 and PERK. All four ISR sensors phosphorylate the eIF2α at serine 51 (Ser51) to inhibit protein synthesis and initiate selective translation. PERK is a transmembrane protein kinase of the ER that activates itself by oligomerization and autophosphorylation at threonine 981 (Thr981) due to ER stress (Costa-Mattioli and Walter, 2020; Parmar et al., 2012). Likewise, the unfolded protein response (UPR) is a network of signalling pathways responsible for reprograming gene transcription, mRNA translation and protein modifications to maintain proteostasis and ER functions. Noteworthy, PERK is a common sensor of ISR and UPR; therefore, eIF2 signalling is involved in both networks (Costa-Mattioli and Walter, 2020).

Mentioned eIF2 signaling is significantly affected by CLN3 KO in HEK cells in both, high glucose and no glucose condition as shown by pathway analysis. Moreover, CLN3 KO had a significant impact on UPR signalling at the transcriptional level in HEK cells starved in no glucose medium. The heatmap below demonstrates the influence of CLN3 KO on the expression of genes associated with eIF2 signalling (Figure 46). As described previously, shades of blue imply decreased gene expression in CLN3 KO HEK cells and shades of red, on contrary, increased gene expression in CLN3 KO HEK cells, inferred from values of the logarithm of base 2 of fold change.

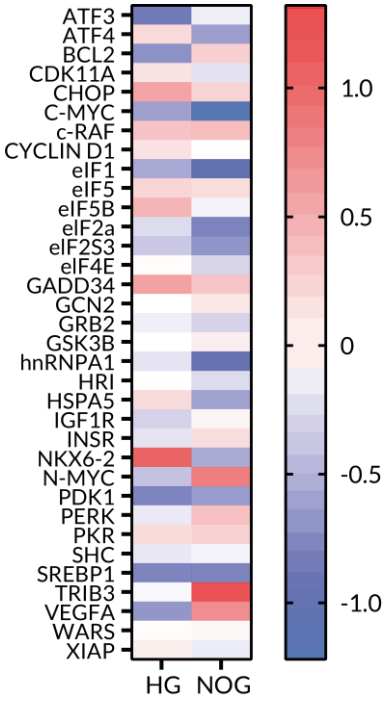

Figure 46. CLN3 KO has a substantial impact on eIF2 alpha signalling at the transcriptional level in HEK cells starved in no glucose medium as revealed by Ingenuity Pathway Analysis. Heatmap represents the logarithm of base 2 of fold change in expression of a given gene in the CLN3 KO/WT NGS dataset. Genes are listed alphabetically.

Moreover, CREB is activated by phosphorylation at serine 133 (Ser133) by several signalling pathways such as calcium and stress signalling. It is involved in various processes of the developing and mature nervous system by controlling the expression of crucial target genes, while its function is modulated by ATF4 (Belgacem and Borodinsky, 2017). We did not observe any statistically significant differences in levels of ER stress and ISR markers in cells grown in a normal medium (Figure 47). Consistently with our transcriptome data, unfolded protein response and integrated stress response are upregulated in CLN3 KO HEK cells starved in no glucose medium what can be inferred from a higher ratio of phosphorylated PERK, eIF2α and CREB to total protein (Figure 48).

Furthermore, activator protein 1 (AP-1) is a transcription factor constituted of one protein of the Jun family and one protein of the Fos family, also implicated in vital regulatory cell functions, such as differentiation, proliferation and apoptosis. Noteworthy, AP-1 and β-catenin cooperate physically and functionally to control TCF-dependent genes (Toualbi et al., 2007). Under ER stress, IRE1α activates chaperone genes and JNK (Urano et al., 2000), which in turn increases transcription activity of AP-1 by phosphorylation of c-JUN on the serine 73 (Ser73). Besides ER stress, JNK is activated due to inflammatory signals, fluctuations in levels of reactive oxygen species and other stress stimuli (Yarza et al., 2016). Thereby, a lower ratio of phosphorylated to total c-JUN suggests that JNK and c-JUN are less active in CLN3 KO HEK cells grown in high glucose medium (Figure 49).

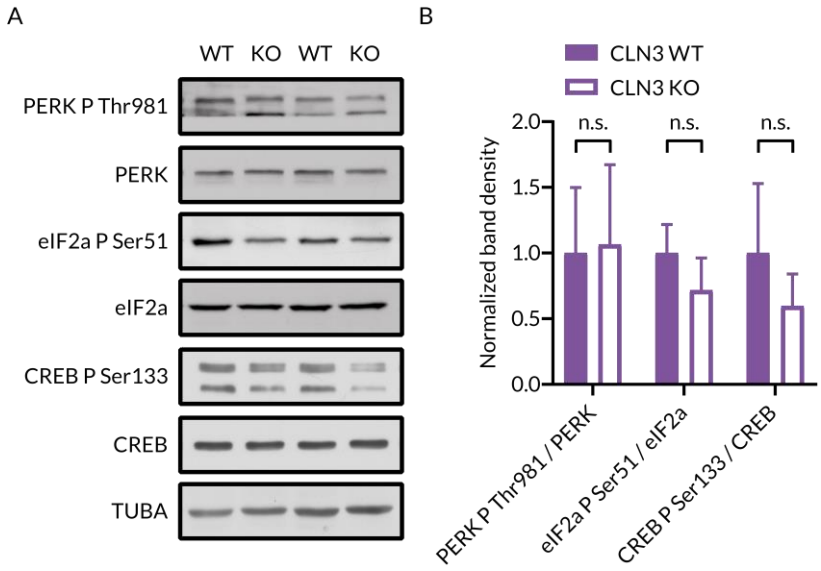

Figure 47. The activity of ER stress markers is not significantly changed in CLN3 KO HEK cells grown in a high glucose medium. A. Immunoblot of PERK, eIF2 alpha and CREB, with α-Tubulin as a loading control in whole cell lysates of CLN3 HEK cells grown in high glucose medium. B. Band density quantifications from the western blot represented in A. Graph represents mean ± SD of experimental triplicates and differences were significant based on the Student's t-test, $p < 0.05$ (*), $p < 0.01$ (**), $p < 0.001$ (***); SD: standard deviation.

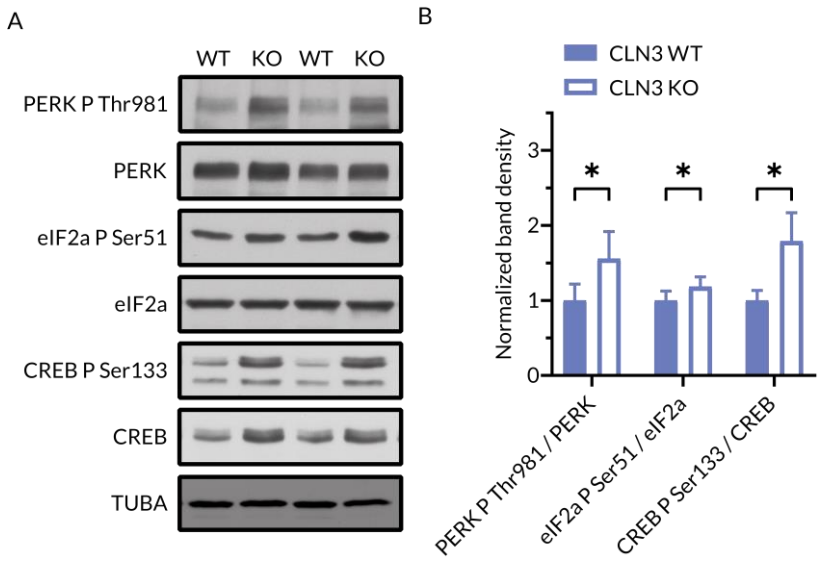

Figure 48. The activity of ER stress markers is significantly increased in CLN3 KO HEK cells starved in no glucose medium. A. Immunoblot of PERK, eIF2α and CREB with α-Tubulin as a loading control in whole cell lysates of CLN3 HEK cells starved in no glucose medium. B. Band density quantifications from the western blot represented in A. Graph represents mean ± SD of experimental triplicates and differences were significant based on the Student's t-test, $p < 0.05$ (*), $p < 0.01$ (**), $p < 0.001$ (***); SD: standard deviation.

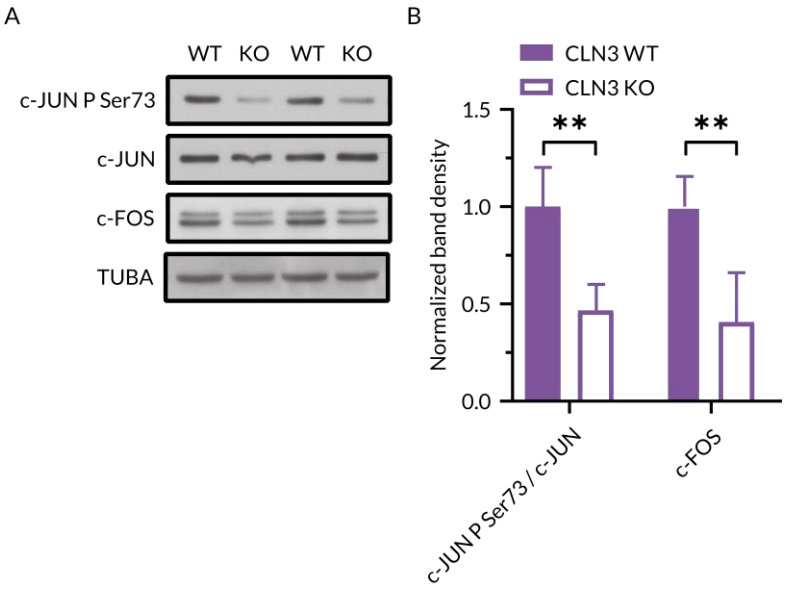

Figure 49. The activity of JNK is significantly decreased in CLN3 KO HEK cells grown in a high glucose medium. A. Immunoblot of c-JUN and c-FOS with α-Tubulin as a loading control in whole cell lysates of CLN3 HEK cells grown in high glucose medium. B. Band density quantifications from the western blot represented in A. Graph represents mean ± SD of experimental triplicates and differences were significant based on the Student's t-test, $p < 0.05$ (*), $p < 0.01$ (**), $p < 0.001$ (***); SD: standard deviation.

4. Discussion

We aimed to study metabolic effects of CLN3 deficiency, reveal the role of organelle crosstalk in Batten disease course and identify signaling pathways relevant for the pathology in HEK cells lacking CLN3. The cellular model was modulated to respond to different metabolic environments like starvation for the purpose of investigating the impact of CLN3 deficiency on metabolism. Provided data should be considered proof of concept and further reproduced in cellular and animal models of Batten disease, including patients cells, to conclusively link presented observations to the disorder.

Our initial experimental model was a HeLa cell line lacking CLN3 and respective WT control, a kind gift from Dr PD Guido Hermey. CLN3 KO HeLa cells have significantly impaired proteolytic activity and mild mitochondrial dysfunction. Informed of modified metabolism (Warburg et al., 1927; reviewed by Vander Heiden et al., 2009), extensive genomic rearrangements and significantly different expression patterns in HeLa cells (Landry et al., 2013), we decided to generate another cellular model modifying HEK cell line with CRISPR/Cas9 technology. Choice of the cell line was motivated by its popularity in the field of cellular signalling related to lysosomal function and NCL, which allows us to compare and possibly combine our data with published and confidentially shared results.

The model, CLN3 KO HEK cells used throughout this project was genotyped by sequencing like other experimental models in the field of NCL (Yasa et al., 2020) due to lack of reliable, specific primary antibody (Mirza et al., 2019; Nelson et al., 2017). The situation will hopefully change in the immediate future and a suitable primary antibody for CLN3 will allow for confirmation of the genotype of experimental models in use. Since cellular systems seem to respond to stress differently depending on its acute or chronic character, we decided to perform 24 hours treatment to simulate the protracted nature of the disease better. Our lab demonstrated before that acute and chronic disturbance of the mitochondrial respiratory chain function impacts lysosomal biogenesis disparately: acute stress activates AMPK- and TFEB/MITF-dependent lysosomal biogenesis, whereas chronic dysfunction represses TFEB/MITF transcriptional activity and lysosomal biogenesis. Change in response was observed after 12-24 hours of treatment (Fernández-Mosquera et al., 2017).

4.1. CLN3 KO results in mitochondrial dysfunction in HEK and HeLa cells

The arrangement of a eukaryotic cell into organelles enables spatial and temporal isolation of incompatible biochemical processes, which must be coordinated to ensure proper cellular function (Cohen et al., 2018). Mitochondria and lysosomes play a key role in cellular metabolism and signalling, including autophagy, proliferation and cell death. Mitochondrial dysfunction was reported in most of the lysosomal storage diseases, and reciprocally, an impaired lysosomal function is observed in multiple mitochondrial diseases. Moreover, defective mitochondria-lysosome crosstalk was described in several neurodegenerative diseases (Deus et al., 2019; Raimundo and Krisko, 2019).

Although the implication of potential involvement of mitochondria in the pathogenesis of Batten disease was for the first time expressed decades ago (Zeman and Donahue,1963) and later well supported by evidence pointing at energy-linked excitotoxicity (Jolly et al., 2002), we are the first to

offer a complex characterization of mitochondrial biogenesis and function in CLN3 deficient HEK grown in normal conditions and exposed to stress through starvation. Several publications present perturbed mitochondria in NCL models (Luiro et al., 2006; Fosalle et al., 2004; Das et al., 2001, 1999; March et al., 1995) and emphasise the role of ER stress in CLN3 pathology (Shematorova and Shpakovski, 2020; Marotta et al., 2017; Wu et al., 2014; Yoon et al., 2011).

Batten disease and other NCL are characterized by selective loss of inhibitory GABAergic interneurons, which are rich in mitochondria, and therefore particularly sensitive to compromised energy production (Luiro et al., 2001). Moreover, neuron loss is observed mainly in the most metabolically active and rich in mitochondria brain areas (Braak and Goebel, 1978). Thereby, mitochondria are considered to contribute to Batten disease pathogenesis (Shematorova and Shpakovski, 2020). Impairment of mitochondrial function correlated with disease progression was reported in several CLN5 KO cell models (Doccini et al., 2020), while CLN5 is known to interact with CLN3 (Scifo et al., 2013; Yasa et al., 2021). Hence, our data are consistent with available literature and give a more detailed insight into the impact of CLN3 defect on mitochondrial function.

4.1.1. Mitochondrial and ER biogenesis is transcriptionally repressed in starved CLN3 KO HEK cells

Considering existing literature, one could expect repressed mitochondrial biogenesis like in some lipid storage diseases (Yambire et al., 2019), it can be surprising that CLN3 KO did not globally affect the biogenesis of any of the organelles in cells grown in a high glucose medium. However, we observe transcriptionally repressed mitochondrial and ER biogenesis in CLN3 KO HEK cells starved in no glucose medium. Moreover, around half of mitochondrial and ER genes are differentially expressed. CLN3-loss-of-function in HEK cells substantially impacts the expression of genes encoding OxPhos proteins, upregulating them under normal conditions and downregulating under starvation. Particularly, 60% of these genes are differentially expressed in CLN3 KO HEK cells starved in no glucose medium consistently with global mitochondrial biogenesis repression at the transcriptional level.

Intriguingly, transcriptional repression of mitochondrial biogenesis was reported only in symptomatic NPC1 KO mice brains, while pre-symptomatic presented the opposite trend (Yambire et al., 2019). A study of organelle biogenesis in pre-symptomatic and symptomatic Batten disease models would allow determining how mitochondrial and ER genes expression is affected in different tissues and phases of the disease. Additionally, evaluation of organelle biogenesis in cells collected from patients throughout the disease would offer a valuable insight into the role of organelle crosstalk in Batten disease pathogenesis.

Since we detected a substantially decreased level of OxPhos proteins in whole cell extracts coming from CLN3 KO HEK cells, we also evaluated the level of native OxPhos complexes in mitochondria isolated from cells grown in high glucose medium and did not discern any significant disparity. Our result can be plausibly explained by reduced mitochondrial mass per cell correspondent with considerably reduced mtDNA copy number and observations in other lysosomal defects (Yambire et al.,

2019). Consequently, the mitochondrial network should be comprehensively assessed in Batten disease models by imaging experiments to determine the impact of CLN3 loss of function on mitochondrial morphology and mass. Similarly, ER and peroxisomal morphology are worth further evaluation.

4.1.2. Mitochondrial function is compromised due to CLN3 KO in HEK and HeLa cells

The said reduction in the level of OxPhos proteins in whole cell extracts is consistent with impaired mitochondrial respiration concluded from a decline in oxygen consumption rate in CLN3 KO HEK cells. Importantly, it is not compensated by an increase in glycolysis which would be reflected in the extracellular acidification rate. Predictably, we also observed lowered mitochondrial membrane potential and increased mitochondrial ROS level indicated by higher mitochondrial superoxide levels in CLN3 KO HEK cells. Similarly, we noticed a mild deficiency in mitochondrial respiration and a slight increase in mitochondrial superoxide levels in CLN3 KO HeLa cells.

Mitochondria utilize oxygen in the respiratory chain to produce ATP and ROS as a by-product. Increased ROS levels can induce intracellular cascades of oxidative stress through DNA and protein oxidation, and induction of lipids peroxidation in the plasma membrane (Kausar et al., 2018). Oxidative stress negatively affects diverse molecules, cellular structures and functions contributing to pathological changes observed in inflammation, ageing, neurodegeneration and cancer (Kudryavtseva et al., 2019; Rimessi et al., 2016; Newsholme et al., 2007; van der Vliet et al., 2018).

Mitochondrial superoxide production is strongly dependent on mitochondrial membrane potential. Expectedly, mitochondrial uncoupling, i.e., decrease in the electrochemical proton gradient in mitochondria, is recognized as a cytoprotective strategy under oxidative stress in diabetes, injury or ageing (Cadenas, 2018). Hence, the observed reduction in mitochondrial membrane potential can be caused by respiratory chain defects but also it can be a part of cellular response to oxidative stress. In many neurodegenerative diseases, mitochondrial dynamics and function are compromised, resulting in reduced ATP generation, excess reactive oxygen species and apoptosis (Jodeiri Farshbaf and Ghaedi, 2017). Additionally, the failure of antioxidant defence is an important factor in neurodegeneration (Sayre et al., 2008).

Additionally, CLN3 KO HEK cells have lower viability, which might be a direct consequence of mitochondrial malfunction, therefore insufficient ATP synthesis. On the other hand, only a major reduction in OxPhos activity leads to a significant decline in ATP production. Considerably impaired mitochondrial ATP synthesis can be compensated as long as glucose is available, hence, overall ATP level may remain unchanged (Area-Gomez et al., 2019). Assessment of mitochondrial and overall ATP production would allay the doubts. Noteworthy, mitochondrial pathological signalling can result in disease regardless of ATP production (Raimundo, 2014). Reduced cell viability of CLN3 KO HEK cells upon both, normal and starvation conditions probably results from multiple aberrations, e.g., in calcium signalling and redox homeostasis, and further study on apoptotic signalling may help elucidate the reason.

All examined aspects were consistent for high- and no glucose conditions and may play a role in disease progression; therefore, it is important to determine their exact cause in future. Observed mitochondrial malfunction may potentially originate from impaired calcium and lipid homeostasis. Common 1kb deletion in CLN3 gene adversely impacts abundance and activity of numerous lysosomal proteins, degradation of lipid droplets and composition of membrane lipids (Schmidtke et al., 2019; Sleat et al., 2019). CLN3-deficient cells are more sensitive to thapsigargin, which increases cytosolic calcium and induces calcium-mediated apoptosis (Chang et al., 2007). Additionally, calcium was implied to play a role in neuronal cell death in CLN3 knock-down SH-SY5Y cells (Warnock et al., 2013; an Haack et al., 2011). Another study indicated significant differences in ER, mitochondrial and lysosomal calcium pools, and in store-operated calcium uptake in murine CLN3$^{\Delta ex7/8}$ neuronal precursor cells (Chandrachud et al., 2015). Aberrant metabolic and calcium signalling was also reported in murine CLN3$^{\Delta ex7/8}$ astrocytes and suggested to contribute to neuronal dysfunction and death (Bosch and Kielian, 2018).

Organelle crosstalk plays an important role in calcium homeostasis. Lysosomal calcium release by transient receptor potential mucolipin 1 promotes calcium transfer to mitochondria, which is mediated by the tethering of mitochondria-lysosome contact sites (Peng et al., 2020). Abnormal ER-mitochondria crosstalk can also affect calcium uptake by mitochondria and, as a result, impact overall calcium signalling and mitochondrial bioenergetics. Moreover, a substantial increase in mitochondrial calcium can reduce membrane potential, induce mitochondrial malfunction and cell death. Interestingly, several proteins linked to neurodegenerative disorders, including α-synuclein, regulate mitochondria-associated ER membranes (Area-Gomez et al., 2019).

Noteworthy, peroxisomes play a key role in lipid and ROS/RNS metabolism and constantly interact functionally and physically with other organelles, in particular with mitochondria and ER. Peroxisomes contribute to several pathological processes of non-peroxisomal origin, including cancer, ageing and Amyotrophic Lateral Sclerosis (Sargsyan and Thoms, 2019; Islinger et al., 2018). Moreover, peroxisomes are involved in intracellular calcium dynamics (Sargsyan et al., 2021), which can play a very important part in Batten disease progression. We did not observe any difference in levels of peroxisomal proteins, which does not implicate proper peroxisomal function and morphology. Hence, an in-depth assessment of peroxisomal function and morphology would provide valuable insight into the role of organelle crosstalk in the pathology of Batten disease.

There is a growing body of evidence of the effectiveness of calcium channel modulators in ameliorating phenotype in LSD (Yu et al., 2020; Scotto Rosato et al., 2019), including calcium channel blocker, verapamil tested in CLN3 disease neuronal cells (Petcherski et al., 2019). Hence, it would be very interesting to verify if these compounds have also a positive impact on mitochondrial function in NCL experimental models. Weaken neurons may benefit from improved mitochondrial respiration even though OxPhos deficiency is not a primary cause of the disease (Area-Gomez et al., 2019).

4.2. CLN3 KO in HEK cells has a substantial impact on proliferation signalling and stress response mechanisms

Improved understanding of the pathways involved in the crosstalk of organelles and affected by their dysfunction may help in finding therapeutic targets that are closer to the source of the problem. Manipulation of the pathological signalling can potentially alleviate symptoms and decelerate disease progression (Deus et al., 2019; Raimundo, 2014). CLN3 and CLN5 form an endosomal complex, which is critical for the efficient endosome-to-TGN trafficking of sortilin. Defective recycling results in impaired lysosomal function (Yasa et al., 2021, 2020). CLN3 plays an important role in cellular and lysosomal homeostasis. The reduced level of multiple lysosomal enzymes in murine $Cln3^{\Delta ex7/8}$ cerebellar cells impacts the lysosomal proteome, the associated degradation of substrates and secondary cellular protein trafficking processes. Hence, CLN3 is functionally related to many other proteins and signaling pathways in neuronal cells (Schmidtke et al., 2019).

4.2.1. Hippo-YAP signaling is significantly affected by CLN3-loss-of-function in HEK cells

The Hippo-YAP signalling pathway integrates signals that modulate cellular proliferation and differentiation. It responds to multiple environmental cues like energy and ER stress. Pathway analysis revealed that YAP is probably activated and plays an important role as a transcription factor in HEK cells lacking CLN3. Furthermore, the Hippo signaling pathway is significantly affected at the transcriptional level in CLN3 KO HEK cells in both, high glucose and no glucose condition.

Phosphorylation of YAP proteins at Ser127 by LATS1/2 promotes their cytoplasmic localization and degradation. The NDR1/2 can phosphorylate YAP at the same sites as LATS1/2 to negatively regulate its activity. We detected a lower ratio of phosphorylated to total YAP, which suggests that YAP is more active in CLN3 KO HEK cells. Notably, the activity of YAP proteins is also regulated by Src family kinases and AMPK through phosphorylation at other sites (Ibar and Irvine, 2020). Therefore, phosphorylation of other residues of YAP protein should be examined to describe its activity in detail. A study of the activity of its upstream regulators, like AMPK, and potential changes in corresponding signaling pathways would be very informative to understand the role of pathological signaling in Batten disease progression.

It was recently reported that YAP promotes autophagosome formation through physical interaction with TFEB. Importantly, activation of autophagy in the presence of lysosome inhibition leads to excessive autophagosome accumulation and as a result, cellular dysfunction. Disruption of YAP function as a cofactor of TFEB can potentially ameliorate the phenotype observed in several LSD through prevention of autophagosome accumulation, and consequent inhibition of apoptosis (Ikeda et al., 2021). It would merit consideration if the enhanced activity of YAP proteins was identified in Batten disease models. Unfortunately, there are no clinically viable drugs that directly target Hippo-YAP signalling (Nguyen and Yi, 2019).

4.2.2. mTOR-S6K1 signalling is considerably altered due to CLN3 KO in starved HEK cells

Protein kinase mTOR combines a variety of environmental signals, such as growth factors, availability of nutrients and energy, to adapt material accumulation and metabolism by adjusting vital cellular processes, such as autophagy, lipid and protein synthesis. Therefore, mTOR plays a crucial role in maintaining cellular and physiological homeostasis (Liu and Sabatini, 2020). The hippo-YAP signalling pathway is modulated by the mTOR signalling providing input from the insulin pathway and nutrients. Furthermore, mTORC1 inhibits autophagy, which can impact and be affected by YAP (Ibar and Irvine, 2020). The activity of the Akt-mTOR pathway was reported to be increased in CLN3 patients fibroblasts (Vidal-Donet et al., 2013).

Pathway analysis completed on our RNA-seq dataset revealed that CLN3 KO had a significant impact on mTOR and S6K1 signaling at the transcriptional level in both, high- and no glucose conditions. We also observed an increased ratio of phosphorylated S6K1 (Thr389) and RPS6 (Ser235) to total protein in CLN3 KO HEK cells starved in no glucose medium, which implies the higher activity of S6K1 and mTORC1. On the other hand, the activity of mTORC1 and S6K1, as well as mTORC2 and Akt seems to remain unaltered due to CLN3 KO under normal conditions. Noteworthy, multisite phosphorylation of S6K1 controls substrate selection and thereby downstream effects (Arif et al., 2019). Similarly, the tested residue of RPS6 can be phosphorylated by multiple kinases besides S6K1 (Biever et al., 2015).

Upstream regulators and downstream effectors of mTOR and S6K1 should therefore be studied to determine the cause and consequences of its higher activity and its role in Batten disease. Since mitochondria and lysosomes play essential roles in metabolism, they are tightly integrated with key hubs of cellular signalling, namely AMPK and mTOR, to preserve the balance between catabolism and anabolism (Deus et al., 2019). It is thus a further reason to study AMPK signalling in CLN3-deficient models to fully explore the effects of CLN3-loss-of-function on metabolism.

4.2.3. Integrated stress response and unfolded protein response are upregulated in starved CLN3 KO HEK cells

The ISR is a central signalling network that aids the cell in restoring homeostasis by reprogramming gene expression. It can be induced by various conditions, such as proteostasis defects, nutrient deprivation, viral infection and oxidative stress. Interestingly, ISR activation is linked to age-related cognitive disorders and mutations in its crucial components are associated with intellectual disability (Costa-Mattioli and Walter, 2020). Similarly, the UPR is a network of signalling pathways responsible for reprograming gene transcription, mRNA translation and protein modifications to restore proteostasis and maintain ER functions (Hetz, 2020). If the just outlined mechanisms fail to restore homeostasis, apoptosis can be activated through the intrinsic pathway to prevent further damage at the level of tissue or organism. Noteworthy, PERK is a common sensor of ISR and UPR; therefore, eIF2 signalling is involved in both networks (Costa-Mattioli and Walter, 2020).

The potential role of oxidative and ER stress in Batten disease was discussed in detail in Marotta et al. (2017), as well as in Shematorova and Shpakovski (2020). Excess of cellular ROS causes damage to

proteins, nucleic acids, lipids, membranes and organelles, which can result in activation of apoptosis. CLN3 in Drosophila melanogaster interacts genetically with key elements of stress signalling pathways, such as JNK, and components of stress granules. CLN3 loss of function resulted in hypersensitivity to oxidative stress but not to other physiological stresses. Although CLN3 mutant flies can sense oxidative stress properly, their ability to react and detoxify ROS is compromised (Tuxworth et al., 2011). Importantly, an accumulation of ROS was observed in CLN3 patients fibroblasts (Vidal-Donet et al., 2013). Interestingly, resveratrol was reported to resolve oxidative and ER stress, as well as protect against apoptosis in Batten disease lymphoblast cells (Yoon et al., 2011). Moreover, a study of ER stress in SH-SY5Y cells indicates that lack of CLN3 function results in deregulation of the ER stress response and as a result, in apoptosis. On the contrary, increased CLN3 gene expression led to a higher level of ER chaperone BiP and a reduced level of CHOP (Wu et al., 2014). Therefore, ER and oxidative stress are considered potential key factors in Batten disease progression (Shematorova and Shpakovski, 2020).

Our pathway analysis demonstrated that eIF2 signaling is significantly affected in CLN3 KO HEK cells in both, high glucose and no glucose condition. Furthermore, UPR signalling is significantly altered in CLN3 KO HEK cells starved in no glucose medium. Consistently with our transcriptome data, ISR and UPR are upregulated in CLN3 KO HEK cells starved in no glucose medium what can be inferred from a higher ratio of phosphorylated PERK, eIF2α and CREB to total protein. A study on downstream effectors of eIF2α, such as ATF4 and proapoptotic CHOP, would provide us with more information about the potential involvement of ISR in Batten disease pathogenesis.

Under ER stress, IRE1α activates chaperone genes and JNK (Urano et al., 2000), which in turn promotes transcription activity of AP-1 by phosphorylation of c-JUN. Besides ER stress, JNK is activated in response to inflammatory signals, fluctuations in levels of reactive oxygen species and other stress stimuli (Yarza et al., 2016). Hence, a lower ratio of phosphorylated to total c-JUN implicates that JNK and c-JUN are less active in CLN3 KO HEK cells grown in a high glucose medium. On the other hand, c-JUN can be also phosphorylated at the same site by vaccinia-related kinase 1 to induce c-JUN stabilization and accumulation (Sevilla et al., 2004), as well as by Cdk5, which regulates the JNK pathway both directly and indirectly (Sun et al., 2009). Importantly, JNK and Cdk5 have been implicated in neuronal-cell death mechanisms in neurodegenerative disorders (de Los Reyes Corrales et al., 2021; Gupta and Singh, 2019). Hence, further investigation of other pathways involved in UPR, such as IRE1α and ATF6, but also JNK and Cdk5 signaling would offer us a deeper insight into the exact role of that network in Batten disease progression.

ISR can be inhibited by ISRIB, a drug-like small molecule, which activates eIF2β and does not impair ISR's cytoprotective function (Costa-Mattioli and Walter, 2020). If induction of ISR was detected in Batten disease models, it would be worth considering the use of ISRIB in rescue trials. Overall, further research contingent on signalling pathways modulation would provide us essential elucidation of their utility as potential therapeutic targets.

4.3. Future perspective

Despite decades of dedicated research, a growing number of clinical trials (Specchio et al., 2021), the availability of multiple cellular (Minnis et al., 2020) and novel animal models (Johnson et al., 2019), the Batten disease mechanism remains elusive. Complete elucidation of CLN3 characteristics would allow determining the best combination therapy and deepening our understanding of other NCL and LSD. In the context of our data, they should be further reproduced in other cellular and animal models of Batten disease, including patients cells, to associate presented observations with the disorder.

Particularly, assessment of organelle biogenesis, morphology and function in patients fibroblasts harbouring different CLN3 mutations would deepen our understanding of the role of organelle crosstalk to the disease progression. Similarly, signaling pathways indicated to be significantly enriched by our transcriptome data analysis should be further studied in patients cells to elucidate the causes and consequences of their deregulation. Additionally, similar experiments performed on cellular models harbouring mutations in CLN3 post-translational modification motifs would facilitate the determination of their role in the CLN3 protein localization and function.

Besides mutation-specific effects, a study of tissue-specific phenotype would offer a valuable insight into grounds for the variable impact of CLN3 mutations in different organs. Just outlined research would help in the determination of disease mechanism and functional role for CLN3 in cellular homeostasis. Importantly, signalling pathways and organelle function can be experimentally manipulated to identify means to ameliorate phenotype and indicate potential therapeutic targets. Noteworthy, NCL proteins are considered to be a part of the same signalling pathway or network, while NCL have common clinical and pathological characteristics. Similar studies in other NCL models would therefore offer a useful insight into the role of NCL proteins and their interdependence.

5. Summary and conclusions

A eukaryotic cell is organized into organelles, whose coordinated function is critical for the health and proper function of a cell. Unsurprisingly, the dysfunction of a single organelle affects the condition of other organelles as a consequence of their strong interdependence (Deus et al., 2019; Sargsyan and Thoms, 2019). Unsurprisingly, impaired mitochondrial function was detected in most of the lysosomal storage diseases and aberrant mitochondria-lysosome crosstalk was observed in several neurodegenerative disorders (Deus et al., 2019; Raimundo and Krisko, 2019). Batten disease is a lysosomal storage disorder and the dominant cause of dementia in children, while its exact mechanism remains to be elucidated (Shematorova and Shpakovski, 2020). Therefore, we intended to improve understanding of the role of organelle crosstalk in the disease progression and deepen knowledge of signaling pathways that might be considered potential therapeutic targets in Batten disease.

Throughout the project presented in this thesis, we evaluated organelle biogenesis and function in CLN3 KO HEK cells and presented comprehensive evidence of mitochondrial dysfunction. Although we do not observe a significant global impact of CLN3 KO on organelle biogenesis at the transcriptional level in HEK cells grown in high glucose medium, we detected transcriptionally repressed mitochondrial and ER biogenesis in CLN3 KO HEK cells starved in no glucose medium. Interestingly, we noticed a substantial decrease in levels of proteins that belong to respiratory chain subunits, except for complex V, in whole cell extracts from CLN3 KO HEK cells under both, normal conditions and starvation. On the other hand, the level of native OxPhos complexes in mitochondria isolated from HEK cells grown in high glucose medium is not altered. Moreover, we report impaired mitochondrial respiration, elevated mitochondrial superoxide levels, reduced mitochondrial membrane potential and decline in cell viability in CLN3 KO HEK cells in both, high glucose and no glucose condition.

Additionally, pathway analysis performed on transcriptome data identified several signaling pathways that are significantly affected by CLN3-loss-of-function and may be relevant for Batten disease progression. Specifically, CLN3 KO in HEK cells had a significant impact on cell proliferation signalling, namely Hippo, mTOR, p70 S6K1, Wnt-β catenin signalling pathways, as well as stress response mechanisms, such as unfolded protein response and eIF2α signalling. Intriguingly, preliminary transcription factor analysis indicated that YAP, associated with Hippo signalling, seems to be a key regulator of the cellular response to the absence of CLN3. These findings were complemented by western blot experiments. We observe increased YAP activity in CLN3 KO HEK cells, implied by a reduced ratio of phosphorylated to total YAP, in both, high glucose and no glucose conditions. Likewise, the detected increased ratio of phosphorylated S6K1 to total protein in CLN3 KO HEK cells starved in no glucose medium implies the higher activity of said kinase and mTORC1. Moreover, integrated stress response and unfolded protein response are upregulated in CLN3 KO HEK cells starved in no glucose medium what can be inferred from a higher ratio of phosphorylated PERK, eIF2α and CREB to total protein.

These pathways can be modulated to potentially ameliorate phenotype, e.g., by calcium channel blockers or integrated stress response inhibitors. Altogether, our findings are consistent with available literature and reveal several prospective therapeutic targets that require further verification. Presented data should be considered proof of concept and replicated in cellular and animal models of Batten disease, including patients cells, to decisively connect provided observations to the disorder.

To conclude, we characterized organelle biogenesis and function and indicated signaling pathways that may play an important role in Batten disease. We are the first to provide an exhaustive demonstration of mitochondrial dysfunction in CLN3 KO cells.

6. Bibliography

A

Abdelmohsen K, Srikantan S, Yang X, et al. Ubiquitin-mediated proteolysis of HuR by heat shock. EMBO J. 2009;28(9):1271-1282. doi:10.1038/emboj.2009.67

Abdulkarim B, Nicolino M, Igoillo-Esteve M, et al. A Missense Mutation in PPP1R15B Causes a Syndrome Including Diabetes, Short Stature, and Microcephaly. Diabetes. 2015;64(11):3951-3962. doi:10.2337/db15-0477

Adams HR, Defendorf S, Vierhile A, Mink JW, Marshall FJ, Augustine EF. A novel, hybrid, single- and multi-site clinical trial design for CLN3 disease, an ultra-rare lysosomal storage disorder. Clin Trials. 2019;16(5):555-560. doi:10.1177/1740774519855715

Aldrich A, Bosch ME, Fallet R, et al. Efficacy of phosphodiesterase-4 inhibitors in juvenile Batten disease (CLN3). Ann Neurol. 2016;80(6):909-923. doi:10.1002/ana.24815

Alonso A, Sasin J, Bottini N, et al. Protein tyrosine phosphatases in the human genome. Cell. 2004;117(6):699-711. doi:10.1016/j.cell.2004.05.018

Amendola R, Cervelli M, Tempera G, et al., Spermine metabolism and radiation-derived reactive oxygen species for future therapeutic implications in cancer: an additive or adaptive response. Amino Acids. 2014;46(3):487-498. doi:10.1007/s00726-013-1579-9

An Haack K, Narayan SB, Li H, Warnock A, Tan L, Bennett MJ. Screening for calcium channel modulators in CLN3 siRNA knock down SH-SY5Y neuroblastoma cells reveals a significant decrease of intracellular calcium levels by selected L-type calcium channel blockers. Biochim Biophys Acta. 2011;1810(2):186-191. doi:10.1016/j.bbagen.2010.09.004

Antoun G, McMurray F, Thrush AB, et al., Impaired mitochondrial oxidative phosphorylation and supercomplex assembly in rectus abdominis muscle of diabetic obese individuals [published correction appears in Diabetologia. 2016 Feb;59(2):396-7]. Diabetologia. 2015;58(12):2861-2866. doi:10.1007/s00125-015-3772-8

Appu AP, Bagh MB, Sadhukhan T, Mondal A, Casey S, Mukherjee AB. Cln3-mutations underlying juvenile neuronal ceroid lipofuscinosis cause significantly reduced levels of Palmitoyl-protein thioesterases-1 (Ppt1)-protein and Ppt1-enzyme activity in the lysosome. J Inherit Metab Dis. 2019;42(5):944-954. doi:10.1002/jimd.12106

Area-Gomez E, Guardia-Laguarta C, Schon EA, Przedborski S. Mitochondria, OxPhos, and neurodegeneration: cells are not just running out of gas. J Clin Invest. 2019;129(1):34-45. doi:10.1172/JCI120848

Arif A, Jia J, Willard B, Li X, Fox PL. Multisite Phosphorylation of S6K1 Directs a Kinase Phospho-code that Determines Substrate Selection. Mol Cell. 2019;73(3):446-457.e6. doi:10.1016/j.molcel.2018.11.017

Artinian N, Cloninger C, Holmes B, Benavides-Serrato A, Bashir T, Gera J. Phosphorylation of the Hippo Pathway Component AMOTL2 by the mTORC2 Kinase Promotes YAP Signaling, Resulting in Enhanced Glioblastoma Growth and Invasiveness. J Biol Chem. 2015;290(32):19387-19401. doi:10.1074/jbc.M115.656587

Augestad LB, Diderichsen J. Nevronale ceroide lipofuscinoser [Neuronal ceroid lipofuscinoses]. Tidsskr Nor Laegeforen. 2006;126(15):1908-1910.

Augustine EF, Beck CA, Adams HR, et al. Short-Term Administration of Mycophenolate Is Well-Tolerated in CLN3 Disease (Juvenile Neuronal Ceroid Lipofuscinosis). JIMD Rep. 2019;43:117-124.

doi:10.1007/8904_2018_113

Axe EL, Walker SA, Manifava M, et al. Autophagosome formation from membrane compartments enriched in phosphatidylinositol 3-phosphate and dynamically connected to the endoplasmic reticulum. J Cell Biol. 2008;182(4):685-701. doi:10.1083/jcb.200803137

B

Balaban RS, Nemoto S, Finkel T. Mitochondria, oxidants, and aging. Cell. 2005;120(4):483-495. doi:10.1016/j.cell.2005.02.001

Balabio A. The awesome lysosome. EMBO Mol Med. 2016;8(2):73-76. doi:10.15252/emmm.201505966

Balch WE, Morimoto RI, Dillin A, Kelly JW. Adapting proteostasis for disease intervention. Science. 2008;319(5865):916-919. doi:10.1126/science.1141448

Banks AS, McAllister FE, Camporez JP, et al. An ERK/Cdk5 axis controls the diabetogenic actions of PPARγ. Nature. 2015;517(7534):391-395. doi:10.1038/nature13887

Baracca A, Chiaradonna F, Sgarbi G, Solaini G, Alberghina L, Lenaz G. Mitochondrial Complex I decrease is responsible for bioenergetic dysfunction in K-ras transformed cells. Biochim Biophys Acta. 2010;1797(2):314-323. doi:10.1016/j.bbabio.2009.11.006

Barb D, Neuwirth A, Mantzoros CS, Balk SP. Adiponectin signals in prostate cancer cells through Akt to activate the mammalian target of rapamycin pathway. Endocr Relat Cancer. 2007;14(4):995-1005. doi:10.1677/ERC-06-0091

Barde MP, Barde PJ. What to use to express the variability of data: Standard deviation or standard error of mean?. Perspect Clin Res. 2012;3(3):113-116. doi:10.4103/2229-3485.100662

Barman A, Deb B, Chakraborty S. A glance at genome editing with CRISPR-Cas9 technology. Curr Genet. 2020;66(3):447-462. doi:10.1007/s00294-019-01040-3

Barrangou R, Fremaux C, Deveau H, et al., CRISPR provides acquired resistance against viruses in prokaryotes. Science. 2007;315(5819):1709-1712. doi:10.1126/science.1138140

Baumgart E, Fahimi HD, Stich A, Völkl A. L-lactate dehydrogenase A4- and A3B isoforms are bona fide peroxisomal enzymes in rat liver. Evidence for involvement in intraperoxisomal NADH reoxidation. J Biol Chem. 1996;271(7):3846-3855. doi:10.1074/jbc.271.7.3846

Bayrhuber M, Meins T, Habeck M, et al., Structure of the human voltage-dependent anion channel. Proc Natl Acad Sci U S A. 2008;105(40):15370-15375. doi:10.1073/pnas.0808115105

Belgacem YH, Borodinsky LN. CREB at the Crossroads of Activity-Dependent Regulation of Nervous System Development and Function. Adv Exp Med Biol. 2017;1015:19-39. doi:10.1007/978-3-319-62817-2_2

Ben-Sahra I, Howell JJ, Asara JM, Manning BD. Stimulation of de novo pyrimidine synthesis by growth signaling through mTOR and S6K1. Science. 2013;339(6125):1323-1328. doi:10.1126/science.1228792

Bertolotto C, Lesueur F, Giuliano S, et al. A SUMOylation-defective MITF germline mutation predisposes to melanoma and renal carcinoma [published correction appears in Nature. 2016 Mar 3;531(7592):126]. Nature. 2011;480(7375):94-98. Published 2011 Oct 19. doi:10.1038/nature10539

Betz C, Stracka D, Prescianotto-Baschong C, Frieden M, Demaurex N, Hall MN. Feature Article: mTOR complex

2-Akt signaling at mitochondria-associated endoplasmic reticulum membranes (MAM) regulates mitochondrial physiology. Proc Natl Acad Sci U S A. 2013;110(31):12526-12534. doi:10.1073/pnas.1302455110

Beyer RE. The participation of coenzyme Q in free radical production and antioxidation. Free Radic Biol Med. 1990;8(6):545-565. doi:10.1016/0891-5849(90)90154-b

Bianconi E, Piovesan A, Facchin F, et al. An estimation of the number of cells in the human body [published correction appears in Ann Hum Biol. 2013 Nov-Dec;40(6):471]. Ann Hum Biol. 2013;40(6):463-471. doi:10.3109/03014460.2013.807878

Bieda M, Xu X, Singer MA, Green R, Farnham PJ. Unbiased location analysis of E2F1-binding sites suggests a widespread role for E2F1 in the human genome. Genome Res. 2006;16(5):595-605. doi:10.1101/gr.4887606

Biever A, Valjent E, Puighermanal E. Ribosomal Protein S6 Phosphorylation in the Nervous System: From Regulation to Function. Front Mol Neurosci. 2015;8:75. Published 2015 Dec 16. doi:10.3389/fnmol.2015.00075

Bolotin E, Liao H, Ta TC, et al. Integrated approach for the identification of human hepatocyte nuclear factor 4alpha target genes using protein binding microarrays. Hepatology. 2010;51(2):642-653. doi:10.1002/hep.23357

Bommiasamy H, Back SH, Fagone P, et al. ATF6alpha induces XBP1-independent expansion of the endoplasmic reticulum. J Cell Sci. 2009;122(Pt 10):1626-1636. doi:10.1242/jcs.045625

Bond ME, Brown R, Rallis C, Bähler J, Mole SE. A central role for TOR signalling in a yeast model for juvenile CLN3 disease. Microb Cell. 2015;2(12):466-480. Published 2015 Nov 11. doi:10.15698/mic2015.12.241

Borck G, Shin BS, Stiller B, et al. eIF2γ mutation that disrupts eIF2 complex integrity links intellectual disability to impaired translation initiation. Mol Cell. 2012;48(4):641-646. doi:10.1016/j.molcel.2012.09.005

Borreguero-Muñoz N, Fletcher GC, Aguilar-Aragon M, Elbediwy A, Vincent-Mistiaen ZI, Thompson BJ. The Hippo pathway integrates PI3K-Akt signals with mechanical and polarity cues to control tissue growth. PLoS Biol. 2019;17(10):e3000509. Published 2019 Oct 15. doi:10.1371/journal.pbio.3000509

Bosch ME, Aldrich A, Fallet R, et al. Self-Complementary AAV9 Gene Delivery Partially Corrects Pathology Associated with Juvenile Neuronal Ceroid Lipofuscinosis (CLN3). J Neurosci. 2016;36(37):9669-9682. doi:10.1523/JNEUROSCI.1635-16.2016

Bosch ME, Kielian T. Astrocytes in juvenile neuronal ceroid lipofuscinosis (CLN3) display metabolic and calcium signaling abnormalities. J Neurochem. 2019;148(5):612-624. doi:10.1111/jnc.14545

Boveris A, Chance B. The mitochondrial generation of hydrogen peroxide. General properties and effect of hyperbaric oxygen. Biochem J. 1973;134(3):707-716. doi:10.1042/bj1340707

Boyd M, Bressendorff S, Møller J, Olsen J, Troelsen JT. Mapping of HNF4alpha target genes in intestinal epithelial cells. BMC Gastroenterol. 2009;9:68. Published 2009 Sep 17. doi:10.1186/1471-230X-9-68

Bradford MM. A rapid and sensitive method for the quantitation of microgram quantities of protein utilizing the principle of protein-dye binding. Anal Biochem. 1976;72:248-254. doi:10.1006/abio.1976.9999

Braak H, Goebel HH. Loss of pigment-laden stellate cells: a severe alteration of the isocortex in juvenile neuronal ceroid-lipofuscinosis. Acta Neuropathol. 1978;42(1):53-57. doi:10.1007/BF01273267

Brand MD. The sites and topology of mitochondrial superoxide production. Exp Gerontol. 2010;45(7-8):466-

472. doi:10.1016/j.exger.2010.01.003

Brand MD. Uncoupling to survive? The role of mitochondrial inefficiency in ageing. Exp Gerontol. 2000;35(6-7):811-820. doi:10.1016/s0531-5565(00)00135-2

Bronner DN, Abuaita BH, Chen X, et al. Endoplasmic Reticulum Stress Activates the Inflammasome via NLRP3- and Caspase-2-Driven Mitochondrial Damage. Immunity. 2015;43(3):451-462. doi:10.1016/j.immuni.2015.08.008

Brookes PS. Mitochondrial H(+) leak and ROS generation: an odd couple. Free Radic Biol Med. 2005;38(1):12-23. doi:10.1016/j.freeradbiomed.2004.10.016

Brown EJ, Albers MW, Shin TB, et al. A mammalian protein targeted by G1-arresting rapamycin-receptor complex. Nature. 1994;369(6483):756-758. doi:10.1038/369756a0

Bucevičius J, Lukinavičius G, Gerasimaitė R. The Use of Hoechst Dyes for DNA Staining and Beyond. Chemosensors. 2018; 6(2):18. doi:10.3390/chemosensors6020018

Buffington SA, Huang W, Costa-Mattioli M. Translational control in synaptic plasticity and cognitive dysfunction. Annu Rev Neurosci. 2014;37:17-38. doi:10.1146/annurev-neuro-071013-014100

Bui HT, Shaw JM. Dynamin assembly strategies and adaptor proteins in mitochondrial fission. Curr Biol. 2013;23(19):R891-R899. doi:10.1016/j.cub.2013.08.040

Burkovetskaya M, Karpuk N, Xiong J, et al. Evidence for aberrant astrocyte hemichannel activity in Juvenile Neuronal Ceroid Lipofuscinosis (JNCL). PLoS One. 2014;9(4):e95023. Published 2014 Apr 15. doi:10.1371/journal.pone.0095023

Burnight ER, Giacalone JC, Cooke JA, et al. CRISPR-Cas9 genome engineering: Treating inherited retinal degeneration. Prog Retin Eye Res. 2018;65:28-49. doi:10.1016/j.preteyeres.2018.03.003

C

Cadenas S. Mitochondrial uncoupling, ROS generation and cardioprotection. Biochim Biophys Acta Bioenerg. 2018;1859(9):940-950. doi:10.1016/j.bbabio.2018.05.019

Calvo SE, Clauser KR, Mootha VK. MitoCarta2.0: an updated inventory of mammalian mitochondrial proteins. Nucleic Acids Res. 2016;44(D1):D1251-D1257. doi:10.1093/nar/gkv1003

Cameron RB, Beeson CC, Schnellmann RG. Development of Therapeutics That Induce Mitochondrial Biogenesis for the Treatment of Acute and Chronic Degenerative Diseases. J Med Chem. 2016;59(23):10411-10434. doi:10.1021/acs.jmedchem.6b00669

Cameron RB, Peterson YK, Beeson CC, Schnellmann RG. Structural and pharmacological basis for the induction of mitochondrial biogenesis by formoterol but not clenbuterol [published correction appears in Sci Rep. 2019 May 1;9(1):6790]. Sci Rep. 2017;7(1):10578. Published 2017 Sep 5. doi:10.1038/s41598-017-11030-5

Cao Y, Espinola JA, Fossale E, et al. Autophagy is disrupted in a knock-in mouse model of juvenile neuronal ceroid lipofuscinosis. J Biol Chem. 2006;281(29):20483-20493. doi:10.1074/jbc.M602180200

Cardol P, Figueroa F, Remacle C, Franzén L, González-Halphen D. Oxidative Phosphorylation: Building Blocks and Related Components. The Chlamydomonas Sourcebook 3-Vol set, (2009), 469-502, 2. doi: 10.1016/B978-0-12-370873-1.00021-6

Cardona F, Rosati E. Neuronal ceroid-lipofuscinoses in Italy: an epidemiological study. Am J Med Genet. 1995;57(2):142-143. doi:10.1002/ajmg.1320570206

Carlson M. org.Hs.eg.db: Genome wide annotation for Human. R package version 3.2.3. (2019).

Carreras-Sureda A, Jaña F, Urra H, et al. Non-canonical function of IRE1α determines mitochondria-associated endoplasmic reticulum composition to control calcium transfer and bioenergetics [published correction appears in Nat Cell Biol. 2019 Jun 14;:]. Nat Cell Biol. 2019;21(6):755-767. doi:10.1038/s41556-019-0329-y

Chae HJ, Kim HR, Xu C, et al. BI-1 regulates an apoptosis pathway linked to endoplasmic reticulum stress. Mol Cell. 2004;15(3):355-366. doi:10.1016/j.molcel.2004.06.038

Chan CH, Mitchison HM, Pearce DA. Transcript and in silico analysis of CLN3 in juvenile neuronal ceroid lipofuscinosis and associated mouse models. Hum Mol Genet. 2008;17(21):3332-3339. doi:10.1093/hmg/ddn228

Chan DC. Mitochondria: dynamic organelles in disease, aging, and development. Cell. 2006;125(7):1241-1252. doi:10.1016/j.cell.2006.06.010

Chan DC. Mitochondrial Dynamics and Its Involvement in Disease. Annu Rev Pathol. 2020;15:235-259. doi:10.1146/annurev-pathmechdis-012419-032711

Chan SW, Lim CJ, Chong YF, Pobbati AV, Huang C, Hong W. Hippo pathway-independent restriction of TAZ and YAP by angiomotin. J Biol Chem. 2011;286(9):7018-7026. doi:10.1074/jbc.C110.212621

Chandel NS. Evolution of Mitochondria as Signaling Organelles. Cell Metab. 2015;22(2):204-206. doi:10.1016/j.cmet.2015.05.013

Chandrachud U, Walker MW, Simas AM, et al., Unbiased Cell-based Screening in a Neuronal Cell Model of Batten Disease Highlights an Interaction between Ca2+ Homeostasis, Autophagy, and CLN3 Protein Function. J Biol Chem. 2015;290(23):14361-14380. doi:10.1074/jbc.M114.621706

Chang JW, Choi H, Kim HJ, et al., Neuronal vulnerability of CLN3 deletion to calcium-induced cytotoxicity is mediated by calsenilin. Hum Mol Genet. 2007;16(3):317-326. doi:10.1093/hmg/ddl466

Chattopadhyay S, Pearce DA. Neural and extraneural expression of the neuronal ceroid lipofuscinoses genes CLN1, CLN2, and CLN3: functional implications for CLN3. Mol Genet Metab. 2000;71(1-2):207-211. doi:10.1006/mgme.2000.3056

Chazotte B. Labeling mitochondria with JC-1. Cold Spring Harb Protoc. 2011; 2011(9):pdb.prot065490. Published 2011 Sep 1. doi:10.1101/pdb.prot065490

Chen H, Detmer SA, Ewald AJ, Griffin EE, Fraser SE, Chan DC. Mitofusins Mfn1 and Mfn2 coordinately regulate mitochondrial fusion and are essential for embryonic development. J Cell Biol. 2003;160(2):189-200. doi:10.1083/jcb.200211046

Chen JJ. Translational control by heme-regulated eIF2α kinase during erythropoiesis. Curr Opin Hematol. 2014;21(3):172-178. doi:10.1097/MOH.0000000000000030

Chen X, Xu H, Yuan P, et al. Integration of external signaling pathways with the core transcriptional network in embryonic stem cells. Cell. 2008;133(6):1106-1117. doi:10.1016/j.cell.2008.04.043

Cho YS, Li S, Wang X, et al. CDK7 regulates organ size and tumor growth by safeguarding the Hippo pathway

effector Yki/Yap/Taz in the nucleus. Genes Dev. 2020;34(1-2):53-71. doi:10.1101/gad.333146.119

Cho YS, Zhu J, Li S, Wang B, Han Y, Jiang J. Regulation of Yki/Yap subcellular localization and Hpo signaling by a nuclear kinase PRP4K. Nat Commun. 2018;9(1):1657. Published 2018 Apr 25. doi:10.1038/s41467-018-04090-2

Chu BB, Liao YC, Qi W, et al. Cholesterol transport through lysosome-peroxisome membrane contacts [published correction appears in Cell. 2021 Jan 7;184(1):289]. Cell. 2015;161(2):291-306. doi:10.1016/j.cell.2015.02.019

Claussen M, Heim P, Knispel J, Goebel HH, Kohlschütter A. Incidence of neuronal ceroid-lipofuscinoses in West Germany: variation of a method for studying autosomal recessive disorders. Am J Med Genet. 1992;42(4):536-538. doi:10.1002/ajmg.1320420422

Codlin S, Haines RL, Mole SE. btn1 affects endocytosis, polarization of sterol-rich membrane domains and polarized growth in Schizosaccharomyces pombe. Traffic. 2008;9(6):936-950. doi:10.1111/j.1600-0854.2008.00735.x

Codlin S, Mole SE. S. pombe btn1, the orthologue of the Batten disease gene CLN3, is required for vacuole protein sorting of Cpy1p and Golgi exit of Vps10p. J Cell Sci. 2009;122(Pt 8):1163-1173. doi:10.1242/jcs.038323

Cogliati S, Calvo E, Loureiro M, et al., Mechanism of super-assembly of respiratory complexes III and IV. Nature. 2016;539(7630):579-582. doi:10.1038/nature20157

Cogliati S, Enriquez JA, Scorrano L. Mitochondrial Cristae: Where Beauty Meets Functionality. Trends Biochem Sci. 2016;41(3):261-273. doi:10.1016/j.tibs.2016.01.001

Cogliati S, Frezza C, Soriano ME, et al., Mitochondrial cristae shape determines respiratory chain supercomplexes assembly and respiratory efficiency. Cell. 2013;155(1):160-171. doi:10.1016/j.cell.2013.08.032

Cohen P. The regulation of protein function by multisite phosphorylation--a 25 year update. Trends Biochem Sci. 2000;25(12):596-601. doi:10.1016/s0968-0004(00)01712-6

Cohen S, Valm AM, Lippincott-Schwartz J. Interacting organelles. Curr Opin Cell Biol. 2018;53:84-91. doi:10.1016/j.ceb.2018.06.003

Cooper JD, Tarczyluk MA, Nelvagal HR. Towards a new understanding of NCL pathogenesis. Biochim Biophys Acta. 2015;1852(10 Pt B):2256-2261. doi:10.1016/j.bbadis.2015.05.014

Costa-Mattioli M, Walter P. The integrated stress response: From mechanism to disease. Science. 2020;368(6489):eaat5314. doi:10.1126/science.aat5314

Costello JL, Castro IG, Hacker C, et al. ACBD5 and VAPB mediate membrane associations between peroxisomes and the ER. J Cell Biol. 2017;216(2):331-342. doi:10.1083/jcb.201607055

Cotman SL, Staropoli JF. The juvenile Batten disease protein, CLN3, and its role in regulating anterograde and retrograde post-Golgi trafficking. Clin Lipidol. 2012;7(1):79-91. doi:10.2217/clp.11.70

Cotney J, Wang Z, Shadel GS. Relative abundance of the human mitochondrial transcription system and distinct roles for h-mtTFB1 and h-mtTFB2 in mitochondrial biogenesis and gene expression. *Nucleic Acids Res*. 2007;35(12):4042-4054. doi:10.1093/nar/gkm424

Cox AG, Tsomides A, Yimlamai D, et al. Yap regulates glucose utilization and sustains nucleotide synthesis to

enable organ growth. EMBO J. 2018;37(22):e100294. doi:10.15252/embj.2018100294

Cox TM, Cachón-González MB. The cellular pathology of lysosomal diseases. J Pathol. 2012;226(2):241-254. doi:10.1002/path.3021

Credle JJ, Finer-Moore JS, Papa FR, Stroud RM, Walter P. On the mechanism of sensing unfolded protein in the endoplasmic reticulum. Proc Natl Acad Sci U S A. 2005;102(52):18773-18784. doi:10.1073/pnas.0509487102

Crouch SP, Kozlowski R, Slater KJ, Fletcher J. The use of ATP bioluminescence as a measure of cell proliferation and cytotoxicity. J Immunol Methods. 1993;160(1):81-88. doi:10.1016/0022-1759(93)90011-u

Cruz-Barrera M, Flórez-Zapata N, Lemus-Diaz N, et al., Integrated Analysis of Transcriptome and Secretome From Umbilical Cord Mesenchymal Stromal Cells Reveal New Mechanisms for the Modulation of Inflammation and Immune Activation. Front Immunol. 2020;11:575488. Published 2020 Sep 30. doi:10.3389/fimmu.2020.575488

Cunningham JT, Rodgers JT, Arlow DH, Vazquez F, Mootha VK, Puigserver P. mTOR controls mitochondrial oxidative function through a YY1-PGC-1alpha transcriptional complex. Nature. 2007;450(7170):736-740. doi:10.1038/nature06322

D

Dancey J. mTOR signaling and drug development in cancer. Nat Rev Clin Oncol. 2010;7(4):209-219. doi:10.1038/nrclinonc.2010.21

Dansen TB, Wirtz KW. The peroxisome in oxidative stress. IUBMB Life. 2001;51(4):223-230. doi:10.1080/152165401753311762

Das AM, Jolly RD, Kohlschütter A. Anomalies of mitochondrial ATP synthase regulation in four different types of neuronal ceroid lipofuscinosis. Mol Genet Metab. 1999;66(4):349-355. doi:10.1006/mgme.1999.2811

Das AM, von Harlem R, Feist M, Lücke T, Kohlschütter A. Altered levels of high-energy phosphate compounds in fibroblasts from different forms of neuronal ceroid lipofuscinoses: further evidence for mitochondrial involvement. Eur J Paediatr Neurol. 2001;5 Suppl A:143-146. doi:10.1053/ejpn.2000.0451

Davies KM, Strauss M, Daum B, et al., Macromolecular organization of ATP synthase and complex I in whole mitochondria. Proc Natl Acad Sci U S A. 2011;108(34):14121-14126. doi:10.1073/pnas.1103621108

Dawson G, Kilkus J, Siakotos AN, Singh I. Mitochondrial abnormalities in CLN2 and CLN3 forms of Batten disease. Mol Chem Neuropathol. 1996;29(2-3):227-235. doi:10.1007/BF02815004

de Duve C. The lysosome turns fifty. Nat Cell Biol. 2005;7(9):847-849. doi:10.1038/ncb0905-847

de Los Reyes Corrales T, Losada-Pérez M, Casas-Tintó S. JNK Pathway in CNS Pathologies. Int J Mol Sci. 2021;22(8):3883. Published 2021 Apr 9. doi:10.3390/ijms22083883

Decraene C, Brugg B, Ruberg M, et al. Identification of genes involved in ceramide-dependent neuronal apoptosis using cDNA arrays. Genome Biol. 2002;3(8):RESEARCH0042. doi:10.1186/gb-2002-3-8-research0042

Dekker PJ, Martin F, Maarse AC, et al., The Tim core complex defines the number of mitochondrial translocation contact sites and can hold arrested preproteins in the absence of matrix Hsp70-Tim44. *EMBO J.* 1997;16(17):5408-5419. doi:10.1093/emboj/16.17.5408

DeRan M, Yang J, Shen CH, et al. Energy stress regulates hippo-YAP signaling involving AMPK-mediated regulation of angiomotin-like 1 protein. Cell Rep. 2014;9(2):495-503. doi:10.1016/j.celrep.2014.09.036

Deus CM, Yambire KF, Oliveira PJ, Raimundo N. Mitochondria-Lysosome Crosstalk: From Physiology to Neurodegeneration. Trends Mol Med. 2020;26(1):71-88. doi:10.1016/j.molmed.2019.10.009

Dias AF, Rodrigues TA, Pedrosa AG, Barros-Barbosa A, Francisco T, Azevedo JE. The peroxisomal matrix protein translocon is a large cavity-forming protein assembly into which PEX5 protein enters to release its cargo. J Biol Chem. 2017;292(37):15287-15300. doi:10.1074/jbc.M117.805044

Diaz F, Enríquez JA, Moraes CT. Cells lacking Rieske iron-sulfur protein have a reactive oxygen species-associated decrease in respiratory complexes I and IV. Mol Cell Biol. 2012;32(2):415-429. doi:10.1128/MCB.06051-11

Dibble CC, Cantley LC. Regulation of mTORC1 by PI3K signaling. Trends Cell Biol. 2015;25(9):545-555. doi:10.1016/j.tcb.2015.06.002

Dibble CC, Elis W, Menon S, et al. TBC1D7 is a third subunit of the TSC1-TSC2 complex upstream of mTORC1. Mol Cell. 2012;47(4):535-546. doi:10.1016/j.molcel.2012.06.009

Ding SL, Tecedor L, Stein CS, Davidson BL. A knock-in reporter mouse model for Batten disease reveals predominant expression of Cln3 in visual, limbic and subcortical motor structures. Neurobiol Dis. 2011;41(2):237-248. doi:10.1016/j.nbd.2010.09.011

Diogo CV, Yambire KF, Fernández Mosquera L, Branco F T, Raimundo N. Mitochondrial adventures at the organelle society. Biochem Biophys Res Commun. 2018;500(1):87-93. doi:10.1016/j.bbrc.2017.04.124

Dobin A, Davis CA, Schlesinger F, et al., STAR: ultrafast universal RNA-seq aligner. Bioinformatics. 2013;29(1):15-21. doi:10.1093/bioinformatics/bts635

Dobin A, Gingeras TR. Mapping RNA-seq Reads with STAR. Curr Protoc Bioinformatics. 2015;51:11.14.1-11.14.19. Published 2015 Sep 3. doi:10.1002/0471250953.bi1114s51

Doccini S, Morani F, Nesti C, et al., Proteomic and functional analyses in disease models reveal CLN5 protein involvement in mitochondrial dysfunction. Cell Death Discov. 2020;6:18. Published 2020 Mar 30. doi:10.1038/s41420-020-0250-y

Dong J, Feldmann G, Huang J, et al. Elucidation of a universal size-control mechanism in Drosophila and mammals. Cell. 2007;130(6):1120-1133. doi:10.1016/j.cell.2007.07.019

Donsante A, Boulis NM. Progress in gene and cell therapies for the neuronal ceroid lipofuscinoses. Expert Opin Biol Ther. 2018;18(7):755-764. doi:10.1080/14712598.2018.1492544

Doudna JA, Charpentier E. Genome editing. The new frontier of genome engineering with CRISPR-Cas9. Science. 2014;346(6213):1258096. doi:10.1126/science.1258096

Drack AV, Mullins RF, Pfeifer WL, Augustine EF, Stasheff SF, Hong SD. Immunosuppressive Treatment for Retinal Degeneration in Juvenile Neuronal Ceroid Lipofuscinosis (Juvenile Batten Disease). Ophthalmic Genet. 2015;36(4):359-364. doi:10.3109/13816810.2014.886271

Dufey E, Bravo-San Pedro JM, Eggers C, et al. Genotoxic stress triggers the activation of IRE1α-dependent RNA decay to modulate the DNA damage response. Nat Commun. 2020;11(1):2401. Published 2020 May 14.

doi:10.1038/s41467-020-15694-y

Dupont S, Morsut L, Aragona M, et al. Role of YAP/TAZ in mechanotransduction. Nature. 2011;474(7350):179-183. Published 2011 Jun 8. doi:10.1038/nature10137

Duvezin-Caubet S, Jagasia R, Wagener J, et al., Proteolytic processing of OPA1 links mitochondrial dysfunction to alterations in mitochondrial morphology. J Biol Chem. 2006;281(49):37972-37979. doi:10.1074/jbc.M6060592

E

Edwards DN, Ngwa VM, Wang S, et al. The receptor tyrosine kinase EphA2 promotes glutamine metabolism in tumors by activating the transcriptional coactivators YAP and TAZ. Sci Signal. 2017;10(508):eaan4667. Published 2017 Dec 5. doi:10.1126/scisignal.aan4667

Egan DF, Shackelford DB, Mihaylova MM, et al. Phosphorylation of ULK1 (hATG1) by AMP-activated protein kinase connects energy sensing to mitophagy. Science. 2011;331(6016):456-461. doi:10.1126/science.1196371

Eisenberg-Bord M, Shai N, Schuldiner M, Bohnert M. A Tether Is a Tether Is a Tether: Tethering at Membrane Contact Sites. Dev Cell. 2016;39(4):395-409. doi:10.1016/j.devcel.2016.10.022

Elgass KD, Smith EA, LeGros MA, Larabell CA, Ryan MT. Analysis of ER-mitochondria contacts using correlative fluorescence microscopy and soft X-ray tomography of mammalian cells. J Cell Sci. 2015;128(15):2795-2804. doi:10.1242/jcs.169136

Eliason SL, Stein CS, Mao Q, et al. A knock-in reporter model of Batten disease. J Neurosci. 2007;27(37):9826-9834. doi:10.1523/JNEUROSCI.1710-07.2007

Ezaki J, Takeda-Ezaki M, Koike M, et al. Characterization of Cln3p, the gene product responsible for juvenile neuronal ceroid lipofuscinosis, as a lysosomal integral membrane glycoprotein. J Neurochem. 2003;87(5):1296-1308. doi:10.1046/j.1471-4159.2003.02132.x

Ezaki J, Takeda-Ezaki M, Kominami E. Tripeptidyl peptidase I, the late infantile neuronal ceroid lipofuscinosis gene product, initiates the lysosomal degradation of subunit c of ATP synthase. J Biochem. 2000;128(3):509-516. doi:10.1093/oxfordjournals.jbchem.a022781

F

Farré JC, Mahalingam SS, Proietto M, Subramani S. Peroxisome biogenesis, membrane contact sites, and quality control. EMBO Rep. 2019;20(1):e46864. doi:10.15252/embr.201846864Fernández-Mosquera L, Diogo CV, Yambire KF, et al., Acute and chronic mitochondrial respiratory chain deficiency differentially regulate lysosomal biogenesis. Sci Rep. 2017;7:45076. Published 2017 Mar 27. doi:10.1038/srep45076

Faust JR, Rodman JS, Daniel PF, Dice JF, Bronson RT. Two related proteolipids and dolichol-linked oligosaccharides accumulate in motor neuron degeneration mice (mnd/mnd), a model for neuronal ceroid lipofuscinosis. J Biol Chem. 1994;269(13):10150-10155.

Fearnley IM, Walker JE, Martinus RD, et al. The sequence of the major protein stored in ovine ceroid lipofuscinosis is identical with that of the dicyclohexylcarbodiimide-reactive proteolipid of mitochondrial ATP synthase. Biochem J. 1990;268(3):751-758. doi:10.1042/bj2680751

Fernando MR, Lechner JM, Löfgren S, Gladyshev VN, Lou MF. Mitochondrial thioltransferase (glutaredoxin 2) has GSH-dependent and thioredoxin reductase-dependent peroxidase activities in vitro and in lens epithelial cells. FASEB J. 2006;20(14):2645-2647. doi:10.1096/fj.06-5919fje

Fietz M, AlSayed M, Burke D, et al. Diagnosis of neuronal ceroid lipofuscinosis type 2 (CLN2 disease): Expert recommendations for early detection and laboratory diagnosis. Mol Genet Metab. 2016;119(1-2):160-167. doi:10.1016/j.ymgme.2016.07.011

Fontana L, Partridge L, Longo VD. Extending healthy life span--from yeast to humans. Science. 2010;328(5976):321-326. doi:10.1126/science.1172539

Forgac M. Vacuolar ATPases: rotary proton pumps in physiology and pathophysiology. Nat Rev Mol Cell Biol. 2007;8(11):917-929. doi:10.1038/nrm2272

Fossale E, Wolf P, Espinola JA, et al., Membrane trafficking and mitochondrial abnormalities precede subunit c deposition in a cerebellar cell model of juvenile neuronal ceroid lipofuscinosis. BMC Neurosci. 2004;5:57. Published 2004 Dec 10. doi:10.1186/1471-2202-5-57

Fransen M, Lismont C, Walton P. The Peroxisome-Mitochondria Connection: How and Why?. Int J Mol Sci. 2017;18(6):1126. Published 2017 May 24. doi:10.3390/ijms18061126

Freeman OJ, Mallucci GR. The UPR and synaptic dysfunction in neurodegeneration. Brain Res. 2016;1648(Pt B):530-537. doi:10.1016/j.brainres.2016.03.029

Frezza C, Cipolat S, Martins de Brito O, et al., OPA1 controls apoptotic cristae remodelling independently from mitochondrial fusion. Cell. 2006;126(1):177-189. doi:10.1016/j.cell.2006.06.025

Frias MA, Thoreen CC, Jaffe JD, et al. mSin1 is necessary for Akt/PKB phosphorylation, and its isoforms define three distinct mTORC2s. Curr Biol. 2006;16(18):1865-1870. doi:10.1016/j.cub.2006.08.001

Friedman JR, Lackner LL, West M, DiBenedetto JR, Nunnari J, Voeltz GK. 2011. ER tubules mark sites of mitochondrial division. Science 334:358–62

Friedrich T, Hellwig P. Redox-induced conformational changes within the Escherichia coli NADH ubiquinone oxidoreductase (complex I): an analysis by mutagenesis and FT-IR spectroscopy. Biochim Biophys Acta. 2010;1797(6-7):659-663. doi:10.1016/j.bbabio.2010.03.002

Fujikake N, Shin M, Shimizu S. Association Between Autophagy and Neurodegenerative Diseases. Front Neurosci. 2018;12:255. Published 2018 May 22. doi:10.3389/fnins.2018.00255

G

Gachet Y, Codlin S, Hyams JS, Mole SE. btn1, the Schizosaccharomyces pombe homologue of the human Batten disease gene CLN3, regulates vacuole homeostasis. J Cell Sci. 2005;118(Pt 23):5525-5536. doi:10.1242/jcs.02656

Galadari S, Rahman A, Pallichankandy S, Thayyullathil F. Reactive oxygen species and cancer paradox: To promote or to suppress?. Free Radic Biol Med. 2017;104:144-164. doi:10.1016/j.freeradbiomed.2017.01.004

Gallagher S, Winston SE, Fuller SA, Hurrell JG. Immunoblotting and immunodetection. Curr Protoc Mol Biol. 2008;Chapter 10:. doi:10.1002/0471142727.mb1008s83

Gallagher SR. One-dimensional SDS gel electrophoresis of proteins. Curr Protoc Protein Sci. 2012;Chapter 10:.

doi:10.1002/0471140864.ps1001s68

Galvin N, Vogler C, Levy B, Kovacs A, Griffey M, Sands MS. A murine model of infantile neuronal ceroid lipofuscinosis-ultrastructural evaluation of storage in the central nervous system and viscera. Pediatr Dev Pathol. 2008;11(3):185-192. doi:10.2350/07-03-0242.1

Gandre-Babbe S, van der Bliek AM. The novel tail-anchored membrane protein Mff controls mitochondrial and peroxisomal fission in mammalian cells. Mol Biol Cell. 2008;19(6):2402-2412. doi:10.1091/mbc.e07-12-1287

García MA, Meurs EF, Esteban M. The dsRNA protein kinase PKR: virus and cell control. Biochimie. 2007;89(6-7):799-811. doi:10.1016/j.biochi.2007.03.001

Gatta AT, Levine TP. Piecing Together the Patchwork of Contact Sites. Trends Cell Biol. 2017;27(3):214-229. doi:10.1016/j.tcb.2016.08.010

Ge L, Melville D, Zhang M, Schekman R. The ER-Golgi intermediate compartment is a key membrane source for the LC3 lipidation step of autophagosome biogenesis. Elife. 2013;2:e00947. Published 2013 Aug 6. doi:10.7554/eLife.00947

Getty A, Kovács AD, Lengyel-Nelson T, et al. Osmotic stress changes the expression and subcellular localization of the Batten disease protein CLN3. PLoS One. 2013;8(6):e66203. Published 2013 Jun 20. doi:10.1371/journal.pone.0066203

Getty AL, Benedict JW, Pearce DA. A novel interaction of CLN3 with nonmuscle myosin-IIB and defects in cell motility of Cln3(-/-) cells. Exp Cell Res. 2011;317(1):51-69. doi:10.1016/j.yexcr.2010.09.007

Gilchrist A, Au CE, Hiding J, et al., Quantitative proteomics analysis of the secretory pathway. Cell. 2006;127(6):1265-1281. doi:10.1016/j.cell.2006.10.036

Girotti M, Banting G. TGN38-green fluorescent protein hybrid proteins expressed in stably transfected eukaryotic cells provide a tool for the real-time, in vivo study of membrane traffic pathways and suggest a possible role for ratTGN38. J Cell Sci. 1996;109 (Pt 12):2915-2926.

Glingston RS, Deb R, Kumar S, Nagotu S. Organelle dynamics and viral infections: at cross roads. Microbes Infect. 2019;21(1):20-32. doi:10.1016/j.micinf.2018.06.002

Golabek AA, Kaczmarski W, Kida E, Kaczmarski A, Michalewski MP, Wisniewski KE. Expression studies of CLN3 protein (battenin) in fusion with the green fluorescent protein in mammalian cells in vitro. Mol Genet Metab. 1999;66(4):277-282. doi:10.1006/mgme.1999.2836

Golabek AA, Kida E, Walus M, Kaczmarski W, Michalewski M, Wisniewski KE. CLN3 protein regulates lysosomal pH and alters intracellular processing of Alzheimer's amyloid-beta protein precursor and cathepsin D in human cells. Mol Genet Metab. 2000;70(3):203-213. doi:10.1006/mgme.2000.3006

Gordaliza-Alaguero I, Cantó C, Zorzano A. Metabolic implications of organelle-mitochondria communication. EMBO Rep. 2019;20(9):e47928. doi:10.15252/embr.201947928

Graber TE, McCamphill PK, Sossin WS. A recollection of mTOR signaling in learning and memory. Learn Mem. 2013;20(10):518-530. Published 2013 Sep 16. doi:10.1101/lm.027664.112

Gravel P. Protein Blotting by the Semidry Method. In: Walker J.M. (eds) The Protein Protocols Handbook. Springer Protocols Handbooks. Humana Press, 2019, Totowa, NJ. doi:10.1007/978-1-59745-198-7_59

Gray MW, Lang BF, Cedergren R, et al., Genome structure and gene content in protist mitochondrial DNAs. Nucleic Acids Res. 1998;26(4):865-878. doi:10.1093/nar/26.4.865

Gregory LC, Ferreira CB, Young-Baird SK, et al. Impaired EIF2S3 function associated with a novel phenotype of X-linked hypopituitarism with glucose dysregulation. EBioMedicine. 2019;42:470-480. doi:10.1016/j.ebiom.2019.03.013

Gu Y, Albuquerque CP, Braas D, et al. mTORC2 Regulates Amino Acid Metabolism in Cancer by Phosphorylation of the Cystine-Glutamate Antiporter xCT. Mol Cell. 2017;67(1):128-138.e7. doi:10.1016/j.molcel.2017.05.030

Guo R, Gu J, Zong S, Wu M, Yang M. Structure and mechanism of mitochondrial electron transport chain. Biomed J. 2018;41(1):9-20. doi:10.1016/j.bj.2017.12.001

Guo Y, Chang C, Huang R, Liu B, Bao L, Liu W. AP1 is essential for generation of autophagosomes from the trans-Golgi network. J Cell Sci. 2012;125(Pt 7):1706-1715. doi:10.1242/jcs.093203

Gupta KK, Singh SK. Cdk5: A main culprit in neurodegeneration. Int J Neurosci. 2019;129(12):1192-1197. doi:10.1080/00207454.2019.1645142

H

Hailey DW, Rambold AS, Satpute-Krishnan P, et al. Mitochondria supply membranes for autophagosome biogenesis during starvation. Cell. 2010;141(4):656-667. doi:10.1016/j.cell.2010.04.009

Haltia M. The neuronal ceroid-lipofuscinoses: from past to present. Biochim Biophys Acta. 2006;1762(10):850-856. doi:10.1016/j.bbadis.2006.06.010Ham AJ, Liebler DC. Vitamin E oxidation in rat liver mitochondria. Biochemistry. 1995;34(17):5754-5761. doi:10.1021/bi00017a007

Hamasaki M, Furuta N, Matsuda A, et al. Autophagosomes form at ER-mitochondria contact sites. Nature. 2013;495(7441):389-393. doi:10.1038/nature11910

Han D, Lerner AG, Vande Walle L, et al. IRE1alpha kinase activation modes control alternate endoribonuclease outputs to determine divergent cell fates. Cell. 2009;138(3):562-575. doi:10.1016/j.cell.2009.07.017

Han J, Back SH, Hur J, et al. ER-stress-induced transcriptional regulation increases protein synthesis leading to cell death. Nat Cell Biol. 2013;15(5):481-490. doi:10.1038/ncb2738

Hannan KM, Brandenburger Y, Jenkins A, et al. mTOR-dependent regulation of ribosomal gene transcription requires S6K1 and is mediated by phosphorylation of the carboxy-terminal activation domain of the nucleolar transcription factor UBF. Mol Cell Biol. 2003;23(23):8862-8877. doi:10.1128/MCB.23.23.8862-8877.2003

Hansen CG, Ng YL, Lam WL, Plouffe SW, Guan KL. The Hippo pathway effectors YAP and TAZ promote cell growth by modulating amino acid signaling to mTORC1. Cell Res. 2015;25(12):1299-1313. doi:10.1038/cr.2015.140

Hanukoglu I. Antioxidant protective mechanisms against reactive oxygen species (ROS) generated by mitochondrial P450 systems in steroidogenic cells. Drug Metab Rev. 2006;38(1-2):171-196. doi:10.1080/03602530600570040

Hara K, Maruki Y, Long X, et al. Raptor, a binding partner of target of rapamycin (TOR), mediates TOR action. Cell. 2002;110(2):177-189. doi:10.1016/s0092-8674(02)00833-4

Hara K, Yonezawa K, Kozlowski MT, et al. Regulation of eIF-4E BP1 phosphorylation by mTOR. J Biol Chem.

1997;272(42):26457-26463. doi:10.1074/jbc.272.42.26457

Hardie DG, Ross FA, Hawley SA. AMPK: a nutrient and energy sensor that maintains energy homeostasis. Nat Rev Mol Cell Biol. 2012;13(4):251-262. Published 2012 Mar 22. doi:10.1038/nrm3311

Harding HP, Novoa I, Zhang Y, et al. Regulated translation initiation controls stress-induced gene expression in mammalian cells. Mol Cell. 2000;6(5):1099-1108. doi:10.1016/s1097-2765(00)00108-8

Harding HP, Zhang Y, Zeng H, et al. An integrated stress response regulates amino acid metabolism and resistance to oxidative stress. Mol Cell. 2003;11(3):619-633. doi:10.1016/s1097-2765(03)00105-9

Haskell RE, Carr CJ, Pearce DA, Bennett MJ, Davidson BL. Batten disease: evaluation of CLN3 mutations on protein localization and function. Hum Mol Genet. 2000;9(5):735-744. doi:10.1093/hmg/9.5.735

Hassler JR, Scheuner DL, Wang S, et al. The IRE1α/XBP1s Pathway Is Essential for the Glucose Response and Protection of β Cells. PLoS Biol. 2015;13(10):e1002277. Published 2015 Oct 15. doi:10.1371/journal.pbio.1002277

Hayashi A, Kasahara T, Iwamoto K, et al. The role of brain-derived neurotrophic factor (BDNF)-induced XBP1 splicing during brain development. J Biol Chem. 2007;282(47):34525-34534. doi:10.1074/jbc.M704300200

Hebert DN, Molinari M. In and out of the ER: protein folding, quality control, degradation, and related human diseases. Physiol Rev. 2007;87(4):1377-1408. doi:10.1152/physrev.00050.2006

Helle SC, Kanfer G, Kolar K, Lang A, Michel AH, Kornmann B. Organization and function of membrane contact sites. Biochim Biophys Acta. 2013;1833(11):2526-2541. doi:10.1016/j.bbamcr.2013.01.028

Hetz C, Bernasconi P, Fisher J, et al. Proapoptotic BAX and BAK modulate the unfolded protein response by a direct interaction with IRE1alpha. Science. 2006;312(5773):572-576. doi:10.1126/science.1123480

Hetz C, Papa FR. The Unfolded Protein Response and Cell Fate Control. Mol Cell. 2018;69(2):169-181. doi:10.1016/j.molcel.2017.06.017

Hetz C, Saxena S. ER stress and the unfolded protein response in neurodegeneration. Nat Rev Neurol. 2017;13(8):477-491. doi:10.1038/nrneurol.2017.99

Hetz C, Zhang K, Kaufman RJ. Mechanisms, regulation and functions of the unfolded protein response. Nat Rev Mol Cell Biol. 2020;21(8):421-438. doi:10.1038/s41580-020-0250-z

Hollenhorst PC, Chandler KJ, Poulsen RL, Johnson WE, Speck NA, Graves BJ. DNA specificity determinants associate with distinct transcription factor functions. PLoS Genet. 2009;5(12):e1000778. doi:10.1371/journal.pgen.1000778

Holmberg CI, Tran SE, Eriksson JE, Sistonen L. Multisite phosphorylation provides sophisticated regulation of transcription factors. Trends Biochem Sci. 2002;27(12):619-627. doi:10.1016/s0968-0004(02)02207-7

Holopainen JM, Saarikoski J, Kinnunen PK, Järvelä I. Elevated lysosomal pH in neuronal ceroid lipofuscinoses (NCLs). Eur J Biochem. 2001;268(22):5851-5856. doi:10.1046/j.0014-2956.2001.02530.x

Hong AW, Meng Z, Yuan HX, et al. Osmotic stress-induced phosphorylation by NLK at Ser128 activates YAP. EMBO Rep. 2017;18(1):72-86. doi:10.15252/embr.201642681

Hong M, Song KD, Lee HK, et al. Fibrates inhibit the apoptosis of Batten disease lymphoblast cells via autophagy

recovery and regulation of mitochondrial membrane potential. In Vitro Cell Dev Biol Anim. 2016;52(3):349-355. doi:10.1007/s11626-015-9979-7

Hoppins S, Collins SR, Cassidy-Stone A, et al., A mitochondrial-focused genetic interaction map reveals a scaffold-like complex required for inner membrane organization in mitochondria. J Cell Biol. 2011;195(2):323-340. doi:10.1083/jcb.201107053

Hornbeck PV, Kornhauser JM, Tkachev S, et al. PhosphoSitePlus: a comprehensive resource for investigating the structure and function of experimentally determined post-translational modifications in man and mouse. Nucleic Acids Res. 2012;40(Database issue):D261-D270. doi:10.1093/nar/gkr1122

Hotamisligil GS, Erbay E. Nutrient sensing and inflammation in metabolic diseases. Nat Rev Immunol. 2008;8(12):923-934. doi:10.1038/nri2449

Hsu PD, Lander ES, Zhang F. Development and applications of CRISPR-Cas9 for genome engineering. Cell. 2014;157(6):1262-1278. doi:10.1016/j.cell.2014.05.010

Hua R, Cheng D, Coyaud É, et al. VAPs and ACBD5 tether peroxisomes to the ER for peroxisome maintenance and lipid homeostasis. J Cell Biol. 2017;216(2):367-377. doi:10.1083/jcb.201608128

Huang C, Wu S, Ji H, et al. Identification of XBP1-u as a novel regulator of the MDM2/p53 axis using an shRNA library. Sci Adv. 2017;3(10):e1701383. Published 2017 Oct 18. doi:10.1126/sciadv.1701383

Huang H, Wu W, Zhang L, Liu XY. Drosophila ste-20 family protein kinase, hippo, modulates fat cell proliferation. PLoS One. 2013;8(4):e61740. Published 2013 Apr 18. doi:10.1371/journal.pone.0061740

Huber AL, Lebeau J, Guillaumot P, et al. p58(IPK)-mediated attenuation of the proapoptotic PERK-CHOP pathway allows malignant progression upon low glucose. Mol Cell. 2013;49(6):1049-1059. doi:10.1016/j.molcel.2013.01.009

Huber RJ. Loss of Cln3 impacts protein secretion in the social amoeba Dictyostelium. Cell Signal. 2017;35:61-72. doi:10.1016/j.cellsig.2017.03.022

Huber RJ, Mathavarajah S. Comparative transcriptomics reveals mechanisms underlying cln3-deficiency phenotypes in Dictyostelium. Cell Signal. 2019;58:79-90. doi:10.1016/j.cellsig.2019.02.004

Humphrey SJ, Yang G, Yang P, et al. Dynamic adipocyte phosphoproteome reveals that Akt directly regulates mTORC2. Cell Metab. 2013;17(6):1009-1020. doi:10.1016/j.cmet.2013.04.010

Hwang JH, Kim AR, Kim KM, et al. TAZ couples Hippo/Wnt signalling and insulin sensitivity through Irs1 expression. Nat Commun. 2019;10(1):421. Published 2019 Jan 24. doi:10.1038/s41467-019-08287-x

I

Ibar C, Irvine KD. Integration of Hippo-YAP Signaling with Metabolism. Dev Cell. 2020;54(2):256-267. doi:10.1016/j.devcel.2020.06.025

Ikeda S, Nah J, Shirakabe A, et al., YAP plays a crucial role in the development of cardiomyopathy in lysosomal storage diseases. J Clin Invest. 2021;131(5):e143173. doi:10.1172/JCI143173

Ikenoue T, Inoki K, Yang Q, Zhou X, Guan KL. Essential function of TORC2 in PKC and Akt turn motif phosphorylation, maturation and signalling [published correction appears in EMBO J. 2008 Aug 20;27(16):2270]. EMBO J. 2008;27(14):1919-1931. doi:10.1038/emboj.2008.119

Inoki K, Li Y, Xu T, Guan KL. Rheb GTPase is a direct target of TSC2 GAP activity and regulates mTOR signaling. Genes Dev. 2003;17(15):1829-1834. doi:10.1101/gad.1110003

Inoki K, Li Y, Zhu T, Wu J, Guan KL. TSC2 is phosphorylated and inhibited by Akt and suppresses mTOR signalling. Nat Cell Biol. 2002;4(9):648-657. doi:10.1038/ncb839

Inoki K, Ouyang H, Zhu T, et al. TSC2 integrates Wnt and energy signals via a coordinated phosphorylation by AMPK and GSK3 to regulate cell growth. Cell. 2006;126(5):955-968. doi:10.1016/j.cell.2006.06.055

Inoki K, Zhu T, Guan KL. TSC2 mediates cellular energy response to control cell growth and survival. Cell. 2003;115(5):577-590. doi:10.1016/s0092-8674(03)00929-2

Ishihara N, Fujita Y, Oka T, Mihara K. Regulation of mitochondrial morphology through proteolytic cleavage of OPA1. EMBO J. 2006;25(13):2966-2977. doi:10.1038/sj.emboj.7601184

Ishiwata-Kimata Y, Yamamoto YH, Takizawa K, Kohno K, Kimata Y. F-actin and a type-II myosin are required for efficient clustering of the ER stress sensor Ire1. Cell Struct Funct. 2013;38(2):135-143. doi:10.1247/csf.12033

Islinger M, Voelkl A, Fahimi HD, Schrader M. The peroxisome: an update on mysteries 2.0. Histochem Cell Biol. 2018;150(5):443-471. doi:10.1007/s00418-018-1722-5

Isolation of a novel gene underlying Batten disease, CLN3. The International Batten Disease Consortium. Cell. 1995;82(6):949-957. doi:10.1016/0092-8674(95)90274-0

J

Jacinto E, Loewith R, Schmidt A, et al. Mammalian TOR complex 2 controls the actin cytoskeleton and is rapamycin insensitive. Nat Cell Biol. 2004;6(11):1122-1128. doi:10.1038/ncb1183

Jalanko A, Braulke T. Neuronal ceroid lipofuscinoses. Biochim Biophys Acta. 2009;1793(4):697-709. doi:10.1016/j.bbamcr.2008.11.004

Janes RW, Munroe PB, Mitchison HM, Gardiner RM, Mole SE, Wallace BA. A model for Batten disease protein CLN3: functional implications from homology and mutations. FEBS Lett. 1996;399(1-2):75-77. doi:10.1016/s0014-5793(96)01290-2

Järvelä I, Lehtovirta M, Tikkanen R, Kyttälä A, Jalanko A. Defective intracellular transport of CLN3 is the molecular basis of Batten disease (JNCL) [published correction appears in Hum Mol Genet 1999 Aug;8(8):1585]. Hum Mol Genet. 1999;8(6):1091-1098. doi:10.1093/hmg/8.6.1091

Järvelä I, Sainio M, Rantamäki T, et al. Biosynthesis and intracellular targeting of the CLN3 protein defective in Batten disease. Hum Mol Genet. 1998;7(1):85-90. doi:10.1093/hmg/7.1.85

Järvelä IE, Mitchison HM, Callen DF, et al. Physical map of the region containing the gene for Batten disease (CLN3). Am J Med Genet. 1995;57(2):316-319. doi:10.1002/ajmg.1320570242

Ji YF, Zhou L, Xie YJ, et al. Upregulation of glutamate transporter GLT-1 by mTOR-Akt-NF-κB cascade in astrocytic oxygen-glucose deprivation. Glia. 2013;61(12):1959-1975. doi:10.1002/glia.22566

Jin VX, Rabinovich A, Squazzo SL, Green R, Farnham PJ. A computational genomics approach to identify cis-regulatory modules from chromatin immunoprecipitation microarray data--a case study using E2F1. Genome Res. 2006;16(12):1585-1595. doi:10.1101/gr.5520206

Jodeiri Farshbaf M, Ghaedi K. Huntington's Disease and Mitochondria. Neurotox Res. 2017;32(3):518-529.

doi:10.1007/s12640-017-9766-1

Johnson LN, Lewis RJ. Structural basis for control by phosphorylation. Chem Rev. 2001;101(8):2209-2242. doi:10.1021/cr000225s

Johnson TB, Cain JT, White KA, Ramirez-Montealegre D, Pearce DA, Weimer JM. Therapeutic landscape for Batten disease: current treatments and future prospects. Nat Rev Neurol. 2019;15(3):161-178. doi:10.1038/s41582-019-0138-8

Johnson TB, Sturdevant DA, White KA, Drack AV, Bhattarai S, Rogers C, Jonathan D. Cooper, David A. Pearce, Jill M. Weimer, Characterization of a novel porcine model of CLN3-Batten disease, Molecular Genetics and Metabolism, Volume 126, Issue 2, 2019, Page S81, ISSN 1096-7192, https://doi.org/10.1016/j.ymgme.2018.12.198.

Jolly RD, Brown S, Das AM, Walkley SU. Mitochondrial dysfunction in the neuronal ceroid-lipofuscinoses (Batten disease). Neurochem Int. 2002;40(6):565-571. doi:10.1016/s0197-0186(01)00128-0

Jousse C, Oyadomari S, Novoa I, et al. Inhibition of a constitutive translation initiation factor 2alpha phosphatase, CReP, promotes survival of stressed cells. J Cell Biol. 2003;163(4):767-775. doi:10.1083/jcb.200308075

K

Kaczmarski W, Wisniewski KE, Golabek A, Kaczmarski A, Kida E, Michalewski M. Studies of membrane association of CLN3 protein. Mol Genet Metab. 1999;66(4):261-264. doi:10.1006/mgme.1999.2833

Kama R, Kanneganti V, Ungermann C, Gerst JE. The yeast Batten disease orthologue Btn1 controls endosome-Golgi retrograde transport via SNARE assembly. J Cell Biol. 2011;195(2):203-215. doi:10.1083/jcb.201102115

Kang SA, Pacold ME, Cervantes CL, et al. mTORC1 phosphorylation sites encode their sensitivity to starvation and rapamycin. Science. 2013;341(6144):1236566. doi:10.1126/science.1236566

Katz ML, Shibuya H, Liu PC, Kaur S, Gao CL, Johnson GS. A mouse gene knockout model for juvenile ceroid-lipofuscinosis (Batten disease). J Neurosci Res. 1999;57(4):551-556.

Kassambara A, Mundt F. factoextra: Extract and visualize the results of multivariate data analyses (Version 1.0.6). (2019).

Katz ML, Johnson GC, Leach SB, et al. Extraneuronal pathology in a canine model of CLN2 neuronal ceroid lipofuscinosis after intracerebroventricular gene therapy that delays neurological disease progression. Gene Ther. 2017;24(4):215-223. doi:10.1038/gt.2017.4

Kaufman RJ. Orchestrating the unfolded protein response in health and disease. J Clin Invest. 2002;110(10):1389-1398. doi:10.1172/JCI16886

Kausar S, Wang F, Cui H. The Role of Mitochondria in Reactive Oxygen Species Generation and Its Implications for Neurodegenerative Diseases. Cells. 2018;7(12):274. Published 2018 Dec 17. doi:10.3390/cells7120274

Kay GW, Jay NP, Palmer DN. The specific loss of GnRH-positive neurons from the hypothalamus of sheep with CLN6 neuronal ceroid lipofuscinosis occurs without glial activation and has only minor effects on reproduction. Neurobiol Dis. 2011;41(3):614-623. doi:10.1016/j.nbd.2010.11.008

Keith CT, Schreiber SL. PIK-related kinases: DNA repair, recombination, and cell cycle checkpoints. Science. 1995;270(5233):50-51. doi:10.1126/science.270.5233.50

Kennedy BK, Lamming DW. The Mechanistic Target of Rapamycin: The Grand ConducTOR of Metabolism and Aging. Cell Metab. 2016;23(6):990-1003. doi:10.1016/j.cmet.2016.05.009

Kent WJ, Sugnet CW, Furey TS, et al. The human genome browser at UCSC. Genome Res. 2002;12(6):996-1006. doi:10.1101/gr.229102

Khoury GA, Baliban RC, Floudas CA. Proteome-wide post-translational modification statistics: frequency analysis and curation of the swiss-prot database. Sci Rep. 2011;1:90. doi:10.1038/srep00090

Kida E, Kaczmarski W, Golabek AA, Kaczmarski A, Michalewski M, Wisniewski KE. Analysis of intracellular distribution and trafficking of the CLN3 protein in fusion with the green fluorescent protein in vitro. Mol Genet Metab. 1999;66(4):265-271. doi:10.1006/mgme.1999.2837

Kim B, Kang S, Kim SJ. Genome-wide pathway analysis reveals different signaling pathways between secreted lactoferrin and intracellular delta-lactoferrin. PLoS One. 2013;8(1):e55338. doi:10.1371/journal.pone.0055338

Kim DH, Sarbassov DD, Ali SM, et al. GbetaL, a positive regulator of the rapamycin-sensitive pathway required for the nutrient-sensitive interaction between raptor and mTOR. Mol Cell. 2003;11(4):895-904. doi:10.1016/s1097-2765(03)00114-x

Kim DH, Sarbassov DD, Ali SM, et al. mTOR interacts with raptor to form a nutrient-sensitive complex that signals to the cell growth machinery. Cell. 2002;110(2):163-175. doi:10.1016/s0092-8674(02)00808-5

Kim E, Goraksha-Hicks P, Li L, Neufeld TP, Guan KL. Regulation of TORC1 by Rag GTPases in nutrient response. Nat Cell Biol. 2008;10(8):935-945. doi:10.1038/ncb1753

Kim H, Williams D, Qiu Y, et al. Regulation of hepatic autophagy by stress-sensing transcription factor CREBH [published correction appears in FASEB J. 2020 Aug;34(8):11311]. FASEB J. 2019;33(7):7896-7914. doi:10.1096/fj.201802528R

Kim H, Zheng Z, Walker PD, Kapatos G, Zhang K. CREBH Maintains Circadian Glucose Homeostasis by Regulating Hepatic Glycogenolysis and Gluconeogenesis. Mol Cell Biol. 2017;37(14):e00048-17. Published 2017 Jun 29. doi:10.1128/MCB.00048-17

Kim J, Kundu M, Viollet B, Guan KL. AMPK and mTOR regulate autophagy through direct phosphorylation of Ulk1. Nat Cell Biol. 2011;13(2):132-141. doi:10.1038/ncb2152

Kim M, Jho EH. Cross-talk between Wnt/β-catenin and Hippo signaling pathways: a brief review. BMB Rep. 2014;47(10):540-545. doi:10.5483/bmbrep.2014.47.10.177

Kim P. Peroxisome Biogenesis: A Union between Two Organelles. Curr Biol. 2017;27(7):R271-R274. doi:10.1016/j.cub.2017.02.052

Kim Y, Ramirez-Montealegre D, Pearce DA. A role in vacuolar arginine transport for yeast Btn1p and for human CLN3, the protein defective in Batten disease. Proc Natl Acad Sci U S A. 2003;100(26):15458-15462. doi:10.1073/pnas.2136651100

Kirkinezos IG, Moraes CT. Reactive oxygen species and mitochondrial diseases. Semin Cell Dev Biol. 2001;12(6):449-457. doi:10.1006/scdb.2001.0282

Koch A, Thiemann M, Grabenbauer M, Yoon Y, McNiven MA, Schrader M. Dynamin-like protein 1 is involved in peroxisomal fission. J Biol Chem. 2003;278(10):8597-8605. doi:10.1074/jbc.M211761200

Koch A, Yoon Y, Bonekamp NA, McNiven MA, Schrader M. A role for Fis1 in both mitochondrial and peroxisomal fission in mammalian cells. Mol Biol Cell. 2005;16(11):5077-5086. doi:10.1091/mbc.e05-02-0159

Koch J, Feichtinger RG, Freisinger P, et al. Disturbed mitochondrial and peroxisomal dynamics due to loss of MFF causes Leigh-like encephalopathy, optic atrophy and peripheral neuropathy. J Med Genet. 2016;53(4):270-278. doi:10.1136/jmedgenet-2015-103500

Korshunov SS, Skulachev VP, Starkov AA. High protonic potential actuates a mechanism of production of reactive oxygen species in mitochondria. FEBS Lett. 1997;416(1):15-18. doi:10.1016/s0014-5793(97)01159-9

Kousi M, Lehesjoki AE, Mole SE. Update of the mutation spectrum and clinical correlations of over 360 mutations in eight genes that underlie the neuronal ceroid lipofuscinoses. Hum Mutat. 2012;33(1):42-63. doi:10.1002/humu.21624

Kruer MC, Pearce DA, Orchard PJ, Steiner RD. Prospects for stem cell therapy in neuronal ceroid lipofuscinosis. Regen Med. 2013;8(5):527-529. doi:10.2217/rme.13.46

Kudryavtseva AV, Krasnov GS, Dmitriev AA, et al., Mitochondrial dysfunction and oxidative stress in aging and cancer. Oncotarget. 2016;7(29):44879-44905. doi:10.18632/oncotarget.9821

Kuper WFE, Oostendorp M, van den Broek BTA, et al. Quantifying lymphocyte vacuolization serves as a measure of CLN3 disease severity. JIMD Rep. 2020;54(1):87-97. Published 2020 Jun 2. doi:10.1002/jmd2.12128

Kuper WFE, van Alfen C, Rigterink RH, Fuchs SA, van Genderen MM, van Hasselt PM. Timing of cognitive decline in CLN3 disease. J Inherit Metab Dis. 2018;41(2):257-261. doi:10.1007/s10545-018-0143-x

Kuper WFE, van Alfen C, van Eck L, et al. Motor function impairment is an early sign of CLN3 disease. Neurology. 2019;93(3):e293-e297. doi:10.1212/WNL.0000000000007773

Kühlbrandt W. Structure and function of mitochondrial membrane protein complexes. BMC Biol. 2015;13:89. Published 2015 Oct 29. doi:10.1186/s12915-015-0201-x 16.

Kyttälä A, Ihrke G, Vesa J, Schell MJ, Luzio JP. Two motifs target Batten disease protein CLN3 to lysosomes in transfected nonneuronal and neuronal cells. Mol Biol Cell. 2004;15(3):1313-1323. doi:10.1091/mbc.e03-02-0120

Kyttälä A, Yliannala K, Schu P, Jalanko A, Luzio JP. AP-1 and AP-3 facilitate lysosomal targeting of Batten disease protein CLN3 via its dileucine motif. J Biol Chem. 2005;280(11):10277-10283. doi:10.1074/jbc.M411862200

L

Lalioti V, Muruais G, Dinarina A, van Damme J, Vandekerckhove J, Sandoval IV. The atypical kinase Cdk5 is activated by insulin, regulates the association between GLUT4 and E-Syt1, and modulates glucose transport in 3T3-L1 adipocytes. Proc Natl Acad Sci U S A. 2009;106(11):4249-4253. doi:10.1073/pnas.0900218106

Lam M, Lawrence DA, Ashkenazi A, Walter P. Confirming a critical role for death receptor 5 and caspase-8 in apoptosis induction by endoplasmic reticulum stress. Cell Death Differ. 2018;25(8):1530-1531. doi:10.1038/s41418-018-0155-y

Lamming DW. Diminished mTOR signaling: a common mode of action for endocrine longevity factors. Springerplus. 2014;3:735. Published 2014 Dec 15. doi:10.1186/2193-1801-3-735

Lamming DW, Bar-Peled L. Lysosome: The metabolic signaling hub. Traffic. 2019;20(1):27-38.

doi:10.1111/tra.12617

Lamming DW, Demirkan G, Boylan JM, et al. Hepatic signaling by the mechanistic target of rapamycin complex 2 (mTORC2) [published correction appears in FASEB J. 2021 Feb;35(2):e21165]. FASEB J. 2014;28(1):300-315. doi:10.1096/fj.13-237743

Lamming DW, Sabatini DM. A Central role for mTOR in lipid homeostasis. Cell Metab. 2013;18(4):465-469. doi:10.1016/j.cmet.2013.08.002

Landry JJ, Pyl PT, Rausch T, et al., The genomic and transcriptomic landscape of a HeLa cell line. G3 (Bethesda). 2013;3(8):1213-1224. Published 2013 Aug 7. doi:10.1534/g3.113.005777

Lange J, Haslett LJ, Lloyd-Evans E, et al. Compromised astrocyte function and survival negatively impact neurons in infantile neuronal ceroid lipofuscinosis. Acta Neuropathol Commun. 2018;6(1):74. Published 2018 Aug 8. doi:10.1186/s40478-018-0575-4

Lavoie H, Li JJ, Thevakumaran N, Therrien M, Sicheri F. Dimerization-induced allostery in protein kinase regulation. Trends Biochem Sci. 2014;39(10):475-486. doi:10.1016/j.tibs.2014.08.004

Lebrun AH, Moll-Khosrawi P, Pohl S, et al. Analysis of potential biomarkers and modifier genes affecting the clinical course of CLN3 disease. Mol Med. 2011;17(11-12):1253-1261. doi:10.2119/molmed.2010.00241

Lee DF, Kuo HP, Chen CT, et al. IKK beta suppression of TSC1 links inflammation and tumor angiogenesis via the mTOR pathway. Cell. 2007;130(3):440-455. doi:10.1016/j.cell.2007.05.058

Lee YA, Noon LA, Akat KM, et al. Autophagy is a gatekeeper of hepatic differentiation and carcinogenesis by controlling the degradation of Yap. Nat Commun. 2018;9(1):4962. Published 2018 Nov 23. doi:10.1038/s41467-018-07338-z

Lenaz G. The mitochondrial production of reactive oxygen species: mechanisms and implications in human pathology. IUBMB Life. 2001;52(3-5):159-164. doi:10.1080/15216540152845957

Leng N, Dawson JA, Thomson JA, et al., EBSeq: an empirical Bayes hierarchical model for inference in RNA-seq experiments [published correction appears in Bioinformatics. 2013 Aug 15;29(16):2073]. Bioinformatics. 2013;29(8):1035-1043. doi:10.1093/bioinformatics/btt087

Lerner AG, Upton JP, Praveen PV, et al. IRE1α induces thioredoxin-interacting protein to activate the NLRP3 inflammasome and promote programmed cell death under irremediable ER stress. Cell Metab. 2012;16(2):250-264. doi:10.1016/j.cmet.2012.07.007

Leung KY, Greene ND, Munroe PB, Mole SE. Analysis of CLN3-protein interactions using the yeast two-hybrid system. Eur J Paediatr Neurol. 2001;5 Suppl A:89-93. doi:10.1053/ejpn.2000.0441

Lewis SC, Uchiyama LF, Nunnari J. 2016. ER–mitochondria contacts couple mtDNA synthesis with mitochondrial division in human cells. Science 353:aaf5549

Li B, Dewey CN. RSEM: accurate transcript quantification from RNA-Seq data with or without a reference genome. BMC Bioinformatics. 2011;12:323. Published 2011 Aug 4. doi:10.1186/1471-2105-12-323

Li H, Handsaker B, Wysoker A, et al., The Sequence Alignment/Map format and SAMtools. Bioinformatics. 2009;25(16):2078-2079. doi:10.1093/bioinformatics/btp352

Li P, Fan W, Xu J, et al. Adipocyte NCoR knockout decreases PPARγ phosphorylation and enhances PPARγ activity and insulin sensitivity. Cell. 2011;147(4):815-826. doi:10.1016/j.cell.2011.09.050

Li P, Silvis MR, Honaker Y, Lien WH, Arron ST, Vasioukhin V. αE-catenin inhibits a Src-YAP1 oncogenic module that couples tyrosine kinases and the effector of Hippo signaling pathway. Genes Dev. 2016;30(7):798-811. doi:10.1101/gad.274951.115

Li X, Gould SJ. The dynamin-like GTPase DLP1 is essential for peroxisome division and is recruited to peroxisomes in part by PEX11. J Biol Chem. 2003;278(19):17012-17020. doi:10.1074/jbc.M212031200

Liang N, Zhang C, Dill P, et al. Regulation of YAP by mTOR and autophagy reveals a therapeutic target of tuberous sclerosis complex. J Exp Med. 2014;211(11):2249-2263. doi:10.1084/jem.20140341

Lin J, Zhang L, Zhang M, et al. Mst1 inhibits CMECs autophagy and participates in the development of diabetic coronary microvascular dysfunction. Sci Rep. 2016;6:34199. Published 2016 Sep 29. doi:10.1038/srep34199

Lin JH, Li H, Yasumura D, et al. IRE1 signaling affects cell fate during the unfolded protein response. Science. 2007;318(5852):944-949. doi:10.1126/science.1146361

Lipton JO, Sahin M. The neurology of mTOR. Neuron. 2014;84(2):275-291. doi:10.1016/j.neuron.2014.09.034

Liu GY, Sabatini DM. mTOR at the nexus of nutrition, growth, ageing and disease [published correction appears in Nat Rev Mol Cell Biol. 2020 Jan 31;:]. Nat Rev Mol Cell Biol. 2020;21(4):183-203. doi:10.1038/s41580-019-0199-y

Liu P, Gan W, Chin YR, et al. PtdIns(3,4,5)P3-Dependent Activation of the mTORC2 Kinase Complex. Cancer Discov. 2015;5(11):1194-1209. doi:10.1158/2159-8290.CD-15-0460

Liu P, Wang Z, Wei W. Phosphorylation of Akt at the C-terminal tail triggers Akt activation. Cell Cycle. 2014;13(14):2162-2164. doi:10.4161/cc.29584

Liu SS. Generating, partitioning, targeting and functioning of superoxide in mitochondria. Biosci Rep. 1997;17(3):259-272. doi:10.1023/a:1027328510931

Lin Z, Xie R, Guan K, Zhang M. A WW Tandem-Mediated Dimerization Mode of SAV1 Essential for Hippo Signaling. Cell Rep. 2020;32(10):108118. doi:10.1016/j.celrep.2020.108118

Lopez-Fabuel I, Resch-Beusher M, Carabias-Carrasco M, Almeida A, Bolaños JP. Mitochondrial Complex I Activity is Conditioned by Supercomplex I-III2-IV Assembly in Brain Cells: Relevance for Parkinson's Disease. Neurochem Res. 2017;42(6):1676-1682. doi:10.1007/s11064-017-2191-2

Losón OC, Song Z, Chen H, Chan DC. 2013. Fis1, Mff, MiD49, and MiD51 mediate Drp1 recruitment in mitochondrial fission. Mol. Biol. Cell 24:659–67

Lu PD, Harding HP, Ron D. Translation reinitiation at alternative open reading frames regulates gene expression in an integrated stress response. J Cell Biol. 2004;167(1):27-33. doi:10.1083/jcb.200408003

Luiro K, Kopra O, Blom T, et al., Batten disease (JNCL) is linked to disturbances in mitochondrial, cytoskeletal, and synaptic compartments. J Neurosci Res. 2006;84(5):1124-1138. doi:10.1002/jnr.21015

Luiro K, Kopra O, Lehtovirta M, Jalanko A. CLN3 protein is targeted to neuronal synapses but excluded from synaptic vesicles: new clues to Batten disease. Hum Mol Genet. 2001;10(19):2123-2131. doi:10.1093/hmg/10.19.2123

Luiro K, Yliannala K, Ahtiainen L, et al. Interconnections of CLN3, Hook1 and Rab proteins link Batten disease to defects in the endocytic pathway. Hum Mol Genet. 2004;13(23):3017-3027. doi:10.1093/hmg/ddh321

Lyly A, von Schantz C, Heine C, et al. Novel interactions of CLN5 support molecular networking between Neuronal Ceroid Lipofuscinosis proteins. BMC Cell Biol. 2009;10:83. Published 2009 Nov 26. doi:10.1186/1471-2121-10-83

M

Ma L, Chen Z, Erdjument-Bromage H, Tempst P, Pandolfi PP. Phosphorylation and functional inactivation of TSC2 by Erk implications for tuberous sclerosis and cancer pathogenesis. Cell. 2005;121(2):179-193. doi:10.1016/j.cell.2005.02.031

Ma XM, Blenis J. Molecular mechanisms of mTOR-mediated translational control. Nat Rev Mol Cell Biol. 2009;10(5):307-318. doi:10.1038/nrm2672

Maejima Y, Kyoi S, Zhai P, et al. Mst1 inhibits autophagy by promoting the interaction between Beclin1 and Bcl-2. Nat Med. 2013;19(11):1478-1488. doi:10.1038/nm.3322

Magistretti PJ, Allaman I. A cellular perspective on brain energy metabolism and functional imaging. Neuron. 2015;86(4):883-901. doi:10.1016/j.neuron.2015.03.035

Magnuson B, Ekim B, Fingar DC. Regulation and function of ribosomal protein S6 kinase (S6K) within mTOR signalling networks. Biochem J. 2012;441(1):1-21. doi:10.1042/BJ20110892

Makoukji J, Saadeh F, Mansour KA, et al. Flupirtine derivatives as potential treatment for the neuronal ceroid lipofuscinoses. Ann Clin Transl Neurol. 2018;5(9):1089-1103. Published 2018 Aug 14. doi:10.1002/acn3.625

Manning G, Whyte DB, Martinez R, Hunter T, Sudarsanam S. The protein kinase complement of the human genome. Science. 2002;298(5600):1912-1934. doi:10.1126/science.1075762

Mao Q, Foster BJ, Xia H, Davidson BL. Membrane topology of CLN3, the protein underlying Batten disease. FEBS Lett. 2003;541(1-3):40-46. doi:10.1016/s0014-5793(03)00284-9

Mao Q, Xia H, Davidson BL. Intracellular trafficking of CLN3, the protein underlying the childhood neurodegenerative disease, Batten disease. FEBS Lett. 2003;555(2):351-357. doi:10.1016/s0014-5793(03)01274-2

March PA, Wurzelmann S, Walkley SU. Morphological alterations in neocortical and cerebellar GABAergic neurons in a canine model of juvenile Batten disease. Am J Med Genet. 1995;57(2):204-212. doi:10.1002/ajmg.1320570219

Marciniak SJ, Yun CY, Oyadomari S, et al. CHOP induces death by promoting protein synthesis and oxidation in the stressed endoplasmic reticulum. Genes Dev. 2004;18(24):3066-3077. doi:10.1101/gad.1250704

Margraf LR, Boriack RL, Routheut AA, et al. Tissue expression and subcellular localization of CLN3, the Batten disease protein. Mol Genet Metab. 1999;66(4):283-289. doi:10.1006/mgme.1999.2830

Marí M, Morales A, Colell A, García-Ruiz C, Fernández-Checa JC. Mitochondrial glutathione, a key survival antioxidant. Antioxid Redox Signal. 2009;11(11):2685-2700. doi:10.1089/ARS.2009.2695

Markham A. Cerliponase Alfa: First Global Approval. Drugs. 2017;77(11):1247-1249. doi:10.1007/s40265-017-0771-8

Marotta D, Tinelli E, Mole SE. NCLs and ER: A stressful relationship. Biochim Biophys Acta Mol Basis Dis.

2017;1863(6):1273-1281. doi:10.1016/j.bbadis.2017.04.003

Marshall FJ, de Blieck EA, Mink JW, et al. A clinical rating scale for Batten disease: reliable and relevant for clinical trials. Neurology. 2005;65(2):275-279. doi:10.1212/01.wnl.0000169019.41332.8a

Martina JA, Chen Y, Gucek M, Puertollano R. MTORC1 functions as a transcriptional regulator of autophagy by preventing nuclear transport of TFEB. Autophagy. 2012;8(6):903-914. doi:10.4161/auto.19653

Mathavarajah S, McLaren MD, Huber RJ. Cln3 function is linked to osmoregulation in a Dictyostelium model of Batten disease. Biochim Biophys Acta Mol Basis Dis. 2018;1864(11):3559-3573. doi:10.1016/j.bbadis.2018.08.013

Mayer C, Zhao J, Yuan X, Grummt I. mTOR-dependent activation of the transcription factor TIF-IA links rRNA synthesis to nutrient availability. Genes Dev. 2004;18(4):423-434. doi:10.1101/gad.285504

Medina DL, Di Paola S, Peluso I, et al. Lysosomal calcium signalling regulates autophagy through calcineurin and TFEB. Nat Cell Biol. 2015;17(3):288-299. doi:10.1038/ncb3114

Meinecke M, Cizmowski C, Schliebs W, et al. The peroxisomal importomer constitutes a large and highly dynamic pore. Nat Cell Biol. 2010;12(3):273-277. doi:10.1038/ncb2027

Metcalf DJ, Calvi AA, Seaman MNj, Mitchison HM, Cutler DF. Loss of the Batten disease gene CLN3 prevents exit from the TGN of the mannose 6-phosphate receptor. Traffic. 2008;9(11):1905-1914. doi:10.1111/j.1600-0854.2008.00807.x

Michalewski MP, Kaczmarski W, Golabek AA, Kida E, Kaczmarski A, Wisniewski KE. Evidence for phosphorylation of CLN3 protein associated with Batten disease. Biochem Biophys Res Commun. 1998;253(2):458-462. doi:10.1006/bbrc.1998.9210

Michalewski MP, Kaczmarski W, Golabek AA, Kida E, Kaczmarski A, Wisniewski KE. Posttranslational modification of CLN3 protein and its possible functional implication. Mol Genet Metab. 1999;66(4):272-276. doi:10.1006/mgme.1999.2818

Miller JN, Chan CH, Pearce DA. The role of nonsense-mediated decay in neuronal ceroid lipofuscinosis. Hum Mol Genet. 2013;22(13):2723-2734. doi:10.1093/hmg/ddt120

Mink JW, Augustine EF, Adams HR, Marshall FJ, Kwon JM. Classification and natural history of the neuronal ceroid lipofuscinoses. J Child Neurol. 2013;28(9):1101-1105. doi:10.1177/0883073813494268

Mirza M, Vainshtein A, DiRonza A, et al. The CLN3 gene and protein: What we know. Mol Genet Genomic Med. 2019;7(12):e859. doi:10.1002/mgg3.859

Mitchell WA, Porter M, Kuwabara P, Mole SE. Genomic structure of three CLN3-like genes in Caenorhabditis elegans. Eur J Paediatr Neurol. 2001;5 Suppl A:121-125. doi:10.1053/ejpn.2000.0447

Mitchison HM, Munroe PB, O'Rawe AM, et al. Genomic structure and complete nucleotide sequence of the Batten disease gene, CLN3. Genomics. 1997;40(2):346-350. doi:10.1006/geno.1996.4576

Mitchison HM, O'Rawe AM, Lerner TJ, et al. Refined localization of the Batten disease gene (CLN3) by haplotype and linkage disequilibrium mapping to D16S288-D16S383 and exclusion from this region of a variant form of Batten disease with granular osmiophilic deposits. Am J Med Genet. 1995;57(2):312-315. doi:10.1002/ajmg.1320570241

Mitchison HM, O'Rawe AM, Taschner PE, et al. Batten disease gene, CLN3: linkage disequilibrium mapping in the Finnish population, and analysis of European haplotypes. Am J Hum Genet. 1995;56(3):654-662.

Mitchison HM, Thompson AD, Mulley JC, et al. Fine genetic mapping of the Batten disease locus (CLN3) by haplotype analysis and demonstration of allelic association with chromosome 16p microsatellite loci. Genomics. 1993;16(2):455-460. doi:10.1006/geno.1993.1210

Misra JR, Irvine KD. The Hippo Signaling Network and Its Biological Functions. Annu Rev Genet. 2018;52:65-87. doi:10.1146/annurev-genet-120417-031621

Mo JS, Meng Z, Kim YC, et al. Cellular energy stress induces AMPK-mediated regulation of YAP and the Hippo pathway. Nat Cell Biol. 2015;17(4):500-510. doi:10.1038/ncb3111

Mole S, Haltia M. The neuronal ceroid-lipofuscinoses (batten disease). In: Rosenberg R, Pascual J, editors. Rosenberg's molecular and genetic basis of neurological and psychiatric disease. 5th ed. Boston: Academic Press; 2015a. p. 793–808. doi:10.1016/B978-0-12-410529-4.00070-X

Mole SE, Anderson G, Band HA, et al. Clinical challenges and future therapeutic approaches for neuronal ceroid lipofuscinosis. Lancet Neurol. 2019;18(1):107-116. doi:10.1016/S1474-4422(18)30368-5

Mole SE, Cotman SL. Genetics of the neuronal ceroid lipofuscinoses (Batten disease). Biochim Biophys Acta. 2015;1852(10 Pt B):2237-2241. doi:10.1016/j.bbadis.2015.05.011

Mole SE, Williams RE, Goebel HH, Machado da Silva G. CLN3-Clinical Data. The neuronal ceroid lipofuscinoses (Batten disease). Cary, North Carolina, Oxford University Press, 2011. Pages 117–119. Print

Montilla-Martinez M, Beck S, Klümper J, et al. Distinct Pores for Peroxisomal Import of PTS1 and PTS2 Proteins. Cell Rep. 2015;13(10):2126-2134. doi:10.1016/j.celrep.2015.11.016

Moon S, Kim W, Kim S, et al. Phosphorylation by NLK inhibits YAP-14-3-3-interactions and induces its nuclear localization. EMBO Rep. 2017;18(1):61-71. doi:10.15252/embr.201642683

Moon SL, Sonenberg N, Parker R. Neuronal Regulation of eIF2α Function in Health and Neurological Disorders. Trends Mol Med. 2018;24(6):575-589. doi:10.1016/j.molmed.2018.04.001

Morita S, Villalta SA, Feldman HC, et al. Targeting ABL-IRE1α Signaling Spares ER-Stressed Pancreatic β Cells to Reverse Autoimmune Diabetes [published correction appears in Cell Metab. 2017 May 2;25(5):1207]. Cell Metab. 2017;25(4):883-897.e8. doi:10.1016/j.cmet.2017.03.018

Michels AA, Robitaille AM, Buczynski-Ruchonnet D, et al. mTORC1 directly phosphorylates and regulates human MAF1. Mol Cell Biol. 2010;30(15):3749-3757. doi:10.1128/MCB.00319-10

Minnis CJ, Thornton CD, FitzPatrick LM, McKay TR. Cellular models of Batten disease. Biochim Biophys Acta Mol Basis Dis. 2020;1866(9):165559. doi:10.1016/j.bbadis.2019.165559

Mishra P, Carelli V, Manfredi G, Chan DC. Proteolytic cleavage of Opa1 stimulates mitochondrial inner membrane fusion and couples fusion to oxidative phosphorylation [published correction appears in Cell Metab. 2014 May 6;19(5):891]. Cell Metab. 2014;19(4):630-641. doi:10.1016/j.cmet.2014.03.011

Monteith AJ, Vincent HA, Kang S, et al. mTORC2 Activity Disrupts Lysosome Acidification in Systemic Lupus Erythematosus by Impairing Caspase-1 Cleavage of Rab39a. J Immunol. 2018;201(2):371-382. doi:10.4049/jimmunol.1701712

Moser BA, Dennis PB, Pullen N, et al. Dual requirement for a newly identified phosphorylation site in p70s6k. Mol Cell Biol. 1997;17(9):5648-5655. doi:10.1128/MCB.17.9.5648

Muñoz JP, Ivanova S, Sánchez-Wandelmer J, et al. Mfn2 modulates the UPR and mitochondrial function via repression of PERK [published correction appears in EMBO J. 2014 Jan 13;33(2):171]. EMBO J. 2013;32(17):2348-2361. doi:10.1038/emboj.2013.168

Muñoz-Pinedo C, López-Rivas A. A role for caspase-8 and TRAIL-R2/DR5 in ER-stress-induced apoptosis. Cell Death Differ. 2018;25(1):226. doi:10.1038/cdd.2017.155

Muzaffar NE, Pearce DA. Analysis of NCL Proteins from an Evolutionary Standpoint. Curr Genomics. 2008;9(2):115-136. doi:10.2174/138920208784139573

N

Nelson T, Pearce DA, Kovács AD. Lack of specificity of antibodies raised against CLN3, the lysosomal/endosomal transmembrane protein mutated in juvenile Batten disease. Biosci Rep. 2017;37(6):BSR20171229. Published 2017 Nov 23. doi:10.1042/BSR20171229

Newsholme P, Haber EP, Hirabara SM, et al., Diabetes associated cell stress and dysfunction: role of mitochondrial and non-mitochondrial ROS production and activity. J Physiol. 2007;583(Pt 1):9-24. doi:10.1113/jphysiol.2007.135871

Nguyen CDK, Yi C. YAP/TAZ Signaling and Resistance to Cancer Therapy. Trends Cancer. 2019;5(5):283-296. doi:10.1016/j.trecan.2019.02.010

Nijssen PC, Ceuterick C, van Diggelen OP, et al. Autosomal dominant adult neuronal ceroid lipofuscinosis: a novel form of NCL with granular osmiophilic deposits without palmitoyl protein thioesterase 1 deficiency. Brain Pathol. 2003;13(4):574-581. doi:10.1111/j.1750-3639.2003.tb00486.x

Nishiyama A, Xin L, Sharov AA, et al. Uncovering early response of gene regulatory networks in ESCs by systematic induction of transcription factors. Cell Stem Cell. 2009;5(4):420-433. doi:10.1016/j.stem.2009.07.012

Nobes CD, Brown GC, Olive PN, Brand MD. Non-ohmic proton conductance of the mitochondrial inner membrane in hepatocytes. J Biol Chem. 1990;265(22):12903-12909.

Nosková L, Stránecký V, Hartmannová H, et al. Mutations in DNAJC5, encoding cysteine-string protein alpha, cause autosomal-dominant adult-onset neuronal ceroid lipofuscinosis [published correction appears in Am J Hum Genet. 2011 Oct 7;89(4):589]. Am J Hum Genet. 2011;89(2):241-252. doi:10.1016/j.ajhg.2011.07.003

Noto A, De Vitis C, Pisanu ME, et al. Stearoyl-CoA-desaturase 1 regulates lung cancer stemness via stabilization and nuclear localization of YAP/TAZ [published correction appears in Oncogene. 2017 Jun 19;:]. Oncogene. 2017;36(32):4573-4584. doi:10.1038/onc.2017.75

Novoa I, Zeng H, Harding HP, Ron D. Feedback inhibition of the unfolded protein response by GADD34-mediated dephosphorylation of eIF2alpha. J Cell Biol. 2001;153(5):1011-1022. doi:10.1083/jcb.153.5.1011

Nugent T, Mole SE, Jones DT. The transmembrane topology of Batten disease protein CLN3 determined by consensus computational prediction constrained by experimental data. FEBS Lett. 2008;582(7):1019-1024. doi:10.1016/j.febslet.2008.02.049

O

Oetjen S, Kuhl D, Hermey G. Revisiting the neuronal localization and trafficking of CLN3 in juvenile neuronal ceroid lipofuscinosis. J Neurochem. 2016;139(3):456-470. doi:10.1111/jnc.13744

Oettinghaus B, Licci M, Scorrano L, Frank S. Less than perfect divorces: dysregulated mitochondrial fission and neurodegeneration. Acta Neuropathol. 2012;123(2):189-203. doi:10.1007/s00401-011-0930-z

Oh H, Irvine KD. In vivo regulation of Yorkie phosphorylation and localization. Development. 2008;135(6):1081-1088. doi:10.1242/dev.015255

Oh H, Reddy BV, Irvine KD. Phosphorylation-independent repression of Yorkie in Fat-Hippo signaling. Dev Biol. 2009;335(1):188-197. doi:10.1016/j.ydbio.2009.08.026

Okado-Matsumoto A, Fridovich I. Subcellular distribution of superoxide dismutases (SOD) in rat liver: Cu,Zn-SOD in mitochondria. J Biol Chem. 2001;276(42):38388-38393. doi:10.1074/jbc.M105395200

Orii Y. The cytochrome c peroxidase activity of cytochrome oxidase. J Biol Chem. 1982;257(16):9246-9248.

Osellame LD, Singh AP, Stroud DA, Palmer CS, Stojanovski D, et al., 2016. Cooperative and independent roles of the Drp1 adaptors Mff,MiD49 and MiD51 in mitochondrial fission. J. Cell Sci. 129:2170–81

Ostergaard JR. Juvenile neuronal ceroid lipofuscinosis (Batten disease): current insights. Degener Neurol Neuromuscul Dis. 2016;6:73-83. Published 2016 Aug 1. doi:10.2147/DNND.S111967

Ostergaard JR, Rasmussen TB, Mølgaard H. Cardiac involvement in juvenile neuronal ceroid lipofuscinosis (Batten disease). Neurology. 2011;76(14):1245-1251. doi:10.1212/WNL.0b013e31821435bd

Oswald MJ, Palmer DN, Kay GW, Shemilt SJ, Rezaie P, Cooper JD. Glial activation spreads from specific cerebral foci and precedes neurodegeneration in presymptomatic ovine neuronal ceroid lipofuscinosis (CLN6). Neurobiol Dis. 2005;20(1):49-63. doi:10.1016/j.nbd.2005.01.025

Otera H, Miyata N, Kuge O, Mihara K. 2016. Drp1-dependent mitochondrial fission via MiD49/51 is essential for apoptotic cristae remodeling. J. Cell Biol. 212:531–44

P

Padilla-López S, Pearce DA. Saccharomyces cerevisiae lacking Btn1p modulate vacuolar ATPase activity to regulate pH imbalance in the vacuole. J Biol Chem. 2006;281(15):10273-10280. doi:10.1074/jbc.M510625200Pagliuso A, Cossart P, Stavru F. 2018. The ever-growing complexity of the mitochondrial fission machinery. Cell Mol. Life Sci. 75:355–74

Palmer DN. The relevance of the storage of subunit c of ATP synthase in different forms and models of Batten disease (NCLs). Biochim Biophys Acta. 2015;1852(10 Pt B):2287-2291. doi:10.1016/j.bbadis.2015.06.014

Palmer DN, Barry LA, Tyynelä J, Cooper JD. NCL disease mechanisms. Biochim Biophys Acta. 2013;1832(11):1882-1893. doi:10.1016/j.bbadis.2013.05.014

Palmer DN, Bayliss SL, Clifton PA, Grant VJ. Storage bodies in the ceroid-lipofuscinoses (Batten disease): low-molecular-weight components, unusual amino acids and reconstitution of fluorescent bodies from non-fluorescent components. J Inherit Metab Dis. 1993;16(2):292-295. doi:10.1007/BF00710268

Palmer DN, Fearnley IM, Walker JE, et al. Mitochondrial ATP synthase subunit c storage in the ceroid-lipofuscinoses (Batten disease). Am J Med Genet. 1992;42(4):561-567. doi:10.1002/ajmg.1320420428

Palmer DN, Husbands DR, Winter PJ, Blunt JW, Jolly RD. Ceroid lipofuscinosis in sheep. I. Bis(monoacylglycero)phosphate, dolichol, ubiquinone, phospholipids, fatty acids, and fluorescence in liver lipopigment lipids. J Biol Chem. 1986;261(4):1766-1772.

Palmer DN, Martinus RD, Cooper SM, Midwinter GG, Reid JC, Jolly RD. Ovine ceroid lipofuscinosis. The major lipopigment protein and the lipid-binding subunit of mitochondrial ATP synthase have the same NH2-terminal sequence. J Biol Chem. 1989;264(10):5736-5740.

Palmer DN, Oswald MJ, Westlake VJ, Kay GW. The origin of fluorescence in the neuronal ceroid lipofuscinoses (Batten disease) and neuron cultures from affected sheep for studies of neurodegeneration. Arch Gerontol Geriatr. 2002;34(3):343-357. doi:10.1016/s0167-4943(02)00011-0

Palmer DN, Tyynelä J, van Mil HC, Westlake VJ, Jolly RD. Accumulation of sphingolipid activator proteins (SAPs) A and D in granular osmiophilic deposits in miniature Schnauzer dogs with ceroid-lipofuscinosis. J Inherit Metab Dis. 1997;20(1):74-84. doi:10.1023/a:1005365709340

Palmieri M, Impey S, Kang H, et al. Characterization of the CLEAR network reveals an integrated control of cellular clearance pathways. Hum Mol Genet. 2011;20(19):3852-3866. doi:10.1093/hmg/ddr306

Palmieri M, Pal R, Nelvagal HR, et al., mTORC1-independent TFEB activation via Akt inhibition promotes cellular clearance in neurodegenerative storage diseases [published correction appears in Nat Commun. 2017 Jun 13;8:15793]. Nat Commun. 2017;8:14338. Published 2017 Feb 6. doi:10.1038/ncomms14338

Pandey R, Mandal AK, Jha V, Mukerji M. Heat shock factor binding in Alu repeats expands its involvement in stress through an antisense mechanism. Genome Biol. 2011;12(11):R117. Published 2011 Nov 23. doi:10.1186/gb-2011-12-11-r117

Papa S, Skulachev VP. Reactive oxygen species, mitochondria, apoptosis and aging. Mol Cell Biochem. 1997;174(1-2):305-319.

Park HK, Ahima RS. Leptin signaling. F1000Prime Rep. 2014;6:73. Published 2014 Sep 4. doi:10.12703/P6-73

Park YY, Sohn BH, Johnson RL, et al. Yes-associated protein 1 and transcriptional coactivator with PDZ-binding motif activate the mammalian target of rapamycin complex 1 pathway by regulating amino acid transporters in hepatocellular carcinoma. Hepatology. 2016;63(1):159-172. doi:10.1002/hep.28223

Parker BW, Gogl G, Bálint M, Hetényi C, Reményi A, Weiss EL. Ndr/Lats Kinases Bind Specific Mob-Family Coactivators through a Conserved and Modular Interface. Biochemistry. 2020;59(17):1688-1700. doi:10.1021/acs.biochem.9b01096

Parmar VM, Schröder M. Sensing endoplasmic reticulum stress. Adv Exp Med Biol. 2012;738:153-168. doi:10.1007/978-1-4614-1680-7_10

Parviainen L, Dihanich S, Anderson GW, et al. Glial cells are functionally impaired in juvenile neuronal ceroid lipofuscinosis and detrimental to neurons. Acta Neuropathol Commun. 2017;5(1):74. Published 2017 Oct 17. doi:10.1186/s40478-017-0476-y

Pawson T, Scott JD. Protein phosphorylation in signaling--50 years and counting. Trends Biochem Sci. 2005;30(6):286-290. doi:10.1016/j.tibs.2005.04.013

Pedraza JM, van Oudenaarden A. Noise propagation in gene networks. Science. 2005;307(5717):1965-1969. doi:10.1126/science.1109090

Pellegrino MW, Haynes CM. Mitophagy and the mitochondrial unfolded protein response in neurodegeneration and bacterial infection. BMC Biol. 2015;13:22. Published 2015 Apr 3. doi:10.1186/s12915-015-0129-1

Peng C, Zhu Y, Zhang W, et al. Regulation of the Hippo-YAP Pathway by Glucose Sensor O-GlcNAcylation. Mol Cell. 2017;68(3):591-604.e5. doi:10.1016/j.molcel.2017.10.010

Peng W, Wong YC, Krainc D. Mitochondria-lysosome contacts regulate mitochondrial Ca2+ dynamics via lysosomal TRPML1. Proc Natl Acad Sci U S A. 2020;117(32):19266-19275. doi:10.1073/pnas.2003236117

Peng Y, Kim MJ, Hullinger R, et al. Improved proteostasis in the secretory pathway rescues Alzheimer's disease in the mouse. Brain. 2016;139(Pt 3):937-952. doi:10.1093/brain/awv385

Peng Y, Puglielli L. Nε-lysine acetylation in the lumen of the endoplasmic reticulum: A way to regulate autophagy and maintain protein homeostasis in the secretory pathway. Autophagy. 2016;12(6):1051-1052. doi:10.1080/15548627.2016.1164369

Perera RM, Zoncu R. The Lysosome as a Regulatory Hub. Annu Rev Cell Dev Biol. 2016;32:223-253. doi:10.1146/annurev-cellbio-111315-125125

Perkins GA, Ellisman MH, Fox DA. Three-dimensional analysis of mouse rod and cone mitochondrial cristae architecture: bioenergetic and functional implications. Mol Vis. 2003;9:60-73. Published 2003 Mar 11.

Pernas L, Scorrano L. Mito-Morphosis: Mitochondrial Fusion, Fission, and Cristae Remodeling as Key Mediators of Cellular Function. Annu Rev Physiol. 2016;78:505-531. doi:10.1146/annurev-physiol-021115-105011

Persaud-Sawin DA, McNamara JO 2nd, Rylova S, Vandongen A, Boustany RM. A galactosylceramide binding domain is involved in trafficking of CLN3 from Golgi to rafts via recycling endosomes. Pediatr Res. 2004;56(3):449-463. doi:10.1203/01.PDR.0000136152.54638.95

Persaud-Sawin DA, Mousallem T, Wang C, Zucker A, Kominami E, Boustany RM. Neuronal ceroid lipofuscinosis: a common pathway?. Pediatr Res. 2007;61(2):146-152. doi:10.1203/pdr.0b013e31802d8a4a

Petcherski A, Chandrachud U, Butz ES, et al., An Autophagy Modifier Screen Identifies Small Molecules Capable of Reducing Autophagosome Accumulation in a Model of CLN3-Mediated Neurodegeneration. Cells. 2019;8(12):1531. Published 2019 Nov 27. doi:10.3390/cells8121531

Pezzini F, Gismondi F, Tessa A, et al., Involvement of the mitochondrial compartment in human NCL fibroblasts. Biochem Biophys Res Commun. 2011;416(1-2):159-164. doi:10.1016/j.bbrc.2011.11.016

Phillips MJ, Voeltz GK. Structure and function of ER membrane contact sites with other organelles. Nat Rev Mol Cell Biol. 2016;17(2):69-82. doi:10.1038/nrm.2015.8

Pinkaew D, Chattopadhyay A, King MD, et al. Fortilin binds IRE1α and prevents ER stress from signaling apoptotic cell death. Nat Commun. 2017;8(1):18. Published 2017 May 26. doi:10.1038/s41467-017-00029-1

Pontikis CC, Cella CV, Parihar N, et al. Late onset neurodegeneration in the Cln3-/- mouse model of juvenile neuronal ceroid lipofuscinosis is preceded by low level glial activation. Brain Res. 2004;1023(2):231-242. doi:10.1016/j.brainres.2004.07.030

Pontikis CC, Cotman SL, MacDonald ME, Cooper JD. Thalamocortical neuron loss and localized astrocytosis in the Cln3Deltaex7/8 knock-in mouse model of Batten disease. Neurobiol Dis. 2005;20(3):823-836. doi:10.1016/j.nbd.2005.05.018

Popov LD. Mitochondrial biogenesis: An update. J Cell Mol Med. 2020;24(9):4892-4899. doi:10.1111/jcmm.15194

Preising MN, Abura M, Jäger M, Wassill KH, Lorenz B. Ocular morphology and function in juvenile neuronal ceroid lipofuscinosis (CLN3) in the first decade of life. Ophthalmic Genet. 2017;38(3):252-259. doi:10.1080/13816810.2016.1210651

Pruitt KD, Brown GR, Hiatt SM, et al. RefSeq: an update on mammalian reference sequences. Nucleic Acids Res. 2014;42(Database issue):D756-D763. doi:10.1093/nar/gkt1114

Puleston D. Detection of Mitochondrial Mass, Damage, and Reactive Oxygen Species by Flow Cytometry. Cold Spring Harb Protoc. 2015;2015(9):pdb.prot086298. Published 2015 Sep 1. doi:10.1101/pdb.prot086298

Pullarkat RK, Morris GN. Farnesylation of Batten disease CLN3 protein. Neuropediatrics. 1997;28(1):42-44. doi:10.1055/s-2007-973665

Pullen N, Dennis PB, Andjelkovic M, et al. Phosphorylation and activation of p70s6k by PDK1. Science. 1998;279(5351):707-710. doi:10.1126/science.279.5351.707

Puranam KL, Guo WX, Qian WH, Nikbakht K, Boustany RM. CLN3 defines a novel antiapoptotic pathway operative in neurodegeneration and mediated by ceramide. Mol Genet Metab. 1999;66(4):294-308. doi:10.1006/mgme.1999.2834

R

R Core Team. R: A Language and Environment for Statistical Computing. Vienna: R Foundation for Statistical Computing (2018).

Rabilloud T, Heller M, Rigobello MP, Bindoli A, Aebersold R, Lunardi J. The mitochondrial antioxidant defence system and its response to oxidative stress. Proteomics. 2001;1(9):1105-1110. doi:10.1002/1615-9861(200109)1:9<1105::AID-PROT1105>3.0.CO;2-M

Radke J, Koll R, Gill E, et al. Autophagic vacuolar myopathy is a common feature of CLN3 disease. Ann Clin Transl Neurol. 2018;5(11):1385-1393. Published 2018 Oct 14. doi:10.1002/acn3.662

Raimundo N. Mitochondrial pathology: stress signals from the energy factory. Trends Mol Med. 2014;20(5):282-292. doi:10.1016/j.molmed.2014.01.005

Raimundo N, Krisko A. Editorial: Mitochondrial Communication in Physiology, Disease and Aging. Front Cell Dev Biol. 2019;7:54. Published 2019 Apr 11. doi:10.3389/fcell.2019.00054

Rambold AS, Cohen S, Lippincott-Schwartz J. Fatty acid trafficking in starved cells: regulation by lipid droplet lipolysis, autophagy, and mitochondrial fusion dynamics. Dev Cell. 2015;32(6):678-692. doi:10.1016/j.devcel.2015.01.029

Ramirez K, Chandler KJ, Spaulding C, et al. Gene deregulation and chronic activation in natural killer cells deficient in the transcription factor ETS1. Immunity. 2012;36(6):921-932. doi:10.1016/j.immuni.2012.04.006

Ratajczak E, Petcherski A, Ramos-Moreno J, Ruonala MO. FRET-assisted determination of CLN3 membrane topology. PLoS One. 2014;9(7):e102593. Published 2014 Jul 22. doi:10.1371/journal.pone.0102593

Ravikumar B, Moreau K, Jahreiss L, Puri C, Rubinsztein DC. Plasma membrane contributes to the formation of pre-autophagosomal structures [published correction appears in Nat Cell Biol. 2010 Oct;12(10):1021]. Nat Cell

Biol. 2010;12(8):747-757. doi:10.1038/ncb2078

Reaves B, Banting G. Overexpression of TGN38/41 leads to mislocalisation of gamma-adaptin. FEBS Lett. 1994;351(3):448-456. doi:10.1016/0014-5793(94)00813-2

Ricquier D. UCP1, the mitochondrial uncoupling protein of brown adipocyte: A personal contribution and a historical perspective. Biochimie. 2017;134:3-8. doi:10.1016/j.biochi.2016.10.018

Rietdorf K, Coode EE, Schulz A, Wibbeler E, Bootman MD, Ostergaard JR. Cardiac pathology in neuronal ceroid lipofuscinoses (NCL): More than a mere co-morbidity. Biochim Biophys Acta Mol Basis Dis. 2020;1866(9):165643. doi:10.1016/j.bbadis.2019.165643

Rimessi A, Previati M, Nigro F, Wieckowski MR, Pinton P. Mitochondrial reactive oxygen species and inflammation: Molecular mechanisms, diseases and promising therapies. Int J Biochem Cell Biol. 2016;81(Pt B):281-293. doi:10.1016/j.biocel.2016.06.015

Rizzuto R, De Stefani D, Raffaello A, Mammucari C. Mitochondria as sensors and regulators of calcium signalling. Nat Rev Mol Cell Biol. 2012;13(9):566-578. doi:10.1038/nrm3412

Roczniak-Ferguson A, Petit CS, Froehlich F, et al. The transcription factor TFEB links mTORC1 signaling to transcriptional control of lysosome homeostasis. Sci Signal. 2012;5(228):ra42. Published 2012 Jun 12. doi:10.1126/scisignal.2002790

Rodriguez DA, Zamorano S, Lisbona F, et al. BH3-only proteins are part of a regulatory network that control the sustained signalling of the unfolded protein response sensor IRE1α. EMBO J. 2012;31(10):2322-2335. doi:10.1038/emboj.2012.84

Rojansky R, Cha MY, Chan DC. 2016. Elimination of paternal mitochondria in mouse embryos occurs through autophagic degradation dependent on PARKIN and MUL1. eLife 5:e17896

Rojas-Rivera D, Armisén R, Colombo A, et al. TMBIM3/GRINA is a novel unfolded protein response (UPR) target gene that controls apoptosis through the modulation of ER calcium homeostasis. Cell Death Differ. 2012;19(6):1013-1026. doi:10.1038/cdd.2011.189

Rolfe DF, Brand MD. Contribution of mitochondrial proton leak to skeletal muscle respiration and to standard metabolic rate. Am J Physiol. 1996;271(4 Pt 1):C1380-C1389. doi:10.1152/ajpcell.1996.271.4.C1380

Rolfe DF, Newman JM, Buckingham JA, Clark MG, Brand MD. Contribution of mitochondrial proton leak to respiration rate in working skeletal muscle and liver and to SMR. Am J Physiol. 1999;276(3):C692-C699. doi:10.1152/ajpcell.1999.276.3.C692

Ron D, Walter P. Signal integration in the endoplasmic reticulum unfolded protein response. Nat Rev Mol Cell Biol. 2007;8(7):519-529. doi:10.1038/nrm2199

Rosario FJ, Dimasuay KG, Kanai Y, Powell TL, Jansson T. Regulation of amino acid transporter trafficking by mTORC1 in primary human trophoblast cells is mediated by the ubiquitin ligase Nedd4-2. Clin Sci (Lond). 2016;130(7):499-512. doi:10.1042/CS20150554

Rosenberg JB, Chen A, Kaminsky SM, Crystal RG, Sondhi D. Advances in the Treatment of Neuronal Ceroid Lipofuscinosis. Expert Opin Orphan Drugs. 2019;7(11):473-500. doi:10.1080/21678707.2019.1684258

Rowland AA, Chitwood PJ, Phillips MJ, Voeltz GK. ER contact sites define the position and timing of endosome

fission. Cell. 2014;159(5):1027-1041. doi:10.1016/j.cell.2014.10.023

Ruvinsky I, Sharon N, Lerer T, et al. Ribosomal protein S6 phosphorylation is a determinant of cell size and glucose homeostasis. Genes Dev. 2005;19(18):2199-2211. doi:10.1101/gad.351605

Rylova SN, Amalfitano A, Persaud-Sawin DA, et al. The CLN3 gene is a novel molecular target for cancer drug discovery. Cancer Res. 2002;62(3):801-808.

S

Sabatini DM, Erdjument-Bromage H, Lui M, Tempst P, Snyder SH. RAFT1: a mammalian protein that binds to FKBP12 in a rapamycin-dependent fashion and is homologous to yeast TORs. Cell. 1994;78(1):35-43. doi:10.1016/0092-8674(94)90570-3

Sabers CJ, Martin MM, Brunn GJ, et al. Isolation of a protein target of the FKBP12-rapamycin complex in mammalian cells. J Biol Chem. 1995;270(2):815-822. doi:10.1074/jbc.270.2.815

Saito A, Cai L, Matsuhisa K, et al. Neuronal activity-dependent local activation of dendritic unfolded protein response promotes expression of brain-derived neurotrophic factor in cell soma. J Neurochem. 2018;144(1):35-49. doi:10.1111/jnc.14221

Sancak Y, Peterson TR, Shaul YD, et al. The Rag GTPases bind raptor and mediate amino acid signaling to mTORC1. Science. 2008;320(5882):1496-1501. doi:10.1126/science.1157535

Sander JD, Joung JK. CRISPR-Cas systems for editing, regulating and targeting genomes. Nat Biotechnol. 2014;32(4):347-355. doi:10.1038/nbt.2842

Sarbassov DD, Ali SM, Kim DH, et al. Rictor, a novel binding partner of mTOR, defines a rapamycin-insensitive and raptor-independent pathway that regulates the cytoskeleton. Curr Biol. 2004;14(14):1296-1302. doi:10.1016/j.cub.2004.06.054

Sarbassov DD, Guertin DA, Ali SM, Sabatini DM. Phosphorylation and regulation of Akt/PKB by the rictor-mTOR complex. Science. 2005;307(5712):1098-1101. doi:10.1126/science.1106148

Sardiello M, Palmieri M, di Ronza A, et al. A gene network regulating lysosomal biogenesis and function. Science. 2009;325(5939):473-477. doi:10.1126/science.1174447

Sargsyan Y, Bickmeyer U, Gibhardt CS, Streckfuss-Bömeke K, Bogeski I, Thoms S. Peroxisomes contribute to intracellular calcium dynamics in cardiomyocytes and non-excitable cells. Life Sci Alliance. 2021;4(9):e202000987. Published 2021 Jul 30. doi:10.26508/lsa.202000987

Sargsyan Y, Thoms S. Staying in Healthy Contact: How Peroxisomes Interact with Other Cell Organelles. Trends Mol Med. 2020;26(2):201-214. doi:10.1016/j.molmed.2019.09.012

Saxton RA, Sabatini DM. mTOR Signaling in Growth, Metabolism, and Disease [published correction appears in Cell. 2017 Apr 6;169(2):361-371]. Cell. 2017;168(6):960-976. doi:10.1016/j.cell.2017.02.004

Sayre LM, Perry G, Smith MA. Oxidative stress and neurotoxicity. Chem Res Toxicol. 2008;21(1):172-188. doi:10.1021/tx700210j

Schägger H. Blue-native gels to isolate protein complexes from mitochondria. Methods Cell Biol. 2001;65:231-244. doi:10.1016/s0091-679x(01)65014-3

Schmidt O, Pfanner N, Meisinger C. Mitochondrial protein import: from proteomics to functional mechanisms.

Nat Rev Mol Cell Biol. 2010;11(9):655-667. doi:10.1038/nrm2959

Schmidtke C, Tiede S, Thelen M, et al., Lysosomal proteome analysis reveals that CLN3-defective cells have multiple enzyme deficiencies associated with changes in intracellular trafficking. J Biol Chem. 2019;294(24):9592-9604. doi:10.1074/jbc.RA119.008852

Schrader M, Costello JL, Godinho LF, Azadi AS, Islinger M. Proliferation and fission of peroxisomes - An update. Biochim Biophys Acta. 2016;1863(5):971-983. doi:10.1016/j.bbamcr.2015.09.024

Schrader M, Costello J, Godinho LF, Islinger M. Peroxisome-mitochondria interplay and disease. J Inherit Metab Dis. 2015;38(4):681-702. doi:10.1007/s10545-015-9819-7

Schrader M, Godinho LF, Costello JL, Islinger M. The different facets of organelle interplay-an overview of organelle interactions. Front Cell Dev Biol. 2015;3:56. Published 2015 Sep 25. doi:10.3389/fcell.2015.00056

Schröder B, Elsässer HP, Schmidt B, Hasilik A. Characterisation of lipofuscin-like lysosomal inclusion bodies from human placenta. FEBS Lett. 2007;581(1):102-108. doi:10.1016/j.febslet.2006.12.005

Schröder BA, Wrocklage C, Hasilik A, Saftig P. The proteome of lysosomes. Proteomics. 2010;10(22):4053-4076. doi:10.1002/pmic.201000196

Schulz A, Ajayi T, Specchio N, et al. Study of Intraventricular Cerliponase Alfa for CLN2 Disease. N Engl J Med. 2018;378(20):1898-1907. doi:10.1056/NEJMoa1712649

Schulz JB. Anti-apoptotic gene therapy in Parkinson's disease. J Neural Transm Suppl. 2006;(70):467-476. doi:10.1007/978-3-211-45295-0_70

Sciarretta S, Zhai P, Maejima Y, et al. mTORC2 regulates cardiac response to stress by inhibiting MST1. Cell Rep. 2015;11(1):125-136. doi:10.1016/j.celrep.2015.03.010

Scifo E, Szwajda A, Dębski J, et al., Drafting the CLN3 protein interactome in SH-SY5Y human neuroblastoma cells: a label-free quantitative proteomics approach [published correction appears in J Proteome Res. 2013 Aug 2;12(8):3822]. J Proteome Res. 2013;12(5):2101-2115. doi:10.1021/pr301125k

Scotto Rosato A, Montefusco S, Soldati C, et al., TRPML1 links lysosomal calcium to autophagosome biogenesis through the activation of the CaMKKβ/VPS34 pathway. Nat Commun. 2019;10(1):5630. Published 2019 Dec 10. doi:10.1038/s41467-019-13572-w

Seehafer SS, Ramirez-Montealegre D, Wong AM, et al. Immunosuppression alters disease severity in juvenile Batten disease mice. J Neuroimmunol. 2011;230(1-2):169-172. doi:10.1016/j.jneuroim.2010.08.024

Seifert C, Storch S, Bähring R. Modulation of Kv4.2/KChIP3 interaction by the ceroid lipofuscinosis neuronal 3 protein CLN3. J Biol Chem. 2020;295(34):12099-12110. doi:10.1074/jbc.RA120.013828

Selden NR, Al-Uzri A, Huhn SL, et al. Central nervous system stem cell transplantation for children with neuronal ceroid lipofuscinosis. J Neurosurg Pediatr. 2013;11(6):643-652. doi:10.3171/2013.3.PEDS12397

Sengupta S, Lorente-Rodríguez A, Earnest S, et al. Regulation of OSR1 and the sodium, potassium, two chloride cotransporter by convergent signals. Proc Natl Acad Sci U S A. 2013;110(47):18826-18831. doi:10.1073/pnas.1318676110

Sengupta S, Peterson TR, Laplante M, Oh S, Sabatini DM. mTORC1 controls fasting-induced ketogenesis and its modulation by ageing. Nature. 2010;468(7327):1100-1104. doi:10.1038/nature09584

Settembre C, Di Malta C, Polito VA, et al. TFEB links autophagy to lysosomal biogenesis. Science. 2011;332(6036):1429-1433. doi:10.1126/science.1204592

Settembre C, Fraldi A, Medina DL, Ballabio A. Signals from the lysosome: a control centre for cellular clearance and energy metabolism. Nat Rev Mol Cell Biol. 2013;14(5):283-296. doi:10.1038/nrm3565

Settembre C, Zoncu R, Medina DL, et al. A lysosome-to-nucleus signalling mechanism senses and regulates the lysosome via mTOR and TFEB. EMBO J. 2012;31(5):1095-1108. doi:10.1038/emboj.2012.32

Sevilla A, Santos CR, Barcia R, Vega FM, Lazo PA. c-Jun phosphorylation by the human vaccinia-related kinase 1 (VRK1) and its cooperation with the N-terminal kinase of c-Jun (JNK). Oncogene. 2004;23(55):8950-8958. doi:10.1038/sj.onc.1208015

Shacka JJ. Mouse models of neuronal ceroid lipofuscinoses: useful pre-clinical tools to delineate disease pathophysiology and validate therapeutics. Brain Res Bull. 2012;88(1):43-57. doi:10.1016/j.brainresbull.2012.03.003

Shaffer AL, Shapiro-Shelef M, Iwakoshi NN, et al. XBP1, downstream of Blimp-1, expands the secretory apparatus and other organelles, and increases protein synthesis in plasma cell differentiation. Immunity. 2004;21(1):81-93. doi:10.1016/j.immuni.2004.06.010

Shamseldin HE, Alshammari M, Al-Sheddi T, et al. Genomic analysis of mitochondrial diseases in a consanguineous population reveals novel candidate disease genes. J Med Genet. 2012;49(4):234-241. doi:10.1136/jmedgenet-2012-100836

Shematorova EK, Shpakovski DG, Chernysheva AD, Shpakovski GV. Molecular mechanisms of the juvenile form of Batten disease: important role of MAPK signaling pathways (ERK1/ERK2, JNK and p38) in pathogenesis of the malady. Biol Direct. 2018;13(1):19. Published 2018 Sep 25. doi:10.1186/s13062-018-0212-y

Shematorova EK, Shpakovski GV. Current Insights in Elucidation of Possible Molecular Mechanisms of the Juvenile Form of Batten Disease. Int J Mol Sci. 2020;21(21):8055. Published 2020 Oct 29. doi:10.3390/ijms21218055

Shen Q, Yamano K, Head BP, Kawajiri S, Cheung JT, et al., 2014. Mutations in Fis1 disrupt orderly disposal of defective mitochondria. Mol. Biol. Cell 25:145–59

Shi L, Wang Z, Liu X, Li M, Zhang S, Song X. Bax inhibitor-1 is required for resisting the Early Brain Injury induced by subarachnoid haemorrhage through regulating IRE1-JNK pathway. Neurol Res. 2018;40(3):189-196. doi:10.1080/01616412.2018.1424699

Shor B, Wu J, Shakey Q, et al. Requirement of the mTOR kinase for the regulation of Maf1 phosphorylation and control of RNA polymerase III-dependent transcription in cancer cells. J Biol Chem. 2010;285(20):15380-15392. doi:10.1074/jbc.M109.071639

Shoulders MD, Ryno LM, Genereux JC, et al. Stress-independent activation of XBP1s and/or ATF6 reveals three functionally diverse ER proteostasis environments. Cell Rep. 2013;3(4):1279-1292. doi:10.1016/j.celrep.2013.03.024

Sigrist CJ, de Castro E, Cerutti L, et al. New and continuing developments at PROSITE. Nucleic Acids Res. 2013;41(Database issue):D344-D347. doi:10.1093/nar/gks1067

Sima N, Li R, Huang W, et al. Neural stem cells for disease modeling and evaluation of therapeutics for infantile (CLN1/PPT1) and late infantile (CLN2/TPP1) neuronal ceroid lipofuscinoses. Orphanet J Rare Dis.

2018;13(1):54. Published 2018 Apr 10. doi:10.1186/s13023-018-0798-2

Skopkova M, Hennig F, Shin BS, et al. EIF2S3 Mutations Associated with Severe X-Linked Intellectual Disability Syndrome MEHMO. Hum Mutat. 2017;38(4):409-425. doi:10.1002/humu.23170

Skulachev VP. Role of uncoupled and non-coupled oxidations in maintenance of safely low levels of oxygen and its one-electron reductants. Q Rev Biophys. 1996;29(2):169-202. doi:10.1017/s0033583500005795

Sleat DE, Tannous A, Sohar I, et al. Proteomic Analysis of Brain and Cerebrospinal Fluid from the Three Major Forms of Neuronal Ceroid Lipofuscinosis Reveals Potential Biomarkers. J Proteome Res. 2017;16(10):3787-3804. doi:10.1021/acs.jproteome.7b00460

Sleat DE, Wiseman JA, El-Banna M, et al. Analysis of Brain and Cerebrospinal Fluid from Mouse Models of the Three Major Forms of Neuronal Ceroid Lipofuscinosis Reveals Changes in the Lysosomal Proteome. Mol Cell Proteomics. 2019;18(11):2244-2261. doi:10.1074/mcp.RA119.001587

Smith HL, Mallucci GR. The unfolded protein response: mechanisms and therapy of neurodegeneration. Brain. 2016;139(Pt 8):2113-2121. doi:10.1093/brain/aww101

Smith JJ, Aitchison JD. Peroxisomes take shape. Nat Rev Mol Cell Biol. 2013;14(12):803-817. doi:10.1038/nrm3700

Snezhkina AV, Kudryavtseva AV, Kardymon OL, et al., ROS Generation and Antioxidant Defense Systems in Normal and Malignant Cells. Oxid Med Cell Longev. 2019;2019:6175804. Published 2019 Aug 5. doi:10.1155/2019/6175804

Sondhi D, Crystal RG, Kaminsky SM. Gene Therapy for Inborn Errors of Metabolism: Batten Disease. In: Tuszynski M. (eds) Translational Neuroscience 2016. Springer, Boston, MA. doi:10.1007/978-1-4899-7654-3_719

Sondhi D, Scott EC, Chen A, et al. Partial correction of the CNS lysosomal storage defect in a mouse model of juvenile neuronal ceroid lipofuscinosis by neonatal CNS administration of an adeno-associated virus serotype rh.10 vector expressing the human CLN3 gene. Hum Gene Ther. 2014;25(3):223-239. doi:10.1089/hum.2012.253

Sorrentino G, Ruggeri N, Specchia V, et al. Metabolic control of YAP and TAZ by the mevalonate pathway. Nat Cell Biol. 2014;16(4):357-366. doi:10.1038/ncb2936

Specchio N, Ferretti A, Trivisano M, et al., Neuronal Ceroid Lipofuscinosis: Potential for Targeted Therapy. Drugs. 2021;81(1):101-123. doi:10.1007/s40265-020-01440-7

Sriburi R, Jackowski S, Mori K, Brewer JW. XBP1: a link between the unfolded protein response, lipid biosynthesis, and biogenesis of the endoplasmic reticulum. J Cell Biol. 2004;167(1):35-41. doi:10.1083/jcb.200406136

Stein CS, Yancey PH, Martins I, Sigmund RD, Stokes JB, Davidson BL. Osmoregulation of ceroid neuronal lipofuscinosis type 3 in the renal medulla. Am J Physiol Cell Physiol. 2010;298(6):C1388-C1400. doi:10.1152/ajpcell.00272.2009

Stengel C. Beretning om et maerkeligt Sygdomstilfaelde hos fire Soedskende I Naerheden af Roeraas, Eyr et medicinsk Tidskrift, 1826;1, 347–352.

Storch S, Pohl S, Braulke T. A dileucine motif and a cluster of acidic amino acids in the second cytoplasmic domain of the batten disease-related CLN3 protein are required for efficient lysosomal targeting. J Biol Chem.

2004;279(51):53625-53634. doi:10.1074/jbc.M410930200

Storch S, Pohl S, Quitsch A, Falley K, Braulke T. C-terminal prenylation of the CLN3 membrane glycoprotein is required for efficient endosomal sorting to lysosomes. Traffic. 2007;8(4):431-444. doi:10.1111/j.1600-0854.2007.00537.x

Storz P. Reactive oxygen species in tumor progression. Front Biosci. 2005;10:1881-1896. Published 2005 May 1. doi:10.2741/1667

Straus W. Isolation and biochemical properties of droplets from the cells of rat kidney. J Biol Chem. 1954;207(2):745-755.

Stuart JA, Cadenas S, Jekabsons MB, Roussel D, Brand MD. Mitochondrial proton leak and the uncoupling protein 1 homologues. Biochim Biophys Acta. 2001;1504(1):144-158. doi:10.1016/s0005-2728(00)00243-7

Sugiura A, Mattie S, Prudent J, McBride HM. Newly born peroxisomes are a hybrid of mitochondrial and ER-derived pre-peroxisomes. Nature. 2017;542(7640):251-254. doi:10.1038/nature21375

Sun KH, Lee HG, Smith MA, Shah K. Direct and indirect roles of cyclin-dependent kinase 5 as an upstream regulator in the c-Jun NH2-terminal kinase cascade: relevance to neurotoxic insults in Alzheimer's disease. Mol Biol Cell. 2009;20(21):4611-4619. doi:10.1091/mbc.e09-05-0433

T

Tabata S, Ikeda R, Yamamoto M, et al., Thymidine phosphorylase enhances reactive oxygen species generation and interleukin-8 expression in human cancer cells. Oncol Rep. 2012;28(3):895-902. doi:10.3892/or.2012.1887

Tamaki SJ, Jacobs Y, Dohse M, et al. Neuroprotection of host cells by human central nervous system stem cells in a mouse model of infantile neuronal ceroid lipofuscinosis. Cell Stem Cell. 2009;5(3):310-319. doi:10.1016/j.stem.2009.05.022

Tammen I, Houweling PJ, Frugier T, et al. A missense mutation (c.184C>T) in ovine CLN6 causes neuronal ceroid lipofuscinosis in Merino sheep whereas affected South Hampshire sheep have reduced levels of CLN6 mRNA. Biochim Biophys Acta. 2006;1762(10):898-905. doi:10.1016/j.bbadis.2006.09.004

Taniguchi K, Wu LW, Grivennikov SI, et al. A gp130-Src-YAP module links inflammation to epithelial regeneration. Nature. 2015;519(7541):57-62. doi:10.1038/nature14228

Taschner PE, de Vos N, Breuning MH. Cross-species homology of the CLN3 gene. Neuropediatrics. 1997;28(1):18-20. doi:10.1055/s-2007-973658

Tasset I, Sánchez F, Túnez I. Bases moleculares de la enfermedad de Huntington: papel del estrés oxidativo [The molecular bases of Huntington's disease: the role played by oxidative stress]. Rev Neurol. 2009;49(8):424-429.

Tecedor L, Stein CS, Schultz ML, Farwanah H, Sandhoff K, Davidson BL. CLN3 loss disturbs membrane microdomain properties and protein transport in brain endothelial cells. J Neurosci. 2013;33(46):18065-18079. doi:10.1523/JNEUROSCI.0498-13.2013

Tejera D, Heneka MT. Microglia in Neurodegenerative Disorders. Methods Mol Biol. 2019;2034:57-67. doi:10.1007/978-1-4939-9658-2_5

Tian J, Cai T, Yuan Z, et al. Binding of Src to Na+/K+-ATPase forms a functional signaling complex. Mol Biol Cell. 2006;17(1):317-326. doi:10.1091/mbc.e05-08-0735

Tian Q, Gromov P, Clement JH, et al. RHEB1 insufficiency in aged male mice is associated with stress-induced seizures. Geroscience. 2017;39(5-6):557-570. doi:10.1007/s11357-017-9997-3

Toualbi K, Güller MC, Mauriz JL, et al., Physical and functional cooperation between AP-1 and beta-catenin for the regulation of TCF-dependent genes. Oncogene. 2007;26(24):3492-3502. doi:10.1038/sj.onc.1210133

Tripathy S, Jump DB. Elovl5 regulates the mTORC2-Akt-FOXO1 pathway by controlling hepatic cis-vaccenic acid synthesis in diet-induced obese mice. J Lipid Res. 2013;54(1):71-84. doi:10.1194/jlr.M028787

Trivisano M, Specchio N. Red flags for neuronal ceroid lipofuscinosis type 2 disease. Dev Med Child Neurol. 2020;62(4):414. doi:10.1111/dmcn.14389

Tsukumo Y, Tsukahara S, Furuno A, Iemura S, Natsume T, Tomida A. TBL2 is a novel PERK-binding protein that modulates stress-signaling and cell survival during endoplasmic reticulum stress. PLoS One. 2014;9(11):e112761. Published 2014 Nov 13. doi:10.1371/journal.pone.0112761

Tumaneng K, Schlegelmilch K, Russell RC, et al. YAP mediates crosstalk between the Hippo and PI(3)K–TOR pathways by suppressing PTEN via miR-29. Nat Cell Biol. 2012;14(12):1322-1329. doi:10.1038/ncb2615

Tuxworth RI, Chen H, Vivancos V, Carvajal N, Huang X, Tear G. The Batten disease gene CLN3 is required for the response to oxidative stress. Hum Mol Genet. 2011;20(10):2037-2047. doi:10.1093/hmg/ddr088

Twig G, Elorza A, Molina AJ, et al., Fission and selective fusion govern mitochondrial segregation and elimination by autophagy. EMBO J. 2008;27(2):433-446. doi:10.1038/sj.emboj.7601963

Tyagi R, Shahani N, Gorgen L, et al. Rheb Inhibits Protein Synthesis by Activating the PERK-eIF2α Signaling Cascade. Cell Rep. 2015;10(5):684-693. doi:10.1016/j.celrep.2015.01.014

Tyynelä J, Palmer DN, Baumann M, Haltia M. Storage of saposins A and D in infantile neuronal ceroid-lipofuscinosis. FEBS Lett. 1993;330(1):8-12. doi:10.1016/0014-5793(93)80908-d

U

U.S. National Library of Medicine. ClinicalTrials.gov. NCT03770572: Gene Transfer Study of AAV9-CLN3 for Treatment NCL Type 3. https://clinicaltrials.gov/ct2/show/NCT03770572. Accessed on 25th July 2021.

Ubersax JA, Ferrell JE Jr. Mechanisms of specificity in protein phosphorylation [published correction appears in Nat Rev Mol Cell Biol. 2007 Aug;8(8):665]. Nat Rev Mol Cell Biol. 2007;8(7):530-541. doi:10.1038/nrm2203

Upton JP, Wang L, Han D, et al. IRE1α cleaves select microRNAs during ER stress to derepress translation of proapoptotic Caspase-2. Science. 2012;338(6108):818-822. doi:10.1126/science.1226191

Urano F, Wang X, Bertolotti A, et al. Coupling of stress in the ER to activation of JNK protein kinases by transmembrane protein kinase IRE1. Science. 2000;287(5453):664-666. doi:10.1126/science.287.5453.664

Urra H, Henriquez DR, Cánovas J, et al. IRE1α governs cytoskeleton remodelling and cell migration through a direct interaction with filamin A [published correction appears in Nat Cell Biol. 2018 Oct;20(10):1228] [published correction appears in Nat Cell Biol. 2021 May;23(5):577]. Nat Cell Biol. 2018;20(8):942-953. doi:10.1038/s41556-018-0141-0

Uusi-Rauva K, Luiro K, Tanhuanpää K, et al. Novel interactions of CLN3 protein link Batten disease to dysregulation of fodrin-Na+, K+ ATPase complex. Exp Cell Res. 2008;314(15):2895-2905. doi:10.1016/j.yexcr.2008.06.016

V

Valm AM, Cohen S, Legant WR, et al. Applying systems-level spectral imaging and analysis to reveal the organelle interactome. Nature. 2017;546(7656):162-167. doi:10.1038/nature22369

Vander Heiden MG, Cantley LC, Thompson CB. Understanding the Warburg effect: the metabolic requirements of cell proliferation. Science. 2009;324(5930):1029-1033. doi:10.1126/science.1160809

van der Oost J, Westra ER, Jackson RN, Wiedenheft B. Unravelling the structural and mechanistic basis of CRISPR-Cas systems. Nat Rev Microbiol. 2014;12(7):479-492. doi:10.1038/nrmicro3279

van der Vliet A, Janssen-Heininger YMW, Anathy V. Oxidative stress in chronic lung disease: From mitochondrial dysfunction to dysregulated redox signaling. Mol Aspects Med. 2018;63:59-69. doi:10.1016/j.mam.2018.08.001

Varanita T, Soriano ME, Romanello V, et al., The OPA1-dependent mitochondrial cristae remodelling pathway controls atrophic, apoptotic, and ischemic tissue damage. Cell Metab. 2015;21(6):834-844. doi:10.1016/j.cmet.2015.05.007

Vasquez-Vivar J, Kalyanaraman B, Kennedy MC. Mitochondrial aconitase is a source of hydroxyl radical. An electron spin resonance investigation. J Biol Chem. 2000;275(19):14064-14069. doi:10.1074/jbc.275.19.14064

Vattem KM, Wek RC. Reinitiation involving upstream ORFs regulates ATF4 mRNA translation in mammalian cells. Proc Natl Acad Sci U S A. 2004;101(31):11269-11274. doi:10.1073/pnas.0400541101

Varelas X. The Hippo pathway effectors TAZ and YAP in development, homeostasis and disease. Development. 2014;141(8):1614-1626. doi:10.1242/dev.102376

Verfaillie T, Rubio N, Garg AD, et al. PERK is required at the ER-mitochondrial contact sites to convey apoptosis after ROS-based ER stress. Cell Death Differ. 2012;19(11):1880-1891. doi:10.1038/cdd.2012.74

Vesa J, Peltonen L. Mutated genes in juvenile and variant late infantile neuronal ceroid lipofuscinoses encode lysosomal proteins. Curr Mol Med. 2002;2(5):439-444. doi:10.2174/1566524023362311

Vidal-Donet JM, Cárcel-Trullols J, Casanova B, Aguado C, Knecht E. Alterations in ROS activity and lysosomal pH account for distinct patterns of macroautophagy in LINCL and JNCL fibroblasts. PLoS One. 2013;8(2):e55526. doi:10.1371/journal.pone.0055526

Volmer R, van der Ploeg K, Ron D. Membrane lipid saturation activates endoplasmic reticulum unfolded protein response transducers through their transmembrane domains. Proc Natl Acad Sci U S A. 2013;110(12):4628-4633. doi:10.1073/pnas.1217611110

von der Malsburg K, Müller JM, Bohnert M, et al., Dual role of mitofilin in mitochondrial membrane organization and protein biogenesis. *Dev Cell*. 2011;21(4):694-707. doi:10.1016/j.devcel.2011.08.026

W

Walton PA, Brees C, Lismont C, Apanasets O, Fransen M. The peroxisomal import receptor PEX5 functions as a stress sensor, retaining catalase in the cytosol in times of oxidative stress. Biochim Biophys Acta Mol Cell Res. 2017;1864(10):1833-1843. doi:10.1016/j.bbamcr.2017.07.013

Wang C, Mao X, Wang L, et al. Adiponectin sensitizes insulin signaling by reducing p70 S6 kinase-mediated serine phosphorylation of IRS-1. J Biol Chem. 2007;282(11):7991-7996. doi:10.1074/jbc.M700098200

Wang JM, Qiu Y, Yang Z, et al. IRE1α prevents hepatic steatosis by processing and promoting the degradation of select microRNAs. Sci Signal. 2018;11(530):eaao4617. Published 2018 May 15. doi:10.1126/scisignal.aao4617

Wang P, Li J, Tao J, Sha B. The luminal domain of the ER stress sensor protein PERK binds misfolded proteins and thereby triggers PERK oligomerization. J Biol Chem. 2018;293(11):4110-4121. doi:10.1074/jbc.RA117.001294

Wang W, Huang J, Chen J. Angiomotin-like proteins associate with and negatively regulate YAP1. J Biol Chem. 2011;286(6):4364-4370. doi:10.1074/jbc.C110.205401

Wang W, Xiao ZD, Li X, et al. AMPK modulates Hippo pathway activity to regulate energy homeostasis. Nat Cell Biol. 2015;17(4):490-499. doi:10.1038/ncb3113

Wang Z, Wu Y, Wang H, et al. Interplay of mevalonate and Hippo pathways regulates RHAMM transcription via YAP to modulate breast cancer cell motility [published correction appears in Proc Natl Acad Sci U S A. 2016 Nov 14;:]. Proc Natl Acad Sci U S A. 2014;111(1):E89-E98. doi:10.1073/pnas.1319190110

Warburg O, Wind F, Negelein E. THE METABOLISM OF TUMORS IN THE BODY. J Gen Physiol. 1927;8(6):519-530. doi:10.1085/jgp.8.6.519

Warnock A, Tan L, Li C, An Haack K, Narayan SB, Bennett MJ. Amlodipine prevents apoptotic cell death by correction of elevated intracellular calcium in a primary neuronal model of Batten disease (CLN3 disease). Biochem Biophys Res Commun. 2013;436(4):645-649. doi:10.1016/j.bbrc.2013.04.113

Waterham HR, Koster J, van Roermund CW, Mooyer PA, Wanders RJ, Leonard JV. A lethal defect of mitochondrial and peroxisomal fission. N Engl J Med. 2007;356(17):1736-1741. doi:10.1056/NEJMoa064436

Wei MC, Zong WX, Cheng EH, et al. Proapoptotic BAX and BAK: a requisite gateway to mitochondrial dysfunction and death. Science. 2001;292(5517):727-730. doi:10.1126/science.1059108

Weir HJ, Yao P, Huynh FK, et al. Dietary Restriction and AMPK Increase Lifespan via Mitochondrial Network and Peroxisome Remodeling. Cell Metab. 2017;26(6):884-896.e5. doi:10.1016/j.cmet.2017.09.024

Wiley LA, Burnight ER, Drack AV, et al. Using Patient-Specific Induced Pluripotent Stem Cells and Wild-Type Mice to Develop a Gene Augmentation-Based Strategy to Treat CLN3-Associated Retinal Degeneration. Hum Gene Ther. 2016;27(10):835-846. doi:10.1089/hum.2016.049

Wong LH, Gatta AT, Levine TP. Lipid transfer proteins: the lipid commute via shuttles, bridges and tubes. Nat Rev Mol Cell Biol. 2019;20(2):85-101. doi:10.1038/s41580-018-0071-5

Wong YC, Ysselstein D, Krainc D. Mitochondria-lysosome contacts regulate mitochondrial fission via RAB7 GTP hydrolysis. Nature. 2018;554(7692):382-386. doi:10.1038/nature25486

Wood Dos Santos T, Cristina Pereira Q, Teixeira L, Gambero A, A Villena J, Lima Ribeiro M. Effects of Polyphenols on Thermogenesis and Mitochondrial Biogenesis. Int J Mol Sci. 2018;19(9):2757. Published 2018 Sep 13. doi:10.3390/ijms19092757

Wright GA, Georgiou M, Robson AG, et al. Juvenile Batten Disease (CLN3): Detailed Ocular Phenotype, Novel Observations, Delayed Diagnosis, Masquerades, and Prospects for Therapy. Ophthalmol Retina. 2020;4(4):433-445. doi:10.1016/j.oret.2019.11.005

Wu D, Liu J, Wu B, Tu B, Zhu W, Luo J. The Batten disease gene CLN3 confers resistance to endoplasmic reticulum stress induced by tunicamycin. Biochem Biophys Res Commun. 2014;447(1):115-120.

doi:10.1016/j.bbrc.2014.03.120

Wu S, Liu Y, Zheng Y, Dong J, Pan D. The TEAD/TEF family protein Scalloped mediates transcriptional output of the Hippo growth-regulatory pathway. Dev Cell. 2008;14(3):388-398. doi:10.1016/j.devcel.2008.01.007

X

Xiong J, Kielian T. Microglia in juvenile neuronal ceroid lipofuscinosis are primed toward a pro-inflammatory phenotype. J Neurochem. 2013;127(2):245-258. doi:10.1111/jnc.12385

Y

Yamano K, Fogel AI, Wang C, van der Bliek AM, Youle RJ. 2014. Mitochondrial Rab GAPs govern autophagosome biogenesis during mitophagy. eLife 3:e01612

Yambire KF, Fernandez-Mosquera L, Steinfeld R, et al., Mitochondrial biogenesis is transcriptionally repressed in lysosomal lipid storage diseases. Elife. 2019;8:e39598. Published 2019 Feb 18. doi:10.7554/eLife.39598

Yang H, Jiang X, Li B, et al. Mechanisms of mTORC1 activation by RHEB and inhibition by PRAS40. Nature. 2017;552(7685):368-373. doi:10.1038/nature25023

Yarza R, Vela S, Solas M, Ramirez MJ. c-Jun N-terminal Kinase (JNK) Signaling as a Therapeutic Target for Alzheimer's Disease. Front Pharmacol. 2016;6:321. Published 2016 Jan 12. doi:10.3389/fphar.2015.00321

Yasa S, Modica G, Sauvageau E, Kaleem A, Hermey G, Lefrancois S. CLN3 regulates endosomal function by modulating Rab7A-effector interactions. J Cell Sci. 2020;133(6):jcs234047. Published 2020 Mar 16. doi:10.1242/jcs.234047

Yasa S, Sauvageau E, Modica G, Lefrancois S. CLN5 and CLN3 function as a complex to regulate endolysosome function [published online ahead of print, 2021 Jun 1]. Biochem J. 2021;BCJ20210171. doi:10.1042/BCJ20210171

Yasui H, Hayashi S, Sakurai H. Possible involvement of singlet oxygen species as multiple oxidants in p450 catalytic reactions. Drug Metab Pharmacokinet. 2005;20(1):1-13. doi:10.2133/dmpk.20.1

Yates AD, Achuthan P, Akanni W, et al., Ensembl 2020. Nucleic Acids Res. 2020;48(D1):D682-D688. doi:10.1093/nar/gkz966

Yifrach E., Fischer S., Oeljeklaus S., Schuldiner M., Zalckvar E., Warscheid B. (2018) Defining the Mammalian Peroxisomal Proteome. In: del Río L., Schrader M. (eds) Proteomics of Peroxisomes. Subcellular Biochemistry, vol 89. Springer, Singapore

Yokokawa T, Kido K, Suga T, Isaka T, Hayashi T, Fujita S. Exercise-induced mitochondrial biogenesis coincides with the expression of mitochondrial translation factors in murine skeletal muscle. Physiol Rep. 2018;6(20):e13893. doi:10.14814/phy2.13893

Yoon DH, Kwon OY, Mang JY, et al., Protective potential of resveratrol against oxidative stress and apoptosis in Batten disease lymphoblast cells. Biochem Biophys Res Commun. 2011;414(1):49-52. doi:10.1016/j.bbrc.2011.09.019

Yu G, Wang LG, Han Y, He QY. clusterProfiler: an R package for comparing biological themes among gene clusters. OMICS. 2012;16(5):284-287. doi:10.1089/omi.2011.0118

Yu L, McPhee CK, Zheng L, et al. Termination of autophagy and reformation of lysosomes regulated by mTOR.

Nature. 2010;465(7300):942-946. doi:10.1038/nature09076

Yu L, Zhang X, Yang Y, et al., Small-molecule activation of lysosomal TRP channels ameliorates Duchenne muscular dystrophy in mouse models. Sci Adv. 2020;6(6):eaaz2736. Published 2020 Feb 7. doi:10.1126/sciadv.aaz2736

Z

Zeman W, Donahue S. FINE STRUCTURE OF THE LIPID BODIES IN JUVENILE AMAUROTIC IDIOCY. Acta Neuropathol. 1963;3:144-149. doi:10.1007/BF00687063

Zerbino DR, Achuthan P, Akanni W, et al. Ensembl 2018. Nucleic Acids Res. 2018;46(D1):D754-D761. doi:10.1093/nar/gkx1098

Zhang J, Wang X, Vikash V, et al. ROS and ROS-Mediated Cellular Signaling. Oxid Med Cell Longev. 2016;2016:4350965. doi:10.1155/2016/4350965

Zhang L, Ren F, Zhang Q, Chen Y, Wang B, Jiang J. The TEAD/TEF family of transcription factor Scalloped mediates Hippo signaling in organ size control. Dev Cell. 2008;14(3):377-387. doi:10.1016/j.devcel.2008.01.006

Zhang M, Zhang L, Hu J, et al. MST1 coordinately regulates autophagy and apoptosis in diabetic cardiomyopathy in mice. Diabetologia. 2016;59(11):2435-2447. doi:10.1007/s00125-016-4070-9

Zhang X, Qiao Y, Wu Q, et al. The essential role of YAP O-GlcNAcylation in high-glucose-stimulated liver tumorigenesis. Nat Commun. 2017;8:15280. Published 2017 May 5. doi:10.1038/ncomms15280

Zhang Y, Gao X, Saucedo LJ, Ru B, Edgar BA, Pan D. Rheb is a direct target of the tuberous sclerosis tumour suppressor proteins. Nat Cell Biol. 2003;5(6):578-581. doi:10.1038/ncb999

Zhang Y, Xu H. Translational regulation of mitochondrial biogenesis. Biochem Soc Trans. 2016;44(6):1717-1724. doi:10.1042/BST20160071C

Zhao B, Li L, Lu Q, et al. Angiomotin is a novel Hippo pathway component that inhibits YAP oncoprotein. Genes Dev. 2011;25(1):51-63. doi:10.1101/gad.2000111

Zhao B, Wei X, Li W, et al. Inactivation of YAP oncoprotein by the Hippo pathway is involved in cell contact inhibition and tissue growth control. Genes Dev. 2007;21(21):2747-2761. doi:10.1101/gad.1602907

Zhao B, Ye X, Yu J, et al. TEAD mediates YAP-dependent gene induction and growth control. Genes Dev. 2008;22(14):1962-1971. doi:10.1101/gad.1664408

Zheng Y, Pan D. The Hippo Signaling Pathway in Development and Disease. Dev Cell. 2019;50(3):264-282. doi:10.1016/j.devcel.2019.06.003

Zheng Z, Kim H, Qiu Y, et al. CREBH Couples Circadian Clock With Hepatic Lipid Metabolism. Diabetes. 2016;65(11):3369-3383. doi:10.2337/db16-0298

Zhou J, Liu CY, Back SH, et al. The crystal structure of human IRE1 luminal domain reveals a conserved dimerization interface required for activation of the unfolded protein response. Proc Natl Acad Sci U S A. 2006;103(39):14343-14348. doi:10.1073/pnas.0606480103

Zhu X, Zhang J, Sun H, et al. Ubiquitination of inositol-requiring enzyme 1 (IRE1) by the E3 ligase CHIP mediates the IRE1/TRAF2/JNK pathway. J Biol Chem. 2014;289(44):30567-30577. doi:10.1074/jbc.M114.562868

Zid BM, Rogers AN, Katewa SD, et al. 4E-BP extends lifespan upon dietary restriction by enhancing mitochondrial activity in Drosophila. Cell. 2009;139(1):149-160. doi:10.1016/j.cell.2009.07.034

Zinzalla V, Stracka D, Oppliger W, Hall MN. Activation of mTORC2 by association with the ribosome. Cell. 2011;144(5):757-768. doi:10.1016/j.cell.2011.02.014

Zoncu R, Bar-Peled L, Efeyan A, Wang S, Sancak Y, Sabatini DM. mTORC1 senses lysosomal amino acids through an inside-out mechanism that requires the vacuolar H(+)-ATPase. Science. 2011;334(6056):678-683. doi:10.1126/science.1207056

7. Appendices

7.1. Award letter

National Contest for Life_NCL

NCL-Stiftung | Holstenwall 10 | D-20355 Hamburg

Ms
Katarzyna Więciorek
University Medical Center Göttingen
Institute of Cellular Biochemistry
Humboldtallee 23, room 01.423
37073 Göttingen

Hamburg, Germany, June 28th, 2018

Dear Ms Więciorek,

Congratulations, you have successfully applied for our NCL PhD fellowship. It is due to your and Dr. Nuno Raimundo's outstanding research proposal "*Metabolic consequences of CLN3 loss-of-function*". The grant money (50.400 EUR) is to be used to cover the fellowship of Katarzyna Więciorek as a PhD student at the University Medical Center Göttingen. The funding is for a thirty-six month period of time that starts on December 1, 2018 to November 30, 2021.

Let me congratulate you personally as well as on behalf of the whole staff of the NCL-Stiftung!

I hope your project will bear many fruits and we look forward to seeing the future results of this work. I wish you and your supervisor a great deal of success.

Once again hearty congratulations!

Sincerely yours,

Frank Stehr

(Dr. Frank Stehr)
(NCL-Stiftung)

NCL-Stiftung (gemeinnützig)
Holstenwall 10, D-20355 Hamburg
Tel./Fax +49-(0)40-69.666.74-0/-69
www.ncl-stiftung.de

Vorstand
Dr. rer. nat. Frank Stehr
frank.stehr@ncl-stiftung.de
Mobil +49-(0)178-3 41 60 57

Spendenkonto
Hamburger Sparkasse
IBAN: DE50 20050550 1059223030
BIC: HASPDEHHXXX

7.2. CV

Katarzyna Więciorek-Płuciennik

Bertheaustrasse 25/27 WE68,
37075 Göttingen, Germany
(+49) 157 71269325
katarzyna.wieciorek@gmail.com

Date of birth: 22 May 1992

Gender: Female

Nationality: Polish

WORK EXPERIENCE

06/2018 – 09/2021 *Graduate Researcher*
University Medical Center Göttingen, Germany

- Study of effect of CLN3-KO on cellular metabolism and signalling
- Successful characterization of mitochondrial function and identification of signalling pathways associated with Batten disease in HEK cells lacking CLN3
- Recommendation of potential therapeutic targets
- Scientific communication through numerous talks and posters at symposia and conferences
- Training and supervision of several master's students

03/2016 – 12/2017 *Trainee in Molecular Biology*
University Medical Center Göttingen, Germany

- Research on links between defective endocytosis and mitochondrial function
- Efficient use of several biochemical and molecular biology techniques in both, cellular and mouse models

02/2014 – 02/2015 *Trainee in Bioinformatics*
University of Lisbon, Portugal

- Study of paced and spontaneous motion using DPARSF Advanced toolbox and MATLAB for fMRI data analysis

EDUCATION AND TRAINING

06/2018 – 09/2021 *Dr rer. nat. in Molecular Medicine*
Georg-August University, Göttingen, Germany
NCL PhD fellowship
Thesis: Effect of CLN3-KO on cellular metabolism and signalling

09/2015 – 12/2017 *Mestre in Biomedical Engineering and Biophysics*
Profile: Medical Biophysics and System Physiology
Faculty of Science, University of Lisbon, Portugal

Final grade: Very good (17/20)
Thesis: Links between defective endocytosis and mitochondria

03/2015 – 09/2015	*Auditor* *Faculty of Science, University of Lisbon, Portugal* Courses of Integrated 2nd cycle in Biomedical and Biophysics Engineering
10/2011 – 02/2015	*Diploma of first cycle programme in biomedical engineering* *International Faculty of Engineering, Lodz University of Technology, Poland* Including two semesters of mobility at the Faculty of Science of the University of Lisbon (2014 and 2014/2015) Final grade: more than good Thesis: The study of paced and spontaneous motion using functional magnetic resonance imaging

SCIENTIFIC AND METHODOLOGICAL EXPERTISE

Cell culture	Culturing, cryopreservation and transfection of various cell lines
Molecular Biology	DNA and RNA isolation from cells and tissues; cDNA synthesis and qPCR; multidimensional NGS data analysis; genome editing with CRISPR-Cas9
Biochemistry	Preparation of whole cell lysates from adherent cells; *Organelle isolation;* SDS-PAGE and BN-PAGE; immunoblotting; preparation of buffers, media and solutions
Functional assays	Flow cytometry; microplate reader assays and real-time cell metabolic analysis; immunofluorescence in light microscopy
Programming	MATLAB, Python, R and COMSOL

IT SKILLS

Graphics	GraphPad Prism, Adobe Illustrator and AutoCAD
Office tools	Microsoft Office on both Windows and macOS

LANGUAGE PROFICIENCY

Polish	Native
English	Advanced, fluent spoken and written (studying, presenting and publishing in English)
German	Independent (living in Germany since 03/2016, language courses since 10/2018)
Portuguese	Elementary (living in Portugal from 2/2014 to 2/2016)

PERSONAL SKILLS

Communication	Outstanding interpersonal, written and public speaking skills developed through teaching and numerous talks and posters at symposia and conferences
Management	Excellent organizing, planning and scheduling assignments as well as events; efficient work without supervision or external motivation
Teamwork	Extensive experience in teamwork in an international environment; constructive feedback, negotiation and conflict management
Problem-solving	Analysis of complex data, quick development and adaptation of new approaches to overcome obstacles